Dry reforming of associated natural gas using catalytic membrane reactors.

TEMIMI, A.R.

2015

Dry Reforming of Associated Natural Gas Using Catalytic Membrane Reactors

By Ali Ramadan Temimi

Thesis submitted for the degree of Doctor of Philosophy

Principal Supervisor:

Professor Edward Gobina

The Robert Gordon University
Faculty of Design and Technology
School of Engineering
Aberdeen, UK
2015

Declaration

This work has been entirely composed by the author and not been accepted in any previous application for a degree. The work has been undertaken by the candidate and all sources of information have been acknowledged.

Mr. Ali.R.Temimi.

Acknowledgements

In the name of God, the Most Gracious, the Most Merciful.

Any piece of research work inevitably involves more than one person before it finally reaches completion. My work has proved to be no exception to this rule and I would like to take this opportunity to acknowledge at least some of the people who have assisted me in this venture. The first and foremost mention must go to Professor Edward Gobina, my principal supervisor and Chair of the Centre for Process Integration and Membrane Technology (CPIMT), for proposing the topic of this research, and for his help, advice, understanding, patience, discussions and supervision. I also wish to express my deepest gratitude to Professor Bob Bradley for being my second supervisor and for providing the use of his equipment and the availability of his research team.

I would like to extend my sincere thanks to the technical staff, namely, Milton Montgomery, Stanley Buchan, Bill Walker, and Allan Harkess, for their unlimited contribution in the installation and maintenance of all the necessary apparatus throughout the research period, and Iain Tough for his precious time and patience in explaining the basics of SEM and analysis of the samples. My full appreciation and acknowledgement goes to Dr. Mohamed Amish for his unlimited support, and also to all the secretarial staff of the School of Engineering for their continuous help and assistance. I should also not forget to thank my colleagues from the Centre for Process Integration and Membrane Technology: Abubakar Alkali, Barry Mackenzie, Ruben Umoh, and Chee Chong Chen, for their support, continuous motivation, friendship and sharing of experiences, from which I gained great benefit.

Finally, I am very much grateful to the authorities of the Petroleum Training and Qualifying Institute (PTQI), Tripoli, Libya, for providing the financial support for my research. Thank you.

Dedication

I would like to dedicate this work to all my family for their patience, especially to my wife for her continuous moral support and encouragement, for making me believe that this could be possible, and for her understanding throughout the years, and also to my beloved parents to whom I owe everything in this life.

Abstract

The mitigation and utilization of greenhouse gases, such as carbon dioxide (CO_2), are among the most important challenges in the area of energy research. Dry reforming of propane (C_3H_8) (DRP), which uses both CO_2 and C_3H_8 as reactants, is a potential method to utilize the previously mentioned gases in the atmosphere. Associated natural gas containing high concentrations of CO_2 and C_3H_8 could therefore be utilized for hydrogen and synthesis gas (syngas) production in the near future, without need for the removal of CO_2 from the source gas. Thus, the DRP reaction is a suitable process to convert C_3H_8 and CO_2 to more useful raw materials.

The reforming of (CO_2) with associated natural gas can be adapted to generate a synthetic gas having 1:1 hydrogen to carbon monoxide (CO) ratio. This type of gas synthesis may be used during the production of a large number of industrially important chemicals. From an environmental point of view, this reaction can also be used to mitigate the so-called ‘‘greenhouse effect’’ since the conversion of these gases into valuable chemical(s) and feed stocks could alleviate and significantly reduce the emissions of CO_2 and associated natural gas to the atmosphere. In this thesis, a catalytic membrane reactor has been used to carry out experiments on the conversion of reactants, product selectivity and distribution, catalyst selection and activity. Interpretation of the reaction mechanism and kinetics of this important reaction are also presented. Previous experimental research has been centered on the reactor development, catalyst impregnation and the feasible applications in industry. The Group VIII metals of the periodic table of elements, supported on oxides have been found to be effective for this reaction. Carbon deposition causing catalyst deactivation was found to be one of the major challenges inhibiting the large-scale application of the reaction. Nickel (Ni)-based catalysts impregnated on an alumina wash-coated tubular membrane supports showed carbon-free operation and was thus used to generate important data regarding the performance of membrane reactors for this reaction.

In this work, the membrane reactor investigated for CO_2 reforming with associated natural gas operated in pore-flow through mode, using a catalyst impregnated porous membrane that had no separating functions but acted as a support for the catalyst. The catalyst was therefore immobilized as highly dispersed nanoparticles in the pore of the membrane structure. CO_2 and associated natural gas were forced through the pores of the membrane

where the catalytic reaction took place. The membrane, in effect, worked as a contact zone for the reactants and the catalyst. Because of fast convective flow, internal diffusion limitations were reduced as the products were immediately removed from the membrane pore, avoiding product accumulation within the membrane and therefore eliminating consecutive reactions. As a consequence, the effective product yield was not influenced by mass transfer limitations and selectivity for the desired product could be increased. The reverse water-gas-shift reaction was a possible cause for the reduced, yield of hydrogen. The reduction or elimination of the mass transfer limitation is particulary important for CO_2 reforming with associated natural gas were there is a high propensity for consecutive reactions.

This research investigated the catalytic dry reforming of propane over Zr/Ni/Pd/Cu/α-Al_2O_3 catalysts under the temperature range 600ºC/873.15ºK to 700ºC/973.15 ºK. These catalysts supported on α-Al_2O_3 were chosen for this study since primary studies showed better selectivity and activity and smaller deactivation resistance than for other catalysts.

The thermal structure, pore size distribution, gas permeability and chemical structure of such Hybrid Ceramic Membranes (HCMs) were characterised using various methods including gas permeability measurement, Scanning Electronic Microscopy (SEM), Accelerated Surface Area and Porosimetry analysis (ASAP), nitrogen Adsorption, Energy Dispersive X-ray Analysis (EDXA) and gas permeation mechanisms through the catalytic porous membrane.

The initial experimental results from the HCMs exhibited good thermal stability, gas permeability and hydrophilic properties as the accompanied water vapour that was formed could permeate through membranes better than the gases that resulted from the dry reforming of propane with CO_2 (C_3H_6, C_2H_6, C_2H_4, CH_4 and CO). Preliminary experiments were conducted to check the working condition of the catalyst testing unit. The results were quantitatively analysed and a typical productive reactive run was selected as a representative sample. The experimental reactive runs were conducted using three different sets of ceramic membrane supports under various operating conditions including pressure at 1.0, 2.0 and 3.0 bars, temperature at 600ºC/873.15ºK, 650ºC/923.15ºK and 700ºC/973.15ºK, and overall inlet premixed reactant fed gas flow rates of 100ml/min, 200ml/min and 300ml/min fed at a flow ratio of 1:1, 1:2 and 2:1. The best experimental reactant fed gas conversion results of 34%, and 58% of CO_2 and C_3H_8

respectively were obtained at a pressure of 2 bar, a temperature of 650ºC/923.15ºK and a flow rate of 200ml/min that was fed at ratio of 2:1. The production gas selectivities were of 68%, 25%, 28%, 26%, and 55% for C_3H_6, C_2H_6, C_2H_4, CH_4, and CO respectively and liquid yield namely water.

Thus a catalytic membrane reactor (CMR) for the dry reforming of CO_2 and propane was presented along with its typical performance characteristics. This reactor structure was implemented here to achieve an efficient integration not only on the reactor section but also in the process scale as recommended in this study.

Table of Contents

List of Tables

List of Figures

Nomenclatures

A	Pre-exponencial factor or frequency factor	
Å	Angstrom	1 angstrom=1.0×10-10 meters
C	Molar concentration	[mol/ml]
ΔH	Heat of reaction	[kJ/mol]
E	Activation energy	[kJ/mol K, kcal/mol K]
F	Molar flow rate	[mol/min]
id	Internal diameter	[mm]
k	Reaction rate constant	
od	External diameter	[mm]
id	Internal diameter	[mm]
P	Pressure	[bar]
r	Rate of reaction	
R	Gas constant	
S	Selectivity	
T	Temperature	[ºK], [ºC]
ts	Internal thickness	[mm]
tw	External thickness	[mm]
V	Volume	[ml, cm3]
Q	Volumetric flow rate	[ml/min]
X	Conversion	
Y	Yield	
y	molar fraction	

SUBSCRIPTS

n place in the reactor

room Room parameter

0 Initial conditions

ABBREVIATIONS

AES Auger Photoelectron Spectrum

ASAP Accelerated Surface Area and Porosimetry analysis

BET Stephen Brumaire; P.H. Emmet; Edward Teller

BJH Elliot P. Barret; Leslie G. Joyner; Paul P. Halenda

CAR Combined Autothermal Reforming

CMR Catalytic Membrane Reactor

CNMR Catalytic Non-permeselective Membrane Reactor

PBCR Packed Bed Catalytic Reactor

PBCMR Packed Bed Catalytic Membrane Reactor

CRM Combined Reforming

CCR Conventional Catalytic Reaction

DRIFTS Diffuse Reflectant Infrared Spectroscopy

EDXA Energy Dispersive x-ray Analysis

FBCMR Fuidized Bed Membrane Reactor

FBMR Fluidized Bed Catalytic Membrane Reactor

FCD Flame Ionization Detector

GTL Gas-to-Liquids

HCMR Hybrid Ceramic Membrane Reactor

LNG Liquefied Natural Gas

HCM Hybrid Ceramic Membrane

MF Microfiltration

NF Nanofiltration

NC-POM Non-catalytic Partial Oxidation

PBCR Packed Bed Catalytic Reactor

PBCMR Packed Bed Catalytic Membrane Reactor

PBMR Packed Bed Membrane Reactor

POM Catalytic Partial Oxidation

SCR Selective Catalytic Reduction

SEM Scanning Electron Microscopy

STP Standard Temperature and Pressure

Syngas Synthesis Gas

TCD Thermal Conductivity Detector

UF Ultrafiltration

WGS Water-Gas-Shift

XPS X-ray Photoelectron Spectroscopy

CONVERSIONS

Pressure

1 bar = 100 000 Pa = 1.987 atm

Energy

1 kcal = 4.1868kJ

Chapter One

Introduction

Chapter 1: Introduction.

1.1 Membrane technology.

Membrane technology is the multidisciplinary science looking at membranes. The term membrane is traditionally associated with the concept of a layered material that is capable of imposing certain restrictions on the permeation flux of some substances. Those molecules meet the permeation requirements can pass through, while the membrane acts as a barrier for the remainder. The **I**nternational **U**nion of **P**ure **A**pplied **C**hemistry [IUPAC] defines a membrane reactor as a device that combines a membrane-based separation process with a chemical reaction step in one unit [1]. There has been rapid development in membrane processes in several different science and technology disciplines over the past two decades. Although much of the development of ceramic membrane technology is fairly recent, however, their first large-scale use actually dates back to the 1930s.

This chapter introduces basic membrane processes together with a brief description of the various types and classifications of membranes available. Chapter 2 presents a more detailed background and literature review, covers the motivation for this study and lists the objectives of this work. Chapter 3 explains in detail the experimental part of the study and Chapter 4 presents and discusses the results. Chapter 5 presents an interpretation of the results, summarizes the main conclusions from the work and suggests recommendations for future work.

1.2 General description.

A **membrane** can be defined as a permeable or semi-permeable phase, often a thin layer, which to some extent restricts the motion of certain species or assists in creating a new species depending upon the purpose for which it was prepared. In other words, a membrane can be simply defined as a barrier between the feed stream (in the case of separation) and the product stream. The two streams are controlled by the relative rates of transport of various species through the membrane. The performance of any membrane is defined in terms of two simple factors such as flux and selectivity [2].

Gas processing using a membrane involves the preferential transport of one constituent in a mixture of gases across a thin barrier-membrane. The resultant product that passes through the membrane is known as permeate. This can be described in technical terms of permeation into the membrane material and diffusion in the membrane. The driving force of the permeation process is due to differences in either one or more operating conditions (such as pressure, temperature, electrochemical potential or concentration of the permeating species) across the membrane barrier, as shown in figure 1.1. This may lead to a membrane separation process where the feed stream has been separated into a retentate and a permeate stream, as shown in figure 1.2.

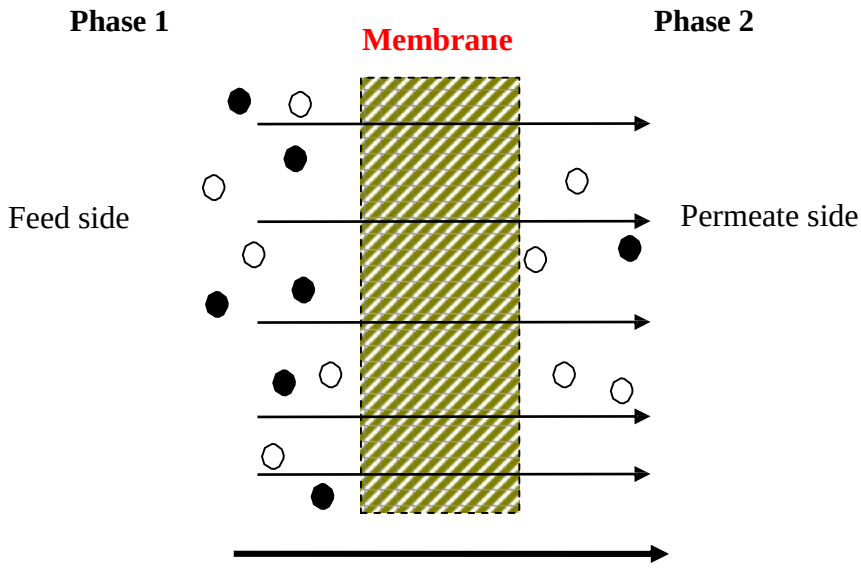

Figure 1.1 Schematic representations for two-phase system separated by a membrane [3].

Driving force = $\Delta P/dt$, $\Delta C/dt$, $\Delta T/dt$ and $\Delta E/dt$, where ΔP represents the pressure differences (i.e.microfiltration, ultrafiltration, nanofiltration, reverse osmosis, gas separation, and pervaporation); ΔC represents the concentration differences (i.e. dialysis, osmosis, and forward osmosis); ΔT represents the temperature differences (i.e. membrane distillation); and ΔE represents the electrochemical potential differences (i.e. electrodialysis, membrane electrolysis, and electrophoresis).

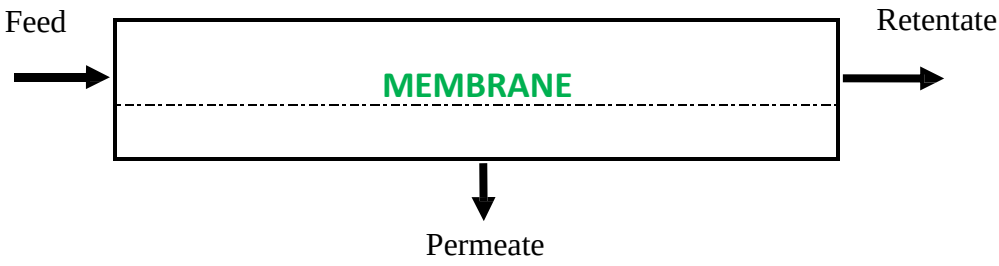

Figure 1.2 Schematic representation of a membrane process where the feed stream has been separated into a retentate and a permeate stream [3].

In this study, commercially available ceramic support materials have been incorporated into catalytic membrane reactors to achieve the conversion of associated natural gas (i.e. propane/CO_2) to lower olefines (C_3H_6 and C_2H_4) and synthesis gas at commercially attractive rates with complete stability of the materials.

1.2.1 Membrane pore size classifications

The pore size is known as the distance between two opposite walls of the pore. According to IUPAC (2-4) definitions, pore diameters are classified as follows:

- Macropores: > 50 nm.
- Mesopores: between 50 nm and 2 nm.
- Micropores: < 2 nm (supermicropores approx 0.7; ultramicropores < 0.7)

Table 1.1 shows that for porous ceramic membranes, their traditional application and separation mechanisms correspond to the pore size of the membranes.

Table 1.1: Category of ceramic membranes [4].

Type	Pore size(nm)	Mechanism	Applications
Macroporous	>50	• Viscous flow. • Molecular sieving.	Ultrafiltration (UF), Microfiltration (MF)
Mesoporous	2-50	• Knudsen diffusion.	UF, Nanofiltration (NF), Gas Separation.
Microporous	<2	• Pore diffusion.	Gas Separation.
Dense	-	• Surface flow. • Solution diffusion.	Gas Separation, Reaction.

1.3 Types of membranes.

Membranes can be classified as organic or inorganic. Inorganic membranes for reactors can be inert or catalytically active, dense or porous, and made from metals, carbon, glass or ceramic. They can be uniform in composition, composite (i.e. made from different materials), [5] and have homogeneous or asymmetric porous structures. Membranes can also be supported on such materials as porous glass, sintered metal, granular carbon or ceramics such as alumina. Even a cursory examination of the variety of membranes that exist makes it evident that a single classification scheme is unlikely to permit a clear and concise presentation. A rather informative picture can, however, be obtained from the following.

1.3.1. Classification by nature of material.

Membranes can be classified according to the nature of the materials they were made of. The most basic division in this system is into living membranes and those made of natural or regenerated substances as shown in figure 1.3.

1.3.2. Classification by structure.

Membranes can be classified based on their structure, including properties such as pore diameter of both porous and non-porous membranes as shown in figure 1.4.

1.3.3. Classification by application.

Membranes can be classified according to the field or system in which they are used, such as those used in gas-liquid systems (figure 1.5).

1.3.4. Classification by mechanism of action.

Figure 1.6 represents membrane classification according to mechanism of action-adsorption, diffusion, or non-selective/inert behaviour.

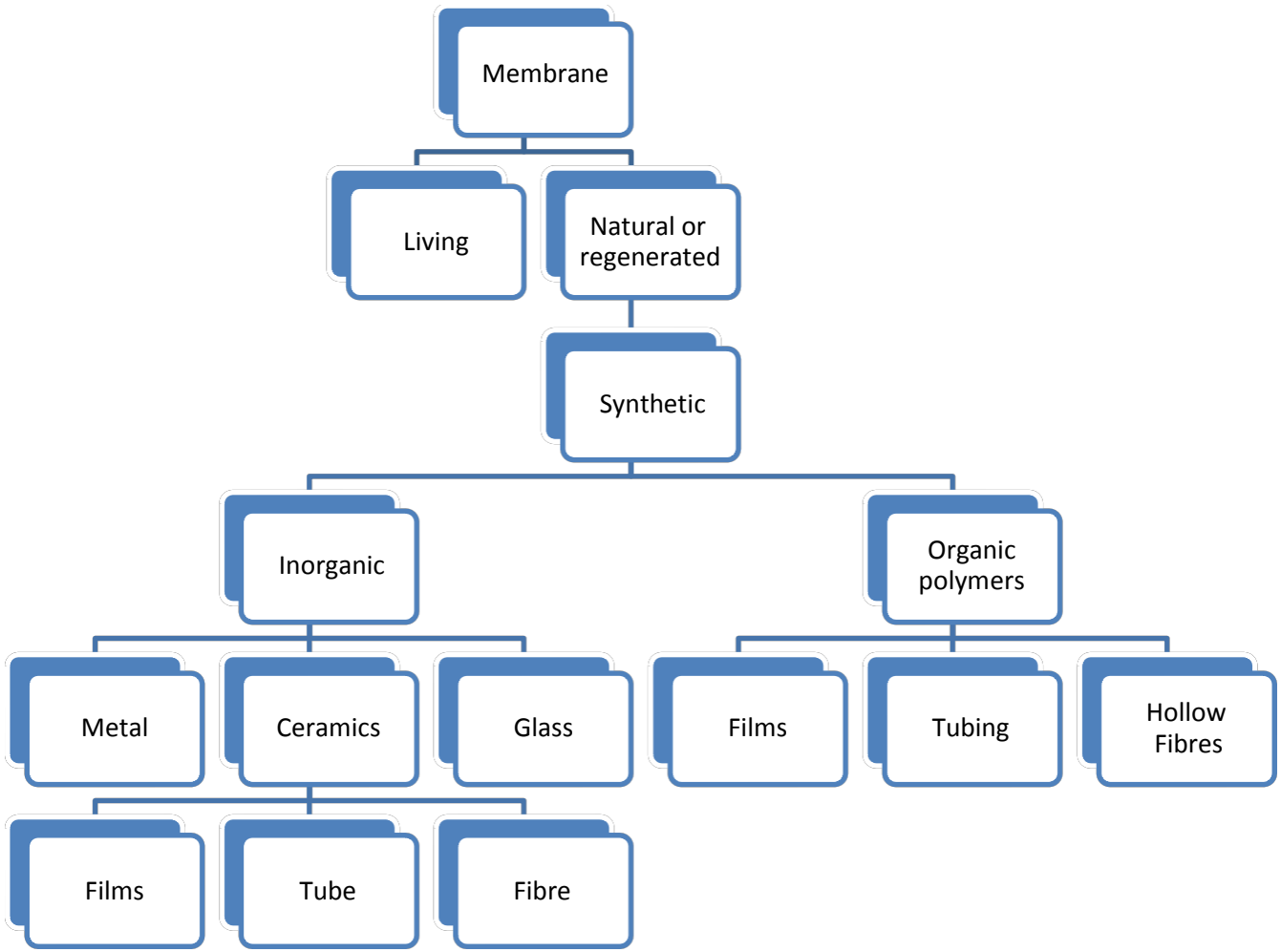

Figure 1.3 Membrane classifications by nature of material.

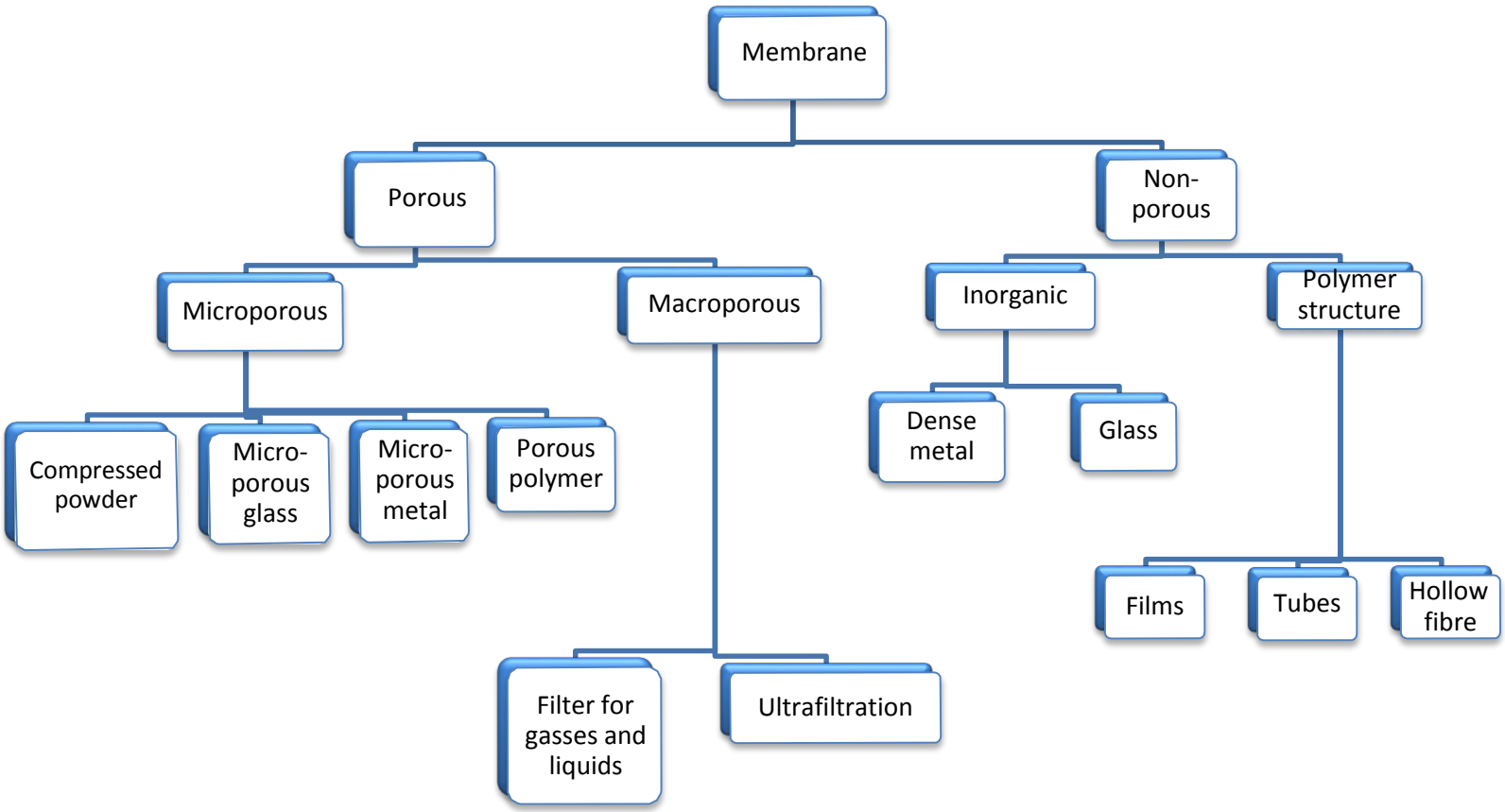

Figure 1.4 Classifications of membranes by the structure of the membrane.

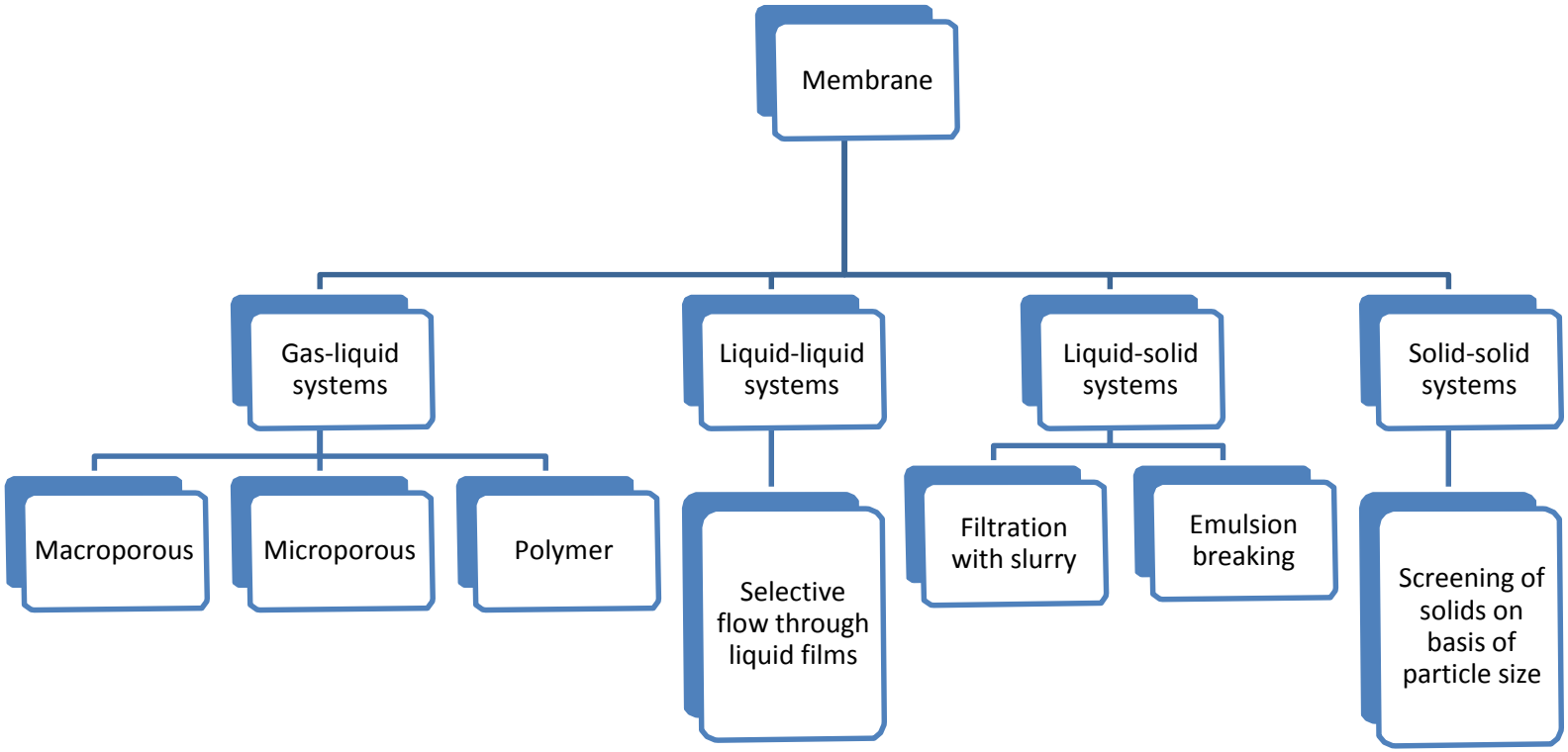

Figure 1.5 Classifications of membranes by their application.

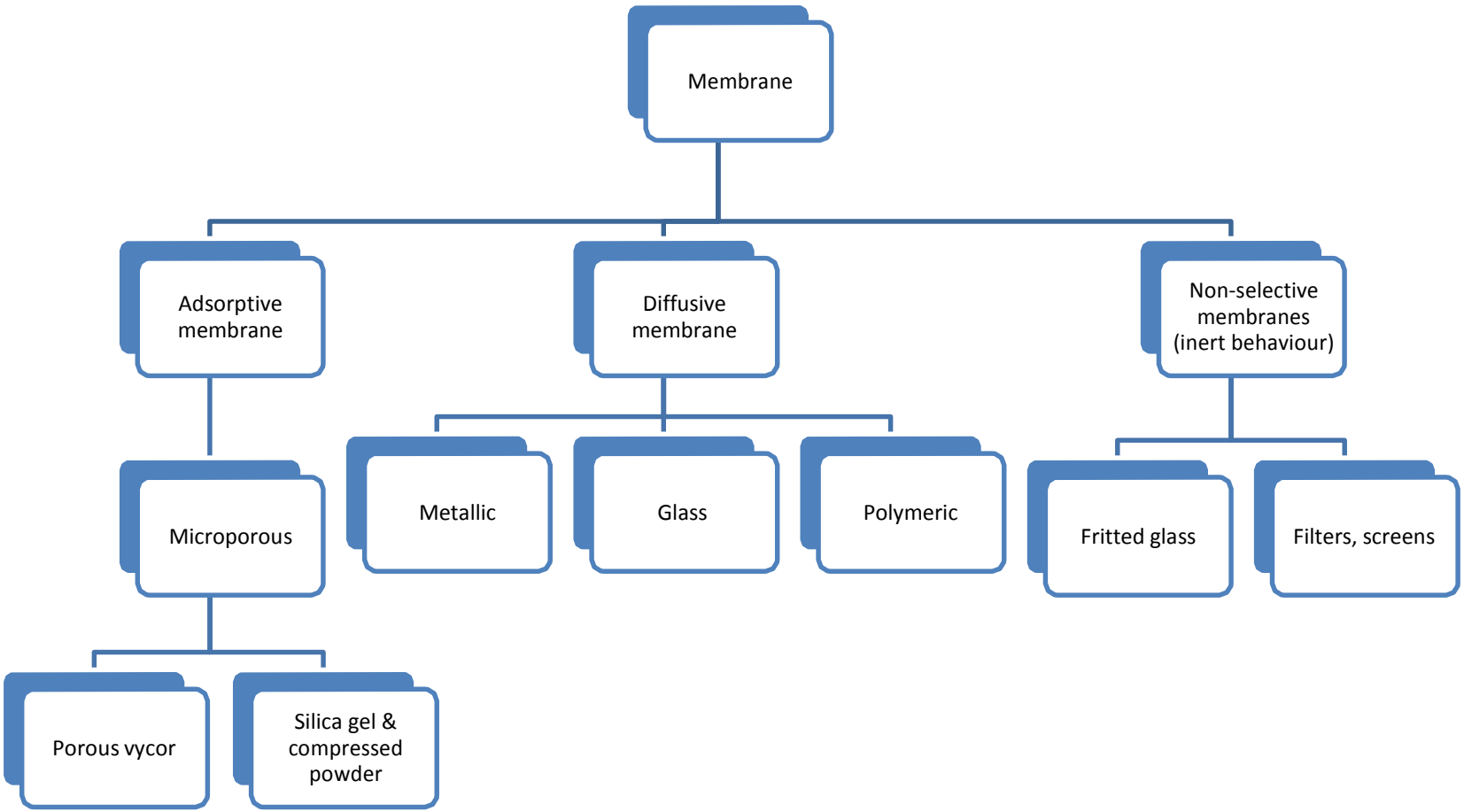

Figure 1.6 Classifications of membranes by mechanism of action.

1.4 Membrane/permeator flow patterns.

In general, the performances of any membrane reactor are affected by the relative direction of feed and permeate flow and/or the relative flow streams in the vicinity of the active layer of the membrane. Membrane flow patterns can generally be described as follows as shown in figure 1.7.

1.4.1. Cross flow.

In cross flow permeation figure 1.7A, the permeate gas in contact with the active layer consists entirely of the gas that has just passed through the membrane. There is no flow of permeate gas past the membrane from adjoining regions on the permeate side of the membrane, so the local permeate composition is not 'coupled' to permeate composition elsewhere along the membrane [3].

1.4.2. Co-current flow.

In this type of flow pattern figure 1.7B, the feed and permeate streams flow through the membrane module in the same direction.

1.4.3. Counter-current flow.

In counter-current flow figure 1.7C, the fluids flow through the membrane module on both the upstream and downstream sides parallel to the membrane surface but in opposite directions. Cross flow permeation can also occur where permeation is perpendicular to the membrane. For co- or counter-current permeation, the gas in contact with the downstream side of the membrane consists of the gas that just permeated through the membrane plus the bulk permeates that is flowing past it.

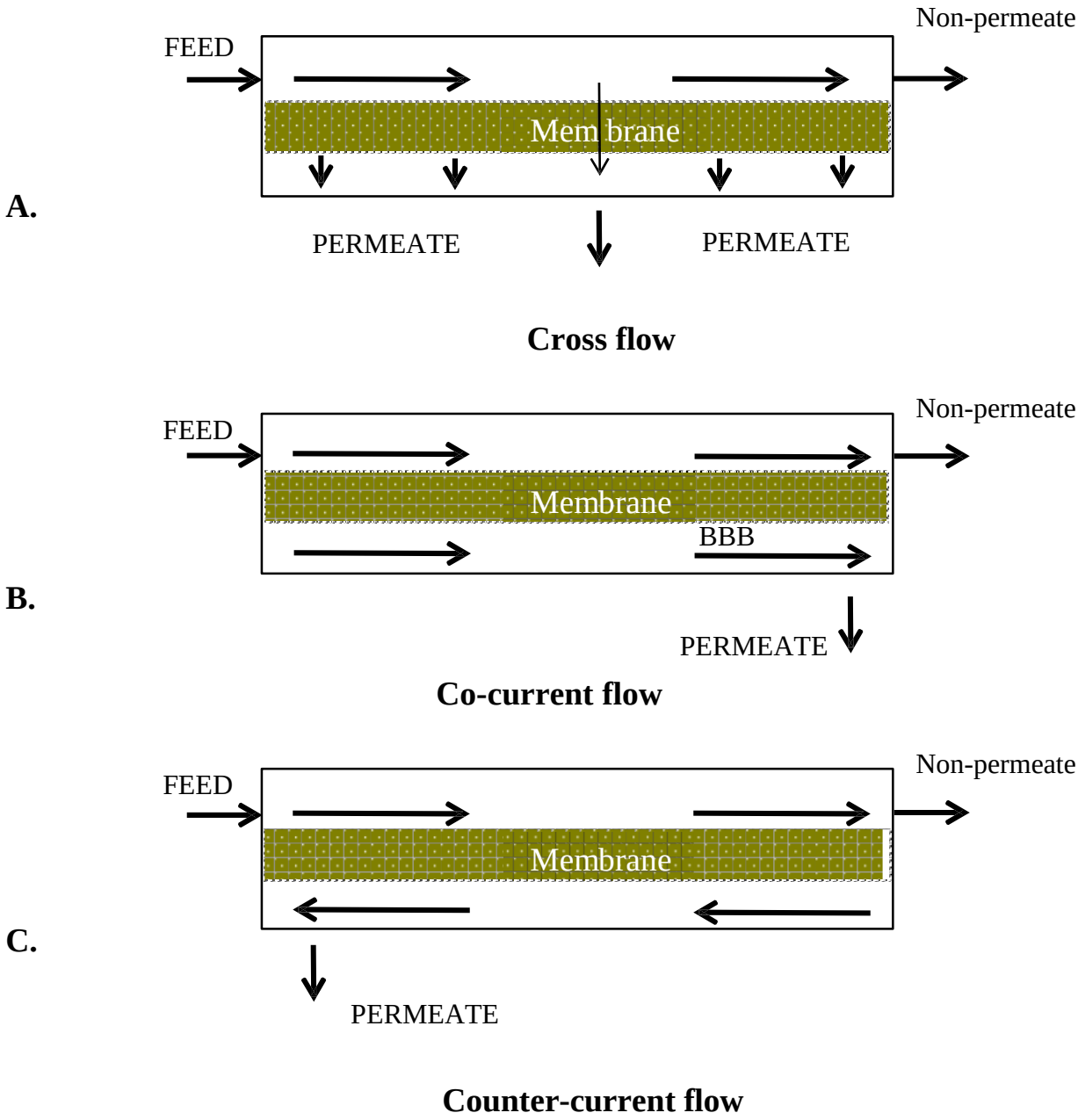

Figure 1.7 Membrane flow patterns [2].

1.5 Gas transport processes.

The gas transport process in any system is the way that the gas travels and behaves as it moves across from one media to another.

1.5.1. Diffusion in gases.

Diffusion is simply defined as the process by which matter is transported from one part of a system to another as a result of random molecular motions. Diffusion plays an important role in chemical engineering as well as in many other disciplines, and thus knowledge of the diffusion coefficient and the mechanism of diffusion are of great importance [6].

1.5.1.1. Types of gas diffusion.

Gas typically moves by three main types of diffusion:

- Gaseous molecular diffusion.
- Steady-state diffusion.
- Non-steady state diffusion.

As figure1.8 shows, gas consists of a large number of individual molecules in rapid motion.

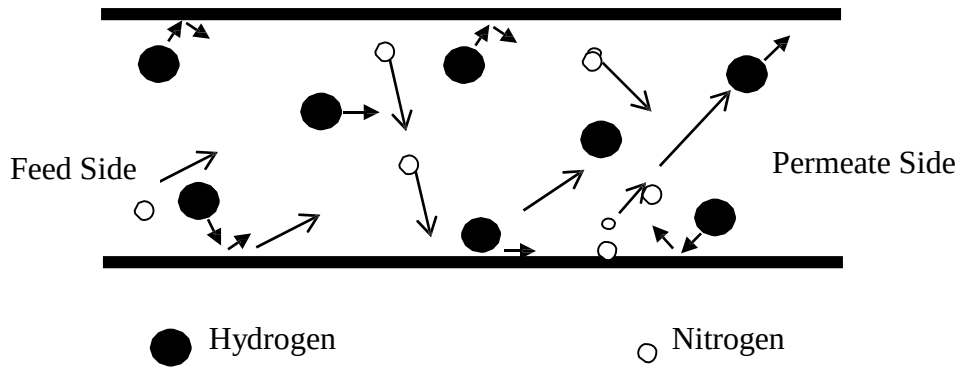

Figure 1.8 Intermolecular momentum transfers.

The molecules move randomly and tend to suffer frequent collisions with one another. The behavior of a molecule upon collision is not definitely known, but approximates to that of a hard elastic sphere. Due to the frequent collisions, molecular velocity is continually changing in both direction and magnitude. Steady-state diffusion may be explained by considering a case of diffusion through a membrane of thickness (δ) and diffusion coefficient (D), whose surface area at x = 0 and retenate δ are maintained at constant concentrations, C1 and C2 respectively. After a steady state is reached, in which the concentration remains constant at all points of the membrane [30] the diffusion equation in one dimension reduces to:

$$\frac{d^2c}{dx^2} = 0 \qquad 1.1$$

Provided that the diffusion coefficient, D is constant, on integrating with respect to x we have:

$$\frac{dc}{dx} = \text{Constant} \qquad 1.2$$

Non steady-state diffusion occurs from the instant diffusion is first admitted to one side of the membrane and prior to the establishment of steady-state. Both flow rate and concentration at any time point of the membrane will then vary with time.

1.6. Gas permeation.

Gas permeation through a micro porous inorganic membrane, as shown in figure 1.9, can be described by one or more of the following mechanisms:

A. Viscous flow (Poisecuille flow).

B. Knudsen flow or “free-molecule diffusion”.

C. Surface adsorption flow.

D. Intermediate flow.

E. Capillary condensation flow.

F. Molecular sieving flow.

A. Viscous flow.

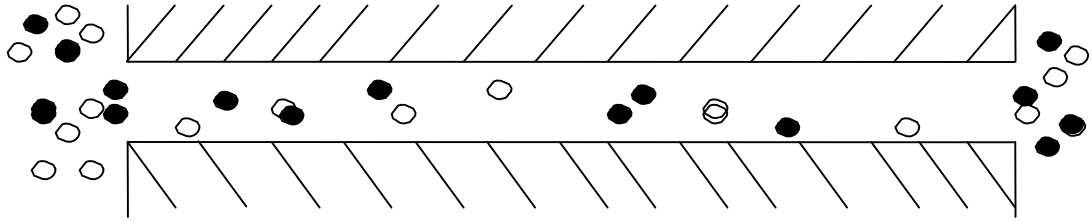

B. Knudsen flow.

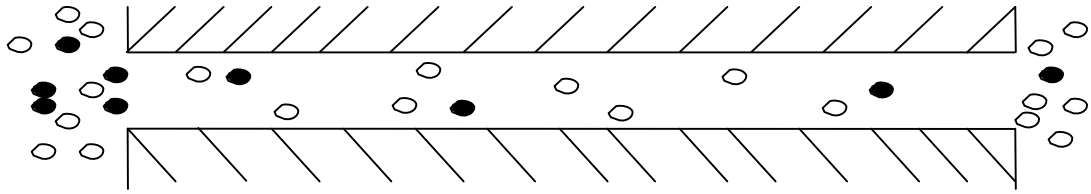

C. Surface adsorption flow.

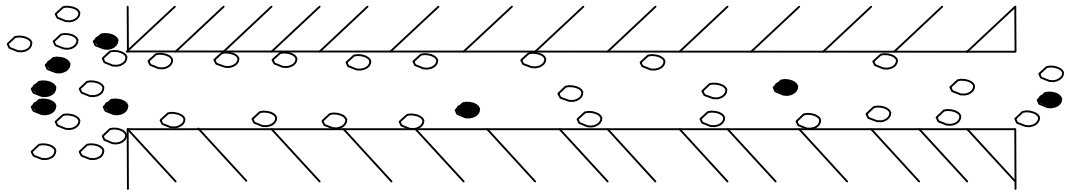

D. Intermediate flow.

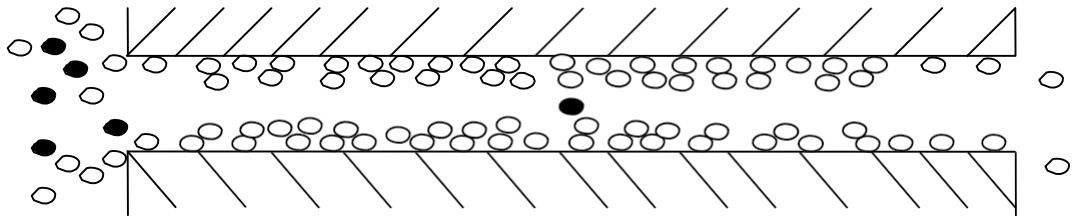

E. Capillary condensation flow.

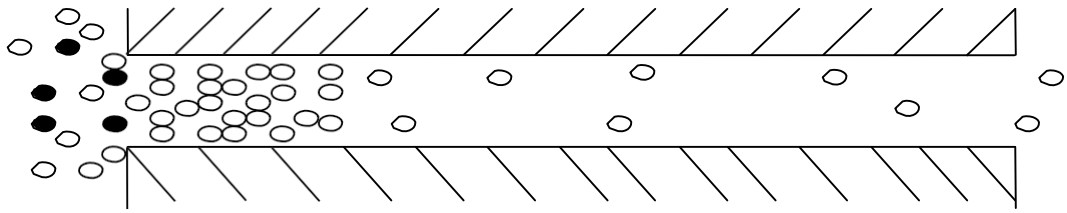

F. Molecular sieving flow.

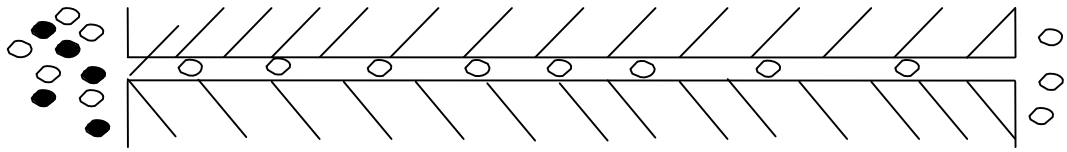

Figure 1.9 Gas permeation mechanisms through a porous media [2].

Figure 1.9A depicts viscous flow, also called Poiseuille flow, in which the gas flow rate is directly proportional to gas pressure and inversely proportional to gas viscosity. This type of flow takes place when the mean pore diameter is larger than the mean free path of the fluid molecules, so that collisions between different molecules are much more frequent than those between molecules and pore walls [7].

As pore size decreases or the mean free path of molecules increases (pressure decreases or temperature rises), the gas molecules collide more with the pore walls than each other and Knudsen flow (1.9B) occurs - the molecules flow almost independently of each other. Surface adsorption flow (1.9C) occurs as gas molecules are adsorbed onto the walls of the porous materials and diffuse on the surface. The mechanism of surface flow is not well understood but it is thought to be an activated type of diffusion, as the surface chemistry of the membrane material significantly affects the flow, and it can be achieved when one permeating species preferentially physisorbs or chemisorbs on the pore walls [8].

When molecule-surface interactions are particularly strong, another flow mechanism exists, which could be regarded as a sort of intermediate flow (1.9D) between surface flow and capillary condensation flow (1.9E). This occurs if one of the gases is a condensable gas and the pressure of the gas is close to its saturation tail allowing it to condense in the pores as a liquid. The choice of membrane material can either enhance or eliminate capillary condensation. Molecular sieving flow (1.9F) takes place whenever the pore diameters are small enough to let only smaller molecules permeate. This occurs with a very small pore size, (i.e. < 10Å) [9], but is a very selective and desirable permeation mechanism.

1.7 Membrane materials.

As an alternative to the classifications mentioned previously, a membrane can simply be defined as an interphase between two bulk phases. It is either a homogenous or heterogeneous collection of phases, and as figure 1.10 shows, depending on the material used, its method of manufacture, and its physical properties, a membrane can be simply classified as organic and inorganic.

The first generation of membranes had found some commercial applications in, for instance, ultra filtration. Those membranes, however, had limited pH, temperature and chlorine tolerance ranges. Moreover, their need to be cleaned to maintain the flux continues to be a major unsolved problem. This motivated the development of a new generation of organic membrane materials that were more resistant to pH, temperature and chlorine. These are now widely used in industry in, for instance, microfiltration (mf) operations. Unfortunately, because of their thermal instability, these membranes are not suitable for high temperature operating environments. This led to a development in material processing techniques and a new class of membranes made from inorganic compounds has emerged. These membranes are formed by deposition of inorganic solutes onto micro porous supports.

In theory, inorganic membranes such as metals, ceramics and glass, should be extremely versatile, since they can be made from various inorganic materials. Further, they should have little or none of the limitations that were associated with polymeric (organic) membranes. Thus, this type of membrane is expected to open up a whole new area of industrial application. They are also limited by two major factors, however, pore structure and permselectivity, as well as by their undesirability for processes that involves very high temperatures and gas separation. Some modification is, therefore, essential to render these membranes suitable for use in many industrial applications under different operating conditions including high temperature and pressure.

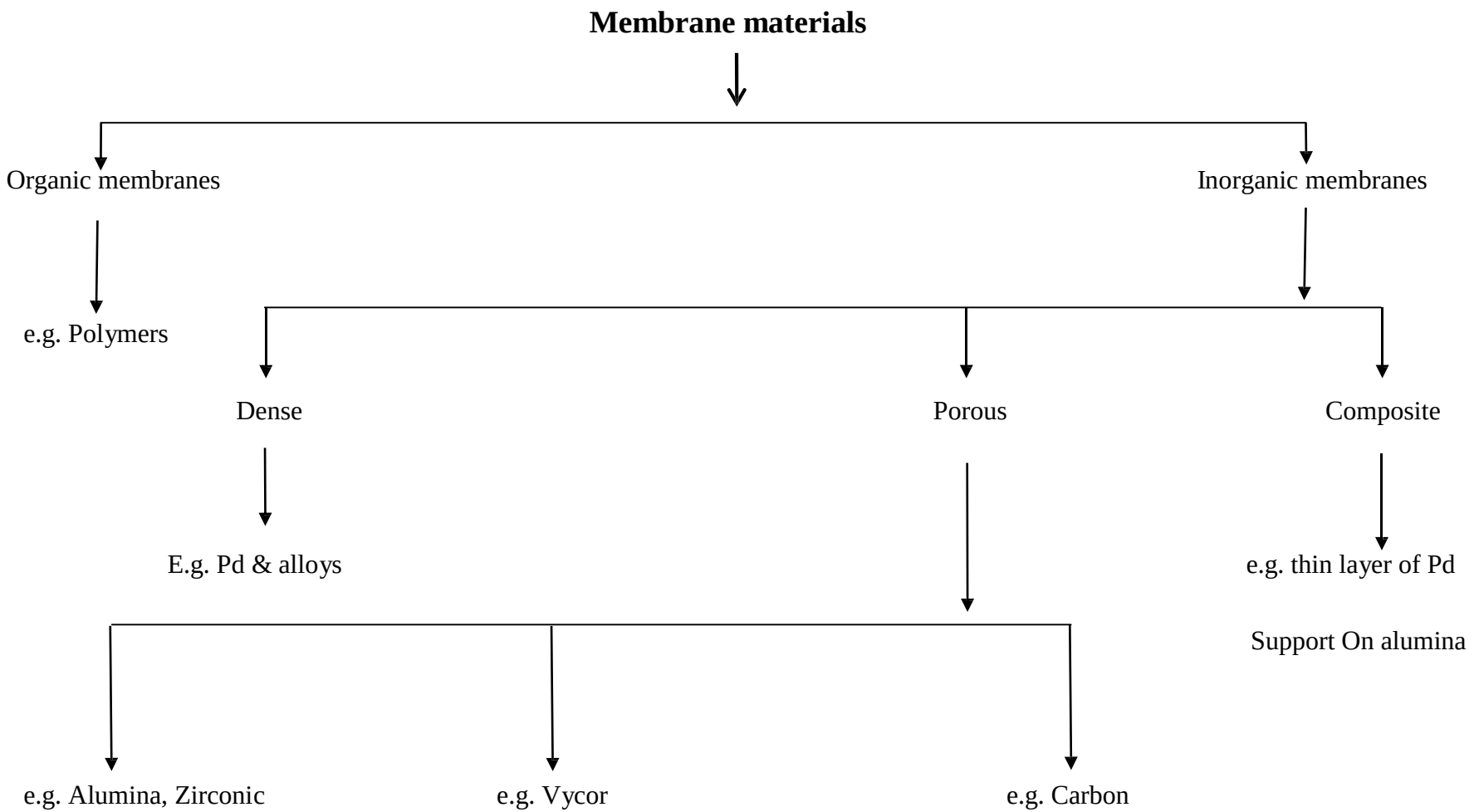

Figure 1.10 Different membrane materials.

1.8 Properties of organic membranes.

Organic membranes:

- cannot withstand harsh conditions, and,
- are restricted to use in the biochemical industry.

1.9 Properties of inorganic membranes.

A better understanding of the properties of membranes, in particular inorganic membranes regardless of whether they are porous or composite, may lead to overcoming many of the challenges and problems associated with their use.

1.9.1 Porous membranes.

Inorganic porous membranes

- can withstand high temperature,
- are less affected by poisoning, and,
- have lower costs than dense membranes.

1.9.2 Composite membranes.

Composite membranes are, in general, an improvement over phase inversion membranes. The composite technique allows the production of a support layer and active (skin) layer from different materials, each selected for optimum function. A thin layer dense membrane deposited on a porous membrane may exhibit the following features:

- High permselectivity.
- Relatively high flux.
- Able to withstand high temperature.
- Lower cost with improvement of implemented techniques.
- High cost due to extensive use of precious metals such as palladium and rhenium used in preparing such membranes.

1.10 Membrane qualities.

Membranes should exhibit some qualities that make them practical for use. These may include:

- High selectivity.
- High permselectivity.
- Mechanical stability.

- Temperature stability.
- Chemical stability.

1.11 General membrane processes considerations.

Membrane processes differ depending on the purpose for which they are used. Thus, before deciding or planning to implement any process there are some general considerations that should be taken into account. These include:

1.11.1 Design considerations.

The design of all membrane systems must be aimed at the ultimate goal of providing a cost effective, robust application technique. Membranes must have very good permeability and permselectivity. They must be compatible with the environment in which they will be used, and they must be mechanically strong enough to be incorporated into permeators without being damaged. They must also be able to withstand the pressure differentials imposed upon them during different operations, but provision should also be made to minimize pressure drops within the reactor housing the membrane.

1.11.2 Economic considerations.

The economic analysis of various membrane processes is intrinsically no different from that of other processes, whether for separation or reaction. However, the cost comparisons involving membranes can be particularly difficult for the following reasons.

a) Membranes do not generally perform under the same conditions or with the same product split as alternative processes.

b) The cost of membrane based processes has been changing due to improved membrane performance and increased competition among various membrane suppliers.

Hence, although membrane systems often offer lower capital maintenance costs than other technologies, the energy requirements will generally be equivalent to or higher than those for other processes. Every implemented membrane process, therefore, has its own economic considerations depending upon the type of membrane used, materials, and operating conditions. For instance, the economic requirements for hydrogen recovery from other gases differ from those of air separation involving various hydrocarbons, and so on. Other membrane applications will no doubt expand as the capabilities of available membranes are improved.

1.12 Membrane reactors.

Membrane reactors may be divided into broad classes according to the area of application.

For many years a number of biochemical processes have used membranes as a means of separation. These include, for instance, immobilisation of enzymes in biochemical reactors, or adding of oxidant gases to a biochemical mass. Examples of such processes include biogas production from wastes, effluent treatment in general and a number of downstream processing operations in biochemical processing. From a reactor point of view, however, the main application is in the area of membrane-fixed enzymes. The second class of membrane reactors is for application in the chemical process industry. This class of reactors, termed catalytic membrane reactors (CMR) because of their incorporation of catalysts, have been the focus of considerable attention since the mid - 1970's [2].

1.13 Reforming reactions.

At present, the cheapest way to produce syngas using a dry reforming process is using natural gas, which is the major feedstock for production of hydrogen via syngas [10]. Natural gas mainly contains CH_4, C_2H_6, C_3H_8 and butane (C_4H_{10}). In contrast, C_3H_8, for instance, is usually easier to deal with since it contains three carbon atoms [11]. reforming to syngas can be achieved using three main reactions:

1) Steam reforming:

$$C_3H_8 + 3H_2O \longleftrightarrow 3CO + 7H_2 \quad \Delta H_{298K} = 498 \text{ kJ/mol} \qquad 1.3$$

2) CO_2 (Dry) Reforming

$$C_3H_8 + 3CO_2 \longleftrightarrow 6CO + 4H_2 \quad \Delta H_{298K} = 621 \text{ kJ/mol} \qquad 1.4$$

3) Partial Oxidation

$$2C_3H_8 + 3O_2 \longleftrightarrow 6CO + 8H_2 \quad \Delta H_{298K} = -455 \text{ kJ/mol} \qquad 1.5$$

Steam reforming has been the most common reaction for syngas production, but recent academic and industrial research has focused on $CO_{2\ dry}$ reforming for environmental reasons [12].

1.14 Dry reforming reactions.

In recent years, CO_2/dry reforming using catalytic membrane reactors (CMRs) has received considerable research interest, and CMRs have become one of the most important areas in new catalytic reaction technology for their potential application in improving the reaction performance. CMRs can also promote reaction conversions, and retain or, to certain extent, avoid side reactions, and hence increase selectivity by

removal of products [13].

1.15 Need for membranes and new catalysts.

Since this reaction is limited thermodynamically and based on LeChatelier's principle, higher temperature or lower pressure is to some extent necessary to achieve high conversion. Furthermore, the high temperature approaches enhance the thermal cracking reaction leading to coke formation and light hydrocarbon production. In fact, reaction temperature depends on the reactor type, apparatus used in the reaction such as the membrane, the operating conditions of the reaction and the type of catalyst. Typically, reaction temperatures between 1073-1173°K (800-900°C) are used for catalytic dry reforming reactions [14], [15]. These extremely high temperatures promote carbon deposition, which can deactivate the catalyst particles in the support [16]. Carbon formation or deposition, however, is the major difficulty related to the CO_2 reforming reaction. The carbon formed quickly deactivates the conventional reforming catalysts via hydrocarbon dehydrogenation and/or CO disproportionation. For this reason many researchers have focused on developing more suitable new catalysts.

1.16 Objectives of this study.

The main aim of this research study was to produce composite membranes made from various catalysts deposited on asymmetric macroporous ceramic supports, which were then used to assess and improve the utilization of CO_2 dry reforming of associated natural gas, namely propane, compared to nickel-zirconium-palladium membrane catalysts. The study concentrated on the following:

a) Designing a membrane reactor (MR) for dry reforming of light alkanes.
b) Selecting suitable modern ceramic supports and examination of their suitability for dry reforming processes.
c) Selecting the most appropriate catalysts available to prepare the membranes and test reactor performance for dry reforming processes.
d) Carrying out a thorough investigation of the performance of the membrane reactor, the catalysts and their appropriateness for dry reforming processes.
e) Characterizing both ceramic fresh supports and the prepared membranes at different stages during use, using the most available techniques.

1.17 Thesis outline.

Chapter two concentrates on the background and a review of the literature on dry reforming, including a brief to definition of natural gas, significance of dry reforming, thermodynamic properties, membrane reactor configuration and membrane catalysis. It

also includes any related literature on associated natural gas dry reforming.

Chapter three explains the experimental work in detail, whilst Chapter four presents the results and discussions. Chapter five discusses, interprets, concludes and suggests recommendations for possible future work.

Appendix 1 shows and explains membrane surface area and volume calculations supported by detailed geometric schematics, and also presents some print outs of the Gas Chromatograph calibration run results.

Appendix 2 shows various result plots for the **H**ybrid **C**eramic **M**embrane HCMC81 and the characterization procedure that was used in this study.

Appendix 3 presents different result plots for **H**ybrid **C**eramic **M**embrane HCMD201 and their characterisation techniques that were used in this study.

Chapter Two

Background and Literature Review

CHAPTER 2: Background and Literature Review

2.1 Sources of associated natural gas.

The term 'associated natural gas' refers to gas that is found associated with most oil reservoirs and coal mines. It consists primarily of CH_4 and is an important fuel source and a major feedstock for many industrial disciplines. However, natural gas itself is often informally referred to simply as gas, especially when compared to other energy sources such as coal and oil. Before natural gas can be used as a fuel, however, it must undergo extensive processing to remove almost all materials other than methane. The by-products of that processing include ethane, propane, butane, pentane and higher molecular weight hydrocarbons, elemental sulfur, and sometimes helium and nitrogen [17].

As mentioned, propane is a by-product of associated natural gas. Processing it via partial oxidation with CO_2 to produce C_3H_6 is important for utilization of carbon resources and environmental protection. C_3H_6 is the second largest petrochemical commodity available. It is used in the production of poly- C_3H_6, acrylonitrile, acrylic acid, acrolein, C_3H_6 oxide and glycols, plasticizer oxo alcohols, cumene, isopropyl alcohol, and acetone. Poly- C_3H_6 produced from C_3H_6 is in great demand for the production of day to day products such as packaging materials and outdoor clothing [18].

Successful application of membrane technology in process industries demands the development of mechanically, thermally and chemically stable composite membranes of high selectivity and permeability for the purpose of producing the desired components. Over the past few decades, researchers have worked to develop such membranes and the first objective of this thesis was to develop composite membranes of superior quality for dry reforming of propane. A number of membranes were considered and subsequent modifications of the membrane preparation procedures are proposed.

Most investigators working on propane dehydrogenation membrane catalysis have performed membrane catalysis by placing the catalyst as pellets in the bore of the tube and coating the membrane support from the outside. Such a design works very well for building a membrane reactor in a research laboratory as it is easy to place the catalyst in a tube. Almost all reaction engineering technologies, however, adapt the usage of jacketed heat transfer through the shell side. The jacket is usually coiled around the shell

of the membrane reactor, and, for the reaction to take place, heat reaches the tube only after crossing over various resistances such as steel, gas film resistance on the shell side and resistance in the composite support. It is easy to conclude that the presence of the gas film on the shell side, as well as in the support, would seriously decrease the value of the overall heat transfer coefficient of the tube. This means that very high temperatures need to be maintained in the shell in order to provide good heating for the reaction to occur in the tube. Placing the catalyst on the shell side would offer more catalyst weight per unit surface area of the membrane support, due to the tube shell side having more surface area than the tube side. A membrane reactor packed with catalyst in the shell side is characterized by a higher reactor volume and higher heat flux. By placing the catalyst in the shell side the reactor behaviour more closely follows the isothermal path, which is the optimal state for endothermic reactions. In addition, control of the reaction conditions is easier when the catalyst is packed into the shell space.

The second objective of this work is to develop a membrane reactor that can be used for catalytic studies considering the aspect of heat transfer.

2.2 Dry reforming reaction of propane.

As discussed, the dry reforming process of associated natural gas can be used for producing syngas, as shown in equation 2.1.

$$CnHm + nCO_2 = 2nCO + (m/2)\ H_2 \qquad 2.1$$

It has recently received quite remarkable attention since operating costs are nearly 20% less than for any other available process [39]. The dry reforming process, however, is thought to be a highly endothermic reaction that favours high temperature, usually between 1073-1173^{o}K (800-900^{o}C). Two boundaries, therefore, need to be taken into account: thermodynamics and kinetics. Thermodynamic calculations for carbon deposition reactions show that in the case of methane, decomposition is a dictating carbon source at temperatures above 973.23^{o}K/700^{o}C. This is known as the reserve Boudoir reaction - a redox reaction with a chemical equilibrium mixture of CO, and (CO_2) at a given temperature. This is a dictating carbon source at lower temperatures due to the fact that the reaction is originally at equilibrium [14]. But from a kinetic point of view, this occurs when the CH_4 decomposes into carbon rather than reacting with CO_2 [10].

2.2.1 Thermodynamics properties.

The thermodynamic properties presented here, and mentioned elsewhere in this thesis, is either calculated based on the value presented by Perry's Chemical Engineers' [19] or based on Hardiman and Mohammed [20]. The relationship between temperature (T) and standard Gibbs free energy (G), that is associated with propane dry reforming and some of the side reactions, are presented in Table 2.1, where ΔG is in kJ/mol and T is in K. It is quite clear that the dry reforming reaction is limited thermodynamically.

Table 2.1 Thermodynamic properties for dry reforming of propane and some other related reactions.

Reaction	AG (T)	Units
$C_3H_8+3CO_2 \rightleftharpoons 6CO + 4H_2$	AG (T) = $623*10^3$ - 796 T	kJ/mol
$C_3H_8 \rightleftharpoons CH_4 + 2C(s) + 2H_2$	AG (T) = $20*10^3$ - 155 T	kJ/mol
$2CO \rightleftharpoons C + CO_2$	AG (T) = $-167*10^3$ + 164 T	kJ/mol
$CO + H_2O \rightleftharpoons CO_2 + H_2$	AG (T) = -40*103 + 45 T	kJ/mol

2.2.2 Related reactions.

One of the reactions that take place concurrently with dry reforming is the reverse water-gas shift reaction (RWGS) equation 2.2.

$$CO + H_2O = CO_2 + H_2 \quad (2.2)$$

The dry reforming reaction is influenced by the RWGS reaction, since the products of the former contribute to the latter. This causes the products ratio in the dry reforming reaction to be lower than the stoichiometric ratio. Other side reactions that might take place in such cases are the propane decomposition equation 2.3 and the carbon deposition reactions of CO disproportionation or the Boudouard reaction equation 2.4.

$$C_3H_8 = CH_4 + 2C_{(s)} + 2H_2 \quad (2.3)$$

$$2CO \rightleftharpoons C + CO_2 \quad (2.4)$$

It is quite clear from Table 2.1 that whilst propane decomposition is an endothermic reaction, the other two side reactions are exothermic. This implies that lower temperature is favourable to obtain higher conversion. At higher temperatures, methanation reactions are unlikely to occur in the forward direction because it seems that they are endothermic reactions.

2.3 Significance of dry reforming.

The global warming phenomenon has motivated researchers to investigate the area of greenhouse gases through the reforming of natural gas and associated natural gases and light hydrocarbons. Dry reforming was first discovered in 1928 by Fischer who studied it using a number of catalysts, but because of severe catalyst deactivation, the research efforts in this field switched to steam reforming. The steam reforming process, where steam reacts and reforms with light hydrocarbons, has several restrictions, including high-energy consumption [21], poor selectivity for CO, and the provisions of a high H_2/CO ratio, i.e. equal to 3, which is unsuitable for methanol and Fisher-Troposh syntheses [22]. On the other hand, reforming using CO_2 instead of steam in producing synthetic gas has gained attention for many reasons [23], [24] and [25]. These include:

- CO_2 is found in considerable amounts in most natural gas fields.
- Dry reforming operation costs are said to be 20% lower than any other reforming processes.
- The capability of CO_2 in chemical energy transmission systems has been studied and found to be useful (e.g. Calleor process and SPARG process).
- The reaction has environmental implications since CO_2 and natural gas, which are greenhouse gases, can be consumed in a useful manner.
- It has the ability to produce a lower syngas ratio (H_2/CO) compared to that produced using steam reforming.

2.4 Hydrocarbon dehydrogenation.

Alkenes are important because they are being increasingly used as industrial intermediates for the manufacture of other chemicals. Industrially, alkenes are mainly produced by the fluid catalytic cracking process or as a by-product from pyrolysis or the

cracking process in refinery furnaces. Existing technological and economic constraints in petrochemical refineries suggest the production of unsaturated hydrocarbons from saturated ones, since the saturated hydrocarbons are of less value than the unsaturated ones. The basic problem of alkane dehydrogenation is that the reaction is thermodynamically limited and reaches an equilibrium conversion. Furthermore, the formation of coke on the surface of the catalyst used to facilitate the reaction hinders the long-term reactivity of the catalyst. Alkane dehydrogenation research has been undertaken from the early 1930s [22].

2.5 Propane dehydrogenation.

Propane dehydrogenation is one of the most important reactions in alkane dehydrogenation schemes. C_3H_6 is a valuable commodity chemical for the production of isopropyl alcohol, an important gasoline blending component, and as a polymer grade chemical [26].

Propane dehydrogenation is expressed as the following reaction:

$$C_3H_8 \longleftrightarrow C_3H_6 + H_2 \qquad 2.5$$

The heat of reaction for propane dehydrogenation at 550^{o}C is 130 KJ/mol and hence the reaction is endothermic. The equilibrium conversion at atmospheric pressure is limited to about 18% at 500 ^{o}C and 50% at 600 ^{o}C, as shown in figure 2.1.

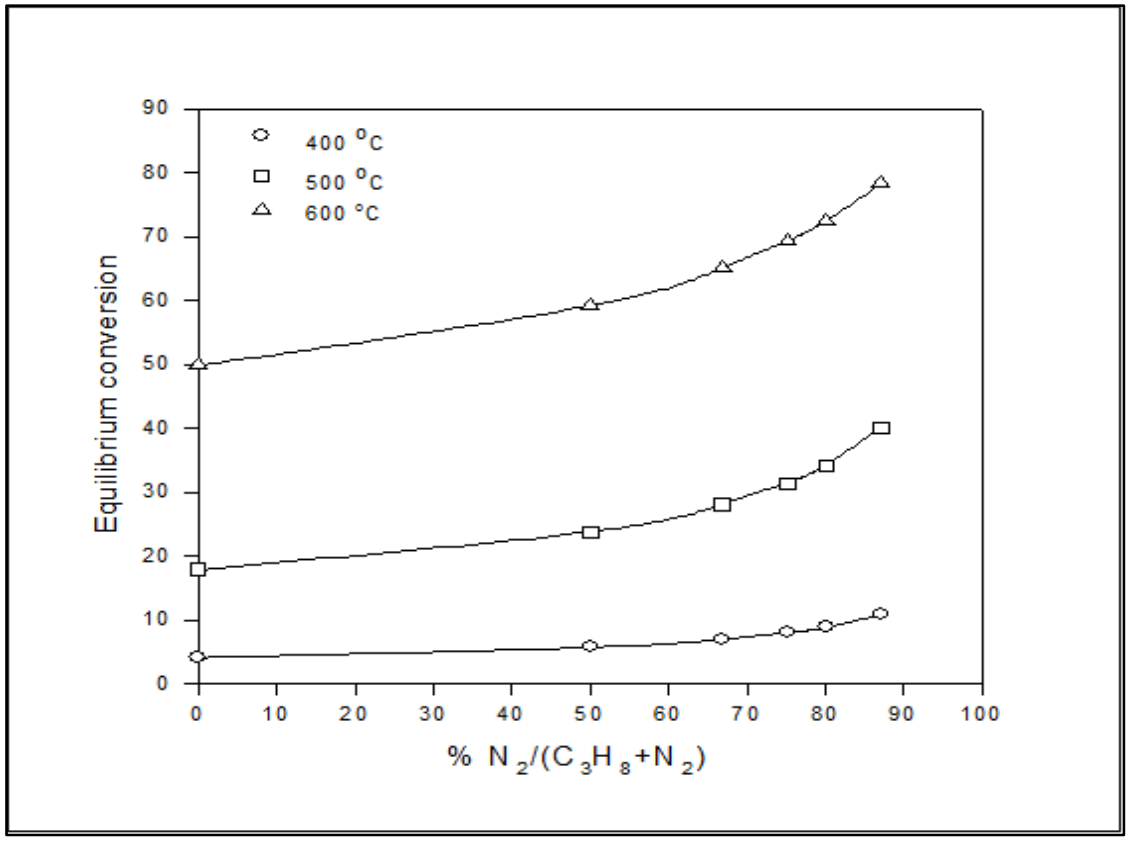

Figure 2.1 Equilibrium conversions of propane and CO_2 as a function of inert composition in the feed [27].

Commercially, propane dehydrogenation is performed using three different catalysts. The most predominant and significant catalyst is 0.5 wt% platinum on alumina pellets. Other catalysts such as palladium deposited on alumina, are also used. Certain operating conditions have been considered to obtain relevant information regarding the reaction. Figure 2.1 summarizes the effect of dilution on the equilibrium conversion at various temperatures [27]. As seen in the graph, the equilibrium conversion increases significantly at higher temperatures (about 600^{o}C). The impact of dilution is not significant at low temperatures (about 400^{o}C). It can be concluded, therefore, that higher conversions can be achieved with a high dilution of propane in the reactor. Dilution can entail additional heat in terms of the heated dilutant feed (nitrogen), but dilution is not a major advantage in operating the reactor. The main factor is that the higher flow rates of the reactor would demand a higher reactor volume to achieve equilibrium conversion. Further, the separation of products along with the dilutant is a major limitation for the utilization of a dilutant.

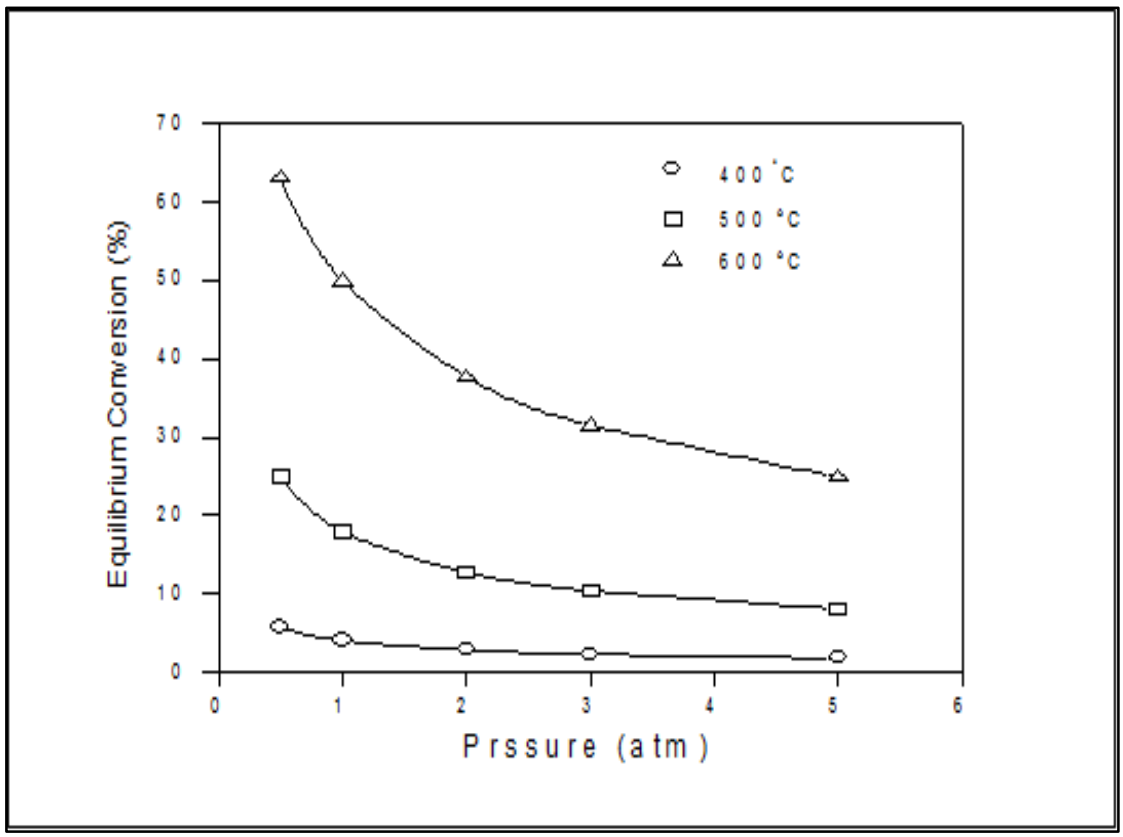

Figure 2.2 Equilibrium conversions of propane CO_2 as a function of pressure [27].

Figure 2.2 presents the variation of equilibrium conversion with respect to the pressure of the system for pure propane dehydrogenation. As shown, the equilibrium conversion decreases significantly at lower temperatures and higher pressures. At low temperatures, pressure variation does not have a significant effect. The effect of pressure on equilibrium conversion is due to the fact that since the propane dehydrogenation reaction produces two reactant molecules for one molecule of propane reacted, any increase in the pressure of the system would have an adverse effect on conversion.

2.6. Reactors

In general, a reactor is simply defined as any device, system or tool that supports a certain process. This could be, for instance, a catalytic chemical reaction process or a separation process that transforms initial compounds to products according to a specific design and modification which helps to contain and house given materials to produce the desired products depending on the process that it has been designed for. In the **I**nternational **U**nion of **P**ure **A**pplied **C**hemistry [IUPAC] definition, a membrane reactor is a device that may combine a separation process with a chemical reaction in one unit [1]. A membrane technology thus finds an application in two areas, namely separation and chemical or

biological reactions, and at times combines the two unit operations in one apparatus. In CO_2 reforming of light hydrocarbons, membrane reactors are used.

2.6.1 Membrane reactors.

Membrane reactors have been used for a number of years and may be classified into many different types according, for example, application, design, and the purpose for which they are being used. Before going into the details of such reactors, it is worth starting with a simple definition of a chemical reactor. A chemical reactor is any device, equipment or system that supports, contains or controls any chemical reaction. Some possible configurations of porous membrane reactors are listed in table 2.2 [28]. Pore-flow through (PFT) catalytic membrane reactors seek to utilize the advantage offered by co-feeding the reactants, which is basically the improvement of the gas-solid contact, leading to improvement in both conversion and selectivity.

Table 2. 2 Possible configurations of porous membrane reactors [28].

Configuration	Advantages sought	Types of membrane
A: Inert membrane reactor (IMR) - permeation of products	Increased reaction yield by equilibrium displacement.	(i) Selective. Thin metallic layers (e.g. Pd or Ag-based alloys on ceramic substrates). (ii) Nonselective,Porous membranes:silica,alumina, titania, glass, etc
B: Permeation of products plus reaction coupling.	As above, although higher yields could be expected due to the thermal/chemical coupling of reactions.	As above
C: IMR- distribution of reactants	Increased selectivity through control of the concentration of selected species along the reactor. Increased reactor safety.	Meso - or microporous membranes.
D: Catalytic membrane reactor (CMR)- Mobile and active lattice oxygen.	Control of oxygen distribution in the reactor. In principle, it is possible to avoid the presence of gas phase oxygen.	(i) Thin layer of Ag-based alloys on top of porous ceramic membranes. (ii) Thin layers of dense oxide on top of porous ceramic membranes.
E: CMR- Segregation of reactants on both sides of the membrane.	Confinement of reaction to a finite thickness zone inside the membrane. Reaction slip is avoided. Improved safety.	Porous catalytic membranes.
F: Inert/catalytic composite membrane.	Control of concentration of a reactant by means of mass transfer resistance in the IMR zone.	Composite membranes: inert (diffusion) zone plus catalytically active zone.
G: CMR-Segregation of liquid and gaseous reactants.	Improved mass transfer in G-L-S reactions.	Porous catalytic membranes.
H: CMR- Joint permeation of reactants.	Improved G-S contact, higher conversions.	Porous catalytic membranes.

2.7 Membrane reactor classifications.

Membrane reactors have received substantial interest from various research groups and the number and variety of applications has continually grown. Different classifications have been tentatively proposed, one of which is based on the area of application.

2.7.1 Separation membrane reactors.

For many years, a number of biochemical processes have used membranes as a means of gas separation, for immobilization of enzymes in biochemical reactors or as a means of adding oxidant gases to a biochemical mass. Examples of such processes may include biogas production from wastes, effluent treatment in general and a number of downstream processing operations in biochemical processing. There are also several other types of separation membrane reactors such as those used for water treatment processes [2].

2.7.2 Catalytic Membrane Reactor (CMR).

This membrane acts as a catalyst and a diffusing element to facilitate simultaneous mass transfer and reactions as shown in figure 2.3A. These types of reactors are designed for application in the chemical process industry. These classes of reactors are termed catalytic membrane reactors because of the incorporation of a catalyst, and have been the focus of considerable attention since the mid-1970s. A number of commercially important reactions can be enhanced by incorporating a membrane in the reactor which would continuously and selectively remove one or more of the products of reaction. This would then drive the reaction towards increased conversion. There are two distinct benefits which arise from the incorporation of a membrane into the reaction system. The main applications, which are still the major areas of interest, are:

i. Removing one or more products from the reaction system,
ii. Influencing the path of a chemical reaction by changing the reaction selectivity.

A good example of the first kind is the dehydrogenation reaction, where removal of the hydrogen product increases the conversion of the reactant. A good simple example of the second type occurs in many oxidation processes. From the processing viewpoint, a major advantage of membrane reactors is that both the reaction and separation stage can [2].

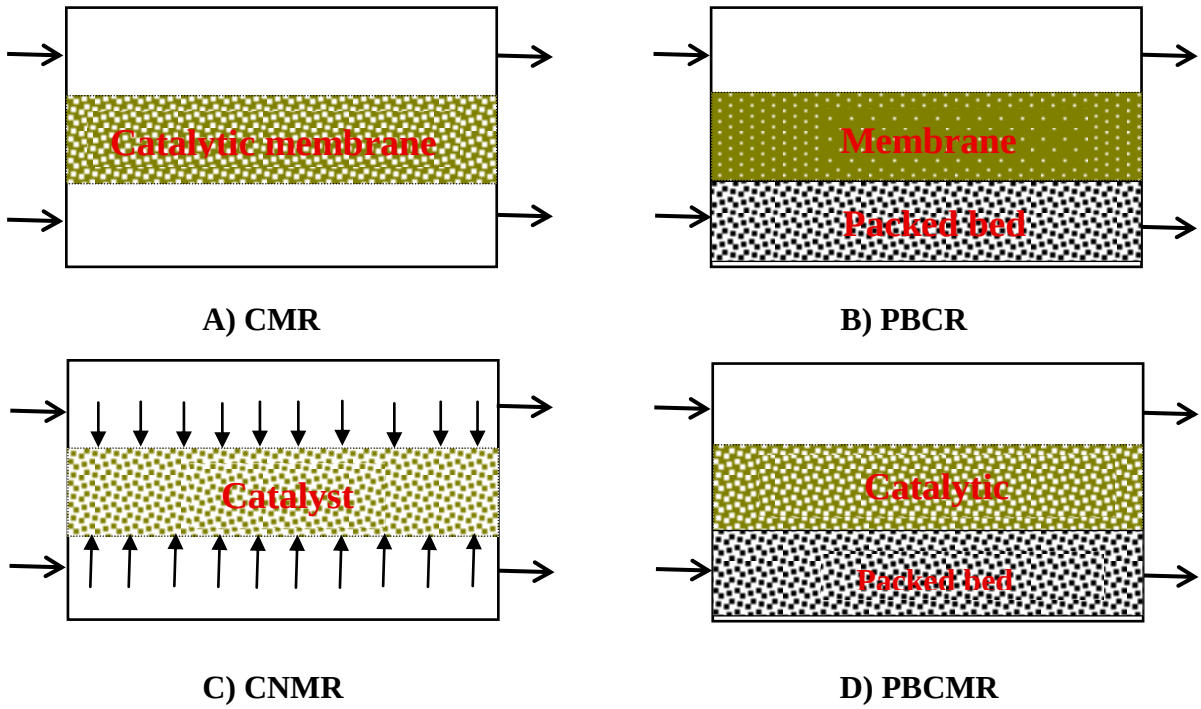

Figure 2.3 Classifications of membrane rectors.

2.7.3 Packed Bed Catalytic Reactor (PBCR).

This membrane acts as a diffusing element and the reaction takes place on a catalyst bed. Such a configuration is significant for dehydrogenation reactions, as shown in figure 2.3B.

2.7.4 Catalytic Non-permselective Membrane Reactor (CNMR).

This membrane acts a catalyst and is non-permselective to the components fed to the system, as shown in figure 2.3C.

2.7.5 Packed Bed Catalytic Membrane Reactor (PBCMR).

This membrane acts as a catalyst and a diffusing element. In addition to the catalytic membrane, a packed bed catalyst, as shown in figure 2.3D, is used to significantly increase the reaction rates.

Academic research using membrane reactors has been directed towards various equilibrium-limited reaction schemes, including the dehydrogenation of C_2H_6, C_3H_8, cyclohexane,

ethylbenzene, hydrogen sulphide decomposition, water-gas shift and steam reforming of CH_4.

The different membranes investigated to date include various composite membranes that are permselective to hydrogen, as hydrogen is one of the key components that needs to be removed for the above mentioned reactions. Since almost all the reactions take place at high temperatures, inorganic membranes perform very well due to their thermal and chemical stability.

Furthermore, research emphasis has been placed on the development of inorganic composite membranes rather than monolithic inorganic membranes, as the former provide very good performance at low cost. Composite membrane preparation has been studied on various supports such as alumina, steel and vycor glass [29]. Deposited thin films include silica, palladium [27] and various palladium alloys such as palladium-silver and palladium-copper [30].

2.7.6 Fixed-bed reactors.

This type of reactors limits intra-particle mass transfer, which of course leads to lowering syngas yield and increasing carbon deposition, yet they are widely used by most research groups compared to fluidized reactors. This may be due to their simplicity of design as well as availability.

2.7.7 Fluidized reactors.

One of the most important advantages of this type of reactors over the fixed bed reactor is that safety is quite high, especially at high temperature and pressure. This is due to continuous catalyst circulation, which of course leads to smoothing of the temperature gradient. Moreover, using a fluid bed reactor (fluidized reactor) means that very fine catalyst particles can be used without the problem of pressure drop, and this means there is a greater active surface area and lower carbon deposition [14].

2.8 Comparison of performance of reaction and mass transport in multiphase reactions between catalytic and fixed-bed reactors.

Mass transfer phenomena play an important role in heterogeneous catalyzed, multiple phase reactions. Dependent on the chosen process parameters, mass transfer can even be the rate determining step. The following mass transfer and reaction steps have to be considered:

1. Mass transfer of the gaseous reactant from the free gas phase into the gas-film interface;

2. Mass transfer by diffusion of the gaseous reactant in the bulk of the gas film;
3. Diffusion of the gaseous reactant through the gas-solid-interface to the catalyst;
4. Diffusion of the reactants within the pores of the catalyst to the active sites-pore diffusion;
5. Adsorption o f the dissolved reactants at the catalytic active surface-Chemisorption;
6. Chemical reaction at the catalyst surface;
7. Desorption of the product;
8. Diffusion of the product out of the pores to the external surface of the catalyst particle and
9. Diffusion of the product through the external gas interface into the bulk of the gas stream.

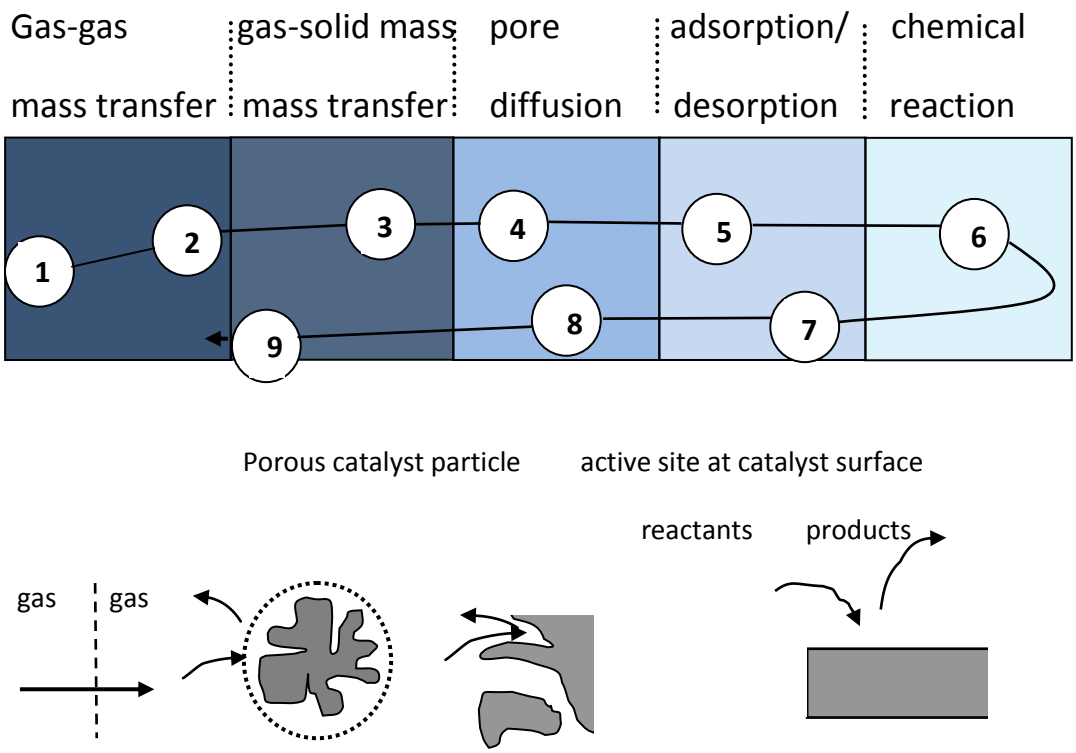

Figure 2.4 Steps in heterogeneous catalyzed, three-phase reaction at a porous catalyst.

Two main problems for reactions in conventional reactor systems become obvious: internal pore diffusion limitations when the catalyst particles in fixed bed reactors are too large (however necessary in order to handle pressure drops) and the difficulty in separating the catalyst from the product when the catalyst particles are too small, which is the case in fixed-bed reactors, as shown in figure 2.4. The motivation for finding a new reactor concept that

solves both problems led to the development of a membrane reactor concept. Numerous types of membrane reactors have been proposed in recent years. Most of them couple a catalytic conversion with a separation effect provided by the integrated membrane. High conversion can, for example, be achieved for equilibrium- restricted reactions if the reaction product is removed from the reaction mixture through a permselective membrane. Additionally, in some catalytic reactions the control of selectivity can be improved in membrane reactors.

The membrane reactor investigated in this work for catalytic reactions operated in pore flow through mode, using a porous membrane that had no separating functions but acted as a support for the catalyst. The catalyst was immobilized as nanoparticles in the membrane pore structure. The premixed reactant fed gases (i.e. C_3H_8 + CO_2) were fed to the actual membrane reactor. The reactants passed through the pores of the membrane where the reaction took place due to contact with the catalysts that were impregnated on the ceramic support. In this way, the membrane worked as a contact zone for the reactants and the catalyst. Because of fast convective flow, internal diffusion limitations were reduced as the products were immediately removed from the membrane pore, which avoided product accumulation within the membrane. As a consequence, the effective reaction rate is not influenced by mass transfer limitations and the selectivity for the desired product can be increased. The latter is particularly important for consecutive reactions figure 2.5 compares the course of a consecutive reaction in a fixed-bed reactor with porous catalyst pellets and in a pore-flow-through membrane reactor. In the pores of the spherical catalyst pellets in the fixed bed reactor, the residence time of the reactants and the product is increased because of internal diffusion limitation. This results in a concentration profile of the reactants in the pores of the catalyst pellet. The concentrations of the reactants **A** and **B** decrease from the shell to the core of the pellet if a fast reaction occurs. With increasing concentration of the product **C** the consecutive reaction to the side product **D** begins. By this, the selectivity of **C** decreases. In the membrane reactor, the reactants and the product are forced through the pores. The residence time in the membrane pores is short which suppresses the consecutive reaction.

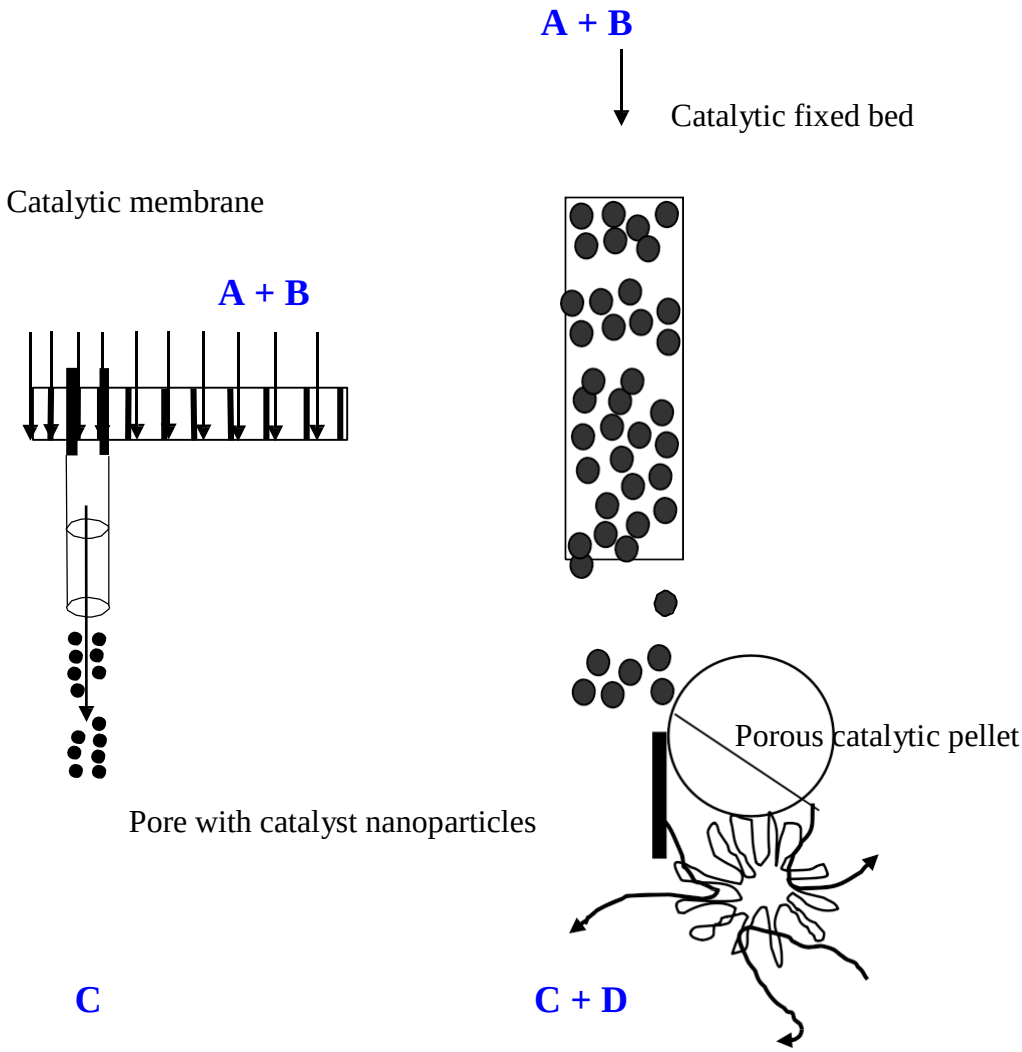

Figure 2.5 Schematic of catalytic consecutive reaction in Pore-Flow-Through (PFT) membrane and fixed-bed reactor.

In this way, the forced-through flow concept of membrane reactors has many advantages compared to fixed-bed and slurry reactors:

- Pore diffusion can be reduced.
- No catalyst separation from the product is necessary.
- Good catalyst accessibility (i.e. less catalyst metal is necessary).

However, some drawbacks have to be thoroughly considered:

- The recycling of large reactant streams is necessary on the expense of energy.
- The development of a new reactor design.
- The pressure drop at the membrane increases with increasing flow velocity and decreasing pore diameter.
- The possibility of pore blocking.

If the benefits of the Pore-Flow-Through (PFT) membrane reactor, such as higher reaction rates, improved selectivity and better product quality, can compensate for these disadvantages, it offers interesting perspectives for an industrial application.

2.8.1 Flow-through Catalytic Membrane Reactor (CMR).

The term "flow-through catalytic membrane reactor" describes a reactor concept for heterogeneous reactions, where the catalyst is immobilized in the pores of a mostly ceramic membrane, which is convectively passed by the reaction mixture. The porous membrane does not perform any separative tasks and is solely used as a microstructured catalyst support. This type of reactor allows for high catalytic activity due to intensive contact between reactants and catalyst and potentially for a narrow residence time distribution [31], [32], [33].

In this research study, however, the catalytic membrane reactor is operated in the forced pore-flow-through (PFT) mode in which the membrane is porous and intrinsically active, having had a catalyst deposited within the pores. The membrane geometry allows for a degree of control of contact time. It is operated in the cross-section mode, in which a mixed stream of all the reactant is forced to flow through the membrane in order to provide a reaction space time with short controlled residence time and high catalytic activity by feeding it to one side of the membrane reactor (i.e. shell side) with a closed exit, as shown in figure 2.6. This configuration gives a uniform time, which can be tailored to a particular reaction by choice of membrane thickness and/or reactant flow rate. The pore size of the membrane controls the diffusion regime. The membrane geometry can also play a role in placing a catalyst in the membrane optimally, or in controlling the partial pressure of the reactant in the phase in contact with the catalyst.

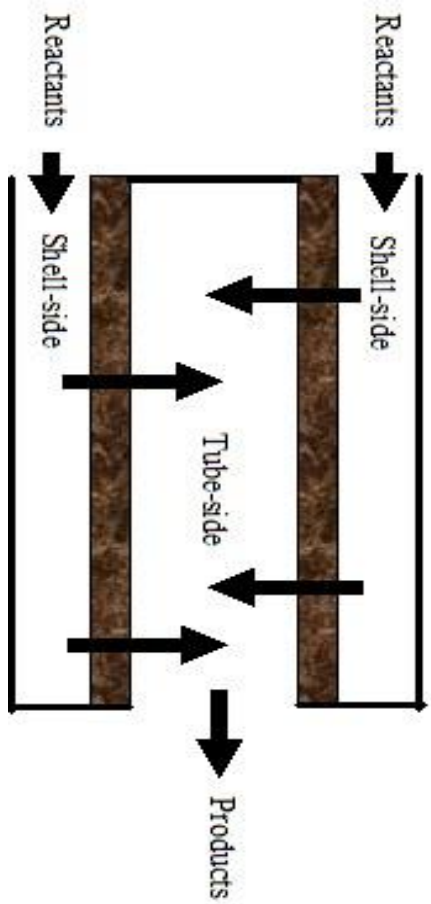

Figure 2.6 Schematic of a catalytic membrane reactor operated in forced pore-flow through mode.

2.9 Applications of membrane reactors.

As mentioned previously, most applications of catalytic reactors have concentrated on minimizing the thermodynamic constraints of equilibrium-limited reactions by removal of reaction products through the membrane and hence enhancing the overall yield. The other main application to date has been the controlled addition of one reactant to another reactant stream. The classic application of the latter approach is in hydrocarbon oxidation reactions where, for example, a hydrocarbon stream can be fed through the tube side of the membrane while the oxidising gas is allowed to permeate from the shell side [23]. In this study, the two reactant gases, namely CO_2 and C_3H_8, were premixed and introduced into the membrane reactor via the shell side, whilst the products were collected from the tube side.

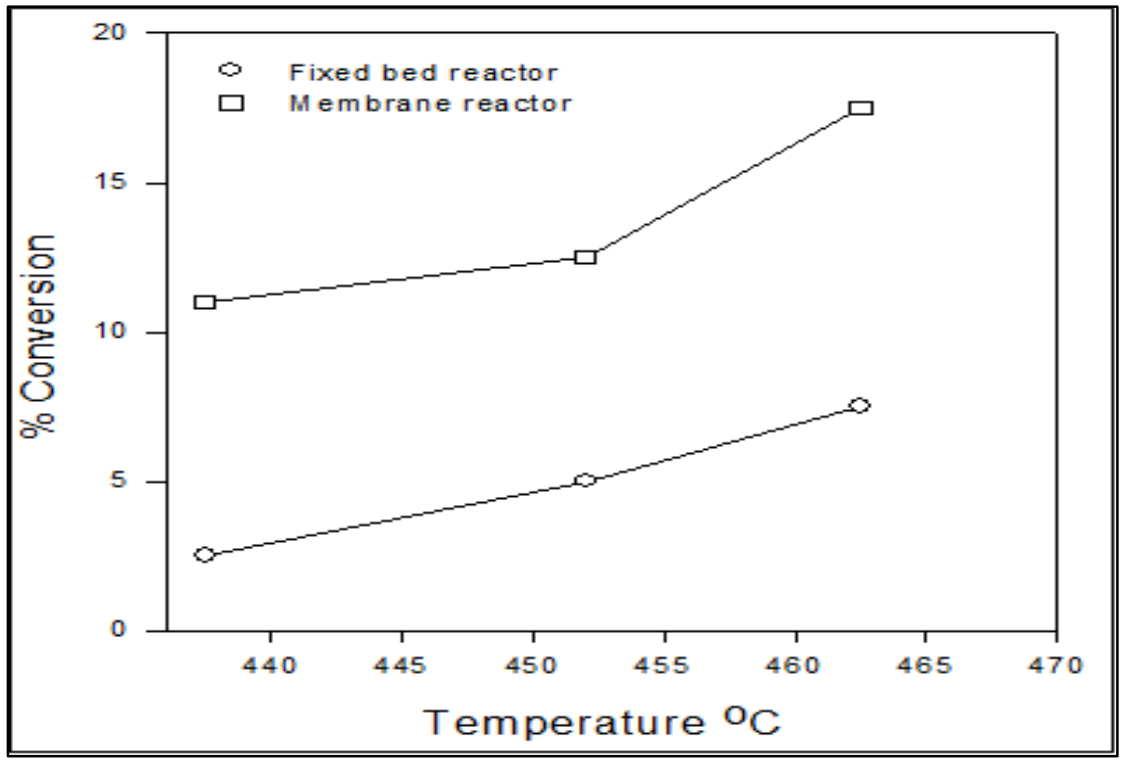

Figure 2.7 Comparison of fixed bed reactor and membrane reactor performance [27].

Yildirim *et.al.* [27] Suggested that a significant improvement in conversion could be achieved using a membrane reactor configuration instead of a fixed bed conventional reactor configuration. Data presented by the authors is illustrated in figure 2.7.

2.10 Conversion enhancement using a membrane reactor.

As explained in the previous section, the conversion of a conventional catalytic reactor for propane dehydrogenation is limited. The equilibrium conversion can be increased predominantly at higher temperature (50% at 600^{o}C compared to 18% at 500^{o}C), but the formation of coke at the higher temperatures drastically reduces the activity of the catalyst. Utilization of a membrane reactor has thus been proposed to overcome this limitation. In a membrane reactor, one of the components (hydrogen in this case) is preferentially removed from the reactor chamber to shift the equilibrium towards the product side. The preferential removal of hydrogen from the reactor is carried out using a membrane. Various membrane reactor configurations have been presented in general in literature [27] and some of them can be classified as described as shown in figure 2.3 earlier.

2.11 Membrane reactors configurations.

The membrane may be coupled with the catalyst in a number of ways. In the simplest

form, the membrane is situated downstream from a catalyst bed and serves essentially to separate the product streams arising from the reaction. More usually in a CMR, the membrane separates the feed and permeates streams in the reactor. The main variation in these systems is the location of the catalytic component. Three basic geometries may be employed and are illustrated in figure 2.8. In figure 2.8A, the membrane is coupled with a conventional pelleted catalyst and the membrane forming the inner wall of the tubular reactor figure 2.8 B. Shows the active catalyst as a thin but dense membrane layer deposited on the surface of a porous support. A potential problem related with this configuration is that the membrane may not have sufficient catalytic area to be totally effective. Figure 2.8C shows a catalyst impregnated into the pores of a microporous material, either as individual particles or as a layer. This geometry is probably one of the easiest to obtain, and is a convenient way of introducing a catalyst into the membrane [2].

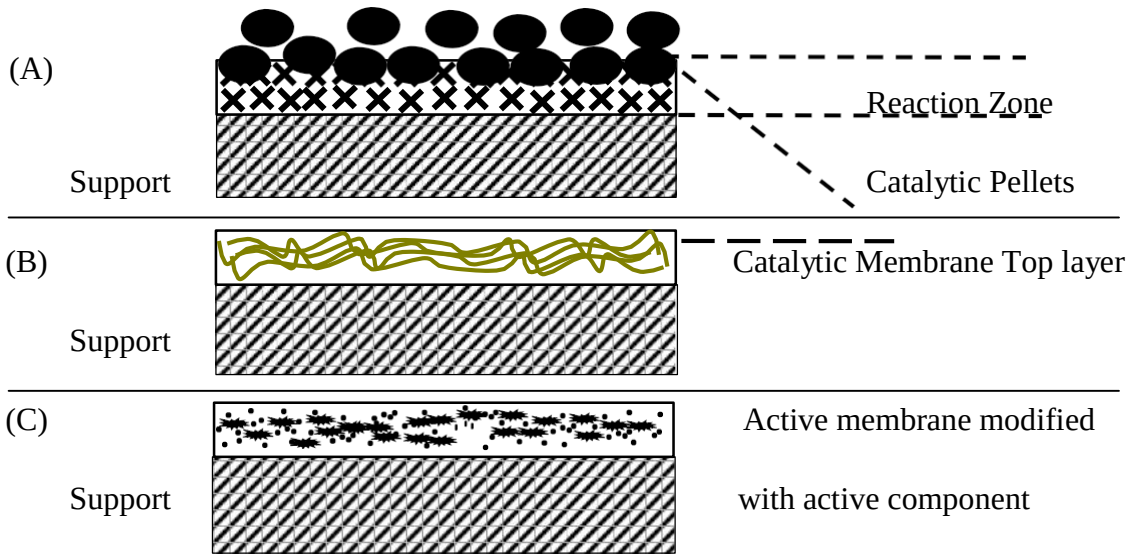

Figure 2. 8 Different membrane/catalyst combination, (a) The catalyst is packed next to the membrane, (b) the membrane is inherently catalytic (c) the membrane is modified with catalytically active components.

2.12 Catalysis and membrane catalysis.

Propane dehydrogenation catalysis and membrane catalysis have been investigated by a number of authors. Bitter *et.al.* [34] Used chromia (Cr_2O_3) on alumina (Al_2O_3) pellets as the catalyst bed at 848^{o}K/575^{o}C for propane dehydrogenation studies. A conversion of 59% and a selectivity of 90% were achieved with pre- and post-dehydrogenation zones installed to convert extra residual propane to C_3H_6. Ziaka *et.al.* [26] Obtained similar results with a Pt-Mg-Al_2O_3 catalyst for the temperature range 793-873^{o}K/520-600^{o}C. Other types of commercially available membranes, such as silicalite-alumina, γ-alumina and Pd-Ag membranes, have been used for membrane catalysis. Sheitntuch *et.al.* [35] Carried out catalytic studies using an alumina-supported platinum catalyst for both palladium-ruthenium and palladium-silver alloy membrane tubes. A C_3H_6 yield of 70% was obtained for the palladium-ruthenium tube at 823^{o}K compared to the equilibrium yield of 32%. It was suggested that the yield of C_3H_6 was limited because of deactivation of the catalyst due to the low hydrogen pressure on the reaction side. Weyten *et.al*. [36] Investigated propane dehydrogenation using a hydrogen-selective silica membrane with a chromia-alumina catalyst. The C_3H_6 yield was reported to be at least two times higher than the value obtained in an equilibrium limited membrane reactor. Yildirim *et.al.* [27] Considered two membrane categories and three types of composite membrane systems (Pd/Ag, silica and Pd- dispersed porous) for propane dehydrogenation. The results indicated that the dense Pd- Ag composite membrane can provide higher conversions than the other systems. The dispersed porous system was also reported to provide significant application due to its higher surface to volume ratio.

2.13 Related literature.

Bitter *et.al.* [37] Published a US patent for propane dehydrogenation membrane reactor catalysis. The process, according to this invention, can be carried out as steam to hydrogen containing propane. Molar steam to hydrogen was specified in the range from 5 to 13, temperature in the range from 673^{o}K/400^{o}C and 1023^{o}K/750^{o}C, pressure in the range of 0.5 to 5 bars, and space velocities in the range of 0.1-5 litre hydrogen containing propane per litre catalyst per hour (measured as liquid). Ziaka.*et.al.*[64] developed a membrane reactor using a 5% Pt-γ Al_2O_3 catalyst and a commercial porous alumina membrane. Hydrogen was used in the feed gas to reduce coking effects. The tube side pressure was maintained at 2-3 psig, shell pressure 0-1 psig and the residence time of the gases was around 2 seconds. Using propane-hydrogen feed with 4:1 molar ratio, a

relative increase of C_3H_6 yield of 26% at 90% selectivity to C_3H_6 was obtained at 833ºK/560ºC (packed bed 80%). C_3H_6 was also used in the feed stream to study the membrane catalysis. The presence of C_3H_6 decreased conversion in both conventional and membrane reactor configurations. In the region of lower C_3H_6 to propane ratios, this decrease in yield is due to a decrease in the reactor conversion. In the region of higher C_3H_6 to propane ratios, however, both the selectivity and conversion decrease simultaneously.

Sheitntuch *et.al.* [35] studied propane dehydrogenation membrane catalysis using commercial palladium-silver (25% Ag) membrane tubes (254μm thickness) and palladium-ruthenium (2% Ru) membranes tubes (76μm thickness) using a fine-grained supported platinum catalyst (0.52 wt. % Pt) diluted with pyrex particles. The shell side of the membrane reactor was swept by a stream of nitrogen or its mixture with hydrogen. Significant gains in yield were reported to have been achieved by separating the hydrogen through the selective palladium membrane. A propane yield of about 70% at 823ºK/550ºC was observed (23% at equilibrium). The performance of the membrane reactor was observed to be strongly dependent on the flow rates of the reactants and the sweep gas. The authors reported that the C_3H_6 yield decreased with time for experiments conducted with a palladium-silver alloy tube at 798ºK/525ºC. The drop in yield was attributed to both membrane and catalyst deactivation.

Yildirim *et.al.* [27] Studied various types of membranes for the catalytic dehydrogenation of propane using 0.5 wt. % Pt/Al_2O_3 or 0.5 wt % Pd/Al_2O_3 cylindrical catalyst pellets (3.4 mm x 3.6 mm). The membranes studied included dense Pd-Ag, silica modified metal impregnated porous and metal sputtered porous membrane systems respectively. The metal impregnated porous system modified with silica gave propane conversions similar to the equilibrium values. Addition of catalytic material in the form of pellets resulted in conversion values significantly above the equilibrium level. The Pd-Ag membrane showed the best performance, giving a four-fold increase in propane conversion at a relatively low temperature of 673ºK/400ºC. Additional features in the work suggested that the membranes needed additional catalyst on the feed side to provide maximum conversions. Weyten *et.al.*[36] Investigated membrane reactors using a silica composite alumina membrane and a chromia-alumina catalyst. Nitrogen was used as the sweep gas and pure propane was fed to the tube side of the reactor. For a weight space hour velocity (WSHV) of 0.16 h^{-1}, the propane conversion was 23.8%, which is 34% higher than the thermodynamic equilibrium conversion for the reaction conditions. The propane selectivity was about 89%. As the WHSV was increased, the

propane yield decreased from a value of 50 at very low values to 20 at 0.75 h^{-1}. Even though the propane yield was high at low WHSV, the selectivity of the dehydrogenation reaction was low. A similar variation in propane yield with respect to system parameters such as pressure, temperature and sweep gas flow rate have been investigated and are summarized in Table 2.3.

Table 2.3. A summary of membrane of the reactor catalysis.

Membrane	Catalyst	Temp ^oC	Reference	Performance
Al_2O_3	5 % Pt- γ Al_2O_3	560	Ziaka et. al. (1993)	26 % conversion
Pd-Ag tube	0.52 % Pt	530	Sheintuch and Dessau (1996)	70% conversion
Dense Pd-Ag Silica porous Sputtered Pd-porous	0.5 wt% Pt/Al_2O_3 0.5 wt.% Pd/Al_2O_3	400	Yildirim et. al. (1997)	four fold increase in conversion with Pd-Ag
SiO_2/Al_2O_3	Cr_2O_3 / Al_2O_3 Cr_2O_3-K/Al_2O_3 Cr_2O_3-Cs-Zr /Al_2O_3	450	Weyten et. al. (1997).	34 % higher conversion from reactor
Pd-Stainless steel Pd-Al_2O_3	Pt-Al_2O_3	400	Quicker et. al. (2000)	Propylene yield 26.1
Pd-Al_2O_3	Pt-Sn-K/Al_2O_3	500	Chang et. al. (2002)	52 % conversion

Propane dehydrogenation using commercial catalysts such as Pt-Sn on alumina with electroless plated palladium-steel, palladium-alumina membranes was studied by [29]. Both propane conversion and C_3H_6 yield with the palladium- ceramic membrane were higher than the values determined in the conventional packed bed reactor. The yield of C_3H_6 increased from 22.2% (conventional packed bed reactor) to 26.1% (Pd-ceramic membrane). Due to the larger amount of hydrogen removed through the palladium-stainless steel membrane, the conversion obtained in this test was even higher. The hydrogen yield increased from 34% (Pd-ceramic membrane) to 39% (Pd-stainless steel membrane), and the conversion from 35.4% to 42%. For the palladium-ceramic membrane, this represents a relative increase in propane conversion of 37.5% compared to the packed bed reactor. Weyten *et.al*. [36] Studied membrane catalysis using palladium–silver and silica-alumina composite membranes with chromia-alumina catalysts. A higher yield was obtained using the Pd-Ag membrane compared to the silica membrane. The propane yield decreased with an increase in WHSV and propane

feed flow rate. The selectivity of the membrane reactor (for both Pd-Ag and SiO_2 membranes) was higher than that found using a conventional plug-flow reactor (under the same operating conditions).

Cheng *et.al*. [25] Employed a K/Sn/γ-Al_2O_3 catalyst in an electroless plated palladium alumina composite membrane. Propane conversion greatly increased above the equilibrium value at 350-500^{o}C. At 500^{o}C, the propane conversion was 52% compared with 28% at equilibrium level. The selectivity of propane was more than 90% below 550^{o}C.

It can, therefore, be seen that membrane catalysis for propane dehydrogenation has involved the utilisation of various catalysts such as platinum–alumina, palladium–alumina and chromia–alumina, and various membranes such as palladium–silver, palladium–ruthenium and silica composites. In general, propane yield decreased as a non-linear function with respect to an increase in propane feed flow rate and WHSV. A reduction in catalyst selectivity is observed at higher values of WHSV due to the formation of by-products. Membrane reactors can operate within the temperature range of 500–600^{o}C. Improvements in catalyst performance (stability and activity for prolonged catalysis), coupled with improvements in membrane technology (thermal, chemical stability as well as consistent performance of inorganic composites at higher temperatures), are very helpful in overcoming the equilibrium limitation. Such improvements can also help to reduce the process economics in industrial scale operations.

Table 2.4 Reaction conditions: 0.1 MPa; space velocity of 1440 h^{-1}; feed gas component $V(CO_2)/V(C3H8)$ = 1 and CO_2 sweep gas velocity 40 ml (STP)/min. Catalyst: Pd-Cu/ MoSiO.

Comparison of reaction results between CCR and MCR				
Reactor	Temp (°K)	sweep gas	X_{C3H8}	S_{C3H6} (%)
Conventional	673	-----	4.1	93.1
PI–SiO_2/SiO_2/K–M	673	CO_2	12.6	97.8
PI–TiO_2/SiO_2/K–M	673	CO_2	12.4	96.6
PI–ZrO_2/SiO_2/K–M	673	CO_2	11.3	95.7

As it can be observed from Table 2.4, the results from three types of hybrid

membranes show excellent gas permeability and hydrophohilic properties. Water vapour could permeate through the three types of hybrid membranes at a greater rate than C_3H_8, C_3H_6, CO_2 and CO gas, which supports the idea that they are excellent membrane catalytic reactor materials for the removal of the product H_2O in the catalytic reaction procedure.

Solymosi *et.al.* [38] Carried out a study that involved CO_2 dry reforming of propane over supported Rh, as it is one of the most active catalysts for dry reforming propane and CH_4 to produce synthesis gas. Its advantage is that it limits the deposition of carbon that causes the significant deterioration of other catalysts. In this study, experiments showed that this process is faster than the reaction between CO_2 and surface carbon formed at high temperature over Rh. Subsequently, these studies confirmed the high activity of Rh and revealed several features of this catalyst. At a later stage, however, it was also observed that the presence of C_2H_6 in the $CH_4 + CO_2$ gas mixture caused the enhancement of carbon deposition and thereby the deactivation of the catalyst. This led to extending the study of the catalytic performance of the Rh catalysts to be used for dry reforming of propane.

2.14 Reaction of propane with CO_2.

Zhang *et.al*. [39] Prepared three types of supported membrane catalysts (Pd- Cu/MoO_3-SiO_2) and studied their application for partial oxidation of propane with CO_2 to C_3H_6. The reaction performance of a conventional catalytic reaction (CCR) was tested on an MRS-901 micro-reactor and the products obtained were fully analyzed by means of online chromatography (GC) with a thermal conductivity detector. The performance of the membrane catalytic reaction (MCR) was measured. At the optimal operation of CCR and MCRs, experiments were carried out to investigate the influence of temperature, space velocity, and reactant composition and sweep gas velocity on the reaction of partial oxidation of propane with CO_2 to C_3H_6. The results obtained are shown in Table 2.4. The presence of CO_2 dramatically influenced the reaction pathway of C_3H_8 and instead of dehydration and cracking; the formation of H_2 and CO came into prominence even though the presence of CO_2 significantly reduced the amount of carbon deposited as it could not prevent its formation. This very unreative carbon is probably responsible for the deactivation of the used catalyst [39], [40]. The formation of carbon in the C_3H_8+CO_2 reaction has been observed on alumina-supported Pt metals. It was not reported by Sutton [11] who, however has said for Ru/Al_2O_3, as in the dry reforming of CH_4, it is assumed that the adsorbed species of each reactant strongly influence the

reactivity of the other. Hence, the dissociated of CO_2 [Equation 2.6],

$$CO_{2\,(g)} = CO_{(a)} + O_{(a)} \quad 2.6$$

Is promoted by CxHy fragments from the decomposition of C_3H_8, and the dissociation of C_3H_8 is facilitated by adsorbed O because it is formed on the support, which does not play any role in the dry reforming of propane. In the latter case, we may take account of a new route for the formation of C_3H_7 and C_3H_6:

$$C_3H_{8\,(a)} + O_{(a)} = C_3H_{7\,(a)} + OH_{(a)} \quad 2.7$$

$$C_3H_{7\,(a)} = C_3H_{6\,(g)} + (½)\,H_{2\,(g)} \quad 2.8$$

Because propane is missing from the reaction products, we may speculate that the C_3H_7 radical decomposes to carbon and hydrogen: Thus, the last two reactions [Equations 2.7 and 2.8] may be shown again in the following basic steps.

$$C_3H_{7\,(a)} \longrightarrow C_{(s)} + H_{2\,(g)} \quad 2.9$$

The C_3H_6 formed in Equation 2.8 may be activated by adsorbed O atoms to give further reactive species:

$$C_3H_{6\,(a)} + O_{(a)} = C_3H_{5\,(a)} + OH_{(a)} \quad 2.10$$

$$C_3H_{5\,(a)} = C_3H_{4\,(a)} + (1/2)\,H_{2\,(g)} \quad 2.11$$

which either react with adsorbed O to give CO or decompose to hydrogen and carbon:

$$C_3H_4 + O_{(a)} = C_2H_{4\,(a)} + CO_{(g)} \quad 2.12$$

$$C_3H_{5\,(a)} = 3\,C_{(s)} + 2\,H_{2\,(g)} \quad 2.13$$

These processes are probably responsible for the addition of a sufficient quantity of CO_2 to propane and the disappearance of propane from the reaction products. In addition to the above elementary steps, a direct reaction of one of the hydrocarbon fragments and CO_2:

$$CxHy_{(a)} + CO_{2\,(a)} \longrightarrow CO_{(g)} + H_{2\,(g)} \quad 2.14$$

Carbon deposited on the catalyst surface can be activated by O or OH to yield CO and H_2:

$$C_{(s)} + O_{(a)} = CO_{(g)} \quad 2.15$$

$$C_{(s)} + OH_{(a)} = CO_{(g)} + (½)\,H_2 \quad 2.16$$

As mentioned previously, most recent research has concentrated on finding suitable new catalysts for the dry reforming processes. It has been well understood by most researchers that the kinetics of such processes depend on catalyst type, as the activities of most catalysts vary with temperature. Giving the kinetic orders of reactions involved in these processes more attention, most of the studies mentioned so far have represented the reaction rate by making use of the simple power-law equation or model:

$$k = A^* \exp^{(-E/R^*T)} \quad 2.17$$

$$R = kP^{m}_{C_3H_8} P^{n}_{CO_2} \quad 2.18$$

Where:

k is the rate coefficient.

A is the exponential factor.

E_a is the activation energy.

R is the universal gas constant.

T is the temperature (in Kelvin).

Equation 2.17, known as the Arrhenius equation, is used by most researchers to test the sensitivity of the reaction towards temperature. According to [11], using a Ru/Al_2O_3 catalyst, the reaction order with respect to C_3H_8 zeros and the order of CO_2 was found to be 0.3. The activation energies were found to be 88 kJ mol^{-1} for C_3H_8, 80 kJ mol^{-1} for H_2 and 66 kJ mol^{-1} for CO. Solymosi *et.al*. [48], used Rh and Re catalysts and applying the same technique reported in their first study that the order of the reaction was also zero in C_3H_8, while it was fractional (0.4-0.45) for CO_2. The linearization for the Arrhenius equation gives activation energy values for H_2 as 87.4 kJ/mol and for CO as 92.2 kJ/mol [40]. In their second study, conducted using a Re/Al_2O_3 catalyst, almost the same findings were obtained – zero order for C_3H_8 and a fractional order of 0.6 for CO_2. The activation energy for dry reforming of propane was found to be 84 kJ mol^{-1} [38].

2.15 Catalyst deactivation.

Catalyst deactivation as a mechanism is very difficult to define precisely, but in simple terms it can be defined as the loss of catalytic activity and/or selectivity over time as the catalyst is exposed to high temperature under fluctuating operating conditions. Catalyst deactivation, in effect, may be considered as a result of the catalyst being subjected to a number of unwanted chemical and physical changes, which cause a decrease in catalyst performance.

2.15.1 Catalyst activity.

The activity of any catalyst depends on various factors including method of preparation, metal loading and type of metal used. Although the preparation method itself sometimes depends on the type of metal and the amount used, most researchers have implemented the incipient wetness impregnation (IWI) technique for preparing metal supported catalysts. The most useful metals groups are the (VIII) that are being used for dry reforming processes reactions, which include Rh, Ru, Ni, Pt, Ir, Co, and Fe. It has been reported that noble metals can be more active and stable than Ni [40], [12]. Rostrup's study shows the order of activity towards the dry reforming reaction as Rh, Ru > Ir >Ni, Pt, Pd. Wang *et.al*.[24] found that for Al_2O_3 support, the order of most active metals was found to be Rh > Ru > Ir > Pd >Pt >Ni > Co >> Fe. Such evaluations may also depend on the metal load. This means that in order to have equal catalyst activity, more catalyst loading is required for Ni and Co catalysts compared to the noble metals. Due to the fact that Ni is much cheaper and more available than other

noble metals, however, it has been suggested that it is the most suitable alternative for research groups nowadays. It has also been reported that bimetallic catalysts offer better selectivity, activity and deactivation resistance compared to those of monometallic catalysts [4 1] . Adding alkali or alkali earth to nickel [42], or possibly using a support with basic characteristics [43], may overcome the problem of carbon deposition. Metal oxide supports have been the most widely used support for dry reforming reaction processes, due to their significant influence on the activity of the catalyst as a result of their acid-base properties and changing the active surface area. This is due to the fact that CO_2 adsorption and dissociation on the catalyst adds to the dry reforming process because of the CO_2 acidic nature, and a basic catalyst might enhance the catalyst activity. It has been reported that the alumina support exhibits a better activity with Ni catalyst than other available oxide supports. Wang *et.al.* [24] Have reported that the sequence of activity of the oxide support for Ni is approximately: $Al_2O_3 > SiO_2 > ZrO_2 > La_2O_3 > MgO > TiO_2$.

The feed ratio is also one of the major factors that may affect catalyst activity because using a feed ratio of less than the stoichiometric could cause serious carbon deposition. To decrease the amount of unwanted carbon being deposited on the used catalyst, feed ratios (CO_2/C_3H_8) must be more than three.

2.16 Types of catalyst deactivations.

Most catalysts in chemical processes, in particular those that are used in hydrocarbon processes, tend to lose their activity with time. Regrettably, this decline in activity cannot be avoided except in a few limited cases, but it can be minimized and kept within certain limits. The three main mechanisms that cause such activity losses are coking (fouling), poisoning and sintering or aging.

2.16.1 Coking (fouling).

The mechanism by which the catalyst losses its activity due to a carbonaceous species being deposited on the surface of the catalyst, especially in hydrocarbon processes, is known as coking or catalyst fouling, and leads to metal sites blocking the pores in the catalyst support. Voorhies was the first scientist to develop an expression for the amount of coke deposited on a surface after time t [43], [44]. This expression equation 2.19 can be used for larger feed streams as well as a large range of catalysts. The relationship is expressed empirically as:

$$Cc = At^{n} \qquad 2.19$$

Where:

Cc = Carbon concentration on the support surface.

T = time.

n and A = are the fouling parameters which depend on the feed rate that could be found out experimentally.

Voorhies found that the deposition rate of carbon was independent of space velocity.

He went on to indicate that the coke time relationship was the solution of the differential equation, dc/dt, to is give $C = A\, t^{½}$. Generally, for a large scale reaction, equation 2.19 turned out to be adequate. It was also found that the amount of cook that could be determined in relation to the catalyst activity (a) as well as the amount of cook that is deposited on the surface) Cc) in other ways:

$a = 1/(C_c{}^{p}+1)$ 2.20

$a = e^{-a}\, 1\, C_c$ 2.21

$a = 1/(1+a_2+C_c)$ 2.22

Generally, carbonaceous deposits on the catalyst surface illustrated the role of the two routes of the hydrocarbon molecule and CO_2 molecule. The first route, which is hydrocarbon decomposition, is more complex than(CO) and gives up a wide range of fragments and species, as showed in figure 2.9. These carbon species are found to be more active than those obtained from the CO route, the latter leading to a smaller amount of coking and higher activity of the Ni catalyst. Other studies have, however, reported that during the hydrocarbon decomposition route, most of the surface carbon species are highly reactive. This takes place when CO_2 is introduced into the system to yield CO, leading to less carbon deposition on the catalyst surface [24], [11], [40]. In the CO route, CO dissociates to produce and form carbon-containing fragments. These fragments/species can be polymerized to form various species of carbon that are different in terms of reactivity.

These include α-C, β-C and γ-C. It has been suggested that α-C species are responsible for CO formation, while, β-C and γ-C species are the source of catalyst deactivation, as illustrated in figure 2.10 [45], [39], [24]. Some of the β-C and γ-C species dissolve into the bulk of the metal forming vermicular carbon, Cv, or metal carbide.

Figure 2.9 Formation gasification and transformation of carbon on nickel from (CO) route [45].

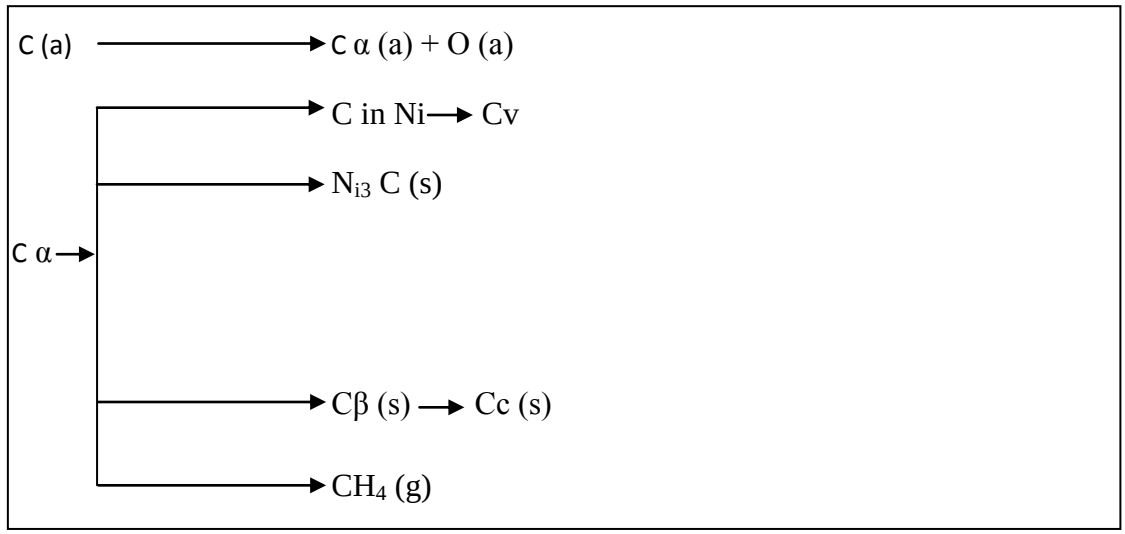

Figure 2.10 Formation gasification and transformation of carbon on metal surface from hydrocarbon route [45].

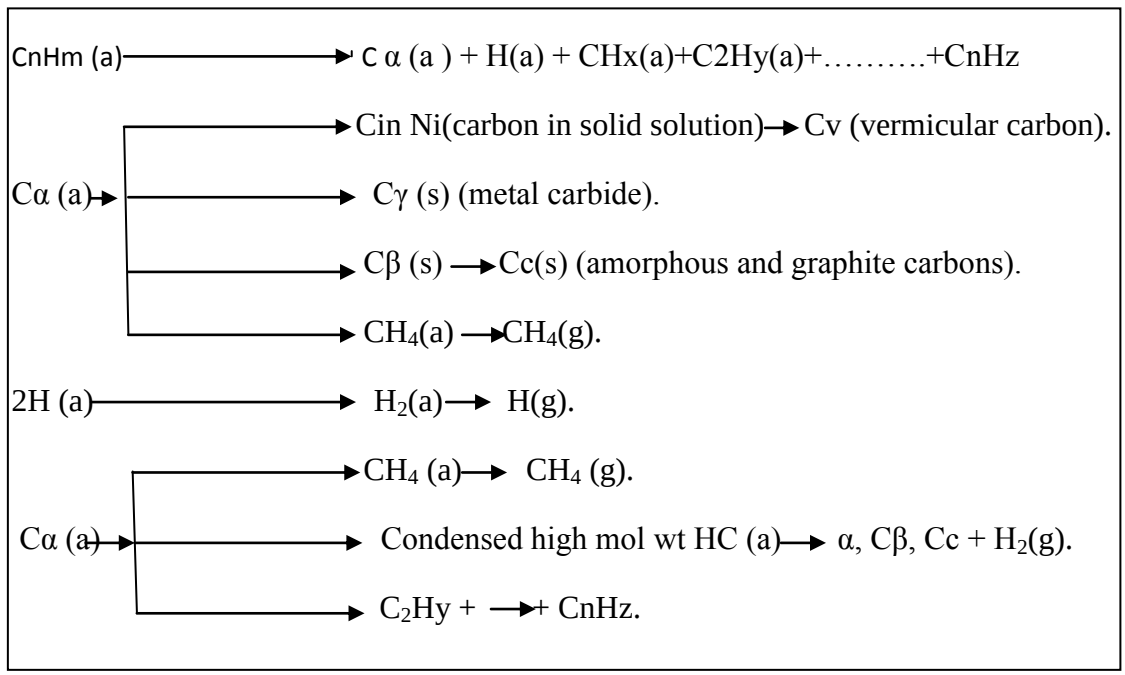

It can be concluded that the coking (fouling) mechanism and other related reactions occurring in any dry reforming system are in equilibrium. The formation of coke via disproportionation, however, decreases as temperature increases. The coke structure through hydrocarbon decomposition becomes very considerable at reasonably high temperatures, depending on the nature of the feed of the dry reforming reaction, and could quickly deactivate the catalyst and hence block the reactor.

2.16.2 Sintering (Aging).

This mechanism describes the process by which the lifetime of the used catalyst active phase should always be stabilized and kept within a desirable limit, when the most useful factor that influences the reaction is the temperature. The catalyst lifetime for research is quite short compared to its industry counterpart. Consequently, keeping the temperatures low over a long period may result in a catalyst structure similar to that caused by elevated temperatures over a short time. The loss of catalyst activity because of the altered structure in the crystal of the catalyst surface is due to high temperature exposure and is known as sintering. This leads to deactivation of the catalyst as the pores inside the activated membrane support become closed or blocked. It can also take place when it grows on the support causing a change in crystal structure. From time to time, the main stream concentration may have an effect on the sintering (aging) deactivation [46]. As far as this mechanism is concerned, however, one of the two theories is crystallite migration and the other is atomic migration. In the former, crystallites tend to move and migrate along the surface until they collide with other crystallites. In the latter, sintering occurs as result of metal atoms migrating away from crystallites as they move across the surface of the support and as a result the migrating atoms colliding with other crystallites [20]. Larger crystallites are more stable than smaller ones, so these processes result in a size increase as the small crystallites vanish or become smaller in size. Fogler *et.al*. [46] Represented and modelled the sintering decay by a second order rate law with respect to the present activity:

$$r_d = -da/dt = k_d a^2 \qquad 2.23$$

Integrating with a =1 at given time t = 0 will give:

$$a(t) = \frac{1}{1 + k_d t} \qquad 2.24$$

Where a (t) at time (t) is the activity of the catalyst and k_d is a constant.

This shows that sintering decay follows the Arrhenius equation.

$$k = A^* \exp^{(-E/R^*T)} \quad 2.25$$

As the temperature decreases, the sintering constant k_d also decreases leading to an activity increase and a subsequent decrease in the sintering decay rate.

2.16.3 Poisoning.

This can be simply defined as the loss of activity due to material depositing on the active portion of the membrane, which results in a decline in the existing active sites for the main reaction. The basic structure of the active sites is not believed to alter during the poisoning process, it seems that the rate depends upon the poisoning molecules and may occur as a result of many reasons, one of which is contamination of the feed by either reactants or products of the main reaction.

2.16.3.1 Poison in the feed.

A good example of this type of poisoning can be the trace contaminants in petroleum stocks, and it is quite expensive to remove these impurities. The rate of this poisoning is fairly slow as the rate of poison from the reactant is believed to be proportional to the number of un-poisoned sites. As a result, each site is assumed to be poisoned by every adsorbed molecule. Considering these assumptions, the decay rate (rd) could be applied to determine the catalyst's activity at any time a (t) [46], [43];

$$r_d = a(t) k_d C_p \quad 2.26$$

Where C_p is the concentration of poison in the gas phase, and k_d is a constant.

2.16.3.2 Poisoning either by product or reactant.

This sort of poisoning occurs as a result the catalyst being deactivated by the products or reactants. The deactivation rate can be represented at a constant concentration of poison:

$$r_d = \frac{da}{dt} = k_d a^q \quad 2.27$$

In such a case, when the decay reaction is quick, the decay will occur around the pore entrance. If this happens to be accompanied by a high diffusion resistance then the pore will be plugged, and this is referred to as pore mouth deactivation [46].

The poison particles can be adsorbed reversibly, irreversibly, or quasi-irreversibly [47]. If reversible, the catalyst activity can be restored provided that the poison is removed from the feed. In this case, the effect of the poison depends upon its strength of adsorption and its concentration because the catalyst recovers its original activity once the poison is removed. The irreversible poisoning process is thought to be due to a lack of desorption between the active site and the poisoning molecule under the operating reaction conditions. This is due to strong bonding to the active site such that its desorption rate is irrelevant. The irreversible poisoning adsorption rate does not depend on the concentration of the poison, but the rate of deactivation does as the catalyst activity stays lower than its original state even before removal of the poison from the feed stream as increasing the temperature from time to time could cause decomposition rather than simple desorption. The term poisoning may at times be inadequate, as it is better described as a deactivation by metal deposition or coke, especially when the adsorbed species condense or polymerize into outsized units on the catalyst surface. A quasi-irreversible poison has the attitudes and features of both reversible and irreversible poisons. Because it is adsorbed onto the active sites, it may decrease the catalytic activity of the membrane, but its very slow desorption rate with respect to the reaction rate indicates that it is a permanent poison. As a result, the inhibition term will include the reversible poison factor, even if the irreversible factor is considered in the rate constant. As the poison is removed, catalyst activity will be partially restored [47].

2.17 Mechanisms of catalyst deactivation.

There are other several factors that may add to the catalyst deactivation mechanisms, such as diffusional effects or mass transfer within the pores of the prepared membrane. It becomes difficult to differentiate between such deactivation mechanisms, however, especially when they occur in combination. When catalyst deactivation is by coking, the carbon deposits on the catalyst pores will cause a change in pore resistance diffusion with an effect on overall reaction rate [48]. According to Levenspiel's classification of mechanisms of catalyst deactivation, there are three kinds these include parallel decay, series decay and side by side decay.

2.17.1 Parallel decay.

In this mechanism, the deactivation is caused by the deposition of side products from the main reaction. This occurs, for example, during coking deactivation.

2.17.2 Series decay.

In this mechanism, the deactivation is due to the reaction product, which could decompose or react further to produce a material that congregates on the surface and causes deactivation.

2.17.3 Side-by-side decay.

This decay occurs when the feed impurities deposit on the catalyst surface causing poisoning deactivation. It is worth mentioning that studies conducted to develop a model for catalyst deactivation, include the pioneer work by Thiele [46]. Who simulated the material balance equations for reaction and diffusion in single catalyst pores. He also went on to develop Thiele's deactivation models Lippens *et.al.* [48] Reported that the progressive drop in concentration of a reactant on moving into the pore is dependent on the dimensionless quantity 'ϕ', which is called the

Thiele modulus that is given by:

$$\phi^2 Exp = \frac{(-r_{rxn} w_{cat}) d^2_p \rho_p}{4 C_{Ag} D_{eff}} \qquad 2.28$$

Where:

$\phi^2 Exp$ is experimental Thiele modulus

$-r'_{rxn}$ is the reaction rate, mol g $^{-1}$ s^{-1}

d_p is the catalyst particle diameter, cm

ρ_p is the particle density, g cm^{-3}

C_{Ag} is the concentration of reacting gas, mol cm $^{-3}$

D_{eff} is the effective diffusity inside the particle, cm^2 s^{-1}

w_{cat} is the catalyst weight, g.

The efficiency of the process may be estimated from the quantity effectiveness factor (η) which measures how far the reaction rate is decreased because of the resistance to pore diffusion. This effectiveness factor (η)is defined using the relation:

$$\eta = \frac{r_{A1}}{r_{A2}} \qquad 2.29$$

Where r_{A1} is the actual reaction rate and r_{A2} is the rate without diffusion resistance.

Many studies have been conducted to investigate the effect of pore diffusion on the reaction rate and have shown that the effect depends on whether the Thiele modulus is large or small. The pore diffusion resistance can be negligible whenever the Thiele modulus (ϕ) is smaller than 0.4. However, it was also observed that the effectiveness factor is almost equal to unity (i.e. the concentration of reactant does not drop significantly within the pore). This shows that the small value of Thiele modulus means a short pore, slow reaction or quick diffusion. Thus, one may conclude that in order to quantify the impact of the different geometries, the overall reaction rate will be compared based on an effectiveness factor found by integrating the concentration of the reactants involved along the reacting boundary. The effectiveness factor is a measure of how much oxygen is reacted, taking diffusion resistance into account.

Chapter Three

Experimental Design

CHAPTER 3: Experimental Designs

3.1 Introduction.

This chapter presents the experimental work that has been carried out. It begins with an explanation of the experimental rig/apparatus setup and the different equipment involved, including a thorough description of all systems, devices and instruments used. It then goes on to show the various materials that were used for this research including gases, chemicals, catalysts and others. It also briefly discusses the catalysts that were utilized to prepare the various membranes, describing the different modification techniques using the desired solutions. This is followed by a detailed explanation of the safety measures that were implemented during the experiments.

The chapter then goes on to briefly discuss the different types of membrane catalyst characterization procedures, and their analysis methods. Finally, it outlines discussions and goes on to draw some conclusions from some of the preliminary test results.

3.2 Experimental setup and design.

Figure 3.1 shows a pictorial view of the whole experimental rig setup, and figure 3.2 shows the schematic diagram for the various systems of the experimental rig. This experimental setup was used for all experiments that were carried out to test the prepared membranes. The schematic consists of a combination of five sub-systems, including gas feed delivery sub-system, gas mixing sub-system, membrane reactor sub-system, H_2O capture sub- system, and the product gas analytical sub-system (i.e. Gas chromatography GC), designated as A, B, C, D and E respectively. The entire experimental rig and some of its accessories were constructed on a 1.50m × 0.75m wooden board, mounted on an upright metal bench frame (as shown in figure 3.1). All the sub-systems will be fully explained and viewed separately later.

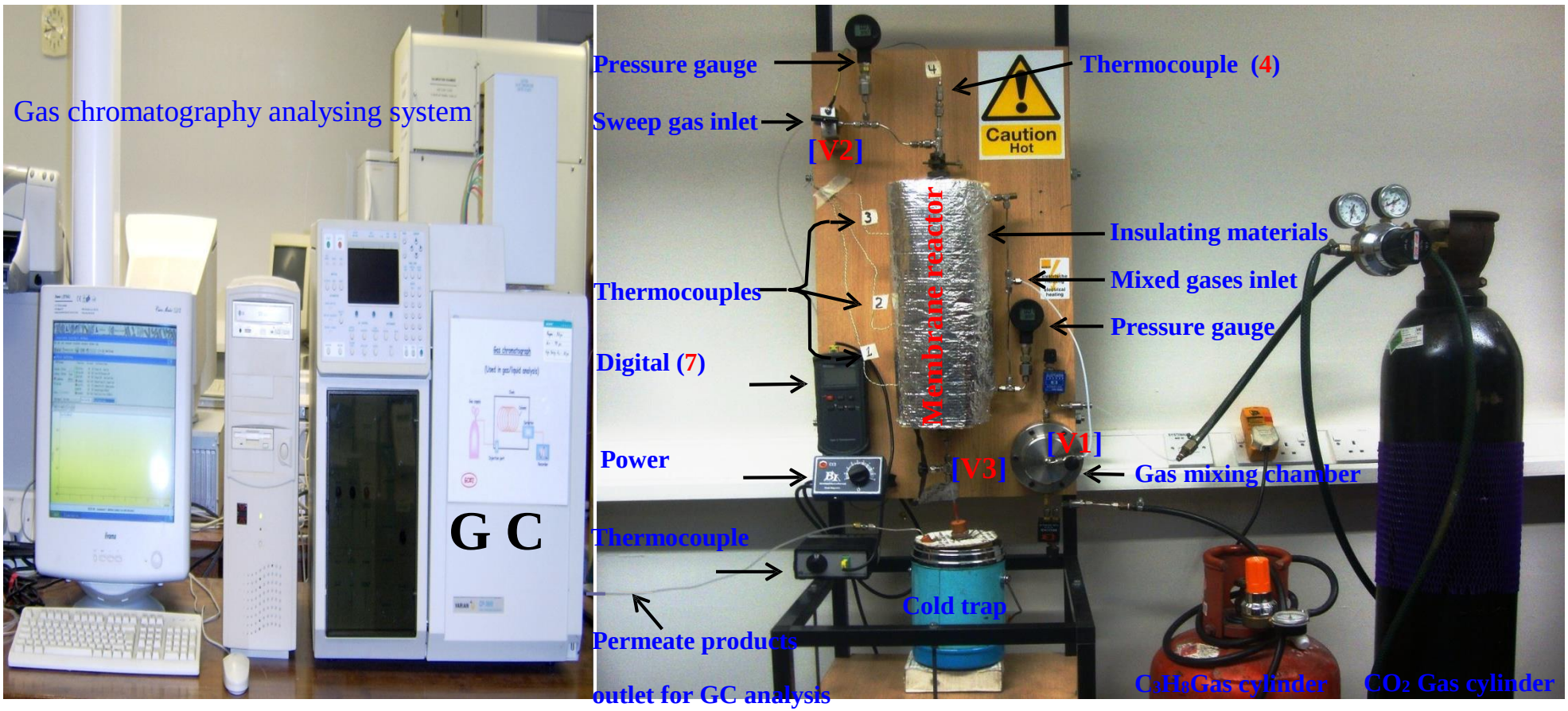

Figure 3.1 Pictorial view of the experimental rig setup.

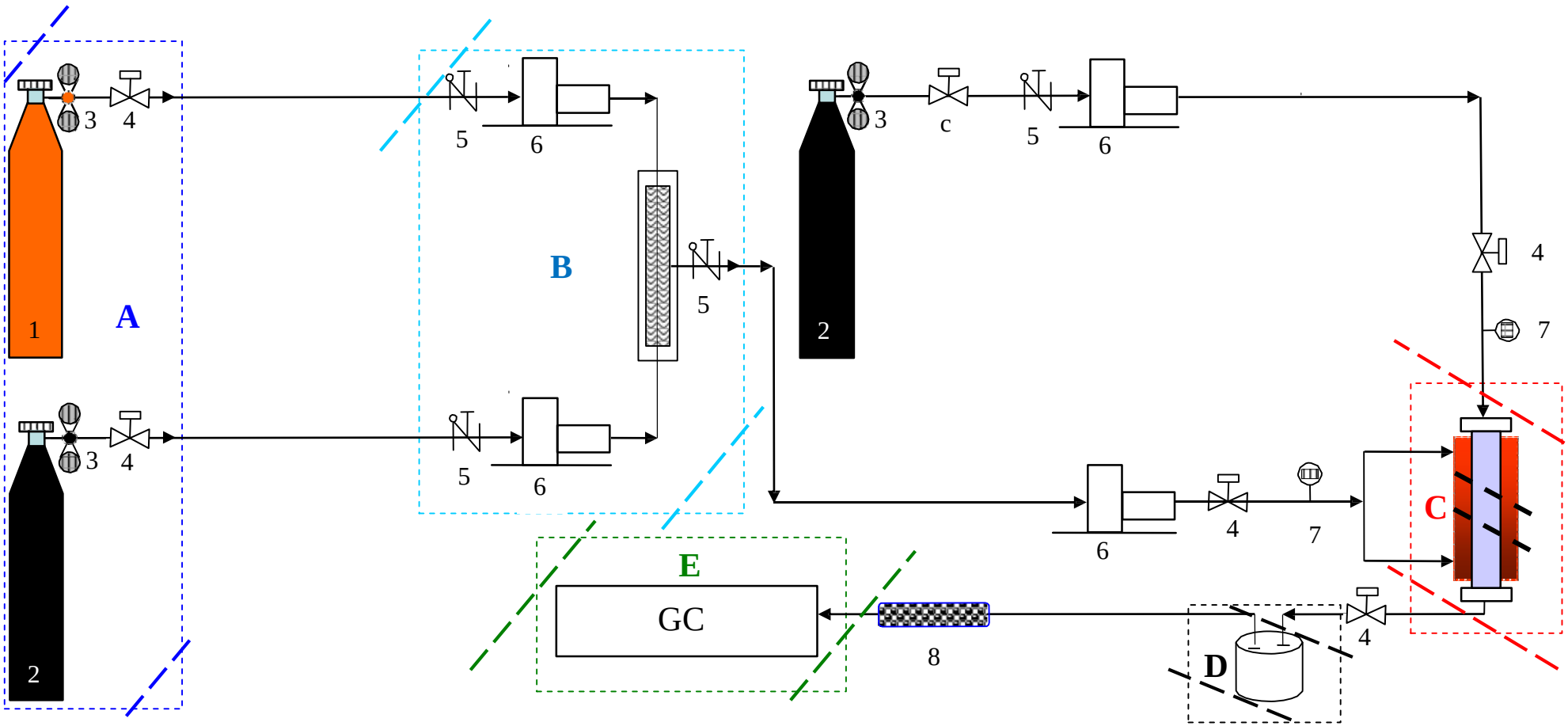

Figure 3.2 Schematic of the experimental setup rig and its accessories and sub-systems, where: (1) C_3H_8 cylinder, (2) CO_2 cylinder, (3) Gas pressure regulator, (4) Screw down valve, (5) Non-return valve, (6) Mass flow controller, (7) Gauge pressure, (8) H_2O trap.

3.2.1 Gas feed sub-system (A).

This sub-system figure 3.3 is a fundamental part of the experimental rig system. It comprises of two gas cylinders, namely propane (C_3H_8) and CO_2 (CO_2), which are used as reactant feed gases. A ¾ inch PFA (perfluoroalkoxy) tubing was employed, due to its ability to resist heat and its unique flexibility, was used as connecting lines. The back-up pressure of both reactant feed gas cylinders was kept constant, monitored and controlled by means of a BOC gas pressure regulator (labelled 3 in the diagram). This was fitted out with two pressure gauges, one indicating the pressure inside the gas cylinder and the other showing the outlet pressure as each reactant feed gas flow stream was passed through a screw down on/off valve (labelled 4) then led into the gas mixing chamber system.

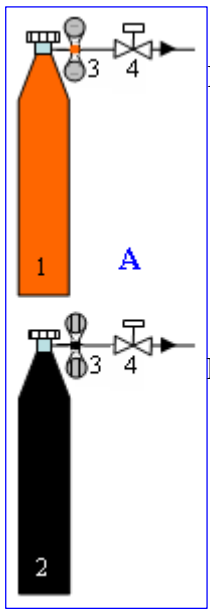

Figure 3.3 Schematic diagram of the feed gas system [A]. 1 = C_3H_8 Gas cylinder, 2 = CO_2 Gas cylinder, 3 = Gas pressure regulator, and 4 = on/off shut valve.

3.2.2 Gas mixing system (B).

The reactant feed gas system (B) is shown as both a schematic and pictorial view in figure 3.4. It consists of a non-return valve (5) to make sure there was no back pressure on the reactant feed gas cylinder being used, and mass flow controllers (6), both of which were supplied by Brooks' Instruments (model 8744), and rated at 1500ml min^{-1} and 1000ml min^{-1} for CO_2 and C_3H_8, respectively. In order to guarantee each of the mass flow controllers provided the specific required amount of reactant feed gas,

they were calibrated on a regular basis using a bubble flow meter. The procedure and results of this calibration are presented later in this chapter. The flow streams of both reactants fed gases are then led into the cylindrical gas mixing chamber that was machined from stainless steel with a capacity of 500ml. The two parts (upper and lower) of this mixing chamber were tightened together by means of five 10mm socket head cap screws. In order to ensure that both reactant fed gases were well mixed before being introduced into the catalytic membrane reactor system, two 50mm in diameter meshed wire steel sheets were placed inside the mixing chamber. This guaranteed that a thorough mixing of the gases was achieved. The system was assembled using machined Swagelok fittings and ¾ inch stainless steel tubing.

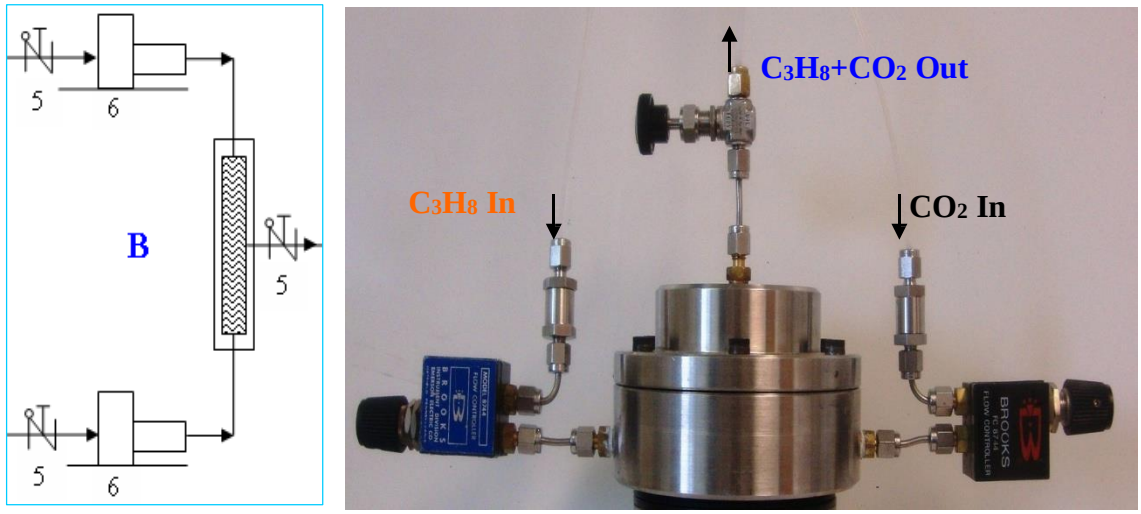

Figure 3.4 Schematic diagrams and pictorial view of the feed gas mixing system [B]; 5 =non-return check valve, 6 = mass flow controller.

3.2.3 Membrane reactor sub-system description (C).

The membrane reactor sub-system comprised the stainless steel membrane reactor itself and accessories such as the ceramic membrane, graphite seals, heating tape, isolating fabric, and the isolating materials.

3.2.3.1 The membrane stainless steel reactor.

The right-hand side of figure 3.5 shows a pictorial view of the stainless steel reactor that was 420 mm in length and lathe machined to accommodate the membranes to be tested. The tube side inlet and outlet were attached at the bottom and top ends of the reactor using machined Swagelok fittings as they were steel welded onto both screw threaded caps. The shell side inlet and outlet were machined and steel welded to the bottom and top sides of the reactor using similar Swagelok fittings. The welding was to

make sure that the system was capable of withstanding both high temperature and pressure. Most of the tasks of this research study involved these harsh operating conditions and as a safety measure, it was recommended that the metal reactor was checked to ensure that it was a leak-free medium prior to every experimental task. This was achieved by pressurising the reactor to 1.5 times the expected operating pressure, in this case 4.5-5.0 bars, by connecting it to a high pressure air supply and then closing all the inlets and outlets and monitoring the pressure gauge that was placed on the system for a few minutes. Simultaneously, applying soap-water solution to all the fittings and metal welded joints ensured that any leaks could easily be visually monitored.

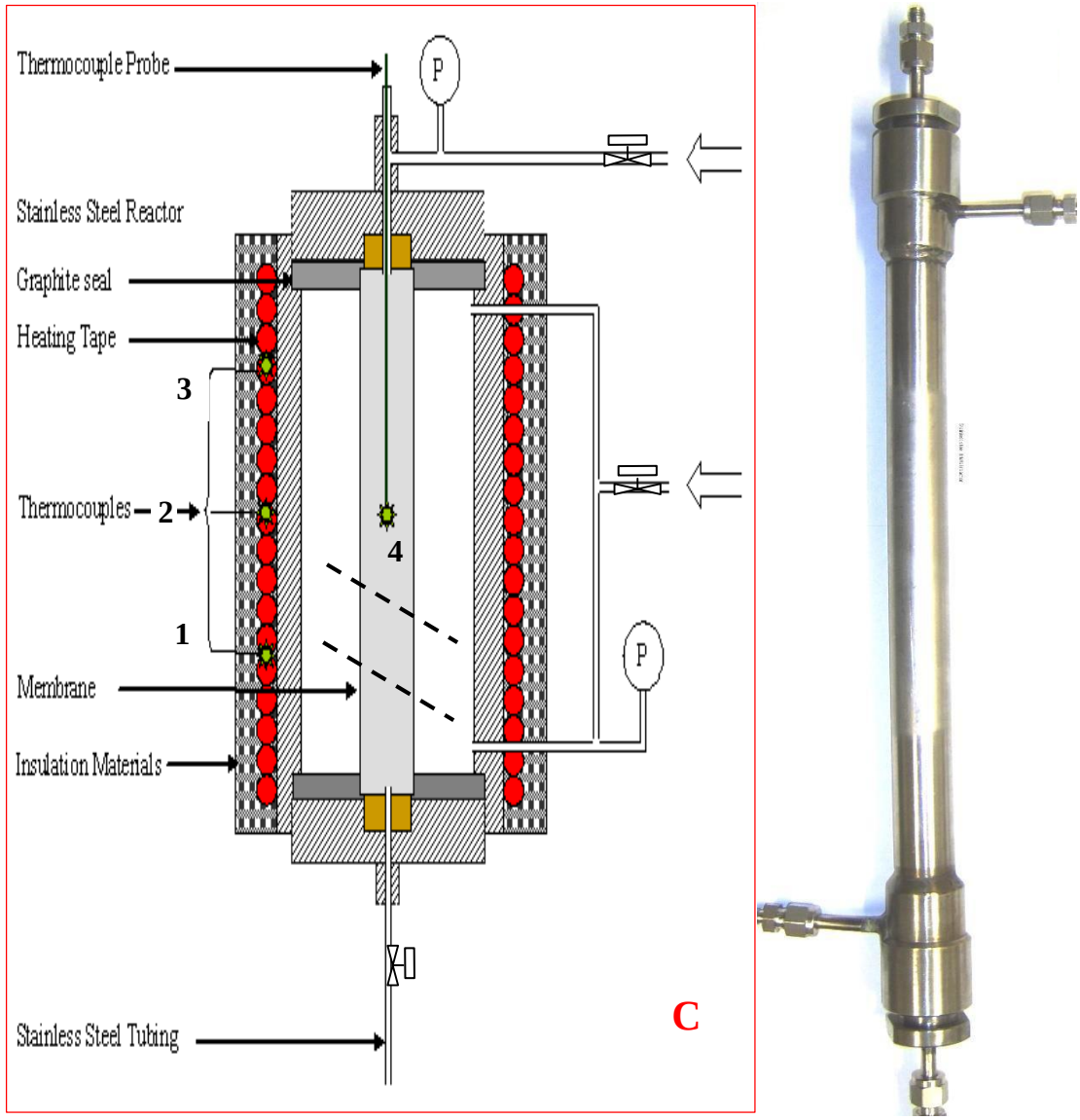

Figure 3.5 Schematic diagram of the membrane reactor assembly system [C] (right) and a cross-sectional view of the catalytic membrane reactor assembly (left).

3.2.3.2 The membrane reactor accessories description.

The left-hand side of figure 3.5 shows a cross-sectional view of the catalytic membrane reactor assembly, comprising the metal membrane reactor housing the tubular ceramic membrane. The membrane was positioned in the middle of the metal reactor and tight-sealed using 98% pure moulded graphite seals, as shown in figure 3.6, with the following technical specifications: an outer diameter o/d of 24mm, inner diameter i/d of 10 mm diameter and thickness of 7mm, which were supplied by Geegraf (Gee Graphite Ltd/West Yorkshire). This guaranteed that the reactant fed gases did not migrate to the other side of the tube by leaking through the seals in any defects

between the ceramic tube and the stainless steel enclosure. A series of leak-free tests were carried out, which demonstrated that graphite seals were the most adequate candidate that met the various operating conditions. The experimental temperature was controlled and maintained by four temperature-sensing NiCr/NiAl-K type, 2m long fibre glass thermocouples (1, 2, 3 and 4), which were positioned at strategic locations on the external surface of the membrane metal reactor. In order to measure reaction temperature inside the tubular membrane, a k-type 1mm (od) stainless steel thermocouple (probe 4 shown in both figure 3.1 and 3.5) was sited axially inside the reactor and fitted on the upper end of the system using a Swagelok fitting. Thermocouples 1, 2, 3, and 4 were connected to a k-type 5- way thermocouple switch box selector 5 in figure 3.1. HBQ heating tape, 2m long, 700 watts, and with a maximum temperature of 1173°K/900°C, supplied by Horst/Germany, was used as a heating source along the metal reactor. The temperature was set and controlled by means of 5 intermittent power controllers 6 in figure 3.1 and observed by the Extech model 421501 digital thermometers 7 in figure 3.1.

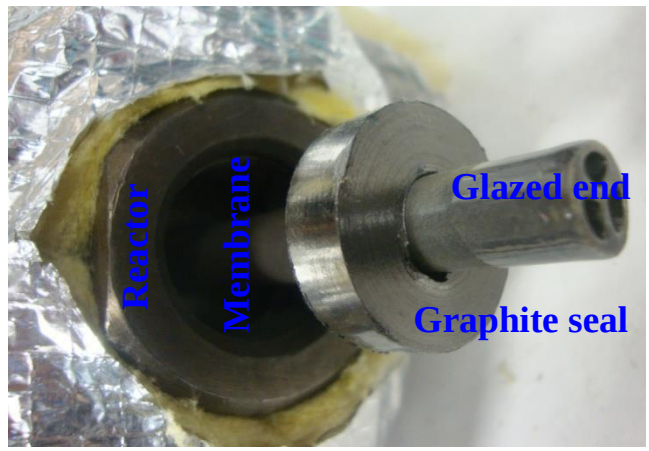

Figure 3.6 Pictorial view of part of the membrane reactor assembly.

In order to maintain the temperature at its desired level and to reduce heat losses in the system, BETEX fabric tape, 4m long by 50mm wide by 2mm thick, was wrapped around the metal reactor. The whole system was covered with thermo 30 mm reflective insulation materials. The membrane support was then installed concentrically inside the metal membrane reactor to be tested, as shown in figure 3.6.

3.2.3.3 Tubular ceramic membrane support description.

Figure 3.7 shows a representative detailed dimensional sketch and cross-sectional view of the tubular ceramic membrane support. The support was 370mm long, including two glazed-ends

of 15mm each on either side for handling, with an outside diameter (o/d) of 10mm, an inside diameter (i/d) of 6mm and a wall thickness (Tw) of 2mm α- alumina tubes washcoated externally with titania (provided by *Ceramiques Techniques et Industrielles* [CTISA] of France) with different pore diameter ranges from 80-6000nm. The ceramic supports were supplied with three internal 2 mm holes to add strength while in use.

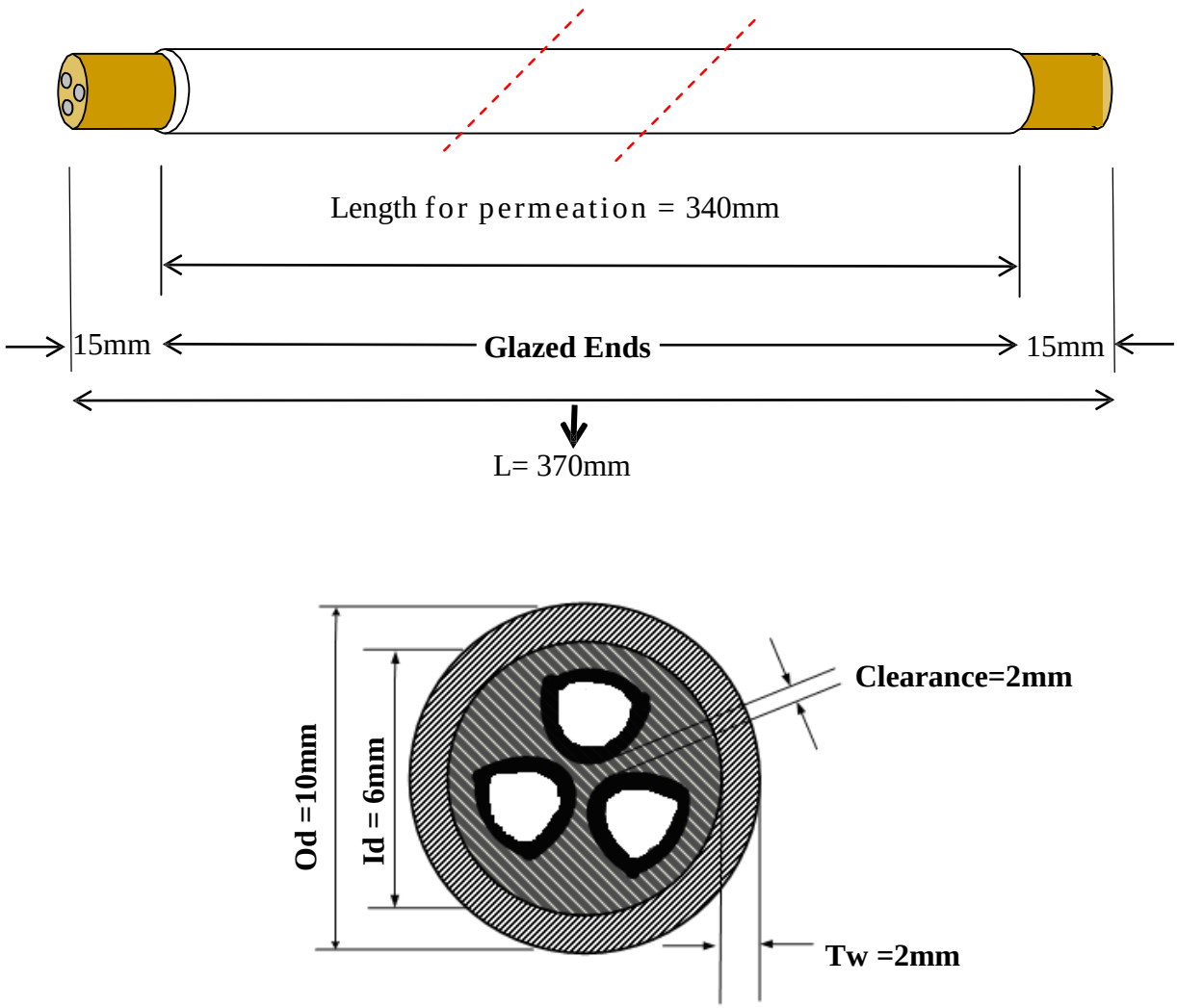

Figure 3.7 Schematic of a cross-sectional view of the membrane support and its specifications.

3.2.4 The cold trap (D).

Figure 3.8 shows the cold trap system, consisting of a 200ml round-bottomed Pyrex glass flask, placed in a 1000ml metal thermos flask filled with ice. The product permeate fluids were directed into the bottom of the flask using ¾ inch PFA tubing via a rubber stopper. Another section of ¾ inch PFA tubing was directed towards the analytical system (E), passing through

a 20cm long glass moisture trap (8) that was filled with recyclable silica gel granules to protect the analytical system from being damaged by possible moisture.

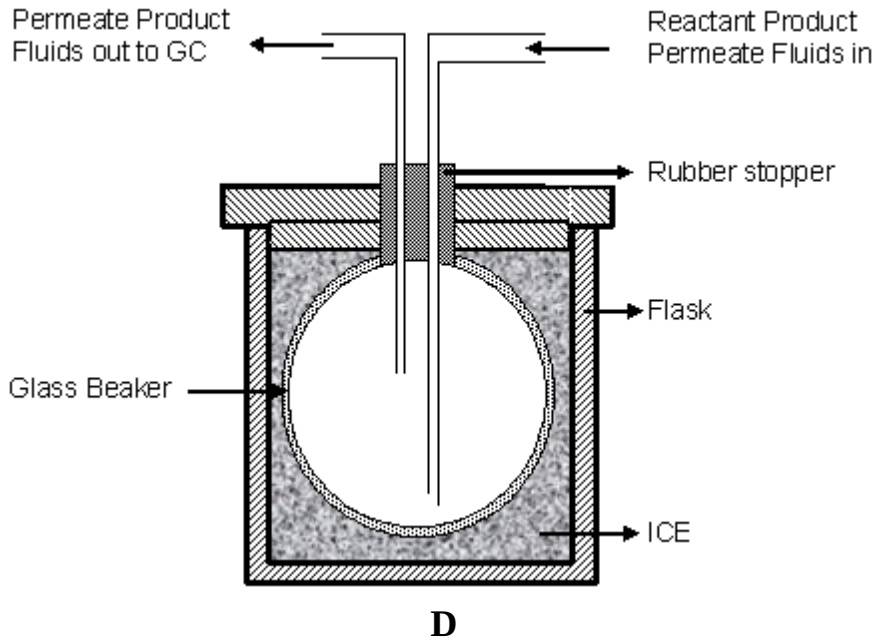

Figure 3.8 Schematic cross-section of the cold trap system [D].

3.2.5 The analytical system (E) Gas Chromatography (GC).

Figure 3.9 presents the pictorial view of the analytical system (E). The analytical system used chromatography, an instrumental technique for the identification and separation of different chemical compounds, which analyzed a sample or sample extract. This was carried out using either of two detectors - a Flame Ionization Detector (FID) or Thermal Conductivity Detector (TCD), as presented in figure 3.10.

Figure 3.9 Pictorial view of the analytical system [E].

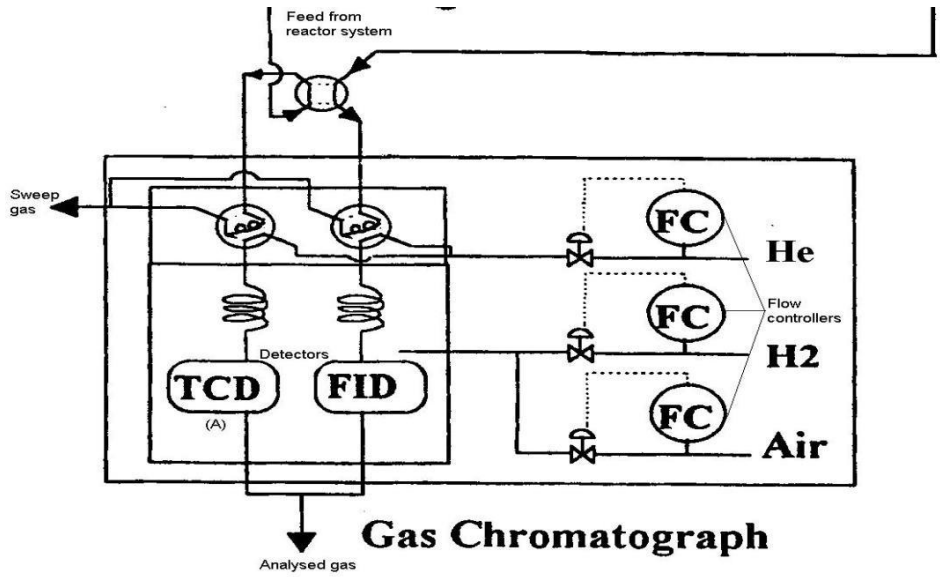

Figure 3.10 Schematic details of gas chromatograph.

3.2.5.1 Flame Ionization Detector (FID).

In this type of detector the specimen to be analysed is dissolved in a soluble phase (which could be a liquid or gas). The mobile medium is then forced through an immobile, immiscible

phase. The two phases are selected in such a way that components of the specimen have differing solubilities in each phase. Components that are quite soluble in the stationary phase tend to take longer to travel through it than components that are not very soluble in the stationary phase but are very soluble in the mobile phase. As a result, the components in the sample become separated from each other as they move through the stationary medium. Once a component has travelled through the stationary phase, it is detected at the other side and a signal is sent to the recording device in a form of curve on the PC monitor. The time between sample injection and an analyte reaching a detector at the end of the GC column is the retention time (t_R). Each analyte in a sample will have a different retention time. Hence, the time for the mobile phase to pass through any GC column is the t_M, as shown in figure 3.11. A GC can separate the compounds, but cannot identify them itself. A GC calibration is, therefore, essential in order to measure the retention time for various sample components before it can be used for identification.

This GC calibration will be discussed in more detail at a later stage.

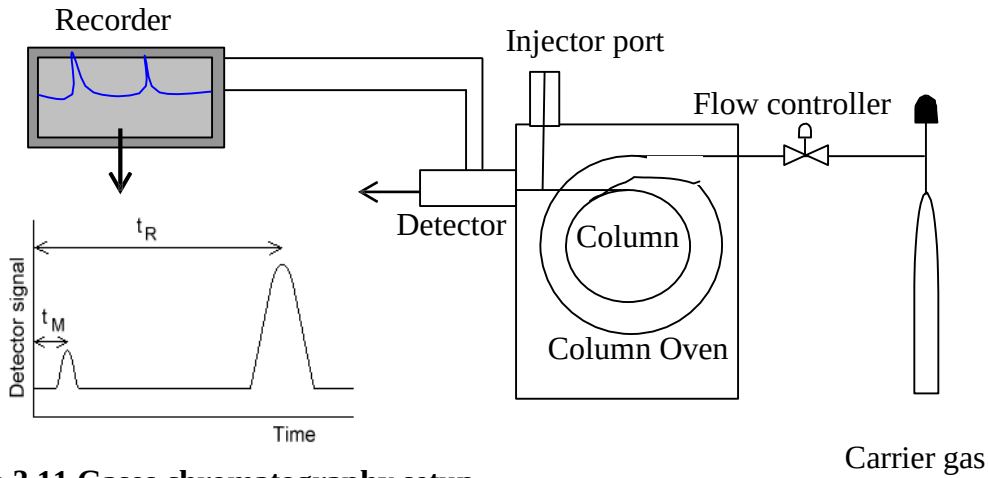

Figure 3.11 Gases chromatography setup.

3.2.5.2 Thermal Conductivity Detector (TCD).

This type of detector consists of an electrically-heated wire, or thermistor. The temperature of the sensing element depends on the thermal conductivity of the gas flowing around it. Changes in thermal conductivity, such as when organic molecules displace some of the carrier gas, cause a temperature rise in the element, which is sensed as a change in resistance. The TCD is not as sensitive as other detectors but it is non- specific and non-destructive.

The analytical system used in this investigation is shown in figure 3.9 and 3.10. The exit streams of the reactor system are lead into a chromatograph Varian CP 3800 for both quantitative and qualitative analysis. The reactant and permeate product gas analyses were achieved using a 2m-long stainless steel column packed with porapak QS 50-80 mesh and a 2m × 1/8" × 2mm stainless steel column packed with molecular sieve 13x mesh using a thermal conductivity detector figure 3.10. Helium was used as a carrier gas and air was used to activate the gas injection valves.

3.3 GC calibration.

In this study most of the expected reactant and product fluids, apart from H_2O, were calibrated on the GC using a calibration method that was created specifically for this purpose with operating conditions as presented in table 3.1. A specially ordered BOC AV size 144 litres, 12.5 bar, gas mixture cylinder (standard gas) with a proved certificate of analysis containing C_3H_6, CO, CO_2, C_3H_8 , C_2H_4, CH_4 and N at 35%, 20%, 15%, 15%, 5%, 5% and 5%, respectively, was used for the calibration to generate a relationship between peak area for each anticipated component and mole %. With the intention of reducing error in the GC reading and to obtain a reliable result, this GC calibration was repeated on a regular basis.

The GC calibration run was conducted by injecting the standard gas into the GC and comparing the area of obtained peaks and retention times for qualitative and quantitative analysis, respectively. For the identification of CO_2, a Porapak column was used, but all other expected products were analysed using the molecular sieve column. A flame ionisation detector (FID) was used to identify the gases exiting both columns. An example print out of the results obtained for the product gases is presented for data, peak area and mol % in figures 3.12 and 3.13.

In order to minimize errors in the GC readings, two approaches were implemented. In the first, the GC was calibrated on a regular basis. In the second, in order to avoid the expected oscillation in GC performance as an outcome of changes in the environmental conditions, the id of normalization of the peak area was applied.

Table 3.1 Operation conditions of the GC calibration run.

Parameter	Setting
Carrier Gas (He)	40ml min^{-1}
Type of Detector (TCD)	Type 3800
Detector Current	50 mA
Detector Voltage	10 volts
Filament Temperature	150 ºC/ 423.15 ºK
Run Time	20 minutes
Number of Column 2	Porapak QS P& molecular sieve

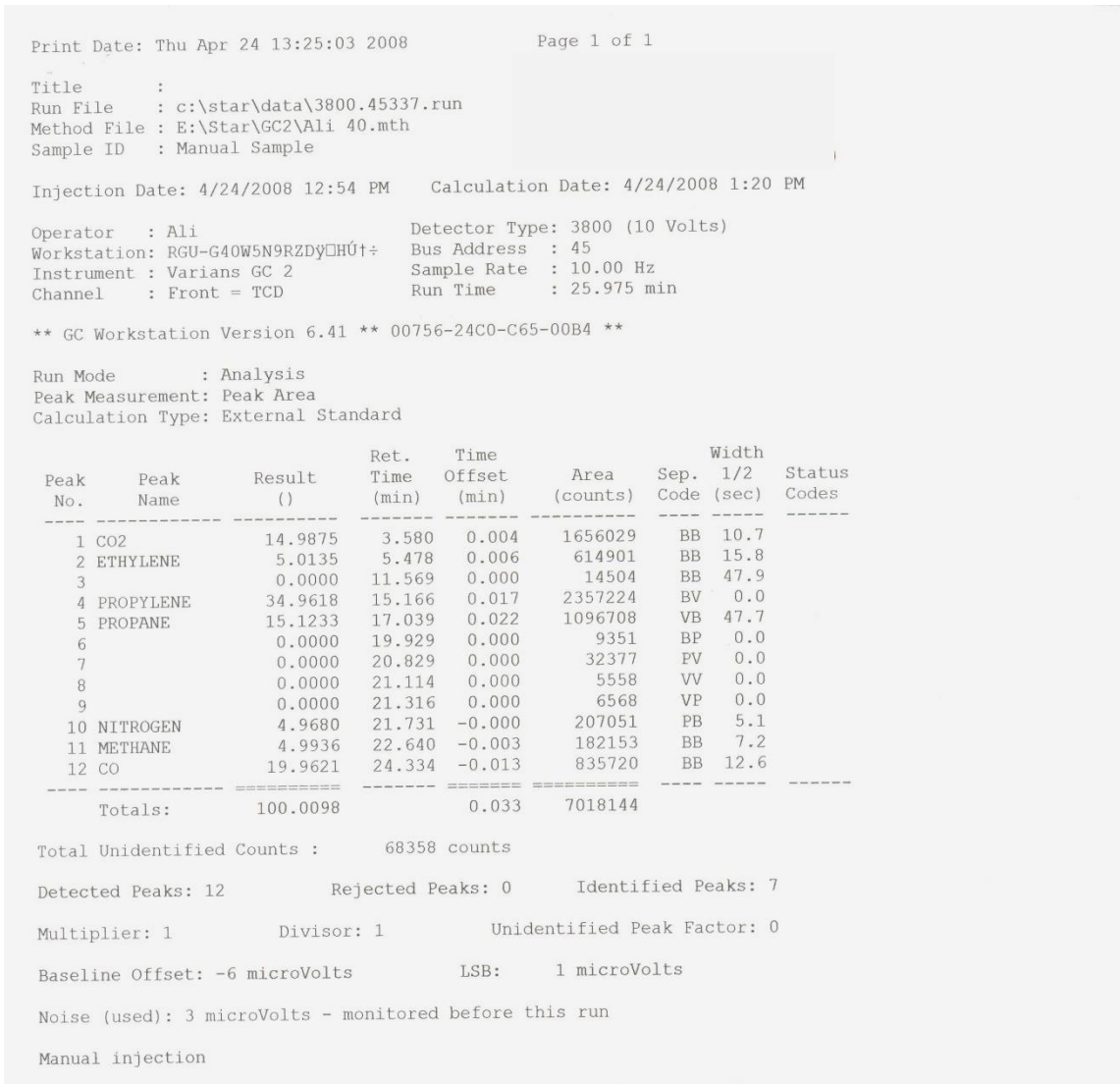

Print Date: Thu Apr 24 13:25:03 2008 Page 1 of 1

Title :
Run File : c:\star\data\3800.45337.run
Method File : E:\Star\GC2\Ali 40.mth
Sample ID : Manual Sample

Injection Date: 4/24/2008 12:54 PM Calculation Date: 4/24/2008 1:20 PM

Operator : Ali Detector Type: 3800 (10 Volts)
Workstation: RGU-G40W5N9RZDÿ□HÚ†÷ Bus Address : 45
Instrument : Varians GC 2 Sample Rate : 10.00 Hz
Channel : Front = TCD Run Time : 25.975 min

** GC Workstation Version 6.41 ** 00756-24C0-C65-00B4 **

Run Mode : Analysis
Peak Measurement: Peak Area
Calculation Type: External Standard

Peak No.	Peak Name	Result ()	Ret. Time (min)	Time Offset (min)	Area (counts)	Sep. Code	Width 1/2 (sec)	Status Codes
1	CO2	14.9875	3.580	0.004	1656029	BB	10.7	
2	ETHYLENE	5.0135	5.478	0.006	614901	BB	15.8	
3		0.0000	11.569	0.000	14504	BB	47.9	
4	PROPYLENE	34.9618	15.166	0.017	2357224	BV	0.0	
5	PROPANE	15.1233	17.039	0.022	1096708	VB	47.7	
6		0.0000	19.929	0.000	9351	BP	0.0	
7		0.0000	20.829	0.000	32377	PV	0.0	
8		0.0000	21.114	0.000	5558	VV	0.0	
9		0.0000	21.316	0.000	6568	VP	0.0	
10	NITROGEN	4.9680	21.731	-0.000	207051	PB	5.1	
11	METHANE	4.9936	22.640	-0.003	182153	BB	7.2	
12	CO	19.9621	24.334	-0.013	835720	BB	12.6	
	Totals:	100.0098		0.033	7018144			

Total Unidentified Counts : 68358 counts

Detected Peaks: 12 Rejected Peaks: 0 Identified Peaks: 7

Multiplier: 1 Divisor: 1 Unidentified Peak Factor: 0

Baseline Offset: -6 microVolts LSB: 1 microVolts

Noise (used): 3 microVolts - monitored before this run

Manual injection

Figure 3.12 GC calibration run result print out.

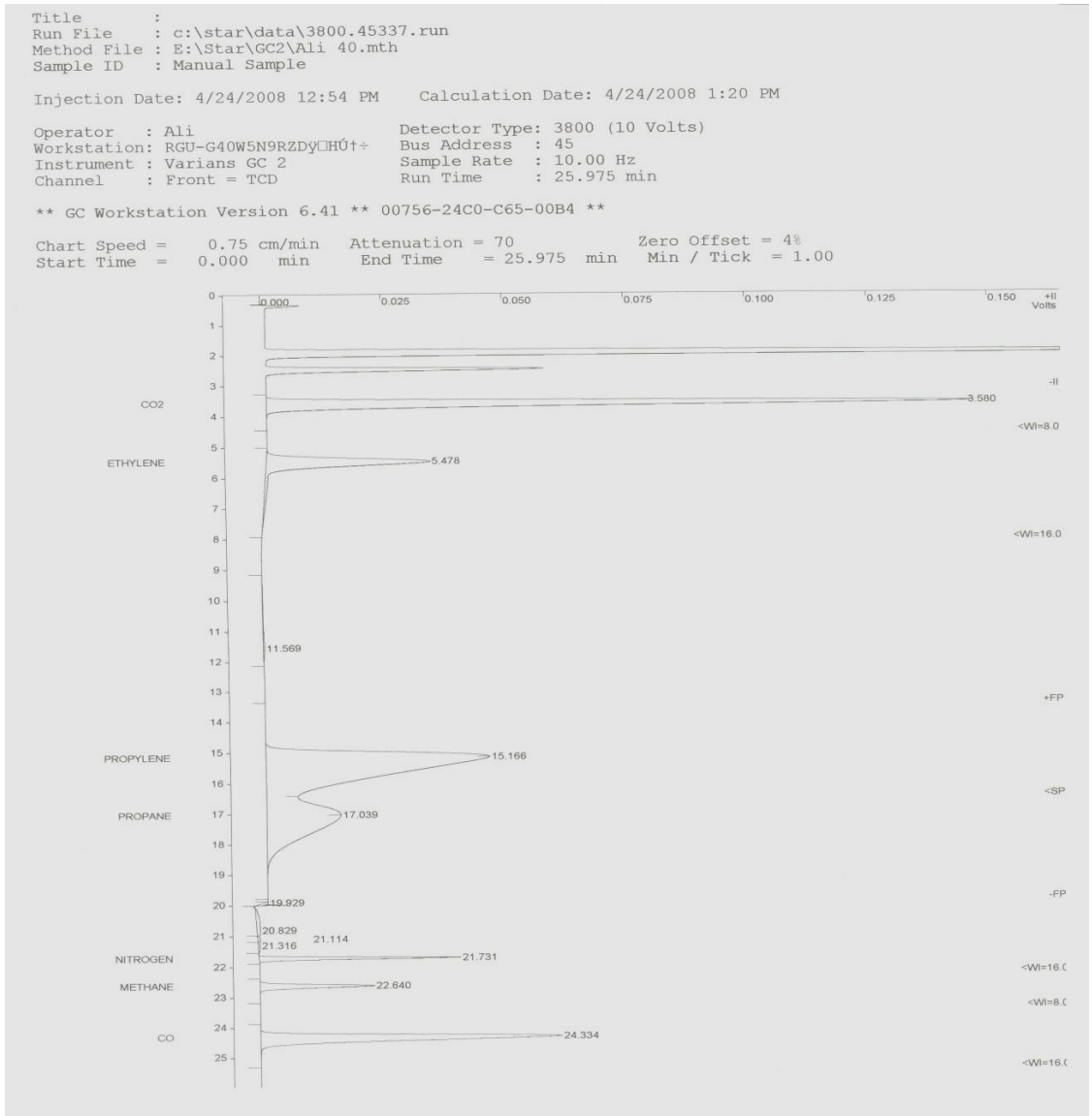

Figure 3.13. An example of the peaks for the calibration runs products.

3.4 Mass flow controller calibration.

One of the most important calibrations needed in this study, was the calibration of the mass flow controllers being used to ensure that the obtained results were accurate and reliable. Each controller was calibrated under the range of anticipated gas flow rates. The calibration was checked from time to time to verify the results obtained for the different gases. Figure 3.14 is selected as an example of a calibration curve for CO_2.

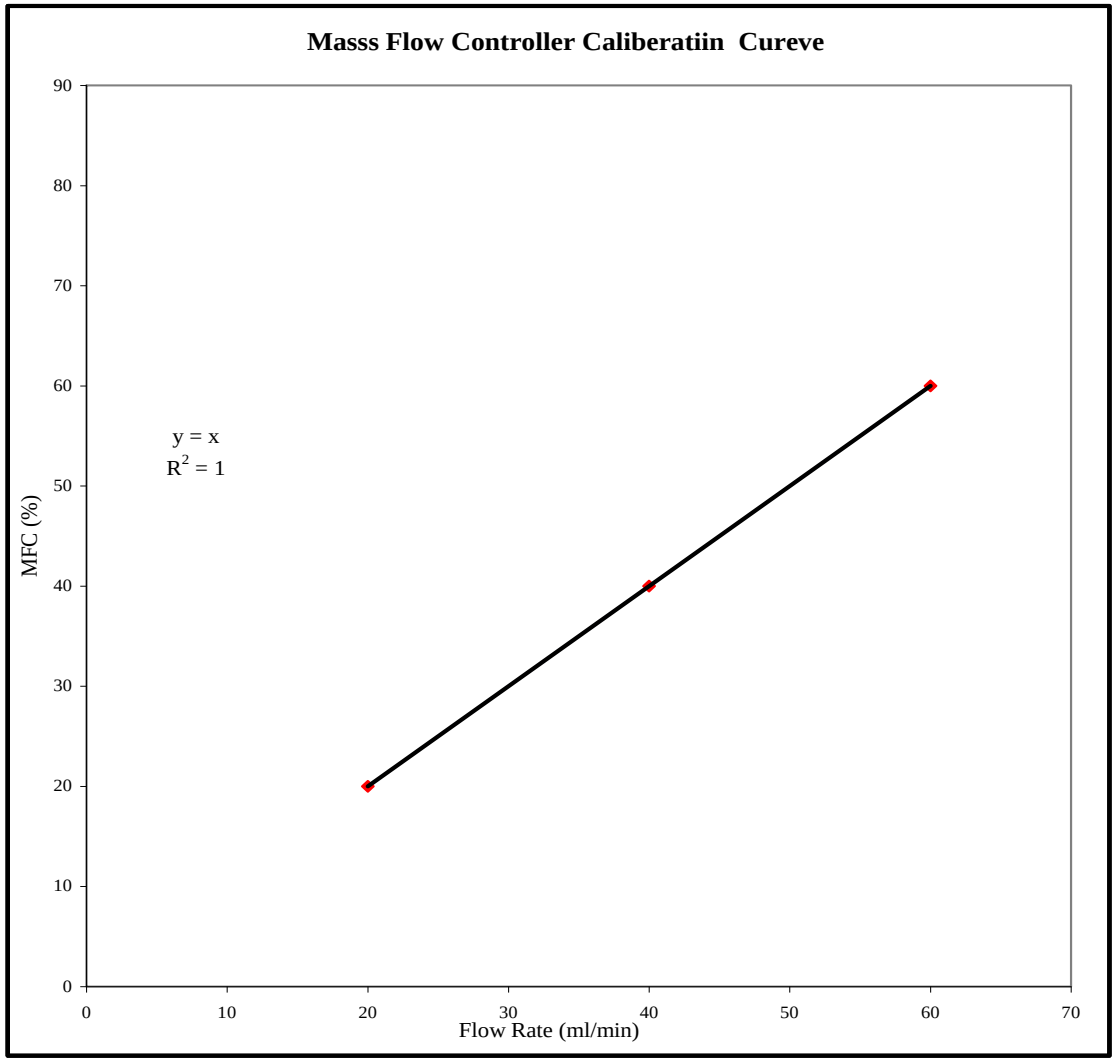

Figure 3.14. Represents mass flow calibration curve for CO_2.

3.5 Materials.

This includes all the items that were used in this research work, including gases, chemicals, reactor heating and wrapping materials, ceramic supports, etc.

3.5.1 Ceramic supports.

All the ceramic supports used in this research study and mentioned earlier, were supplied by *Ceramiques Techniques et Industrials* (CTISA) of France. The supports with an average pore size of 6 microns (based on supplier's information) were selected for this work to enhance the forced pore flow-through (PFT) concept used in these contactor membranes. Such supports could be easily distinguished by the colour of their glazed ends. More detailed information on these supports, including a pictorial view, was presented earlier in this chapter.

Support pore size is known to greatly influence the property and catalytic performance of supported catalysts [49]. Apart from determining the particle and hence the reducibility of the

active metal, the pore size of the support also affects the level of dispersion of the active used material. Permeation tests were thus carried out on supports with different pore sizes impregnated with equal amounts of catalysts in order to determine the most suitable support for the membranes under study.

3.5.2 Choice of promoters.

The choice of promoters for the catalytic membranes was based on the need to improve and enhance their overall activity and selectivity.

3.5.3 Chemicals and associate relevant materials.

The chemicals used in this research study are presented in Table 3.2, and were provided by Sigma-Aldrich. Other materials used with the membrane reactor system, such as HBQ heating, BETEX fabric, GKB heat proof tapes and thermo-reflective insulation materials were provided by Horst-Germany.

Table 3.2 Specifications of chemicals and materials used in this research study.

Chemical and materials	Formula	Application	Grade and Purity
Copper Nitrate	$Cu(NO_3)_2.2.5H_2O$	Catalyst Preparation	> 98%
Nickel Nitrate	$Ni(NO_3)_2.6H_2O$	Catalyst Preparation	> 98%
Palladium Chloride	$PdCl_2$	Catalyst Preparation	> 99 +%
Boehmite	γ -ALO(OH)	Catalyst Preparation	-
Zirconium Oxychloride Octahydrate	$ZrOCl_2.8H_2O$	Catalyst Preparation	> 98%
Hydrogen Chloride Solution	HCl	Catalyst Preparation	
α- Alumina Tubes	Al_2O_3	Support	80nm, 200nm and 6000nm
Anhydrous Sodium Silicate(Silica Gel)	Na_2SiO_3	Moisture Stripper	> 98%
HBQ Heating Tape	-	Used as Heating Tape	2.0m-700 watts T max 900 ºC
Thermo reflective Insulation Materials	-	Used as Heat Isolator	30mm
BETEX fabric Tape	-	Used as Heat Isolator	50mm*2mm T max 900 ºC
GKB Heat Proof Adhesive Tape			
Thermo reflective Insulation Materials	-	Used as Heat Isolator	30mm

3.5.4 Gases.

All the gases used in this work were provided by the British Gas Company BOC Ltd, in high pressure bottles fitted with appropriate pressure gauges and flow regulators. The gas applications and grades are listed in table 3.3.

Table 3.3 Presents applications and specifications of gases.

Gas	Application	Purity
Air	Membrane Cleaning and GC	21% O_2, N_2 Balance
CO_2	Reactant	99.9% High purity
C_3H_8	Reactant	99.9% High purity
C_3H_6, CO, CO_2,C_3H_8, C_2H_4, CH_4 and N_2	GC Calibration (Standard Cylinder)	35%, 20%, 15%, 15%, 5%, 5%, and 5% respectively
H_2	Catalyst Reduction, and GC	99.9% High purity
He	BET surface Area analysis and GC	99.9% High purity
N_2	BET Surface Area Analysis	Liquid

3.6 Catalyst preparation.

It is of great importance that proper steps are followed in preparing any catalyst as they play a key role in industry, as well as in everyday of life. The main function of any catalyst is to increase the rate of the reaction in which it is involved without being highly consumed.

3.6.1 Screening tests.

In this study, a series of trial membranes were prepared using various membrane catalytic solutions. Several reaction runs were then conducted to determine the best catalytic membrane, identify the most adequate inlet parameters and identify the chemical reaction products. Published literature indicates that a possible wide range of available techniques may lead to enhancement of the membrane performance. These include proper support selection, support modification techniques, reactor design and catalyst materials.

3.6.2 Support modification and treatment.

As previously mentioned, and shown in figure 3.7, three ceramic support tubes (i.e. 80nm, 200 nm and 6000 nm) were used in this work as a ceramic support. These consisted of a α-alumina structure washcoated externally with TiO_2 resulting in a composition of ~77% α-alumina and ~23% TiO_2. The outer diameter (od) was ~10mm, inner diameter (id) ~6mm and the wall thickness ~2mm, and with three different average pore size diameters of C80nm, D200nm and E6000nm, as provided by the supplier.

The dry reforming reaction is an endothermic process which requires elevated pressure. One of the best candidates for this process is alumina, due to its ability to be operated at quite harsh conditions for extended periods without losing its reliability, provided that it is modified by calcination, and thermal heating prior to application to guarantee material stability. In order to modify each selected support it was, therefore, first dried in the oven at 473°K/200°C for two hours to get rid of any impurities and H_2O vapour.

The full support modification procedure was as follows:

1. Mix silica-alumina powder with boehmite γ-ALO(OH).
2. Dissolve the mixture in HNO_3 – the total amount of solid in the slurry should be 25% of the total used weight.
3. Pour the mixture into a 200ml graduated cylinder and mix vigorously using a magnetic stirrer that is equipped with a stir bar continuously for 1 hour.
4. Dip-coat the support in the slurry for at least 30 minutes.
5. Slowly blow air through the support to remove excess slurry.
6. Place the support in the oven to dry at 338ºK/65ºC overnight, followed by drying at 363ºK/90ºC for at least 1 hour.
7. Calcine at 823ºK/550ºC for three hours (ramp rate 10ºK/min).
8. Repeat steps 4-7 to obtain the desired amount of washcoat loading (Approximately 25% of the total used weight).

3.6.3 Catalyst preparation method.

The catalyst preparation technique plays an important role in any experimental study. Based on the literature, the most widespread methods of catalyst preparation are Incipient Water Impregnation (IWI) and co-precipitation (CPT). The second method seems to be preferred to a certain extent when a high metal catalyst surface area is required, but the IWI technique is one of the most common methods used for dry reforming catalyst preparation due to its ability to develop a higher mechanical strength and because it can also be used for low metal loading. This method of supported catalyst preparation involves a number of steps that include proper catalyst candidate selection, drying and calcining, which play an important role in both support thermal stability and phase. The catalyst itself is easy to prepare using this technique but it can be difficult to obtain the desired metal loading on the support due to solubility of the metal compounds. This difficulty can be overcome by repeating the process many times until the desired amount of catalyst loading is obtained.

3.6.4 Incipient Wetness Impregnation (IWI) technique.

In the IWI technique, the active metal precursor is dissolved in an aqueous or organic solution. This metal-containing solution is then added to a catalyst support containing the same pore volume as the volume of solution that was added. Capillary action draws the solution into the pores. The catalyst is then dried and calcined to drive off the volatile components within the solution, depositing the metal on the catalyst surface. The maximum loading is limited by the solubility of the precursor in the solution. The concentration profile of the impregnated compound depends on the mass transfer conditions within the pores during impregnation and drying [17].

3.6.5 Catalytic solutions.

A variety of catalytic solutions were prepared for use with the ceramic hybrid tubular membranes used in this research study.

3.6.5.1 Solution SA (Cu-Pd catalyst).

A few grams of palladium chloride ($PdCl_2$) was dissolved in 25ml dilute hydrogen chloride (HCl) in a 200ml beaker under continuous stirring, using a magnetic stirrer for 30 mins. The solution temperature was monitored using a thermometer and kept constant at 50°C by a temperature control switch provided with the heating element base of the magnetic stirrer. The produced solution was added drop-wise to 225ml of another solution containing a few grams of copper nitrate ($Cu(NO_3)_2$) dissolved in deionised water, under vigorous continuous stirring for 1 hour at room temperature. The final solution was kept in a sealed bottle for later use.

3.6.5.2 Solution SB (Zr-Ni catalyst).

This solution was prepared by dissolving a few grams of zirconyl (iv) chloride octahydrate ($ZrOCl_2.8H_2O$) in 25ml of deionised water in a small beaker on a magnetic stirrer under continuous vigorous stirring for 1 hour. The resulting solution was then added drop wise to 225ml of a well-mixed nickel nitrate ($Ni(NO_3)_2$) /deionised water solution. The solutions were kept under continuous stirring for 4 hours at a monitored temperature of 288°K/15°C. The temperature was then raised to 298°K/25°C for 3 hours. The resulting solution was kept in sealed bottle for later use.

3.6.5.3 Solution SC.

This solution was prepared by mixing both solutions SA and SB. This was achieved by pouring solution SA into a 500ml graduated cylinder on a magnetic stirrer under continuous stirring. Solution SB was added gradually and stirred continuously for 1 hour

until a homogenous solution of $PdCl_2$-$Cu(NO_3)_2$ +$ZrCl_2$-$Ni(NO_3)_2$ was obtained.

3.7 Membrane preparation.

The three different pore size ceramic tubular supports selected for this study were nominated as HCMC81, HCMD201 and HCME6001, having a pore size of 80nm, 200nm, and 6000nm respectively. The first three letters (**HCM**) stand for Hybrid Ceramic Membrane, as given by the researcher, the fourth letter (**C**, **D**, or **E**) was specified by the support manufacturer (CTI, France), and the digits that follow refer to the approximate pore diameter in nm with the last digit specifying the number of the membrane from the same support type, as given by the researcher as the research work progressed.

3.7.1 Hybrid Ceramic Membrane HCMC81.

An 80nm support, after modification following the procedure mentioned earlier, was prepared using the following procedure:

1. Air-dried at 65°C for 1 hour and weight noted using a digital scale.

2. Immersed for 30 minutes in a 250ml graduated cylinder containing solution SC, which had already been stirred continuously for at least 1 hour using the magnetic stirrer prior to support immersion.

3. One end of the support was attached to a PFA tube to be held in the catalyst solution by a metal stand, whilst the other end of the support was attached to a PFA tube with a plastic centraliser attached to it to ensure that it would not be damaged while being immersed and pulled out of the solution figure 3.15. Continuous solution stirring was maintained by means of a small stir bar or flea to guarantee catalyst solution homogeneity.

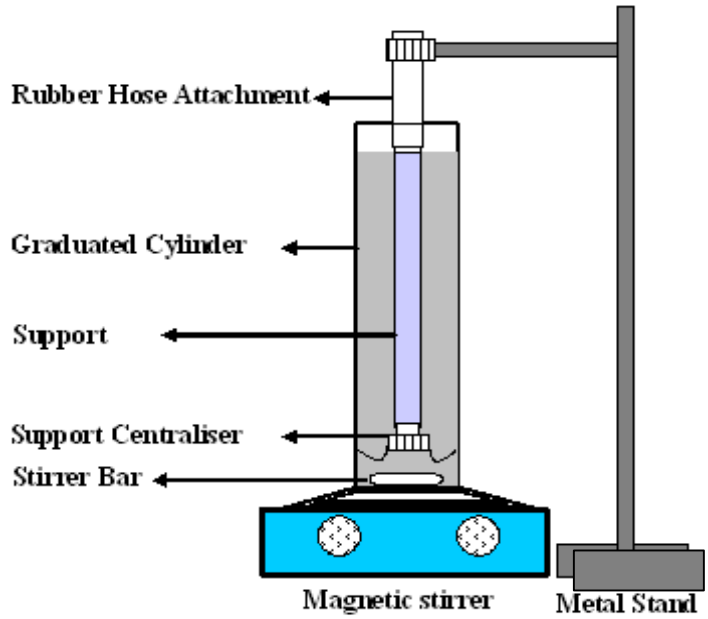

Figure 3.15 Schematic of the membrane preparation IWI stage assembly.

4. The support was then pulled out of the solution and placed on a low-speed DC motor assembly figure 3.16 for evaporation. The motor was kept running at a very low speed for at least 2 hours to ensure that proper vaporisation was established and a uniform catalyst distribution was obtained.

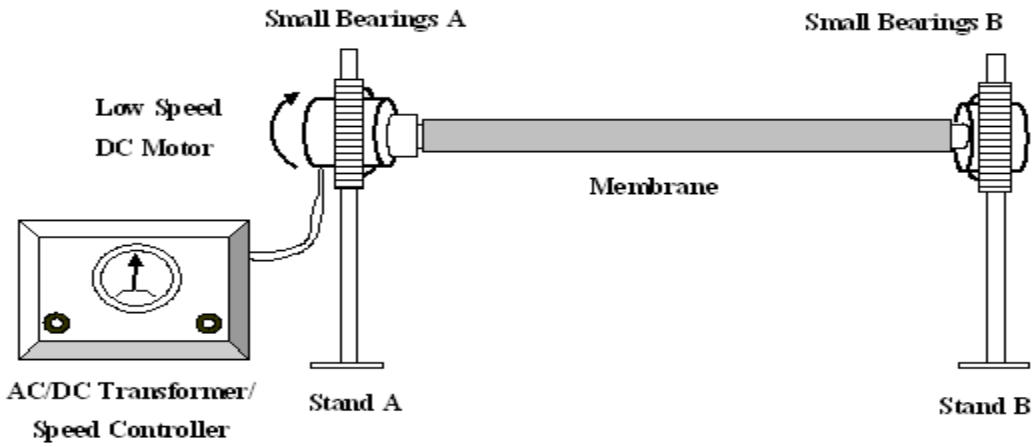

Figure 3.16 Schematic of the membrane vaporisation stage assembly.

5. The resulting membrane was then placed in an oven to be air-dried overnight at 90°C. Following this, it was heat-treated/calcined in the furnace according to the temperature profile shown in figure 3.17. It is important to know the decomposition temperature of all used catalysts/salts in order to determine the final calcination temperature and Table 3.4 shows the decomposition temperature of the salts used in this work. This step in catalytic membrane production leads to the reduction of the metallic oxides produced in the calcination step to the required metal. The effectiveness of this reduction is very important to ensure that the active metal needed for catalysis is produced. All precursor salts and chemical regents used in the study were high purity (98% and above) as supplied by Fisher Scientific and Sigma-Aldrich.

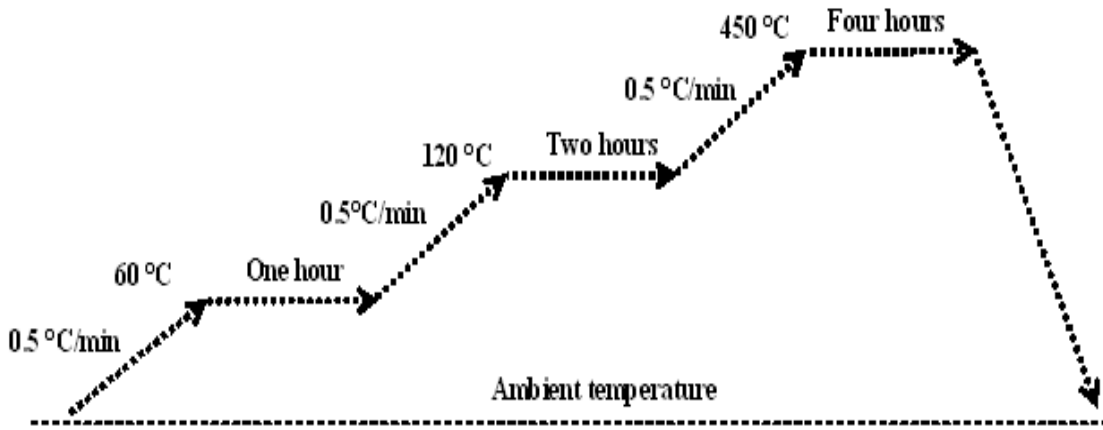

Figure 3.17 Typical calcinations profile in catalyst preparation.

Table 3.4 Decomposition temperature of precursor salts.

Precursor salt	Decomposition temperature (°C)
Nickel nitrat30e[$Ni(NO_3)_2$]	310
Cupper nitrate [$Cu(NO_3)_2$]	200
Palladium Chloride [Pl Cl_2]	518
Zirconium chloride [Zr Cl_2]	437

6. Steps 1-5 were repeated for every membrane till the required membrane catalyst loading amount was achieved.

At this stage the membrane was ready to be placed in the reactor to be exposed to initial testing. In order to define a reaction volume, it was essential to define the region in which permeation was occurring. Assuming high dispersion of catalyst over the surface, the whole permeate membrane volume was considered as reaction volume.

Following the steps above, a membrane such as the one shown in figure 3.18 was obtained. The same steps were followed up to prepare various membranes.

Figure 3.18 Pictorial views showing the fabrication of a membrane (from a fresh ceramic support to metallic composite membrane).

3.8. Safety.

Safety is a very important issue that must be considered in research laboratories. Different types of hazardous materials are present, including gases as well as chemicals and extra care, precautions and proper measures were taken into account when working in the lab.

3.8.1. Safety characteristics of propane.

Propane is non-toxic and so is not harmful to humans or the environment if handled properly. It contains very low levels of Sulphur, is lead free, and has a narrow flammability range. It won't ignite when combined with air unless the source of ignition reaches at least 940° Fahrenheit. If liquid propane leaks from its container, it vaporizes and dissipates into the air, but as it is virtually odourless and colourless in its natural state, a commercial odorant is added so any leaks can be detected.

3.8.2. Safety characteristics of C_3H_6.

C_3H_6 is a colourless and odourless gas that has a specific density of 0.5g/cm^3 at 15°C, and is slightly soluble in water at 100°F. It is very dangerous to humans as it may cause central nervous system disorder that leads to coma and death if inhaled in high enough concentration. It will also cause irritation if in contact with the eye.

3.8.3. Safety characteristics of C_2H_4.

C_2H_4 is a colourless, flammable gas that has a sweet odour and a density of 2.085 kg/m3 in its gaseous state. It is not very soluble in water Like all other hydrocarbons, it is an asphyxiant and combustible, but there is no evidence of it being toxic hence it has been used as an anesthetic.

3.8.4. Safety characteristics of C_2H_6.

At room temperature, CH_4 is a gas that is less dense than air. It melts at 90.15°K and boils at 109.15°K. It is not very soluble in water. CH_4 is combustible, and mixtures of about 5 to 15 percent in air are explosive. CH_4 is not toxic when inhaled, but it can produce suffocation by reducing the concentration of oxygen inhaled. An undetected gas leak could result in an explosion or asphyxiation.

3.8.5. Safety characteristics of hydrogen.

Hydrogen has a specific gravity of -0.0694 so is much lighter than air. It has practically no toxicity except that it may asphyxiate. It has a highly flammable and explosive when exposed to heat, flame, oxidizers, O_2 or chlorine. Its range of flammability in air ranges from 4% to 72%. The small size of the molecule makes containing hydrogen more difficult than larger gaseous molecules.

3.8.6. Safety characteristics of CO.

CO is an extremely dangerous poison, and as it is odourless and tasteless, it gives no warning of its presence. It binds to the hemoglobin in blood to form a compound that is

so stable that it cannot be broken down by body processes. When the hemoglobin is combined with CO, it cannot combine with oxygen, thus destroying the ability of hemoglobin to carry essential oxygen to all parts of the body. Suffocation can occur if sufficient amounts of CO are present to form complexes with the hemoglobin. It is also a dangerous fire hazard when exposed to flame.

3.8.7. Safety characteristics of CO_2.

CO_2 is a colourless and essentially odourless gas that is 1.5 times as dense as air. It is not toxic, although a large concentration could result in suffocation simply by causing a lack of oxygen in the body. CO_2 is also used as a fire extinguisher, because most substances do not burn in it, and it is readily available and inexpensive. Air containing as little as 2.5 percent CO_2 extinguishes a flame.

3.8.8. Safety characteristics of nitrogen.

Nitrogen is considered to be an inert gas that is colourless, tasteless. At standard conditions it constitutes almost 78% by volume of the earth's atmosphere. It is a non-toxic, non-flammable gas. Quick release of nitrogen gas into an enclosed space can dislocate oxygen, and hence represents an asphyxiation hazard unless it is being used as inert replacement for air where oxidation is unwanted. If nitrogen liquid comes into direct contact with the skin, it may cause serious frostbite burns.

3.8.9. Safety characteristics of copper nitrate.

Copper nitrate is a blue crystalline powder that is stable, a very strong oxidant, has a melting point of 114°C, and, if heated, emits fumes of NO_x. It can be very harmful to both humans and the environment. It is particularly harmful to humans if swallowed and may cause burns in contact with the skin and serious irritation to eyes. In solid form, it is a strong oxidizing agent and contact with combustible materials can lead to fire.

3.8.10. Safety characteristics of boehmite.

Boehmite is considered non-hazardous.

3.8.11. Safety characteristics of palladium chloride.

Palladium chloride is a red-brown powder, a weak oxidizing agent that decomposes at high temperature to metallic palladium and chlorine. It is deliquescent and water soluble. It is very hazardous to humans if ingested or inhaled, slightly hazardous when in contact with the skin, and an irritant when in contact with the eye.

3.8.12. Safety characteristics of zirconium chloride.

Zirconium chloride is shiny grey-white in colour, has a high resistance to corrosion, a high melting point and stays hard when very hot. It has a density of 6.5 g/cm^3 (i.e. 6.5 times the density of water). Chloride is hazardous to both environment and humans as it may cause burns.

3.8.13 Safety characteristics of silica gel (moisture stripper).

Silica gel is considered to be non-flammable, non-toxic, and stable with usage, but can cause irritation to both eyes and skin due to contact with dust from silica beads. Some precautions should therefore be taken when the material is being handled.

3.9. Membrane characterization.

It was important to have information on membrane properties to lead to a better understanding of membranes and how to enhance and improve their performance. Information was obtained using a number of characterisation methods, some of which are discussed below.

3.9.1. Scanning Electron Microscopy (SEM).

The SEM generates a finely focused beam of electrons which is made to scan across the sample under inspection. The beam originates from the heating of a tungsten wire filament (thermionic emission), housed in an electron gun at the top of the microscope column. The beam of electrons is accelerated towards the specimen by means of an applied accelerating voltage between the filament assembly and an anode plate. The SEM column and sample chamber are maintained under a high vacuum so the electrons in the beam have an unhindered path between the filament and the sample surface [52].

As the beam travels down the column, it undergoes electron optical demagnification as it passes through two electromagnetic lenses (condenser lenses). Just above the specimen, the beam comes under the influence of a set of scan coils that deflect the beam in a faster pattern across the sample surface. This scanning section is synchronised with the monitor which displays an image of the sample surface. Available magnification may exceed 300,000 xs with a resolution of 3-4nm [53].This compares with a resolution capability of a light microscope of approximately 2550nm.

The equipment used in this study was a Leo model S430 SEM. An example of SEM image of the surface of the support used in this study is shown in figure 3.19.

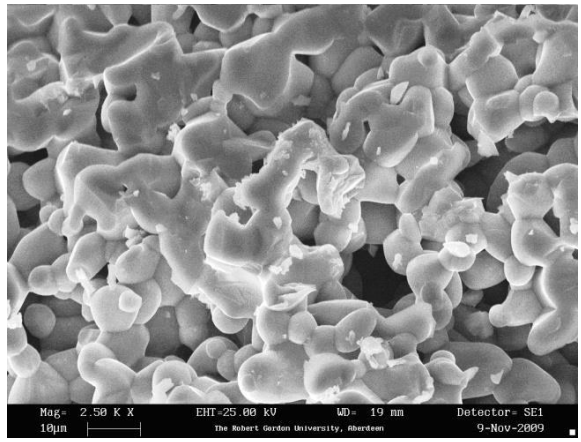

Figure 3.19 SEM **image for ceramic support**.

3.9.2. X-Ray Photoelectron Spectroscopy (XPS).

X-ray Photoelectron Spectroscopy (XPS), also known by the synonym ESCA (Electron spectroscopy for Chemical Analysis), is the method of choice to provide high-resolution compositional material surfaces [50]. XPS identifies all elements, except H_2 and He, present in the outer 10 nanometres of a surface at concentrations exceeding 0.1 atomic percent. It determines the approximate surface composition (10%) semi- quantitatively, and also gives bonding information and molecular environments (oxidation states, bonding partners) in surface zone[50] XPS is based on photoemission of core level electrons in an atom. Incident X-rays with energy, usually monochromatic on modern systems, liberate core-level electrons with sufficient kinetic energy to escape from the material and pass through the vacuum chamber to the energy spectrum analyser.

In this work, the XPS was used mainly for quantitative and qualitative compositional surface analyses. The equipment used was a Kratos Axis Hsi 5 channel imaging x-ray photoelectron spectrometer using monochromated AlK (alpha) radiation.

3.9.3. Accelerated Surface Area and Porosimetry analysis (ASAP).

In order to characterise the surface of the porous catalytic membrane, pore volume, pore diameter and surface area were computed. Nitrogen adsorption of the samples was measured at –195.8ºC (77.35ºK) with an ASAP 2010 micrometrics apparatus. A pictorial view of this apparatus is shown in figure 3.20. Prior to taking measurements, the samples were degassed at 673.15ºK over night, at a pressure less than 1.4Pa.

For a better understanding of the techniques used to compute the surface area, pore volume, and pore diameter, a brief description of the different theories is presented below. Brunauer *et.al*. [54] Carried out a derivation of the isotherm equation for

multimolecular adsorption by a method that is a generalisation of Langmuir's treatment of the unimolecular layer. The assumption was that the same forces that produce condensation are chiefly responsible for the binding energy of multimolecular adsorption. As nitrogen is a non-polar gas, and assuming the samples analysed are not ionic, the DeBoer and Zwicker's method, which assumes dipole formation for adsorption calculation, is not used in this work. Instead, the BET method has been adopted.

Considering Shull's assumption that states the BET thickness became much larger than the experimental thicknesses for flat surfaces in the high pressure region, the BJH technique [7] for estimating the volume of porous materials was also used. This technique was developed to deal with relatively coarsely porous materials exhibiting a wide range of pore sizes, but the procedure appears to be applicable to porous solids of any nature.

Burret *et.al*. [7] Carried out a formal analysis of the relationship between nitrogen desorption isotherms at liquid nitrogen temperatures and the distribution of pore volume and area with respect to the pore radius. It was assumed that the equilibrium between the gas phase and the adsorbed phase during desorption is determined by two mechanisms: (1) physical adsorption *on* the pore walls (which would occur to the sa me extent whether the area involved constituted a wall of pores or a flat surface impenetrable to nitrogen), and (2) capillary condensation in the inner capillary volume [7].

The experimental values of the volume of nitrogen adsorbed in cm^3 STP/g of adsorbent, obtained as a function of the relative pressure (P/Po), may be transformed to functions of thickness of the multimolecular layer of adsorbed nitrogen. By plotting the volume of adsorbed nitrogen for an unknown sample as a function of the experimental thickness, a straight line is obtained as long as the multilayer is formed unhindered. The straight line goes to the origin and its slope is a measure of surface area. The surface area will not be exactly equal to the BET surface area, as the BET equation depends on the sample. This plot is a t-plot, independent of the nature of the sample [55]. As the adsorption behaviour of nitrogen depends on the surface characteristics and on the pore diameter, both of which can change during membrane preparation, the results of nitrogen adsorption have to be interpreted with much caution. It must also be taken into account that the values of the surface and the pore volume are referenced to the sample weight. Nonetheless, the BJH method is usually adopted as the standard method for pore size determination and is well suited to analyse trends in similar samples [56].

Figure 3.20 Pictorial views of the ASAP 2010 Micrometrics apparatus.

An example of the values obtained for the pore structure of the original alumina tube is:

Surface area [m^2/g]

Single point 99.50

BET 260.9962

BJH 181.4751

Pore volume [cm^3/g]

Single point 0.213349

BJH 0.195347

Pore size (diameter) [nm].

Average BET 3.2698

BJH 4.3057

It should be pointed out that the ASAP 2010 apparatus is only capable of determining the pore diameter of materials that have a pore diameter between 0-200nm. This meant it could be used for the characterization of the HCMC81 and HCMD201 membranes used in this study. An example of a print out from the ASAP 2010 for C80nm fresh support material sample is shown in figure 3.21.

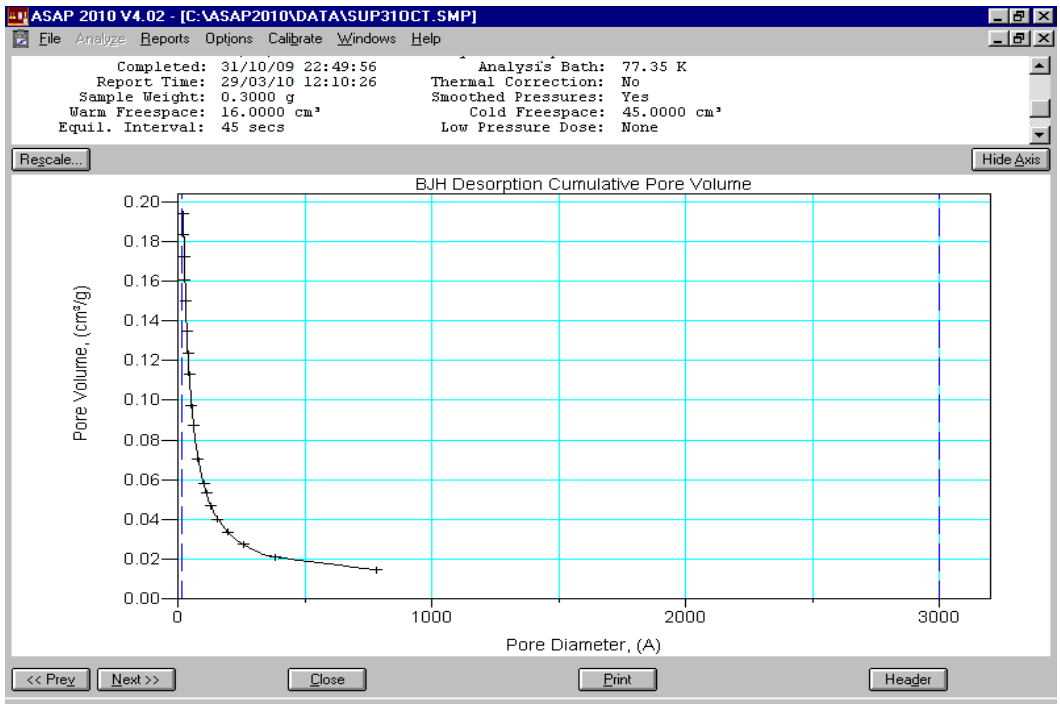

Figure 3.21 A typical print out from the ASAP 2010 Micrometrics apparatus for a fresh ceramic support C80nm material sample.

3.9.4. Energy Dispersive X-ray Analysis (EDXA).

As the SEM uses a high energy electron beam to illuminate a specimen, one of the by-products is the generation of x-rays as primary beam electrons interact with specimen electrons. The production of x-rays occurs in two basic ways. As an electron in the primary beam enters the volume of a specimen atom, it can be scattered inelastically in various ways. Primary electrons may slow down by interaction with forces present within the volume of an atom resulting in the electron giving up energy. This energy loss can be accomplished by the emission of x-ray radiation. This type of radiation is known as braking radiation and is observed as a continuous spectrum. This continuous spectrum is regarded as background radiation for EDXA spectrometers.

Inelastic scattering also occurs due to collisions between primary electrons and electrons within specimen atoms. The consequent rearrangement of electrons within electron shells, as atoms strive to reach their lowest energy states, results in the release of energy in the form of x-ray photons. As the energy of these photons is related to the energy between electron shells, the x-ray photons are characteristic of the element present in the specimen. By collecting and analysing these x-rays, qualitative and quantitative information about the component elements of a specimen may be obtained [53]. The additional hardware required to detect and measure the energy of the characteristic x-rays was a Link exL2 EDXA system (Oxford Microanalysis Group). A

typical Elemental composition based on Energy Dispersive X-ray Analysis (EDXA) for C80 fresh support material sample is shown below in figure 3.22.

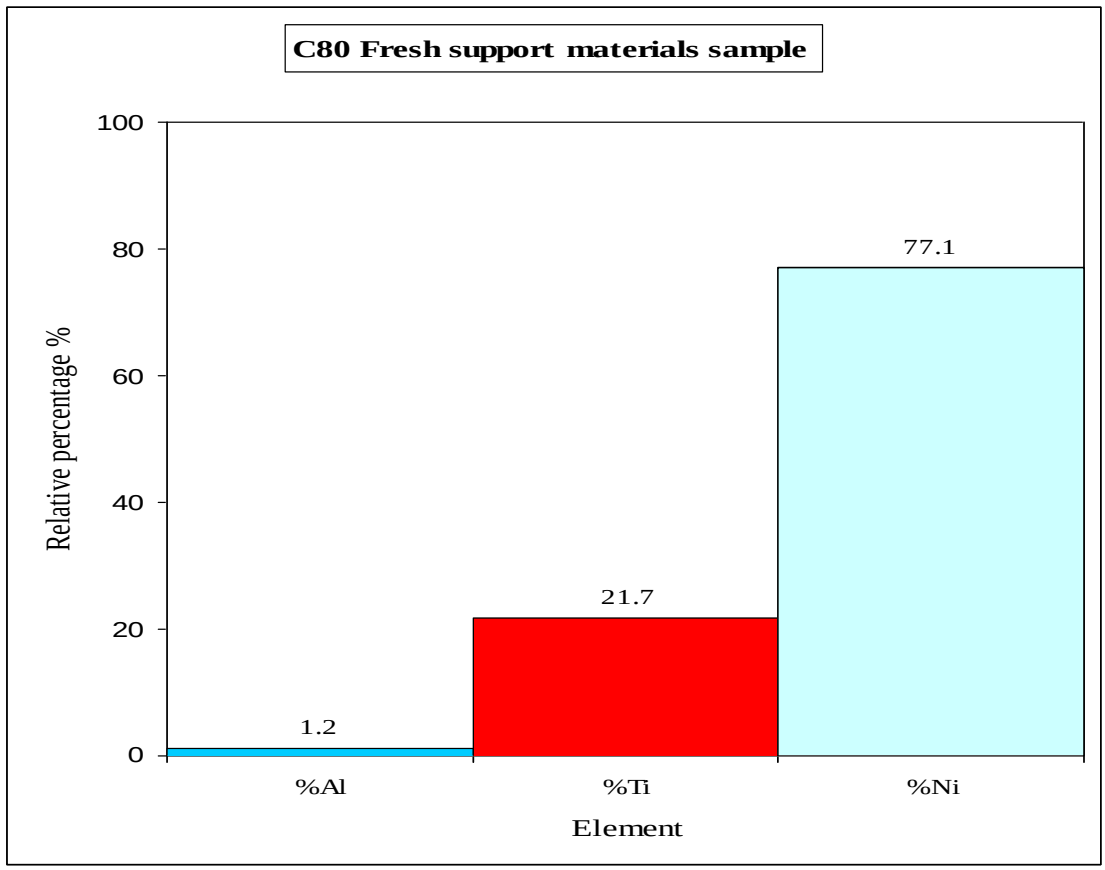

Figure 3.22. A typical print out of 'Elemental composition based on Energy Dispersive X-ray Analysis (EDXA)' for C80 fresh ceramic support sample.

3.9.5 Flux characterization.

Flux characterization involves studying and analysing gas mass transport mechanisms through the catalytic membranes. As for organic membrane supports, basic flux characterization studies suggest two types of analysis. In the first, the capability of such catalytic membranes, and how they respond as different gas and gas mixtures permeate through them, is examined. Subsequent results can lead to the determination of average pore size of the membrane support. These estimated values can be used for comparison with that obtained (observed) from SEM micrographs. Extra time was spent on these results, and they are presented in the results and discussion chapter later in this thesis.

3.10 The membrane test run.

As shown in figure 3.2, the temperature of the reactor system was gradually raised to the expected reaction temperature by means of the power controller with an inert gas such as argon flowing through both the shell and tube side of the reactor at a very low flow rate of 50ml/min. Once the desired reaction temperature was reached (i.e. 873.23°K/600°C, 923.23°K/650°C or 973.23°K/700°C), the flow of argon gas was stopped and a flow of hydrogen at 100ml/min was run for 2 hours to reduce the catalyst. The dry reforming reaction test run was then initiated by introducing the reactant gases to the reactor via the gas mixing chamber, at the pre-determined flow rate, through the shell side by slowly opening valve V_1 with propane. The pressure on the shell side of the reactor (reaction side) was adjusted using a back-pressure regulator. Meanwhile, the tube side (permeate side) was kept at atmospheric pressure and the flow passed through the cold trap, then through the moisture trap to the analysis system (i.e. the GC).

Once proper experimental operating conditions were established and the reaction steady state was reached, the experiment was kept running for 2-3 hours. The reaction products were fed into the GC for identification and monitoring. The products typically consisted of C_3H_6, C_2H_6, C_2H_4, CH_4 and CO, plus the unreacted CO_2 and C_3H_8 reactant fed gases, and the H_2O that was stripped out in the cold trap and the moisture capture unit. To confirm those results were accurate and reliable; the experiment was repeated several times based on a daily experimental run of 6 hours. The membrane test run results are presented in the results and discussions chapter.

3.11 The membrane test experimental procedure/GC calibration procedure.

The analytical system used in this research comprised the water trap and the gas chromatograph which was equipped with a thermal conductivity detector (TCD). A calibration method was devised in which the oven temperature was maintained at 423.15°K/150°C for a pair of stainless steel columns packed with porapak QS and molecular sieve, respectively. The relevant retention times for the product gases were recorded and compared to those of the standard gas (standard cylinder). Standard gas was used for calibrating the GC regularly before each run. In this research, the main variables that were under investigation were the feed ratio for both CO_2 and propane, the temperature and total feed rate of the reaction, and the pressure at which the reaction takes place. After selecting the membrane to be used, an experiment plan was drawn up incorporating the different variables (see table 3.6).

Table 3.5. Summary of the various kinetic runs.

First set of kinetic runs (1-5)						**Second set of kinetic runs (6-10)**					
Pressure 0.05 [bars]	Run 1	Run 2	Run 3	Run 4	Run 5	Pressure 1.0 [bars]	Run 6	Run 7	Run 8	Run 9	Run 10
Temperature [°K]	823.15 923.15 973.15	823.15 923.15 973.15	823.15 923.15 973.15	923.15	923.15	Temperature [°K]	823.15 923.15 973.15	823.15 923.15 973.15	823.15 923.15 973.15	923.15	923.15
C_3H_8 feed flow rate[ml/min]	50	100	150	100	200	C_3H_8 feed flow rate[ml/min]	50	100	150	100	200
Ratio	1:1	1:1	1:1	1:2	2:1	Ratio	1:1	1:1	1:1	1:2	2:1
CO_2 feed flow rate[ml/min]	50	100	150	200	100	CO_2 feed flow rate[ml/min]	50	100	150	200	100
Ratio	1:1	1:1	1:1	1:2	2:1	Ratio	1:1	1:1	1:1	1:2	2:1
Total feed flow rate [ml/min]	100	200	300	300	300	Total feed flow rate [ml/min]	100	200	300	300	300

Third set of kinetic runs (11-15)						**Fourth set of kinetic runs (16-20)**					
Pressure 2.0 [bars]	Run 11	Run 12	Run 13	Run 14	Run 15	Pressure 3.0 [bars]	Run 16	Run 17	Run 18	Run 19	Run 20
Temperature [°K]	823.15 923.15 973.15	823.15 923.15 973.15	823.15 923.15 973.15	923.15	923.15	Temperature [°K]	823.15 923.15 973.15	823.15 923.15 973.15	823.15 923.15 973.15	923.15	923.15
C_3H_8 feed flow rate[ml/min]	50	100	150	100	200	C_3H_8 feed flow rate[ml/min]	50	100	150	100	200
Ratio	1:1	1:1	1:1	1:2	2:1	Ratio	1:1	1:1	1:1	1:2	2:1
CO_2 feed flow rate[ml/min]	50	100	150	200	100	CO_2 feed flow rate[ml/min]	50	100	150	200	100
Ratio	1:1	1:1	1:1	1:2	2:1	Ratio	1:1	1:1	1:1	1:2	2:1
Total feed flow rate [ml/min]	100	200	300	300	300	Total feed flow rate [ml/min]	100	200	300	300	300

The kinetic studies were carried out under conditions of constant catalyst load. In total, four kinetic sets were conducted containing 20 runs. The variables were pressure (0.05, 1, 2, or 3 bars), flow rate (100, 200 or 300 ml/min), gas feed ratio (1:1, 1:2 or 2:1), and temperature (823.15°K/600°C, 923.15°K/650°C, and 973.15°K/700°C).

The first set of kinetic runs (1-5) included:

1- Pressure maintained constant at 0.05bar, gas fed flow rate maintained at 100ml/min at a ratio of 1:1, and temperature was varied (an average of 5 measurements was taken).

2- Pressure maintained constant at 0.05bar, gas fed flow rate was increased to 200ml/min at a ratio of 1:1, and temperature was varied (an average of 5 measurements was taken).

3- Pressure maintained constant at 0.05bar, gas fed flow rate was increased to 300ml/min at a ratio of 1:1, and temperature was varied (an average of 5 measurements was taken).

4- Both temperature and pressure were maintained constant at 0.05bar and 923.15°K respectively, gas fed flow rate was maintained constant at 300ml/min but the fed ratio was varied to 1:2 (an average of 5 measurements was taken).

5- Both temperature and pressure were maintained constant at 0.05 bar and 923.15°K respectively, gas fed flow rate was maintained constant at 300ml/min but the fed ration was varied to 2:1 (an average of 5 measurements was taken).

In the second set of kinetic runs (6-10), the pressure was increased as follows:

6- Pressure maintained constant at 1.0bar, gas fed flow rate maintained at 100ml/min at a ratio of 1:1, and temperature was varied (an average of 5 measurements was taken).

7- Pressure maintained constant at 1.0bar, gas fed flow rate was increased to 200ml/min at a ratio of 1:1, and temperature was varied (an average of 5 measurements was taken).

8- Pressure maintained constant at 1.0bar, gas fed flow rate was increased to 300ml/min at a ratio of 1:1, and temperature was varied (an average of 5 measurements was taken).

9- Both temperature and pressure were maintained constant at 1.0bar and 923.15°K respectively, gas fed flow rate was maintained constant at 300ml/min but the fed ratio was varied to 1:2 (an average of 5 measurements was taken).

10- Both temperature and pressure were maintained constant at 1.0bar and 923.15°K

respectively, gas fed flow rate was maintained constant at 300ml/min but the fed ratio was varied to 2:1 (an average of 5 measurements was taken).

In the third set of kinetic runs (11-15), the pressure was increased again as follows:

11- Pressure maintained constant at 2.0bar, gas fed flow rate maintained at 100ml/min at a ratio of 1:1, and temperature was varied (an average of 5 measurements was taken).

12- Pressure maintained constant at 2.0bar, gas fed flow rate was increased to 200ml/min at a ratio of 1:1, and temperature was varied (an average of 5 measurements was taken).

13- Pressure maintained constant at 2.0bar, gas fed flow rate was increased to 300ml/min at a ratio of 1:1, and temperature was varied (an average of 5 measurements was taken).

14- Both temperature and pressure were maintained constant at 2.0bar and 923.15°K respectively, gas fed flow rate was maintained constant at 300ml/min but the fed ratio was varied to 1:2 (an average of 5 measurements was taken).

15- Both temperature and pressure were maintained constant at 2.0bar and 923.15°K respectively, gas fed flow rate was maintained constant at 300ml/min but the fed ratio was varied to 2:1 (an average of 5 measurements was taken).

In the final set of kinetic runs (16-20), the pressure was increased to 3.0bars and includes the following:

16- Pressure maintained constant at 3.0bar, gas fed flow rate maintained at 100ml;min at a ratio of 1:1, and temperature was varied (an average of 5 measurements was taken).

17- Pressure maintained constant at 3.0bar, gas fed flow rate was increased to 200ml/min at a ratio of 1:1, and temperature was varied (an average of 5 measurements was taken).

18- Pressure maintained constant at 3.0bar, gas fed flow rate was increased to 300ml/min at a ratio of 1:1, and temperature was varied (an average of 5 measurements was taken).

19- Both temperature and pressure were maintained constant at 3.0bar and 923.15°K respectively, gas fed flow rate was maintained constant at 300ml/min but the fed ratio was varied to 1:2 (an average of 5 measurements was taken).

20- Both temperature and pressure were maintained constant at 3.0bar and 923.15°K respectively, gas fed flow rate was maintained constant at 300ml/min but the fed ratio was varied to 2:1 (an average of 5 measurements was taken).

3.11.1 Membrane reactor operation kinetic runs explained.

Once the experimental rig was set up as required, the concerned membrane was placed in the reactor and the fed reactant gas cylinders were connected to the reactor system. The power supply for the heating tape was switched on and observed using the digital thermometer that was attached to thermocouples 1, 2 and 3, located in various places along the entire membrane reactor heating zone. The temperature was set to 573.15°K/300°C and as the temperature reached the set value a stream of hydrogen was introduced at a flow rate of 100-150ml/min to both shell and tube side of the reactor system to reduce the catalyst and activate the membrane. The permeate outlet was put into a beaker full of water as a safety precaution measure and the apparatus was left running for at least 3 hours. A standard sample was injected directly into the analytical system (GC) in order to check the apparatus pre-calibration. If the retention times and composition of gases did not match to the initial calibration, maybe due to different atmospheric operation conditions, a new calibration became necessary at this stage and was carried out. After the calibration was complete, the pre-determined feed flow rates of both reactant gases (C_3H_8 and CO_2) were set according to the chosen run using the digital mass flow controller and passed to the shell-side through V1 figure 3.1 via the gas mixing chamber system. The heating of the reactor was increased to the desired set temperature value by means of the power controller. A steady temperature was reached when several readings from the reactor were found to be constant. The digital thermometer was monitored and the attached thermocouples 1, 2, 3, and 4 alternated via the thermocouple selector. Once the temperature of the heating tape used in the system was stabilised the system was allowed to run for an hour or so. When stabilization was attained, analysis of the reaction products would start and they would be sent to the analytical system (GC) after the pressure across the membrane system was set as required by gradually closing the valve V3 located on the product stream outlet, passing it through the cold trap system and the H_2O trap. More kinetic runs were conducted to determine the activity of the catalyst, which seemed to initially decrease, but then reach a steady value after a few runs.

The membrane reactor run tests were repeated with varied feed composition, flow rate, operating pressures and temperatures according to the schedule in Table 3.6. Each run was allowed to stabilize after checking and adjusting the various parameters. The reactant products were then sent to the GC for analysis.

Once product analysis was complete, the reactant gas cylinder supplies were closed and

the heating tape system shut down by turning off the power supply. At this stage the fed gas was replaced by an inert gas, either nitrogen or argon, at a flow rate of 100ml/min for a few hours to purge or cool down the reactor system until it approached room temperature. Simultaneously, all the associated electronic systems were also switched off.

3.12 Initial membrane test results.

Preliminary test results for the three prepared catalytic membranes, HCMC81, HCMD201, and HCME6001, are presented in Table 3.6. The results demonstrate that it is indeed possible for the dry reforming reaction to take place as some conversion of the fed gases was observed and some product GC peaks for different gases were observed. Unfortunately, at this trial phase of the experimental tests for the membranes, it was difficult to detect the extent the GC gas peaks. As the work progressed, however, it was possible at a later stage to detect the presence of water in the cold trap plus some other reaction gas products such as C_3H_6, C2H4, C_2H_6, CH_4 and CO via the GC analytical system.

3.12.1 Discussion.

Results from the initial test runs on the initially prepared membranes were not easily attained. This was due at first to a lack of experience in operating the different sections of the experimental set up. Secondly, the equipment was not accurately calibrated. It was, however, considered important to obtain qualitative analysis of the reactant products at this stage because these initial results allowed the set up of the experimental rig to be optimised.

3.12.2 Conclusion.

Initial conclusions suggest that the catalyst produced good results for the purpose for which it was designed, and seemed to be promising under this reaction as more preliminary result tests were conducted to check the working conditions of the catalyst testing unit. Prior to catalytic testing, blank reaction tests were performed without catalysts to determine the activity of the reactor and its accessories. To achieve the desired experimental aims, more time and effort should be devoted to further understanding of the different experimental rig sections in order to use them effectively. The equipment also requires regular calibration to gain the best outcome. The best experimental operating conditions need to be selected - flow rate, pressure and temperature, and this can only be done more work and trials are first carried out.

Table 3.6 Presents some membrane initial test results.

Membrane	Reactant fed gases	Reaction products	GC ret result %
HCMC81	Propane (C_3H_8) Carbon Dioxide (CO_2)	Propylene (C_3H_6)	0.8
		Ethylene (C_2H_6)	0.3
		Ethane (C_2H_4)	0.2
		Methane (CH_4)	0.1
		Carbon monoxide (CO)	2.2
		Propane (C_3H_8)	47.0
		Carbon dioxide (CO_2)	49.0
HCMD201	Propane (C_3H_8) Carbon Dioxide (CO_2)	Propylene (C_3H_6)	1.4
		Ethylene (C_2H_6)	2.0
		Ethane (C_2H_4)	1.3
		Methane (CH_4)	0.7
		Carbon monoxide (CO)	3.0
		Propane (C_3H_8)	45.0
		Carbon dioxide (CO_2)	46.0
HCME6001	Propane (C_3H_8) Carbon Dioxide (CO_2)	Propylene (C_3H_6)	4.0
		Ethylene (C_2H_6)	3.0
		Ethane (C_2H_4)	2.0
		Methane (CH_4)	1.5
		Carbon monoxide (CO)	6.0
		Propane (C_3H_8)	42.0
		Carbon dioxide (CO_2)	41.0

Chapter Four

Results and Discussion

CHAPTER 4: Results and Discussion

4.1 Membrane reactor characteristics, performance and stability.

Since the dimensions of the steel membrane reactor used in this study were lab-scale, the catalyst beds employed were also small so that a reasonable approach to isothermal conditions could be obtained. When higher conversions were required, the amount of catalyst involved usually increased. The temperature was recorded by means of three different thermocouples placed along the length of the reactor and a fourth placed inside the membrane reactor as described in the experimental section. It was important to assess the magnitude of the temperature gradients in the bed when significant conversions were reached. Figure 4.1 shows temperature profile along the permeation zone.

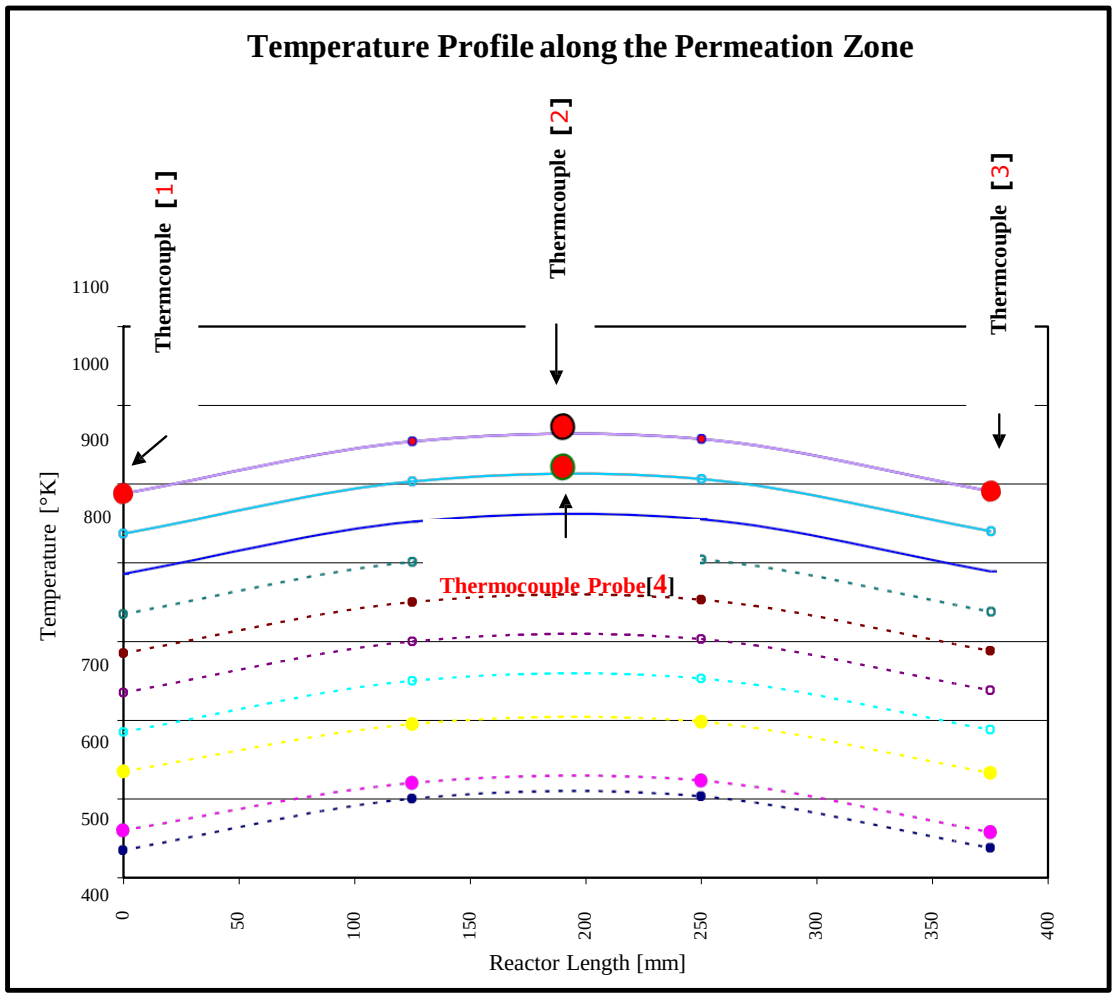

Figure 4.1 The membrane reactor temperature profile along the permeation zone.

The profile indicates that the temperatures along the reactor seemed to be higher in the middle (detected by thermocouple 2) than at the upper and lower ends of the reactor (detected by thermocouples 1 and 3). The highest temperature was detected by thermocouple 4, as was expected, possibly due to the influence of the gas reaction operation. The temperature profile shows that over the length of the main reaction area, between the first and second thermocouple, the temperature was roughly constant. The lower temperature at both extremities can be explained by the limits of the heat insulation system and also by the heat exchange between the reactor and the feed gases.

4.2 Membrane catalyst loading and their activities.

In this study, it was found that one of the most important factors that influenced the amount of catalyst that could be loaded onto any ceramic support was the type of loading technique being used. Figure 4.2 represents a plot of weight of membrane versus the number of **I**ncipient **W**etness **I**mpregnations (IWI) conducted. The amount of catalyst loaded almost doubled when a low speed (d/c) motor was used instead of the conventional dip coating technique. The amount of catalyst membrane gain was calculated by weighing the support before and after each IWI step. The steps were repeated until there was no weight gain observed, at which stage it was assumed that all the support was filled with catalyst. Catalyst loading increased from 4.113g to 8.605g giving a substantial increase in %wt of catalyst loading – an improvement of almost 52% for the HCME6001 membrane. The low speed rotation of the membrane support meant that the catalyst remained on the support instead of draining off due to gravity. A similar improvement was obtained for the other two membranes. The HCMC81 membrane showed catalyst loading increasing from 2.801g to 3.421g with a %wt catalyst loading improvement of almost 8.0%, and the HCMD201 membrane showed an increase from 3.451g to 4.802g with %wt of catalyst loading improvement of 28% (see Appendices 2 and 3).

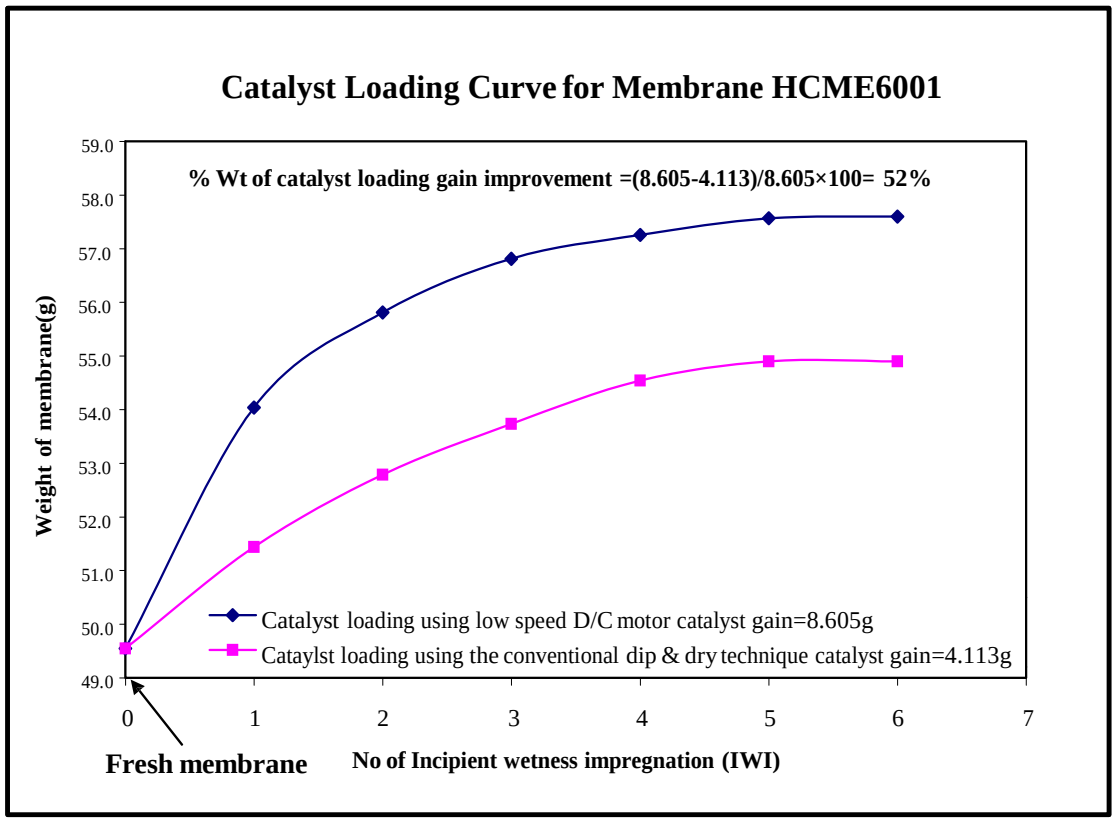

4.2 Catalyst [$PdCl_2$-Cu $(NO_3)_2$ + $ZrCl_2$-Ni $(NO_3)_2$] loading curve for membrane HCME6001.

The activity of the catalyst, however, always depends on various factors, one of which is the preparation method, the nature of the support used, type of metal used, and so on. Most researchers have used the IWI technique to prepare metal supported catalysts. The majority of the group VIII metals (Ru, Rh, Ni, Pd, Pt, Ir ,Co and Fe) have been found to be very useful in the dry reforming reaction. Noble metals were, in fact, found to be more active and stable than Ni [40].

4.3 Membrane characterization.

Membrane characterization is an important procedure that involves various available techniques to confirm its performance in terms of mechanical, chemical and thermal stability, pore size, and pore size distribution. Such techniques may include Scanning

Electronic Microscopy (SEM), Accelerated Surface Area and Porosimetry (ASAP), Energy Dispersive X-Ray Analysis (EDXA), X-ray photoelectron spectroscopy (XPS) and single gas mass transport flux measurements through the catalytic membrane.

4.3.1 Scanning Electron Microscope (SEM) analysis.

The SEM technique was used in this study to provide details of the pore structure of the membrane as it is went through different modifications, and enabled broader characterizations to be achieved. Figure 4.3 shows SEM images for membrane HCME6001. Figure 4.3(A) is a plan view and 4.3(B) a cross sectional area of a fresh unmodified 6000nm support shows a reasonably uniform pore distribution. Figures 4.3(C) and (D) show SEM images for the surface and cross-sectional area of the support after being dip- coated three times in the [$PdCl_2$-Cu $(NO_3)_2$ +$ZrCl_2$-Ni $(NO_3)_2$] catalyst (SC) solution, and figures 4.3(E) and (F) show the same after five dip-coatings.

Scanning electron microscopy (SEM) confirms the observations from the nitrogen adsorption characterization, presenting in a pictorial view the modifications to the crystal structures in the various steps during the membrane preparation.

γ-alumina modification is clearly visible on the inner pore structure. The increase in pore diameter is clear, confirming the ASAP for monolayer analysis (BET).

The effectiveness of the first two catalysts (i.e. $PdCl_2$-Cu $(NO_3)_2$ +$ZrCl_2$-Ni $(NO_3)_2$] impregnations can also be observed, and no major modification occurred on the surface following subsequent impregnations. The decrease in pore diameter and rhodium deposition is also evident from the SEMs.

$PdCl_2$-Cu $(NO_3)_2$ +$ZrCl_2$-Ni $(NO_3)_2$ depositions can be observed on the SEMs and a very clean surface is shown on figure 4.3 A, and B for the sample after the heat treatment in hydrogen atmosphere.

SEMs with different magnifications are shown in figures 4.3 C, D, E, and F. The outer surface micrographs show the non-homogeneity of the surface, for example the support has a flat area that can be simply structural modification during its extrusion in the manufacturing process. The non-homogeneity is less evident after the heating for the γ-alumina modification.

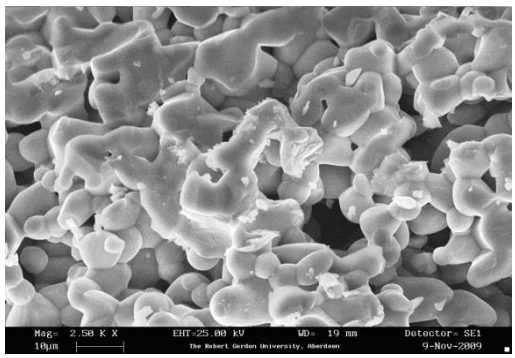

(A) Fresh support

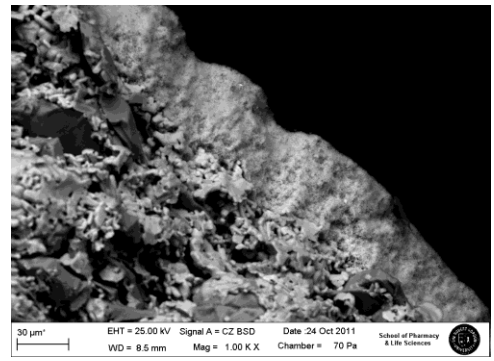

(B) Surface & cross sectional area of fresh support

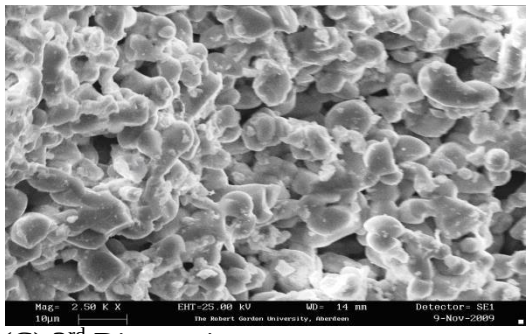

(C) 3rd Dip-coating

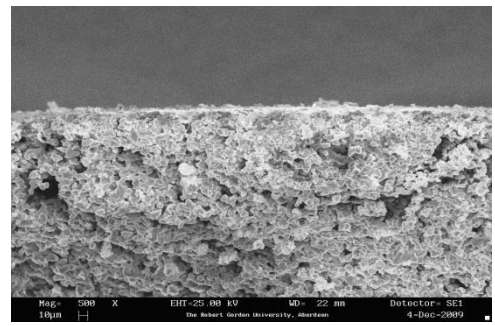

(D) Surface & Cross sectional area

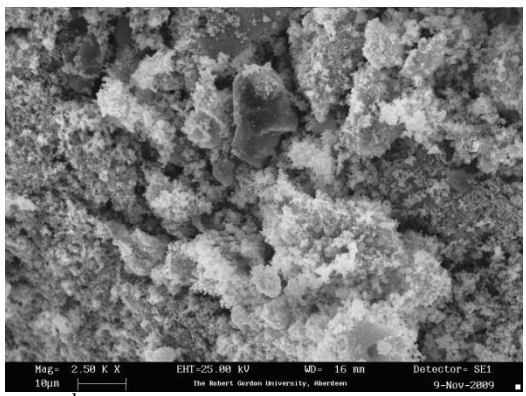

(E) 5th Dip-coating

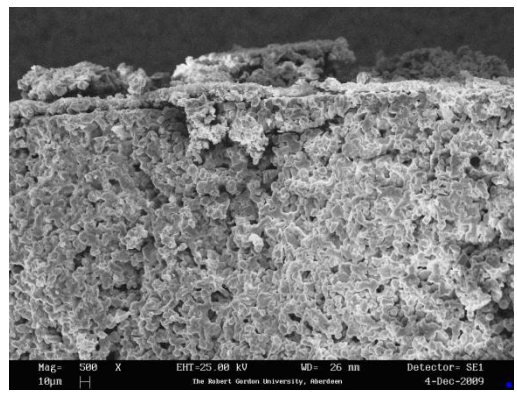

(F) Surface and Cross sectional area

Figure 4.3 SEM images for membrane HCME6001.

4.3.2 Accelerated Surface Area and Porosimetry (ASAP) analysis.

The surface area of the ceramic support employed in this study is presented in table 4.1 and shown in figure 4.4. It was determined by single point (P/Po 0.8), BET, Langmuir, BJH adsorption and BJH desorption, for cumulative surface area of pores between 80nm and 200nm.

Table 4.1 Surface area [m^2/g of sample] for membrane HCME6001

Sample	Single point	BET	Langmuir	BJH (adsorption)	BJH (desorption)
1st IWI	98.5654	275.2321	8656.2343	191.2134	185.5678
2nd IWI	87.4543	222.5456	6432.4533	185.4354	176.3644
3rd IWI	99.5465	277.4543	8643.3453	190.4353	184.5463
4th IWI	87.5436	223.4543	6453.546	186.3454	176.4543
5th IWI	97.5465	276.5432	8664.5434	192.4356	185.5432
6th IWI	89.5654	224.5432	6345.5432	188.3654	177.3463

The first γ-alumina modification exhibited the smallest surface area, possibly due to its crystal structure, but after the second γ-alumina modification, the surface area increased, giving a suitable value for the catalyst impregnation. It should be borne in mind that the γ-alumina modifications took place on the inner surfaces of the tube. After the first catalytic dip-coating, the surface area significantly increased due to the fact that at this stage both sides (i.e. inner and outer tube surfaces) of the tube were exposed to the catalytic IWI solution and that was expected because the tube support pore diameter was quite large at 6000nm. This was supported by the amount of catalytic solution consumed in the first dip coating as the solution seem to have occupied some of the support free pores.

As the procedure was repeated again and again, the membrane was exposed to higher temperature and in the hydrogen atmosphere (where catalytic reduction was taking place) the palladium, zirconium, and nickel chlorides were reduced to their metallic forms, and the crystals seem to be rearranged. These new arrangements result in a significant increase in surface area so that the surface area obtained was even larger than the ceramic support surface area. This enhanced or optimised the surface/volume ratio and therefore improved the catalytic activity of the concerned membrane. Figure 4.4 indicates that the Langmuir surface area is larger that the single point, BET and BJH. This was due to consolidation of a monolayer adsorption following the same profile previously described.

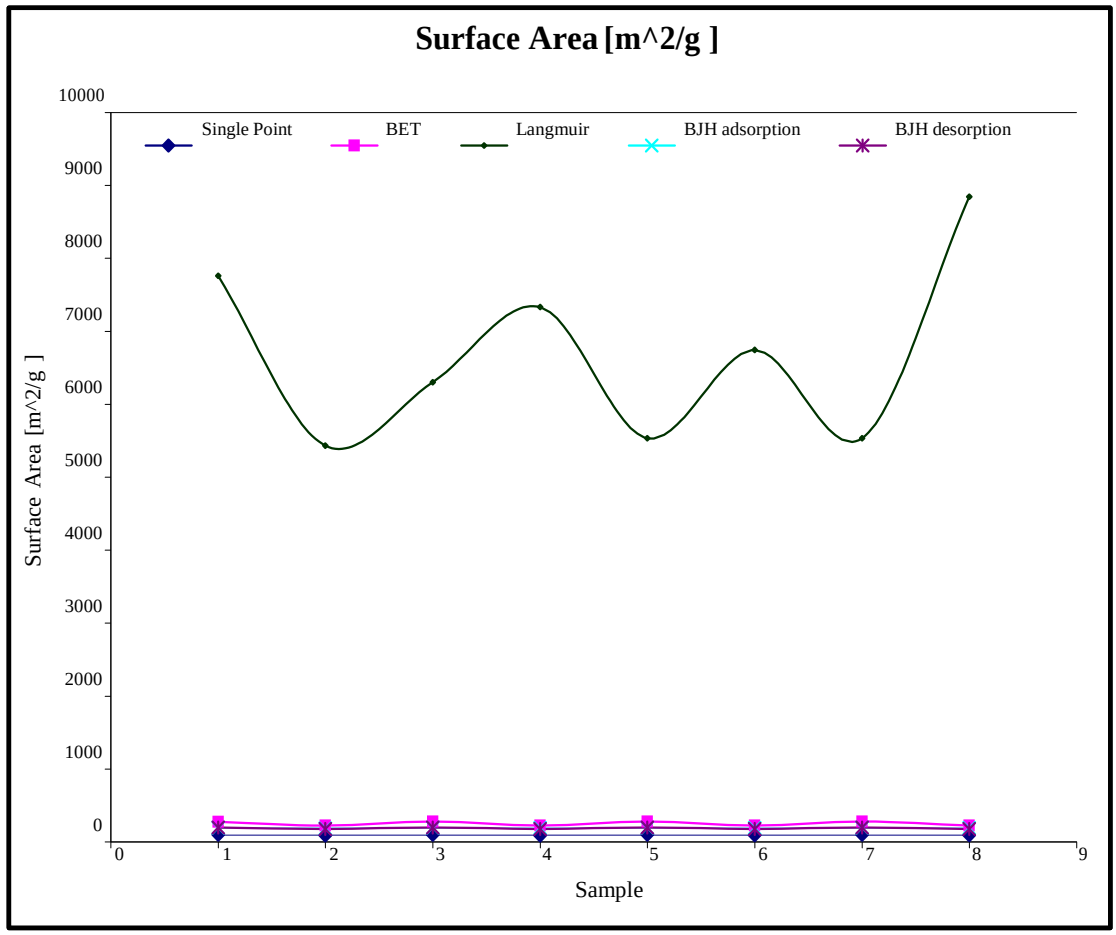

Figure 4.4 The effect of modification on the surface area [m^2/g of sample] for membrane HCME6001.

Pore volume table 4.2 and figure 4.5 was established on a single point of pores with less than 80nm diameter at P/Po 1.2, BJH adsorption and adsorption cumulative of pores between 80 and 200nm diameter.

Table 4.2 Pore volume [m^3/g of sample] for membrane HCME6001.

Sample	Single Point	BJH(adsorption)	BJH(desorption)
1st IWI	0.32	0.26	0.23
2nd IWI	0.20	0.27	0.24
3rd IWI	0.25	0.28	0.25
4th IWI	0.24	0.29	0.26
5th IWI	0.24	0.28	0.27
6th IWI	0.23	0.27	0.26

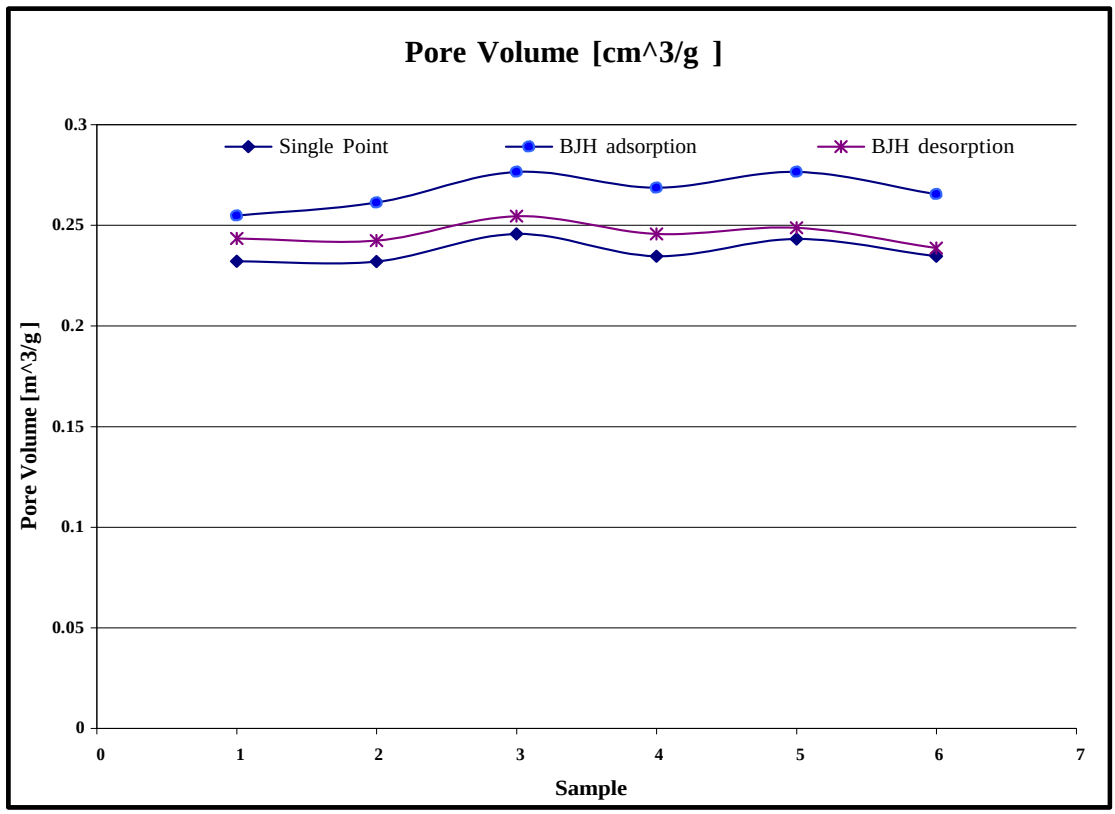

Figure 4.5 The effect of modification on pore volume [cm^3/g of sample] for membrane HCME6001.

The first γ-alumina support modification and heat treatment was not sufficient to influence the pore volume notably, but after the second calcination following the γ-alumina modification, the crystals tended to restructure. This is indicated by the increase in pore volume, which is also confirmed by the increase in pore diameter. The first catalytic coating occurred inside the pores of the modified support, and caused an increase in pore volume and a decrease in pore diameter, as seen in figures 4.5 and 4.6.

This validates the earlier suggestion that the third catalytic layer is deployed within the available free pores. The pore volume is slightly higher than after the first catalytic layer in a similar way as the increase in pore volume of the modified support after the first catalytic solution coating. Calcinations with hydrogen activate sites increased pore volume. The deviation of the BJH desorption values may be due to the possible entrapment of nitrogen molecules inside the pores. These values are related to the weight of sample used, so some probable variation in the values mentioned must be taken into account.

Table 4.3: Pore diameter [nm] of sample] for membrane HCME6001.

Sample	BET	BJH(adsorption)	BJH(desorption)
1st IWI	6.643	8.232	8.123
2nd IWI	6.854	8.012	8.231
3rd IWI	6.987	8.321	8.453
4th IWI	6.676	8.343	8.435
5th IWI	6.645	8.345	8.423
6th IWI	6.654	8.354	8.342

Actual print outs of the ASAP2010 for BJH Desorption dV/dLog(D) Pore Volume of membrane HCME6001 are presented in figures 4.5, 4.6, 4.7 and 4.9 for the fresh support 1st IWI, 3rd IWI, and 5th IWI, respectively, at various membrane preparation stages. These indicate a decrease in both pore volume (cm^3/g) and pore diameter (Å) with increased stages of IWI.

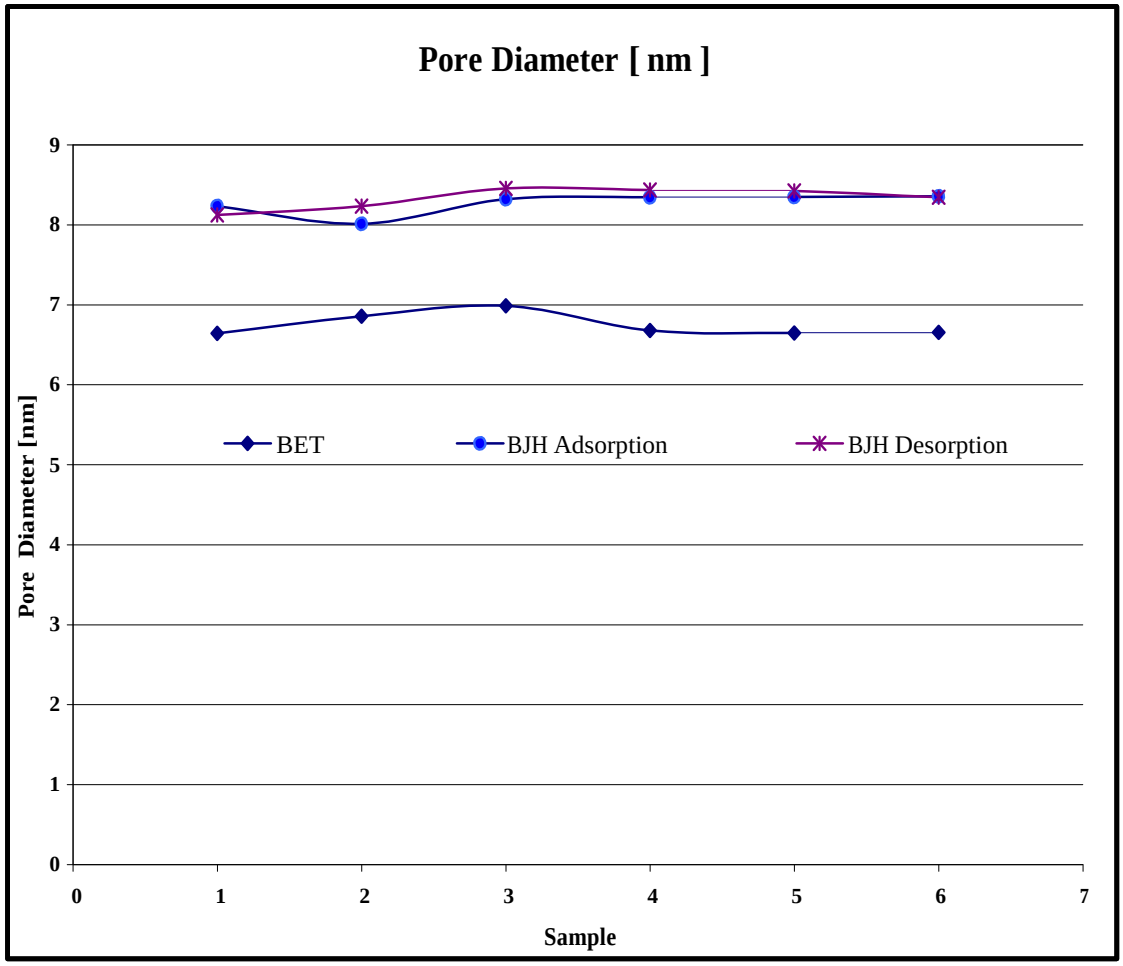

Figure 4.6 Pore diameters [nm] for the membrane HCME6001.

BJH DESORPTION dV/dLog(D)Pore Volume

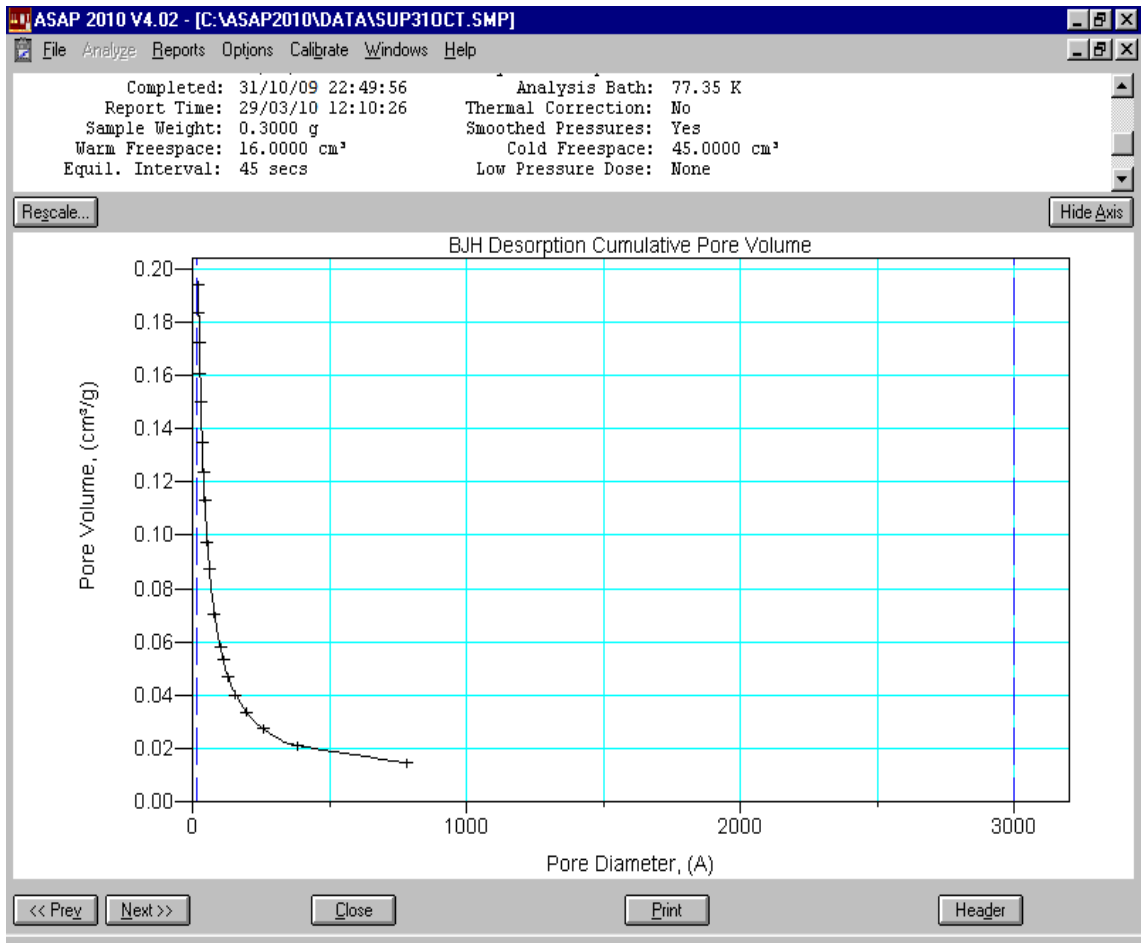

Figure 4.7 The ASAP curve for membrane HCME6001nm support.

BJH DESORPTION dV/dLog(D)Pore Volume

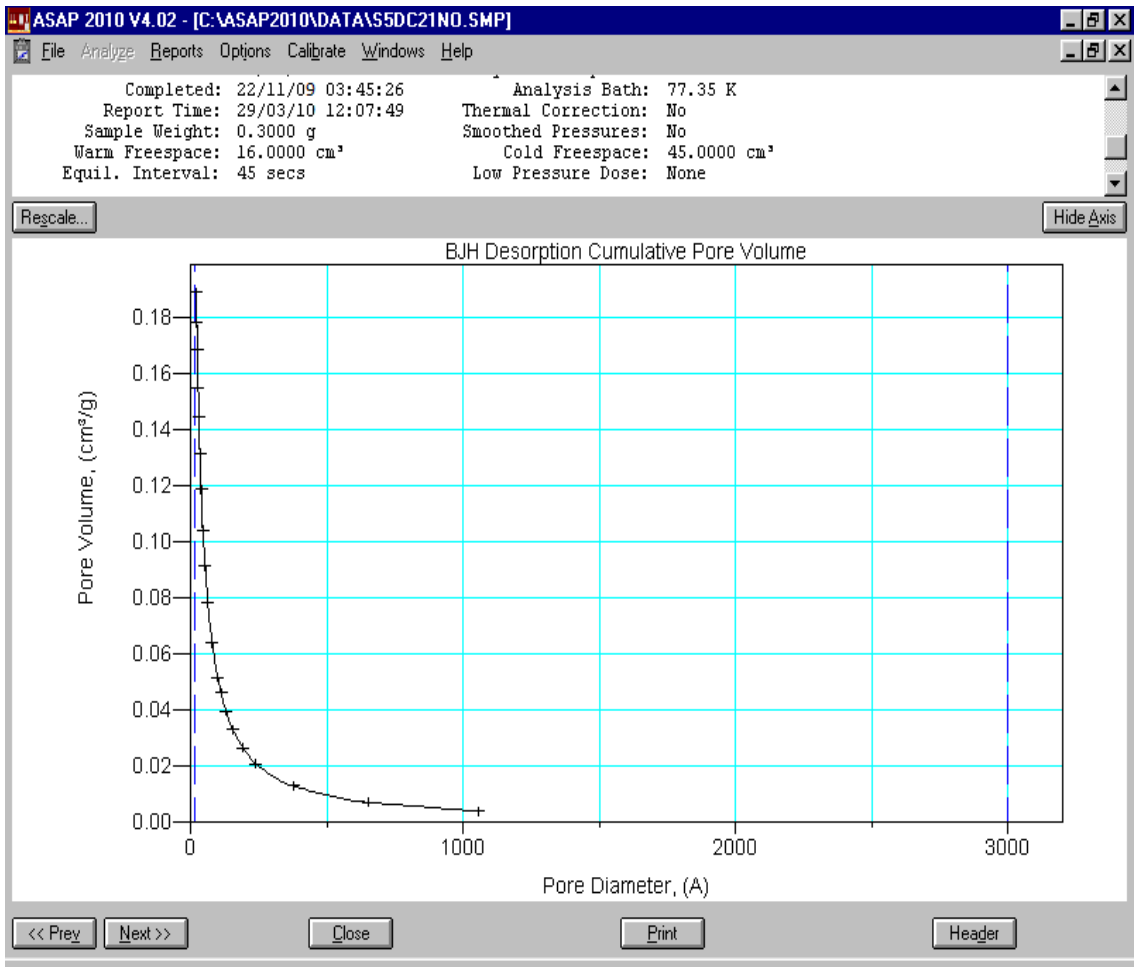

Figure 4.8 The ASAP curve for membrane HCME6001 1st dip-coating.

BJH DESORPTION dV/dLog(D)Pore Volume

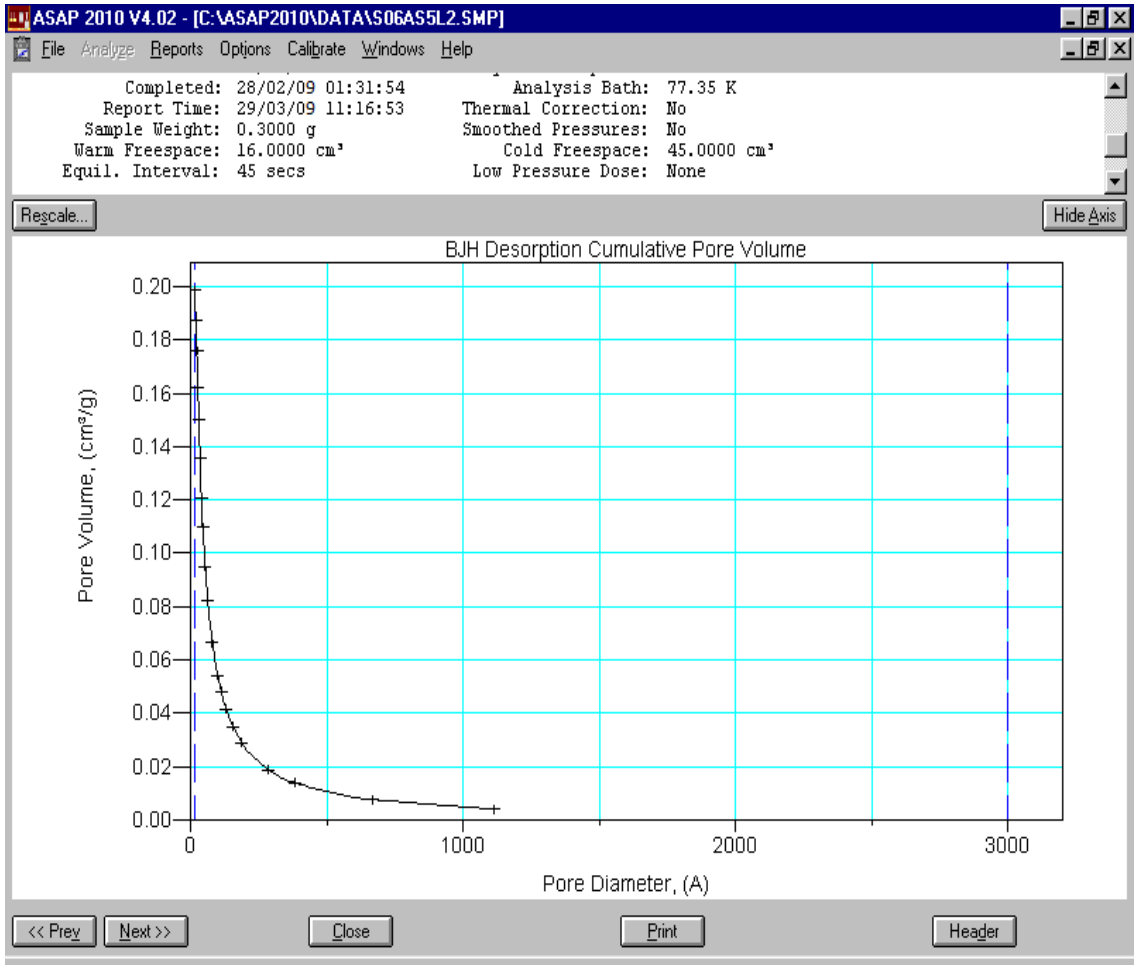

Figure 4.9 The ASAP curve for membrane HCME6001 3rd dip-coating.

BJH DESORPTION dV/dLog(D)Pore Volume

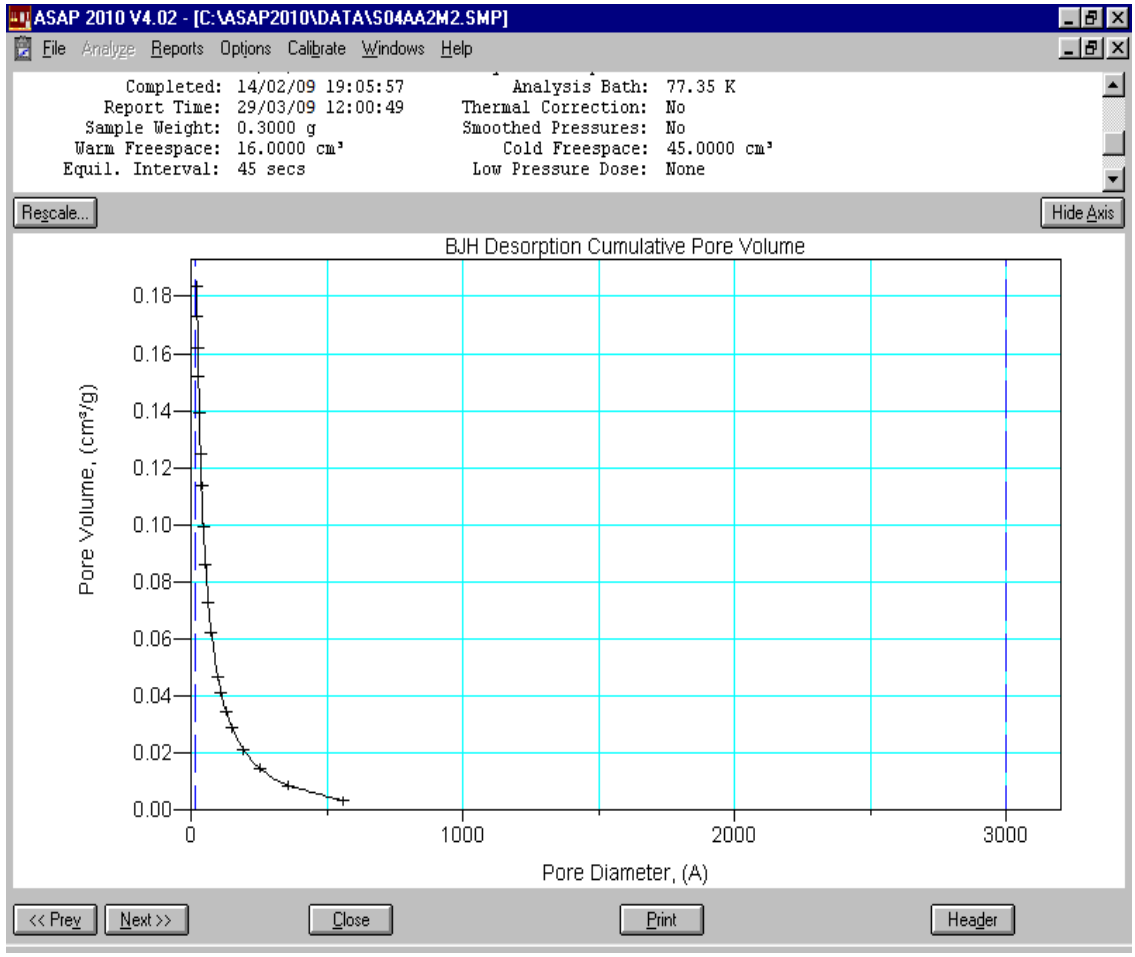

Figure 4.10 The ASAP curve for membrane HCME6001 5th dip-coating.

4.3.3 X-ray Photoelectron Spectroscopy (XPS) analysis.

XPS analysis is an elemental surface analysis technique, in which a small top layer (i.e. 10nm) of the final obtained membrane was taken at various membrane preparation stages and analysed. It should be mentioned that this surface composition analysis technique could be misleading at times due to the possibility of surface contamination during handling. Such limitation or drawbacks would not be possible in the EDXA technique, which gives information on the bulk material content. Results for the tube side and shell side XPS analyses are presented in tables 4.4 and 4.5.

Table 4.4 XPS analysis- shell side for membrane HCME6001.

Sample	%Si	%Ti	%Al	%Pd	%Zr	%Ni	%Cu	%O	C	%Cl
1st IWI	7.87	9.46	11.53	1.12	1.23	1.18	0.31	46.74	22.72	0
2nd IWI	6.66	10.22	11.97	0.88	1.19	0.98	0.22	47.86	22.97	0
3rd IWI	5.98	9.86	12.33	0.80	1.21	0.86	0.11	48.73	23.22	0
4th IWI	5.76	9.65	12.53	0.71	0.99	0.75	0.09	49.63	22.42	0.21
5th IWI	4.44	8.54	13.82	0.65	0.91	0.54	0.05	49.76	21.22	0.01
6th IWI	4.37	8.32	13.58	0.52	0.77	0.31	0.04	49.81	20.97	0.06

Table 4.5 XPS Analysis for tube-side for membrane HCME6001.

Sample	%Si	%Ti	%Al	%Pd	%Zr	%Ni	%Cu	%O	C	%Cl
1st IWI	7.11	9.44	11.23	1.02	1.13	0.98	0.21	46.54	22.32	0
2nd IWI	6.43	10.12	11.87	0.78	1.09	0.88	0.12	47.76	22.87	0
3rd IWI	5.78	9.66	12.03	0.70	1.01	0.76	0.10	48.43	23.12	0
4th IWI	5.41	9.55	12.13	0.61	0.98	0.65	0.06	49.43	22.32	0.21
5th IWI	4.12	8.34	13.32	0.55	0.88	0.44	0.04	49.56	21.12	0.01
6th IWI	4.21	8.12	13.48	0.42	0.67	0.21	0.03	49.61	20.87	0.04

4.3.4 Energy Dispersive X-ray (EDXA) Analysis.

The samples used for this analysis were the same as those used for the SEM. They were obtained by cutting a small piece (3-5mm^2) from the membrane itself at various preparation stages. Such pieces were firstly analysed by the SEM, and then by EDXA. The EXDA analysis was carried out at five different points on the surface of the ~5mm^2 pieces and then the averages of those results were calculated and are presented in tables 4.6 and 4.7.

Table 4.6 EDXA presents a sample of results of inner surface analysis for tube-side for membrane HCME6001.

Sample	%Na	%Mg	%P	%Si	%Ti	%Al	%Pd	%Zr	%Ni	%Cu
1st IWI	0.03	0.04	0.03	1.87	3.46	4.53	0.44	0.23	0.18	0.01
2nd IWI	0.04	0.04	0.04	2.66	4.22	4.97	0.68	0.87	0.24	0.02
3rd IWI	0.03	0.05	0.05	2.89	4.56	5.33	0.810	0.98	0.43	0.011
4th IWI	0.05	0.06	0.04	3.23	4.65	5.53	0.91	1.12	0.55	0.19
5th IWI	0.05	0.05	0.04	3.44	5.34	5.82	1.05	1.34	0.64	0.15
6th IWI	0.6	0.06	0.05	3.65	5.62	5.98	1.23	1.47	0.66	0.17

Table 4.7 Presents a sample of results of outer surface (shell side) EDXA analysis for membrane HCME6001.

Sample	%Na	%Mg	P%	%Si	%Ti	%Al	%Pd	%Zr	%Ni	%Cu
1st IWI	0.01	0.02	0.01	2.11	9344	2.23	0.07	0.13	0.07	0.01
2nd IWI	0.02	0.02	0.02	2.43	3.12	2.87	0.08	0.29	0.08	0.02
3rd IWI	0.03	0.03	0.03	2.23	3.66	2.03	0.09	0.34	0.12	0.04
4th IWI	0.02	0.04	0.03	2.41	3.75	3.34	1.05	0.67	0.15	0.06
5th IWI	0.03	0.03	0.03	3.67	3.87	3.56	1.21	0.88	0.23	0.04
6th IWI	0.03	0.04	0.04	4.01	3.97	3.78	1.23	0.97	0.32	0.01

The data presented in Tables 4.6 and 4.7 show that, even though considerable care was taken to avoid sample contamination, it seemed impossible to avoid. There are many sources of contamination during membrane preparation, including handling, the water used for dissolving chemicals, or contact with laboratory equipment. Table 6 indicates that the shell side was more affected by contamination, due to its exposure, whereas the tube side (Table 4.7) was usually only contaminated from the water used for chemical preparation. Impurities such as magnesium, phosphorus, calcium and sodium are commonly found in water.

The Elemental composition based on Energy Dispersive X-ray Analysis (EDXA) in figure 4.11 for membrane HCME6001 indicates that membrane calcination in the

presence of the hydrogen stream seemed to remove some of the impurities, which were burned off as chemical thermal decomposition took place. Both tables 4.6 and 4.7 show detailed variation of the element concentration in the concerned membrane at various membrane preparation stages.

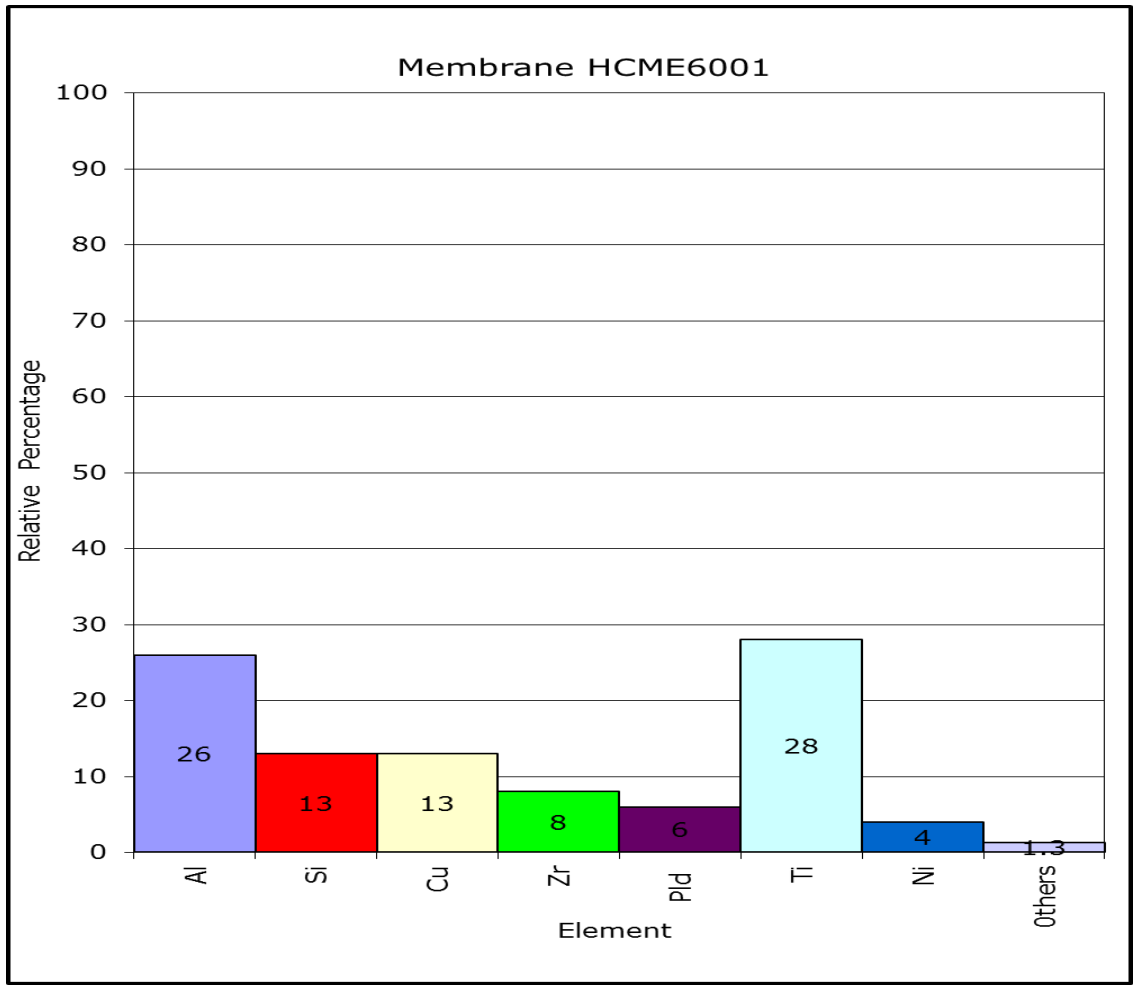

Figure 4.11 A typical print out of 'Elemental composition based on Energy Dispersive X-ray Analysis (EDXA)' for membrane HCME6001.

4.3.5 Catalytic membrane characterization using single gas permeation tests.

The ceramic membrane was fixed in the tubular permeation cell, and the membrane ceramic support was sandwiched between either end of the tube with clamps. The permeation cell was assembled using tightening screws. Leaks through the permeation cell were tested using soap solution. Once the permeation cell was ready for use, the shell of the permeation cell was connected to the selected gas, and the other end to a pressure gauge to measure the retentate pressure (Pr), whilst permeate pressure was also noted down (Pp). Gas flow rate through membrane support was measured using either the bubble flow meter/or the digital flow meter. The pressure at the feed side started at

1.0 bar and was increased gradually by 1.0 bar at a time up to 4.0 bars. Gas permeation tests were used to establish flow characteristics through the HCME6001 membrane. The tests were carried out using a permeation cell and two gases, hydrogen and CO_2. They revealed that flow through these membranes could be characterized mostly by the viscous convective regime at ambient temperature. Plots of those tests are shown in figure 4.12.

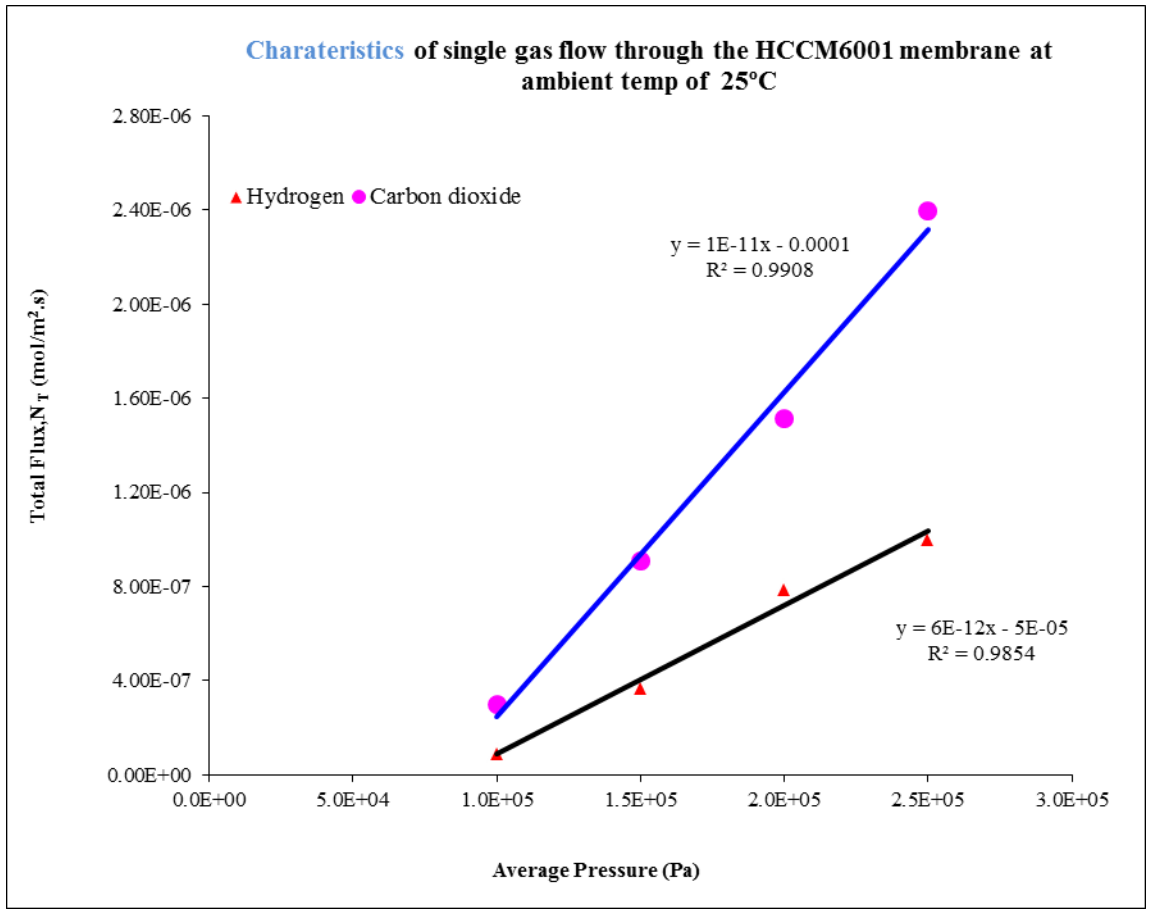

Figure 4.12 Characteristics of gas flow through the membrane at 300°K.

As the mass transport of a single gas through a porous media is usually well described by Fick's and Darcy's laws, and the net flux of non-absorbable gas, N_T is a contribution of Knudsen

diffusion and viscous flow. Accompanied by, an increase of permeability with pressure is a sign of that viscous flow of gases might be responsible for mass transfer, since Knudsen diffusion does not show dependency on pressure as the permeation is due the free molecules flow. The linear zed equation for gas flux through a porous media is given as [55]:

$$N_T = K_0 + B_o\overline{P} \qquad 4.1$$

Where N_T is the total flux (mol/m^2.s), $\overline{P}$ is the mean pressure (Pa), and K_o and B_o are parameters that characterise the structure of the porous matrix. If equation 4.1 when plotted is of the form, $N_T=K_o$, the permeation is characterised by Knudsen flow; if it hasthe form $N_T=B_o$, $\overline{P}$, then the flow is in the viscous regime. The constant K*o* and *Bo*, are defined by equation 4.2 and 4.3 respectively.

$$K_0 = \frac{8r_p}{3(2\pi MRT)^{1/2}} \qquad \left(\frac{mol}{m^2 s P_a}\right) \qquad 4.2$$

$$B_0 = \frac{r_p^{\,2}}{8\mu RT} \qquad \left(\frac{mol}{m^2 s P_a}\right) \qquad 4.3$$

A plot of the type of shown in equation 4.1 indicates a combined Knudsen and viscous flow condition. Figure 4.12 seems to suggest that there is a small contribution of Knudsen flow to the total flux. In the viscous flow regime, gas flux through a porous membrane is inversely proportional to the viscosity of the gas $(i.e. B_0 \alpha 1/\mu)$, but under Knudsen flow conditions, it is inversely proportional to the square root of the molecular weight of the gas $(i.e. k_0 \alpha 1/\sqrt{M})$ [Silva.R. *et al*., 2008].

However, a consideration of pattern of ratios of fluxes of gases to be inverse of both the ratio of viscosities and square root of the ratio of molecular weights will therefore help to determine the actual flow characterise through the concerned membrane.

For Knudsen flow, the ratio of fluxes for gas 1 and 2:

$$\frac{N_1}{N_2} = \sqrt{\frac{M_2}{M_1}} \qquad 4.4.$$

Where M is the molecular weight of gases, and for viscous flow;

$$\frac{N_1}{N_2} = \frac{\mu_2}{\mu_1} \qquad 4.5$$

Where: μ is the viscosity of the gases involved.

Table 4.8 represents the fluxes and flow ratios obtained for hydrogen and CO_2 in the gas permeation test that were carried out.

Table 4.8: Presents ratios of fluxes for hydrogen and CO_2 at 300 ºK.

Δ P(bar)	N_{H2}(ml/min)	N_{CO2}(ml/min)	N_{H2}/F_{CO2}
1.0	43	22.43	1.91707534
2.0	112	59.65	1.98019802
3.0	214	103	2.07766990
4.0	335	158	2.12025316

The viscosity of hydrogen μH_2 = 8.870774245421 × 10^{-6} kg/m.s and that of CO_2, μCO_2 = 1.5127490355989465 × 10^{-5} kg/m.s [http://www.1mnoeng.com, 2009]. The ratio of viscosities of CO_2 to H_2 = 1.7, while the ratio of the square root of molecular weights = 4.67. Thus it could be safely concluded that under the conditions of the experiments reported in this research thesis, viscous flow characteristics was maintained by the membrane. The small deviation from ideal viscous flow seen in figure 4.12 could have arisen as a result the presence of micropores within the macroporous membrane. During catalytic tests, it is very important to maintain viscous flow through the membrane to guarantee that no separation of gas mixture takes place, as this would change the ratio fed reactant gases required for their conversions to the desired products. Thus, having established that the dominant flow characteristic through the tested membrane is the viscous regime, the pore size of the membrane may be estimated from the slope of the graph using equation 4.3.

For CO_2, Bo = 3.222346 × 10^{-12} mol /m^2.Pa and kg/m.s and μ_{CO2}= 1.5127490355989465 × 10^{-5} kg/m.s at 300K. Hence, solving equation 4.3 gives r_p=9.82093 × 10^{-7} m. This therefore means that the estimated pore radius is 0.99 microns. Using the obtained slope from figure 4.12 for hydrogen, B_o=7.07546767432 × 10^{-12} mol/m^2.s Pa. The viscosity of hydrogen at 300K is 8.88777245421 × 10^{-6} kg/m.s. Equation 4.3 gives a value for r_p = 1.23214 × 10^{-6}m.

Therefore, the calculated values of r_p range from 0.99 microns to 1.23 microns or pore diameter d_p of 1.98 - 2.46 microns (i.e. $r_p \times 2$) that looks to be in agreement with the pore size of about 2 microns that was obtained from SEM that is mentioned else where in this study. Thus the pore size of the support had been reduced from its original 6 microns once it had been impregnated by the catalysts.

4.4. Gas conversions.

Conversion in general is normally defined to be that the fraction of a component that has converted to products by the reaction network. Gas conversion of fed components (*i*) is simply defined as the amount of the reactant gases, namely propane and CO_2 fed into the reactor which then is converted into anticipated products passing through the membrane reactor.

Such relation can be expressed as follows:

$$C_i(\%) = \frac{molar\%\ (i)_{in} - molar\%\ (i)_{out}}{molar\%\ (i)_{in}} \qquad 4.6$$

Where:

i = C_3H_8 , CO_2

Thus conversion of propane is

$$C_{C_3H_8}(\%) = \frac{molar\%\ (H_3C_8)_{in} - molar\%\ (H_3C_8)_{out}}{molar\%\ (H_3C_8)_{in}} \qquad 4.7$$

And also conversion of CO_2 (CO_2) is

$$C_{CO_2}(\%) = \frac{molar\%\ (CO_2)_{in} - molar\%\ (CO_2)_{out}}{molar\%\ (CO_2)_{in}} \qquad 4.8$$

4.4.1. Product gas selectivity.

Product gas selectivity can be simply either point selectivity or overall selectivity.

Selectivity of product gases may be expressed as

$$S_j(\%) = \frac{\text{molar\% } j_{out}}{\sum(\text{ molar\% of } j)_{out}} \qquad 4.9$$

Where:

$$j = CH_4 , C_2H_4 , C_2H_6 , C_3H_6 , CO_2 , CO$$

For instance selectivity of C_3H_6 is

$$S_{C_3H_6}(\ \%) = \frac{\text{molar\% } C_3H_6 \text{ out}}{\sum(\text{ molar\% of } C_3H_6)_{out}} \qquad 4.10$$

4.4.1.1. Point gas selectivity.

The point selectivity (or instantaneous) selectivity is defined as the ratio of the production of one component to production rate of another component.

4.4.1.2. Overall gas selectivity.

The overall selectivity is the ratio of the amount of component produced to the amount of another component produced. However, selectivity in this study is defined as the molar percentage of propane that reacts with CO_2 to produce the desired products.

4.4.1.3. Chemical reaction yield.

Yield, also referred to as chemical yield and reaction yield, and it is the amount of product obtained in a chemical reaction and it can be given as the weight in grams or in moles (molar yield). In this study the yield happened to be liquid namely water that was formed as C_3H_6, CO the later reacted with the H_2 to produce H_2O which is known as RWGS.

4.5. Membrane reaction products identification distribution.

As previously mentioned elsewhere a Gas Chromatography (GC) was used to identify the products of the reaction. The main product happened to be C_3H_6 besides C_2H_4, C_2H_6, CH_4 and CO. Hence, a series of trial membranes was prepared and few reaction runs were conducted in order to identify the best catalytic membrane composition, define the most adequate inlet parameters and also give some guidance to precise identification of such membrane reaction products using gas chromatography.

As shown in the chemical reaction equations (4.11, 4.12, 4.13 and 4.14) and according to the CMR experimental reaction some reactive species products were formed those include, C_3H_6, C_2H_4, C_2H_6, CH_4, CO and water.

$$C_3H_8 + CO_2 \longrightarrow C_3H_6 + H_2O + CO \qquad 4.11$$

$$C_3H_8 + 2CO_2 \longrightarrow C_2H_6 + H_2O + 3CO \qquad 4.12$$

$C_3H_8 + 3CO_2 \longrightarrow 2C_2H_4 + H_2O + 4CO$ 4.13

$C_3H_8 + 3CO_2 \longrightarrow CH_4 + 2H_2O + 5CO$ 4.14

Thus, assuming that such membrane catalytic reaction takes place simultaneously requires combining chemical reaction equations involved 4.11.4.12, 4.13 and 4.14 gives equation 4.15.

$3C_3H_8+2CO_2 \longrightarrow C_3H_6+C_2H_6+C_2H_4+CH_4+ 2H_2O+2CO+C$ 4.15

4.6 Parameters affecting the reaction products outcome.

In order to improve and enhance the reaction products, various parameters were varied and refined to optimise the results of the membranes under investigation. These parameters included gas flow rate, and pressure and temperature at which the investigations were conducted. The parameters were presented in more details in chapter three tables 3.5. Whereas plots of the experimental runs results are presented in this chapter.

4.6.1 Flow rate dependencies.

Table 4.9 represents flow rates of the composition of the inlet/fed reactant gases.CO_2 and C_3H_8 were fed into the membrane reactor using three different flow rates, 100ml/min, 200ml/min and 300ml/min, at ratios of 1:1, 1:2 and 2:1 CO_2,:C_3H_8 respectively. Figure 4.13 shows that, regardless of the flow ratio 1:1, 1:2 or 2:1, the flow rate was stable over time. This is quite understandable since the flow passing the membrane reactor stayed the same throughout the experiment period.

Table 4.9 Flow rates of the composition of the inlet/fed reactant gases and their ratios.

Flow rate [ml/min]	Gas and ratio					
	CO_2 1	C_3H_8 1	CO_2 1	C_3H_8 2	CO_2 2	C_3H_8 1
100	50	50	33.33	66.66	66.66	33.33
200	100	100	66.66	133.33	133.33	66.66
300	150	150	100	200	200	100

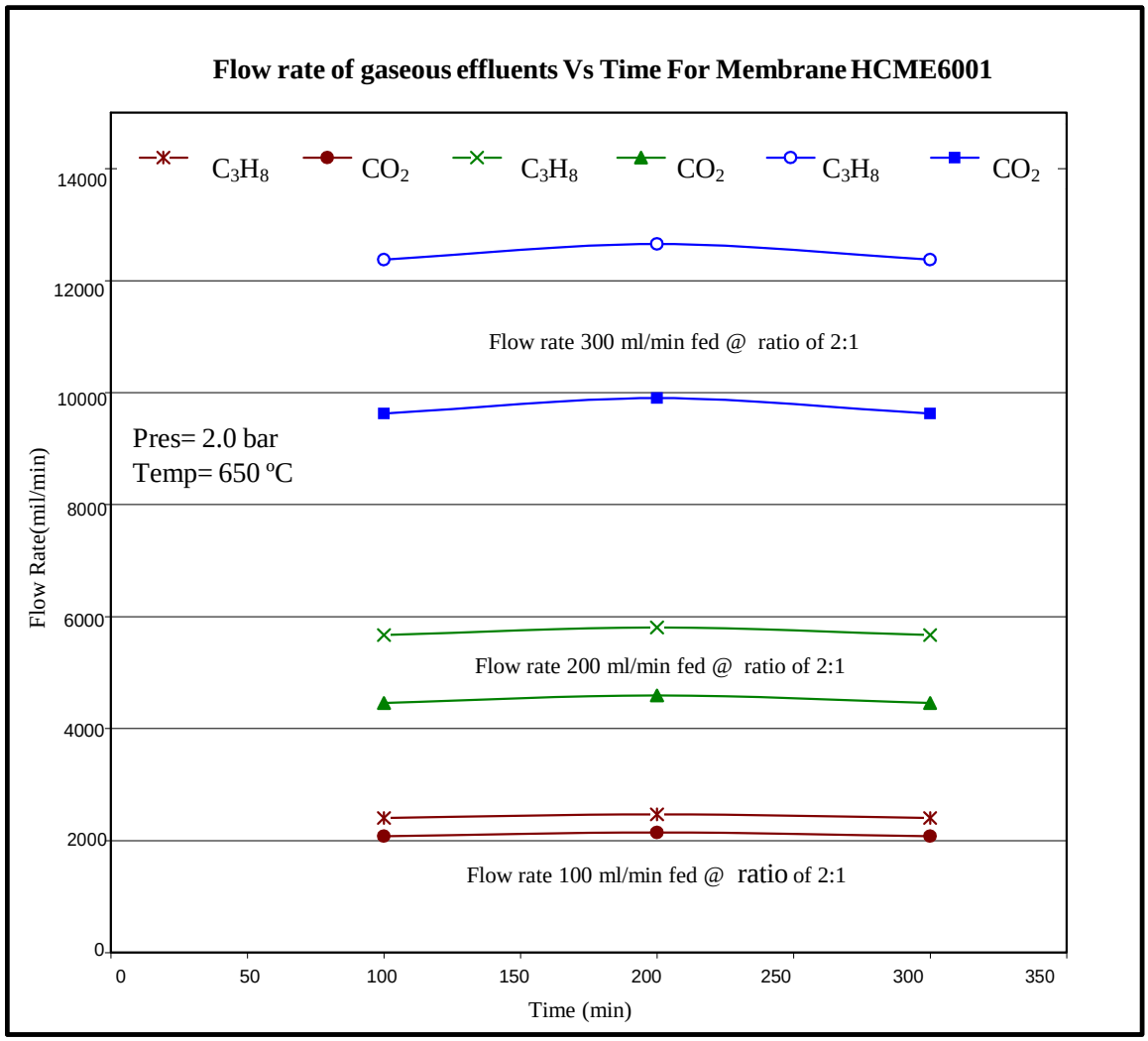

Figure 4.13 Flow rates of gaseous effluents vs time for membrane HCME6001 fed at ratio of 2:1.

4.6.1.1 The influence of fed gas flow rate ratios on conversion.

The three flow rate ratios seemed to influence the conversion and utilization of the reactants (CO_2, C_3H_8). This was calculated using equation 1.16 using the molar flow
rates of each species from the inlet and outlet of the membrane reactor:

$$\mathrm{Xi} = \frac{y_{\mathrm{A,\ in}}\ F_{in} - y_{A,\ out}\ F_{out}}{y_{A,\ in}\ F_{in}} \qquad 4.16$$

where both $y_{A,in}$ and $y_{A,out}$ represent the mole fraction of component A in the feed and product lines respectively, and $F_{in,}$ and F_{out} represent the total molar rates (mole. S^{-1}) in both feed and product streams. Results of such calculations are plotted in figure 4.14, showing an increase in conversion of the reactant gases as their inlet flow rate was increased from 100 to 200 ml/min at a ratio of 2:1 for CO_2:C_3H_8 respectively (i.e. 52%). The conversion of CO_2 increased considerably from 18% to 52% as the flow rate ratios increased from 1:2 to 2:1 using the same flow rates, and the conversion of C_3H_8 decreased from 50% to 18% as its flow rate ratios were decreased from 2:1 to 1:2 at the same flow rate (i.e. 100 ml/min and 300 ml/min). This behaviour could be due to the increase in the amount of CO_2 which reacted with propane, producing more gases such as C_3H_6 and CO, which later reacted with the H_2 to produce H_2O (RWGS).

4.6.1.2 The influence of feed gas flow rates on product selectivities.

The influence of fed gas flow rate on product gas (C_3H_6, C_2H_6, C_2H_4, CH_4 and CO) selectivity seemed to vary depending on the amount of reactant fed gases and the ratios at which they were fed into the CMR. They were significantly different and as can be seen in figure 4.15, the selectivities fluctuated from 10% to 80%. It is worth pointing out those results for these product gases were collected at a MR reaction temperature of 923.15ºK/650ºC and a pressure of 2 bars, as such operating conditions had produced the maximum reactant yield outcome.

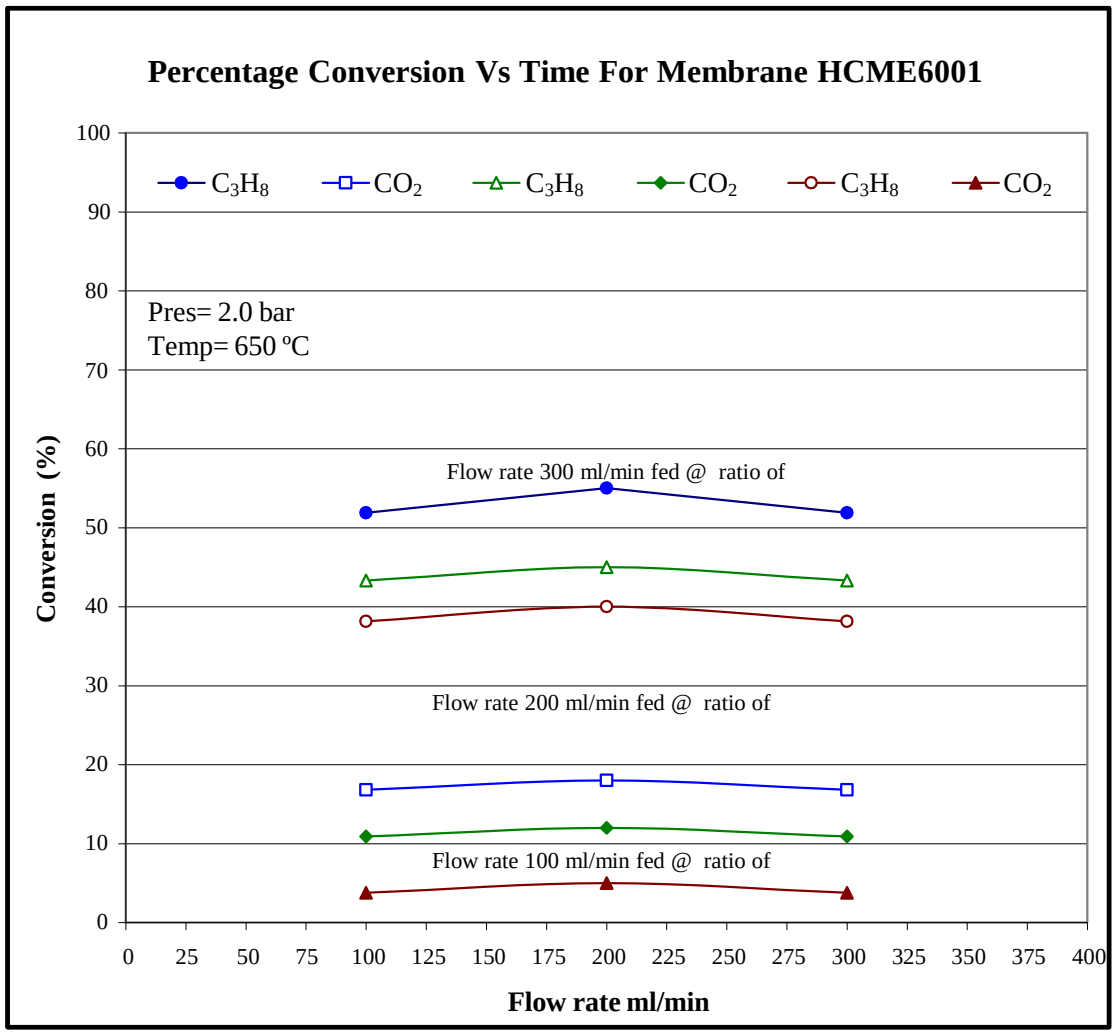

Figure 4.14 An verage conversion vs flow rate for membrane HCME6001 fed at ratio of 2:1.

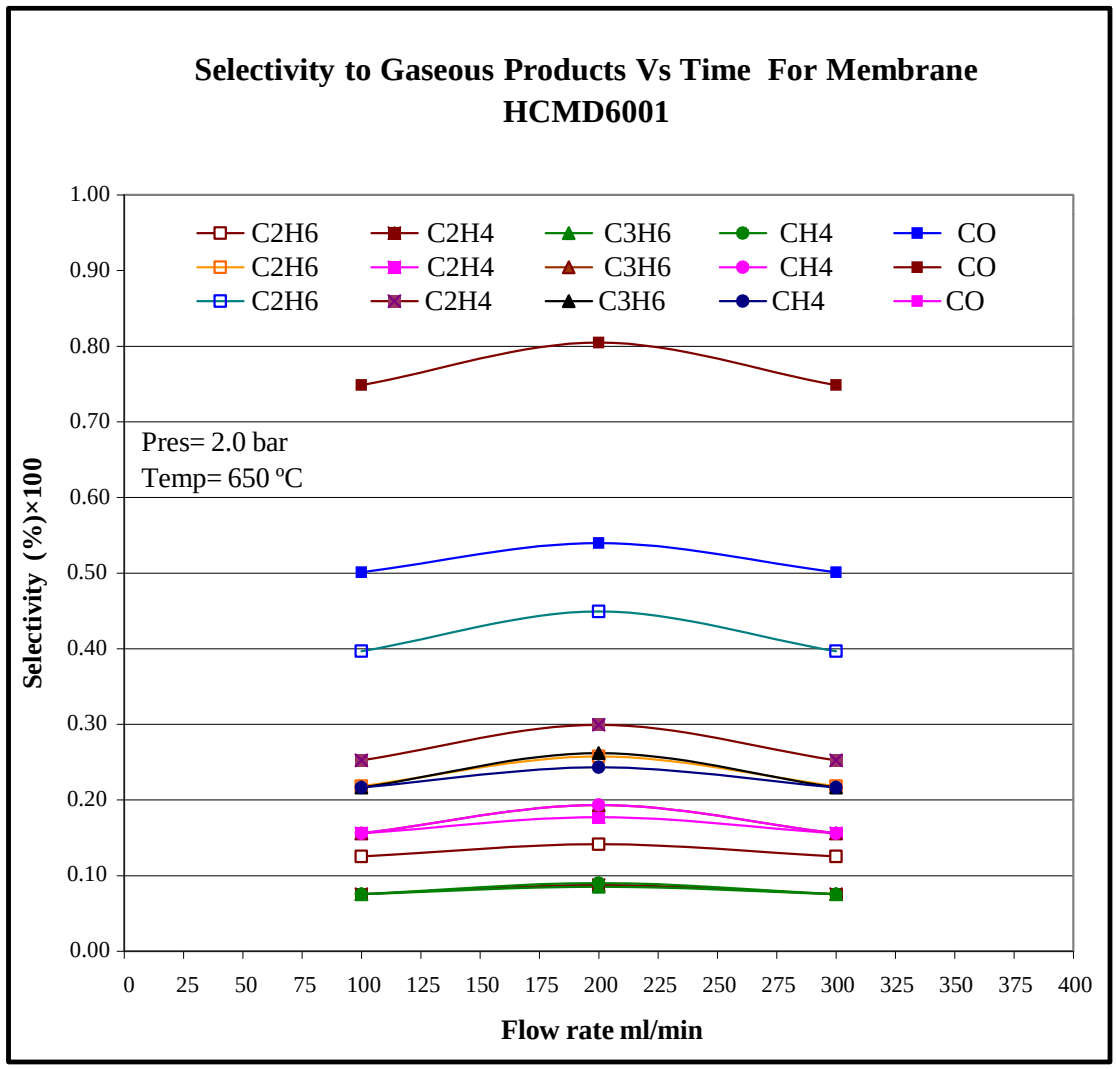

Figure 4.15 Selectivity of gaseous products vs flow rate for membrane HCME6001 fed at ratio of 2:1.

4.6.2 Pressure dependencies

Pressure is an important parameter that has a substantial effect on the performance of the membrane reactor, and on the experimental conversions of both CO_2 and C_3H_8. This is due to the increased number of moles in the dry-reforming reaction and the influence of pressure on the feed reactant gases and their selectivties. The effect of pressure on both reactant gas conversions and yields is presented in figures 4.16, 4.17 and 4.18.

4.6.2.1 The influence of pressure of fed reactant gases on their conversion.

Figure 4.16 shows a plot of conversion % versus differential pressure in bars. Conversions of CO_2 and C_3H_8 increased as the pressure was increased from atmospheric pressure (20% and 28%) to 71% and 45% for C_3H_8 and CO_2 respectively, then decreased considerably as the pressure increased above 2 bars.

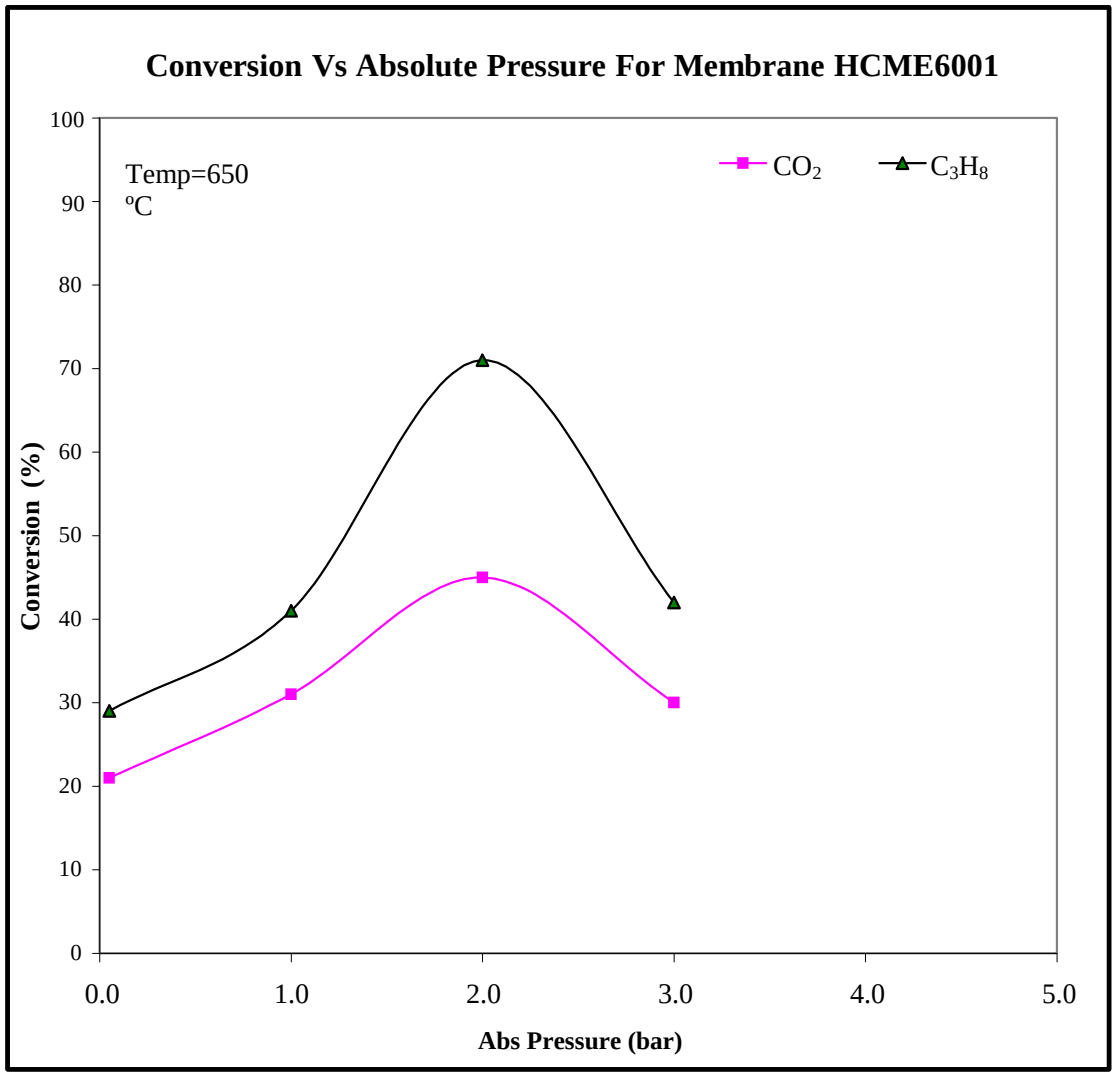

Figure 4.16 Conversion vs absolute pressure for membrane HCME6001.

4.6.2.2 The influence of pressure of feed reactant gases on product selectivities.

Figure 4.17 shows that the selectivity values of the products increased, following the same trend as the reactant gas. This was expected due to the fact that the fed reactant gas conversions increased with the increase of reactant pressure across the membrane reactor (MR). The reactant products kept on increasing along with the reactant differential pressure across the MR and reached their peak, C_3H_6 = 68%, CO = 55%, C_2H_6 = 28%, C_2H_4 = 24% and CH_4 = 12%, at abs pressure of 2 bars.

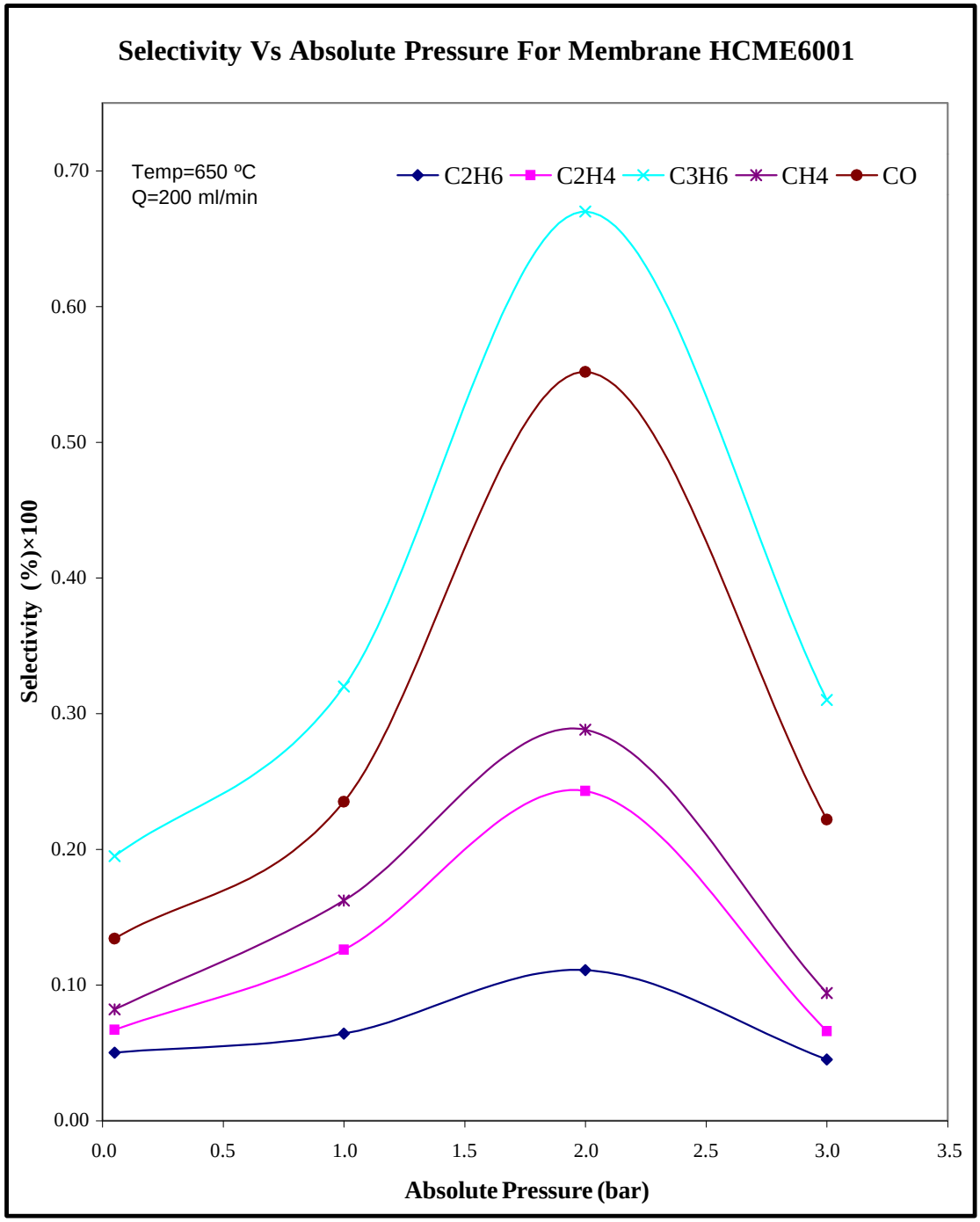

Figure 4.17 Selectivity vs absolute pressure for membrane HCME6001.

4.6.2.3 The influence of pressure of feed reactant gases on yield of liquid product.

Figure 4.18 shows that the dry-reforming reaction was accompanied by the reverse water gas shift (RWGS) reaction, which was found to have a serious impact on the dry-

reforming reaction. Its effect was minimal at atmospheric pressure but at high pressure the suppression of the dry-reforming reaction caused much of the hydrogen produced to convert to water. At the same time, as the pressure was increased across the MR the reactant gas products were increased accordingly. As a consequence, the liquid yields in the MR (water) at first increased with pressure because of increasing of gas yield up to about 1.25%, but then had a tendency to drop down beyond 2 bars, probably because of the unfavourable RWGS reaction.

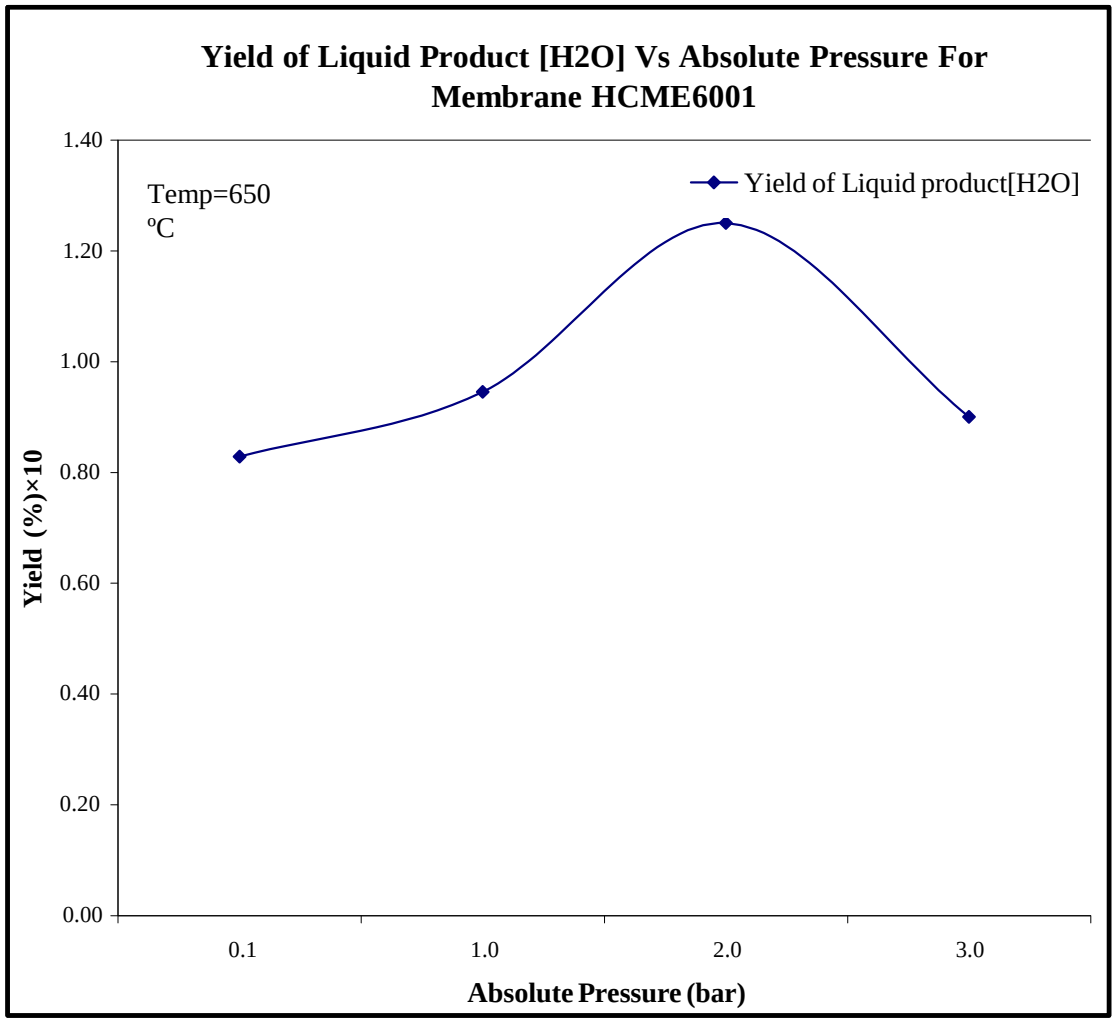

Figure 4.18 Yield of liquid products (H_2O) vs absolute pressure for membrane HCME6001.

The RWGS reaction may be considered to have played an extremely important role in minimising the amount of hydrogen that could be produced at high pressures, and this might lead to the production of many other undesired products.

The results indicated that CO_2 conversion is higher than C_3H_8 conversion at all temperatures. This is due to the occurrence of RWGS side reaction together with CORM process in which CO_2 will react with H_2 formed to produce water and CO. Besides, the C3H8 conversion is found to approach CO_2 conversion as the temperature increases because of the high endothermic nature of CORM process and the less favorable RWGS reaction at high temperature.

When membrane reactor is applied in this process, the results illustrated that C_3H_8 conversion increases with the increment of H_2 permeation while the CO_2 conversion only increases slightly. This has proven that preferential removal of H_2 using membrane reactor is able to increase the reactants (more noteworthy for C_3H_8) conversion. Furthermore, a relatively small increment of CO_2 conversion than C_3H_8 conversion also proves that the introduction of membrane reactor is able to suppress the RWGS side reaction. As both C_3H_8 and CO_2 conversions are tend to be equivalent, according to the reaction stoichiometric, the side reactions will be suppressed.

4.6.3 The influence of temperature on catalytic chemical reaction.

As seen in figures 4.19, 4.20 and 4.21, the influence of temperature plays a vital role. The two reactant gases (CO_2 and C_3H_8) were fed into the MR providing sufficient energy for the chemical reaction to take place in the presence of the catalyst on the membrane, which contributed to speeding up the reaction. From the initial experimental membrane tests on operating conditions, three temperature sets were selected, 600ºC/873.15ºK,

650ºC/923, 15ºK and 700ºC/973.15ºK. The initial tests had indicated that the reaction seemed to occur within this range, especially the middle temperature, which exhibited higher reactant gas conversions, product gas selectivities and liquid yield products.

4.6.3.1 The influence of temperature on reactant fed gases conversion.

Figure 4.19 represents a plot of temperature in ºC versus the feed reactant gas conversion (%). It shows that an increase in temperature from 600 to 650ºC led to a rapid increase in the conversion of the reactant gas propane from 42% to 58%, but that a temperature increase beyond 650ºC tended to decrease conversion.

A similar behavioural trend was also demonstrated by CO_2, with an increase from almost 22% to 33% conversion as the reaction temperature increased from 600 to 650ºC, then a decrease back to almost 22% as the temperature was further increased to 700ºC.

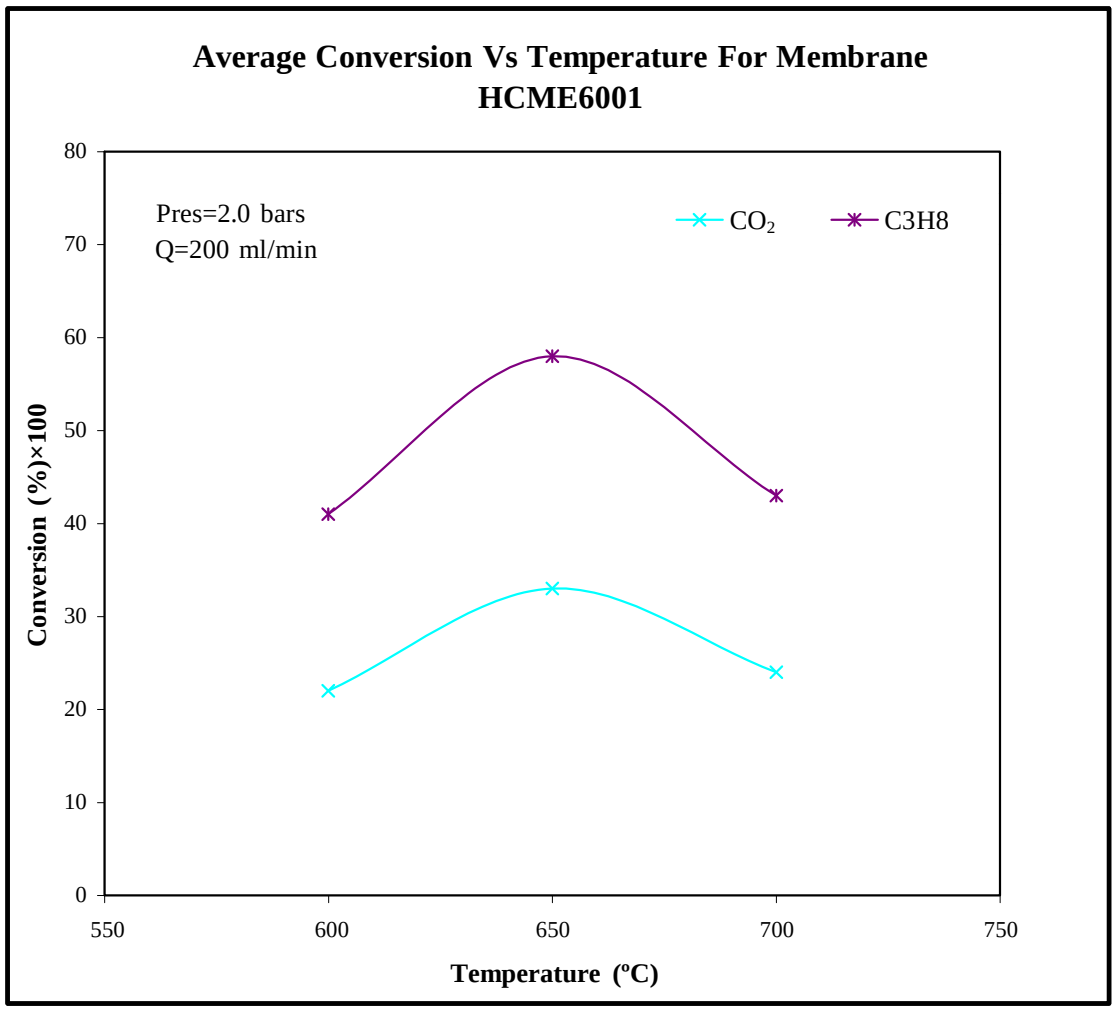

Figure 4.19 An average conversions vs temperature for membrane HCME6001.

4.6.3.2 The influence of temperature on product selectivities.

Figure 4.20 represents the plot of MR feed reactant gas temperature in ºC versus the reactant product gas selectivities in %. A reaction temperature increase from 600 to 650ºC was accompanied by an increase in the product selectivities from 28%, 32%, 24%, 21% and 17% to 44%, 41%, 29%, 27% and 15% for CO, C_3H_6, C_2H_6, CH_4 and C_2H_4, respectively. As reaction temperature was further increased to 700ºC, the selectivities of the product gases decreased to values close to those attained in 600ºC.

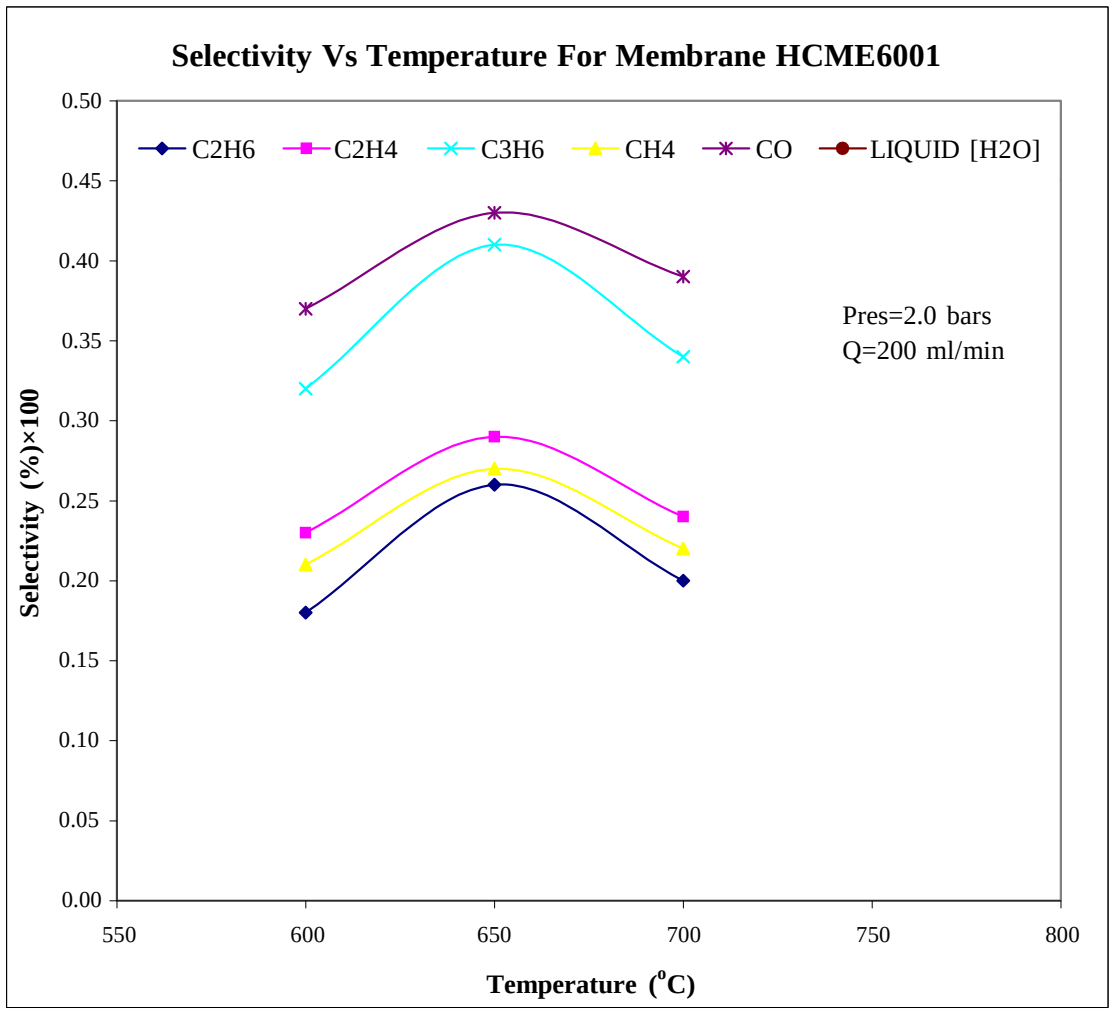

Figure 4.20 Selectivity vs temperature for membrane HCME6001.

4.6.3.3 The influence of temperature on yield of liquid product.

Following the explanation earlier concerning both feed gas conversions and reactant product gas selectivities, it can be deduced that such an increase is clearly expected to be accompanied by a similar trend in the yield of liquid product. The reaction behaviour of water did indeed follow the same trend. As temperature increased from 600ºC/873.15ºK to 650ºC/923.15ºK the liquid yield also increased from 11% to 18%, followed by a decrease back to 12% as the reaction temperature was increased to 700ºC/923.15ºK. The HCMR behaviour as the relationship between reactant temperature and the liquid yield % is presented in figure 4.21.

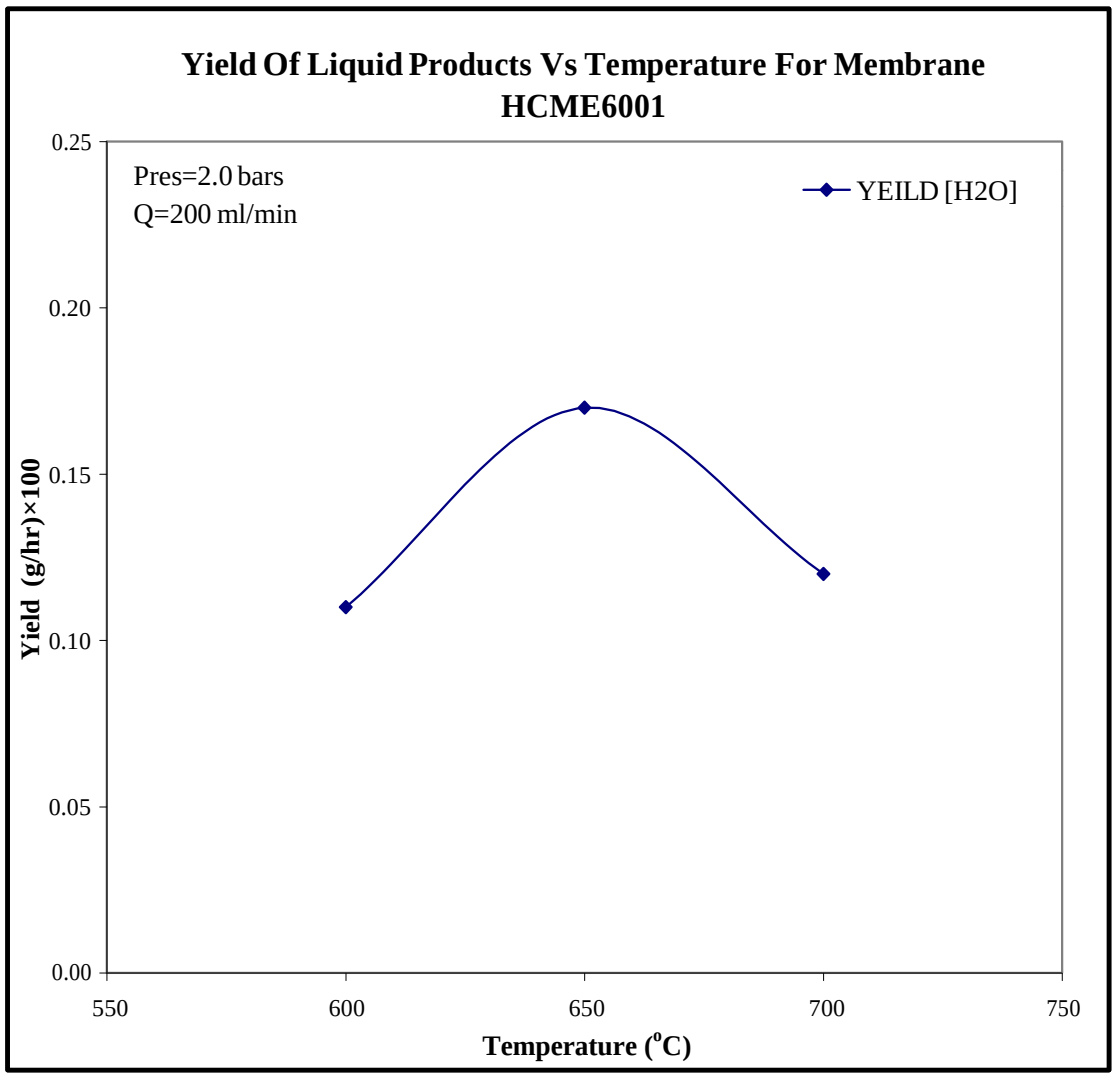

Figure 4.21 Yield of liquid products vs temperature for membrane HCME6001.

4.7 Catalytic membrane reactor performance.

One of the most important properties affecting the quality or superiority and the performance of the HCMR, is whether it can maintain the same behaviour while in constant use after reaching stability, i.e. can it produce the same liquid products, reactant product gas selectivities, and have the same reactant gas conversions under the same operating conditions. Results indicated that both constancy and consistency of the HCMR seemed to be achievable as the experimental work proceeded, which to some extent contributes to extending the life time of the catalyst. This goal could only be acquired by maintaining proper reaction operating conditions, including pressure and temperature, especially the latter as excessive heating may lead to catalyst deactivation (or sintering).

4.7.1 Catalytic membrane reactor re-producibility.

Figure 4.22 shows the plot of average conversion of reactant gases in % versus the number of runs using the HCME6001 membrane that attained similar or identical activity. The reactant product gases selectivities were found to remain constant over several experimental runs. This successful HCMR re-producibility is quite clear in figure 4.23, which shows a plot of reactant product gas average selectivities vs the number of experimental runs.

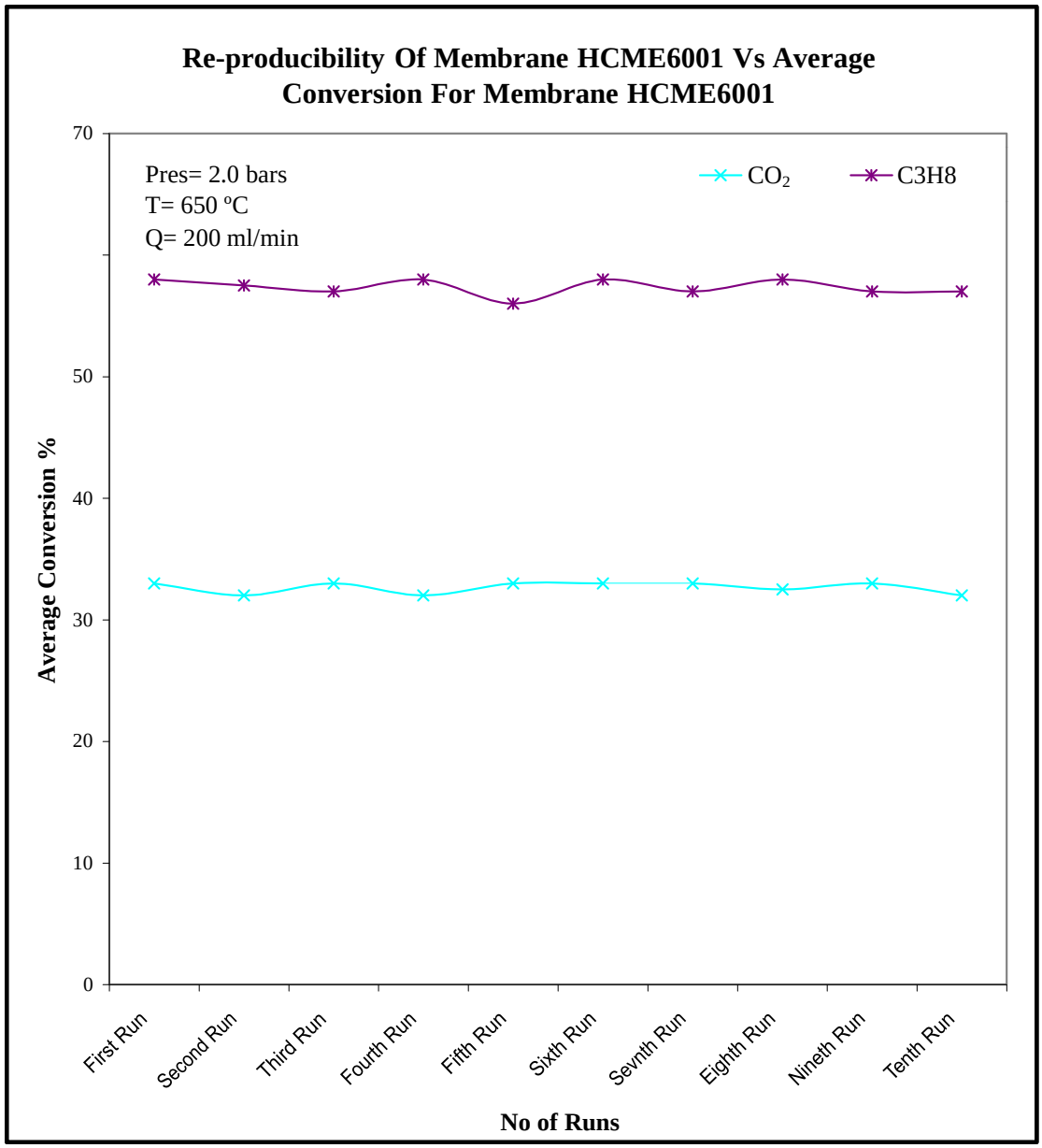

Figure 4.22 Re-producibility of membrane HCME6001 vs. its average conversion.

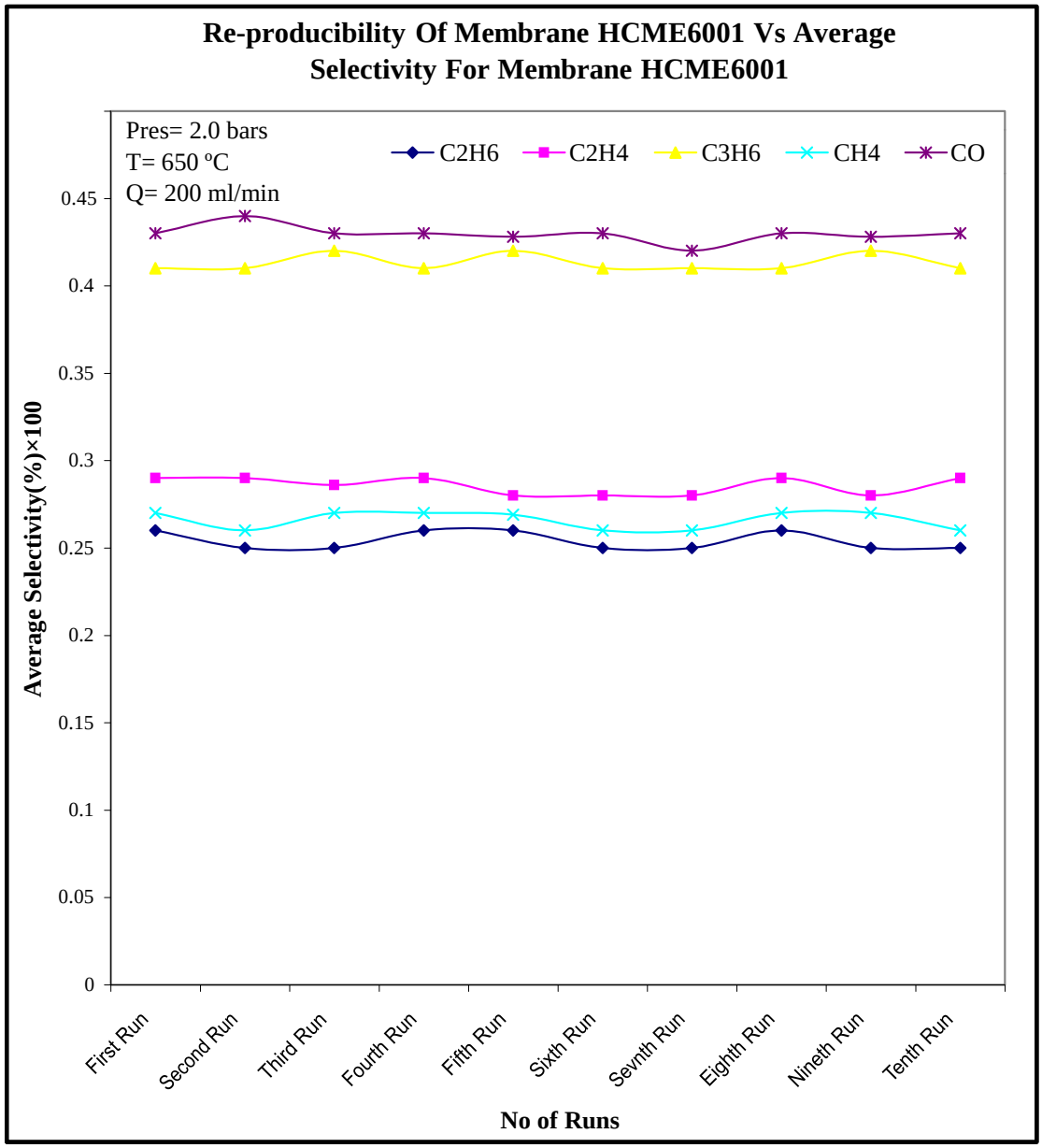

Figure 4.23 Re-producibility of membrane HCME6001 vs its average selectivity.

4.7.2 Catalytic membrane reactor durability.

As previously mentioned, an HCMR should always have and sustain certain qualities that directly affect its reaction performance. Besides reproducibility, another important property is durability. This refers to the capability of the membrane material to withstand wear and tear over a long period of time and to be used over and over again. This is highly influenced by quality and structure figures 4.24 and 4.25 represent the average

reactant feed gas conversions (%) versus lapsed time over four months and the average reactant product gas selectivities (%) versus lapsed time over four months, respectively. From these representative plots, it seems that the capability of the MR g r a d u a l l y declined as time passed. This may be attributed to wear and tear deactivating the catalyst during the continuous heating as the experimental work proceeded. This was expected as the amount of catalyst present on the support was very small. This challenging drawback is, however, likely to be avoided or overcome if the HCMR is used on a larger industrial scale - durability could be improved since larger amounts of catalysts would be used.

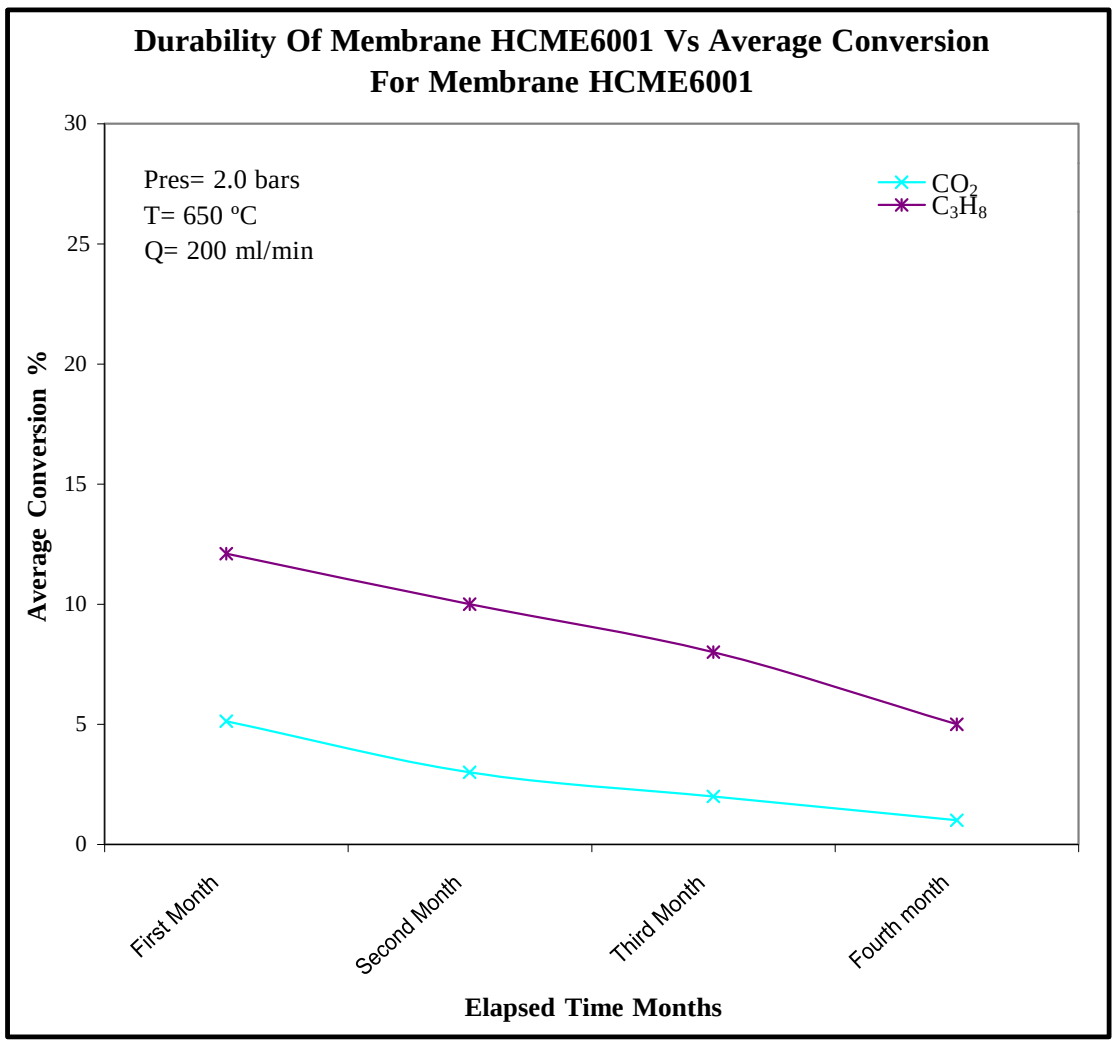

Figure 4.24 Durability of membrane HCME6001 vs its average conversion.

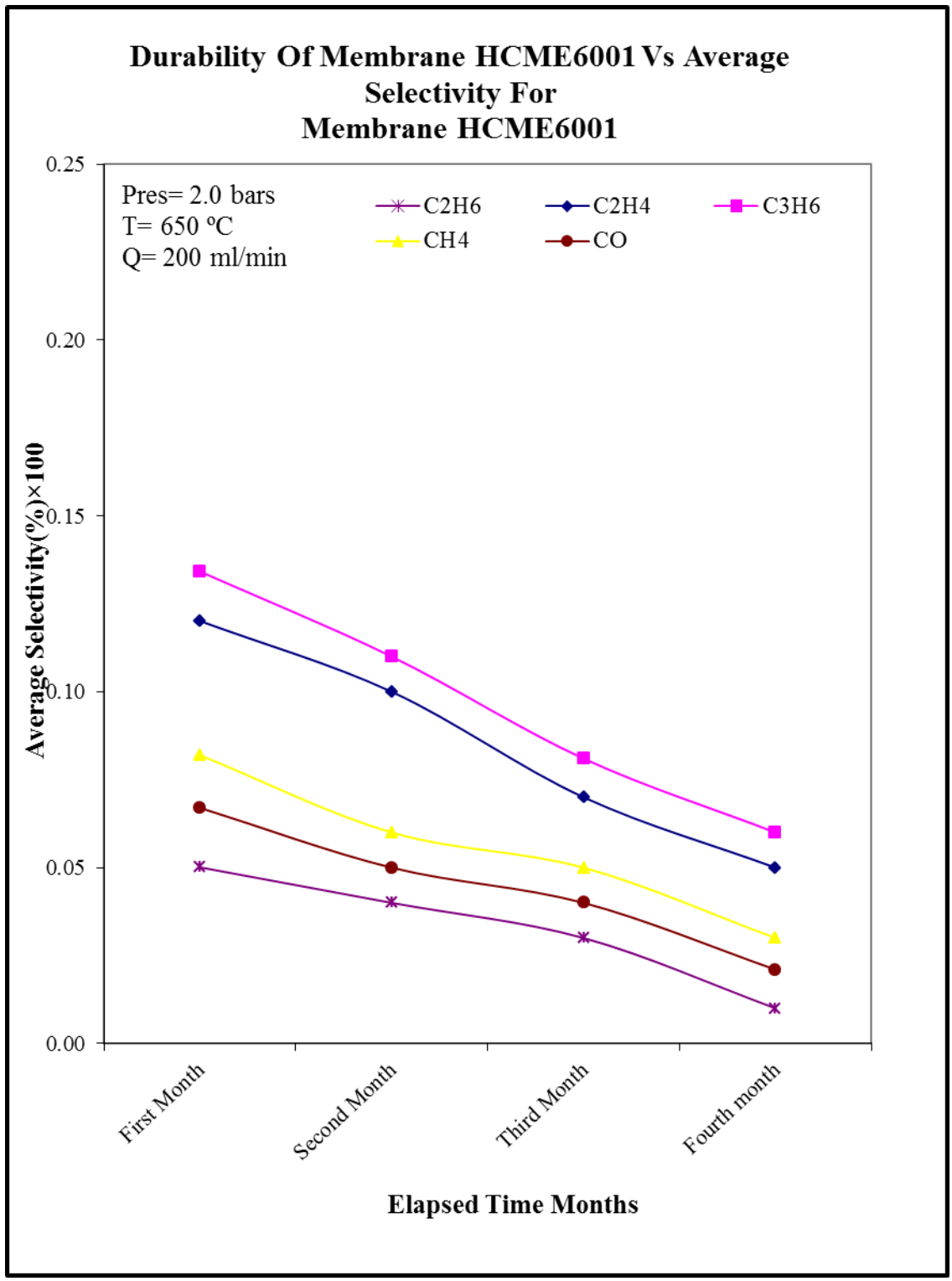

Figure 4.25 Durability of membrane HCME6001 vs its average selectivity.

4.8 Membrane pore diameter effect on HCM performance and behavior.

In order to assess the influence of membrane pore diameter on the performance and behaviour of Hybrid Ceramic Membranes (HCMs), three sets of ceramic supports with different pore diameters were selected to prepare HCMs (HCMC81, HCMD201, and HCME6001). These were then used to conduct experiments to explore their performance and behaviour as they were exposed to various experimental operating conditions such as flow rate pressure and temperature. Some preliminary results for HCMC81 and HCMD201 and their experimental characterisations are presented in Appendices A2 and A3. The results indicated that membrane pore diameter had a great influence on the performance and behaviour of HCMs, including reactant feed gas conversion, reactant gas product selectivities and liquid yield products. The amount of catalyst that could be loaded onto the support varied due to the fact that the void space of the 6000nm support was much greater than that of the 200nm support, which in turn was greater than that of the 80nm support. This leads to the membrane with the highest pore space potentially having more active and reactive capabilities. Several relationship plots of these results are presented in figures 4.26 to 4.36 to demonstrate the various influences showing that the higher the pore diameter, the higher the activation energy.

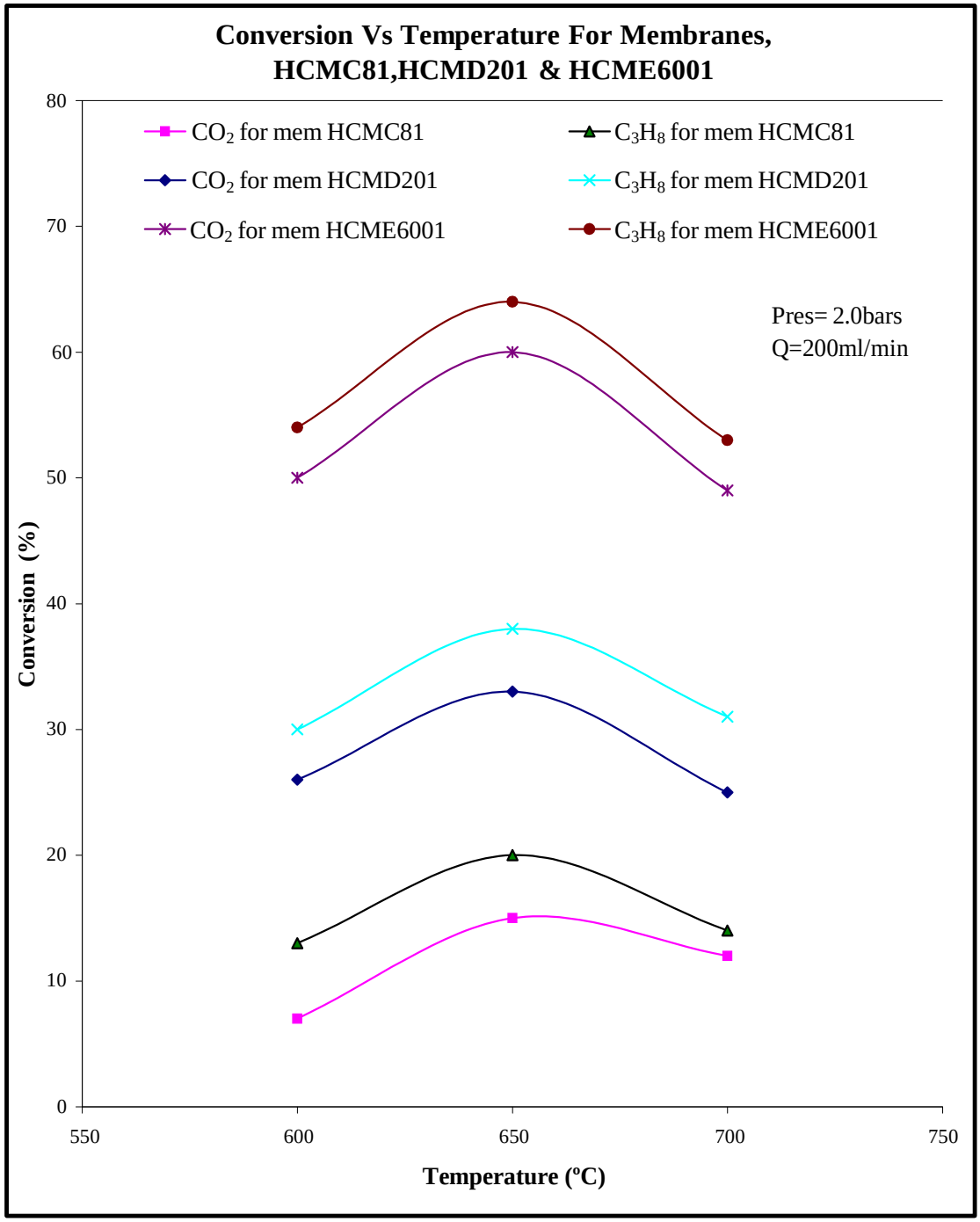

Figure 4.26 Performance comparison curve conversion vs temperature for membranes HCMC81, HCMD201 & HCME6001.

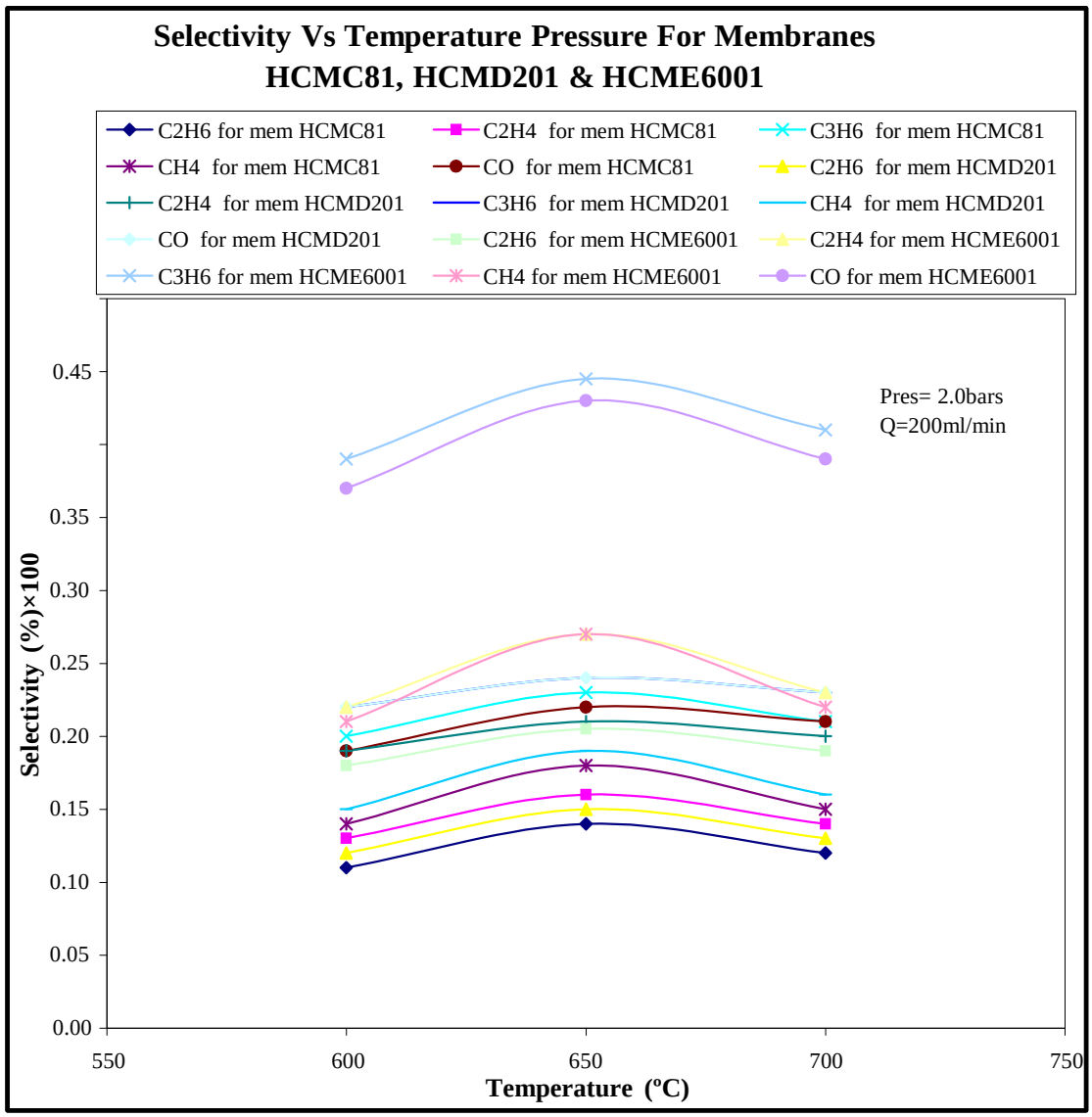

Figure 4.27 Performance comparison curve selectivity vs temperature for membranes HCMC81, HCMD201 & HCME6001.

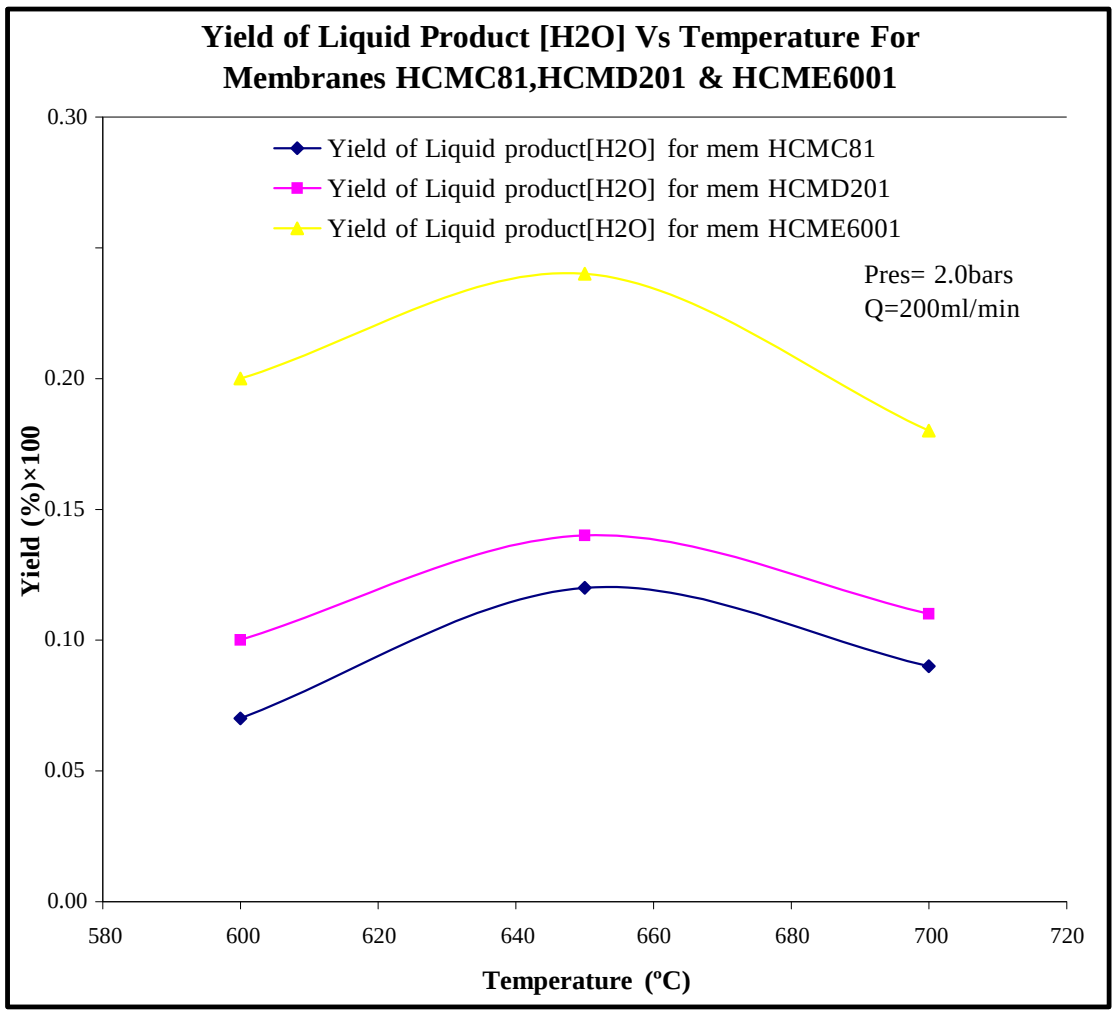

Figure 4.28 Performance comparison curve yield of liquid product [H_2O] vs temperature for membranes HCMC81, HCMD201 & HCME6001.

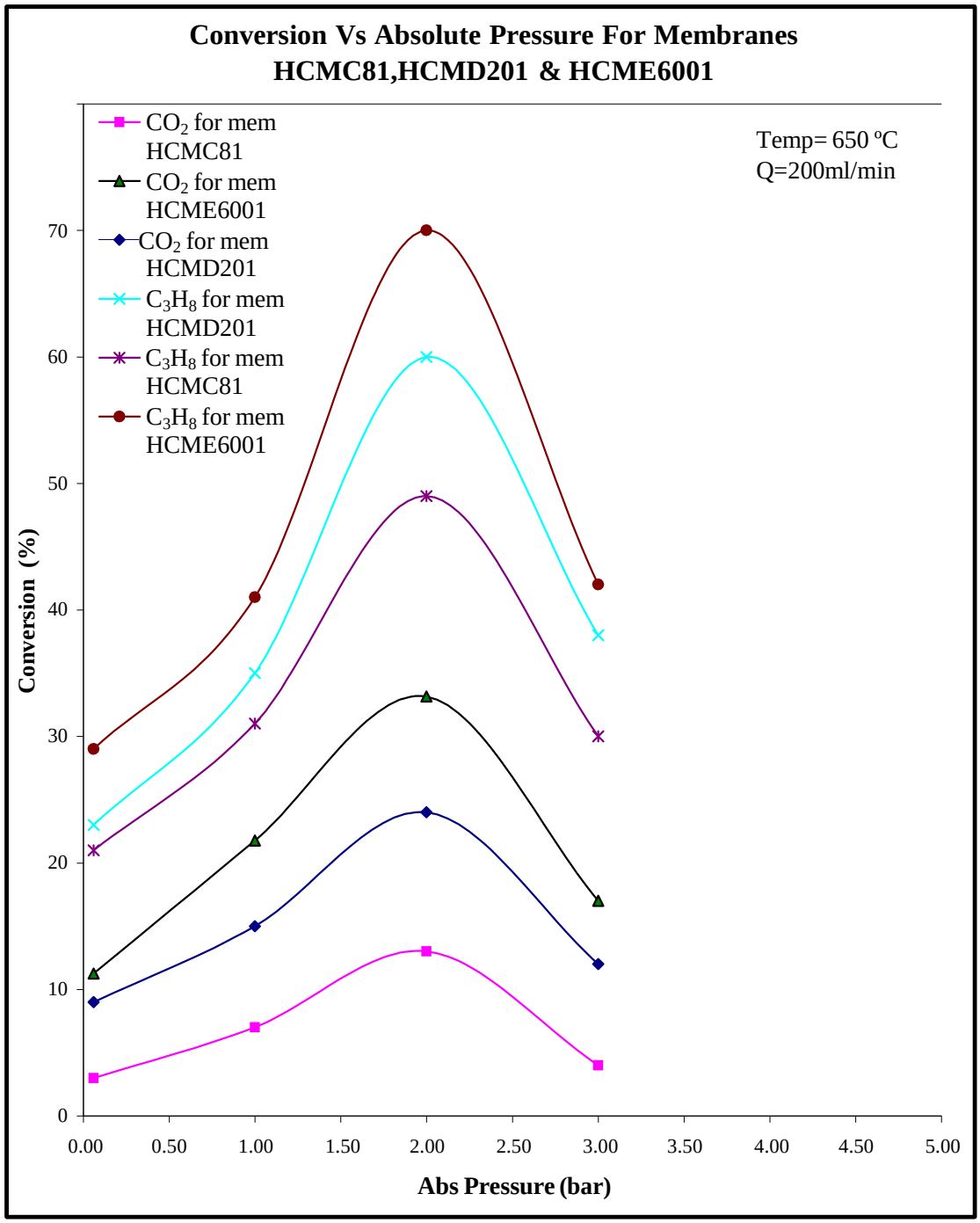

Figure 4.29 Performance comparison curve conversion vs absolute pressure for membranes HCMC81, HCMD201 & HCME6001.

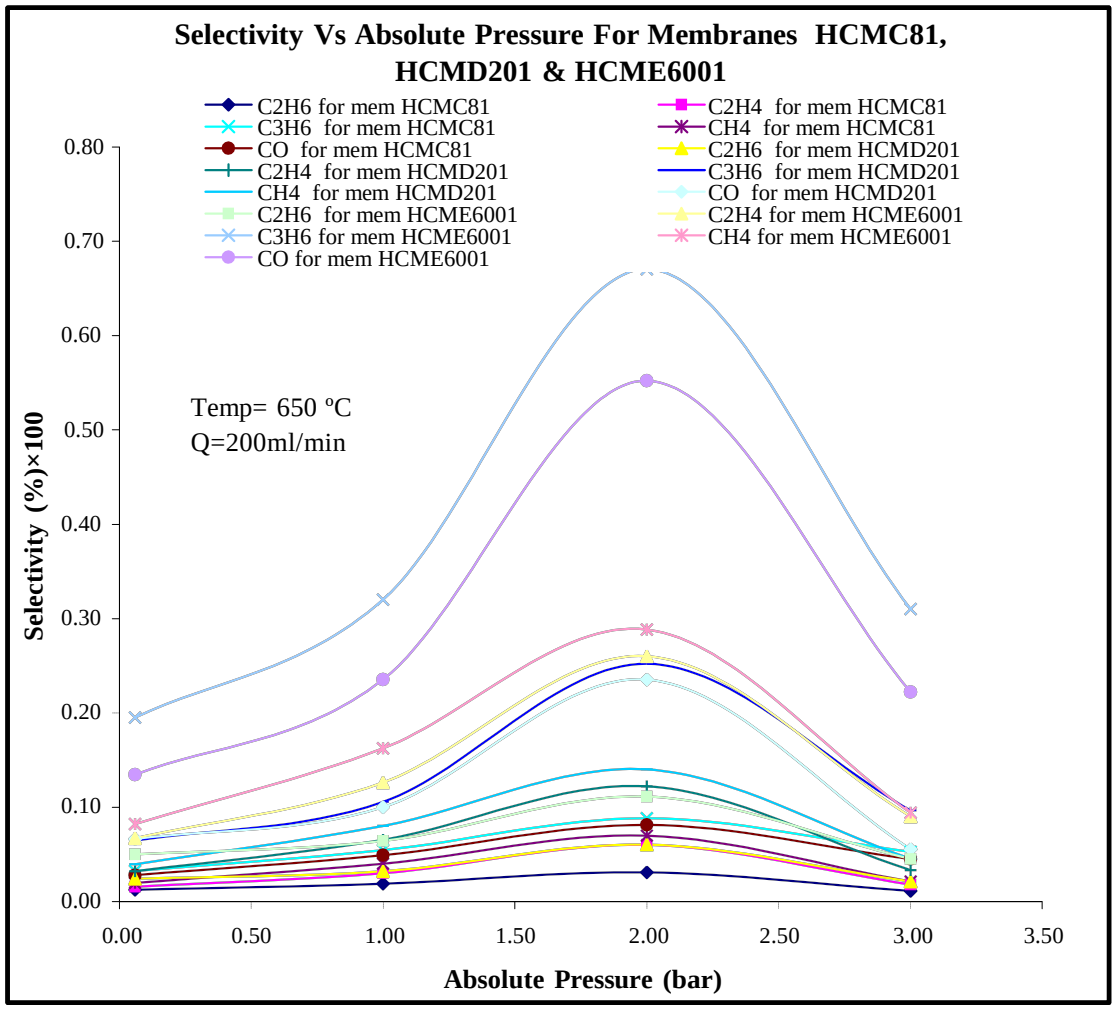

Figure 4.30 Performance comparison curve selectivity vs absolute pressure for membranes HCMC81, HCMD201 & HCME6001.

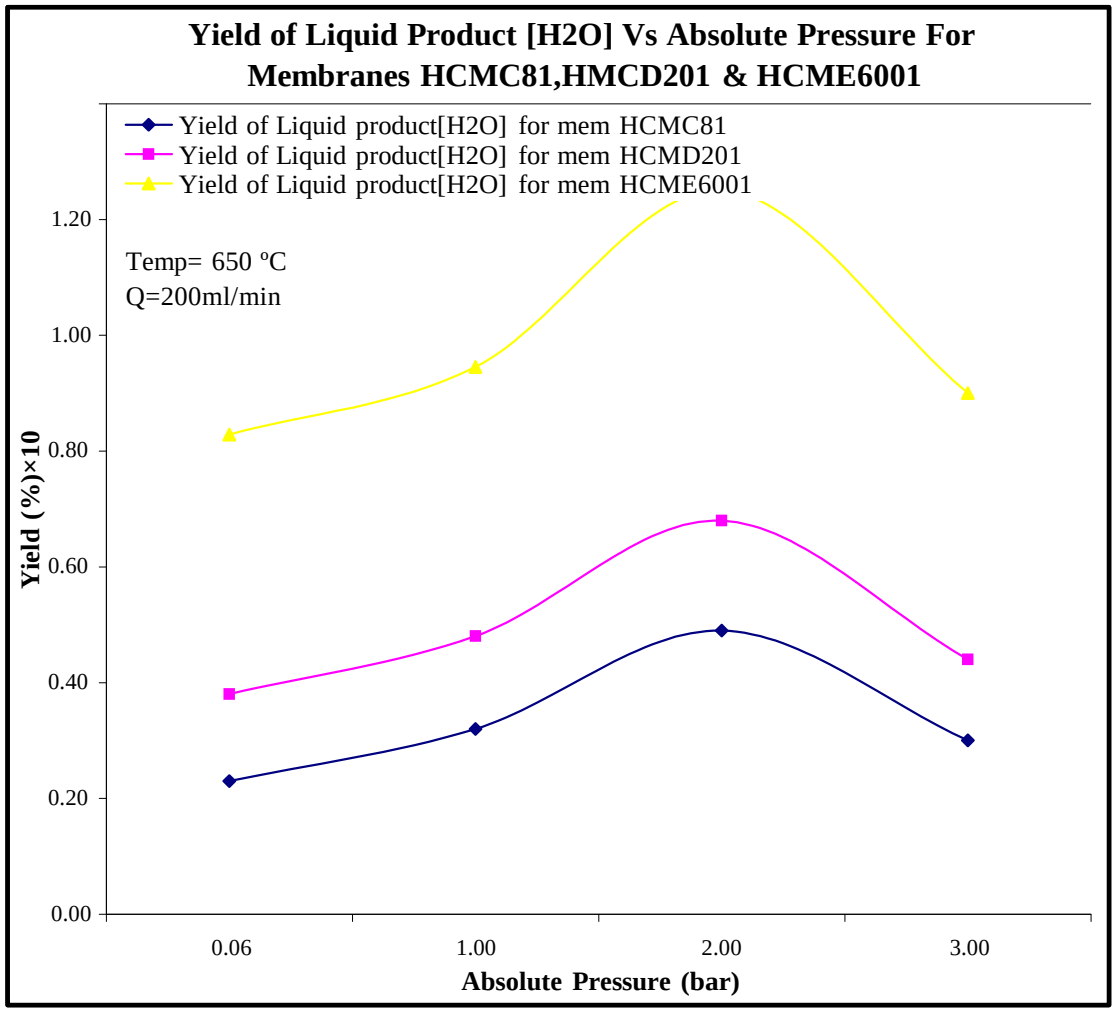

Figure 4.31 Performance comparison curve yield of liquid product [H_2O] vs absolute pressure for membranes HCMC81, HCMD201 & HCME6001.

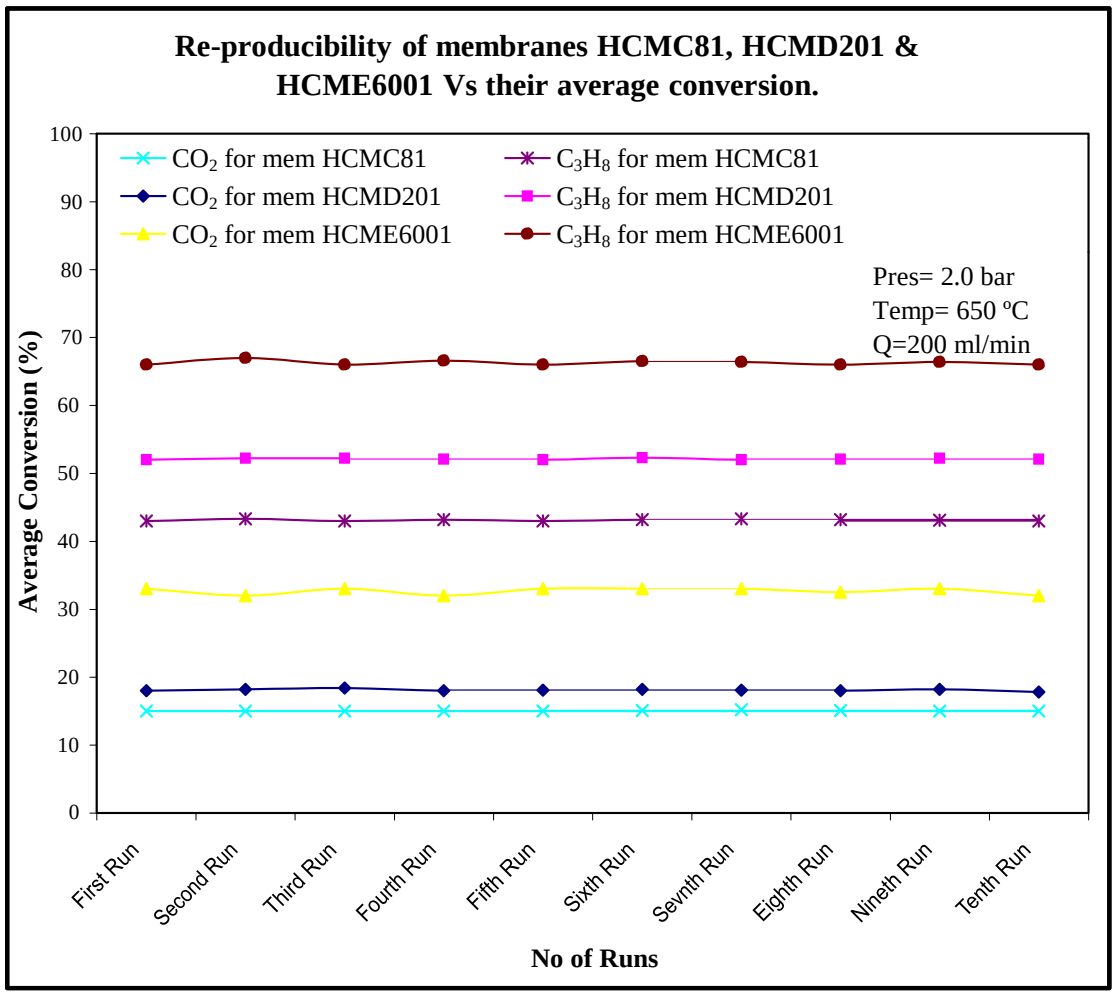

Figure 4.32 Performance comparison curve reproducibility of membranes HCMC81, HCMD201 & HCME6001 vs their average conversion.

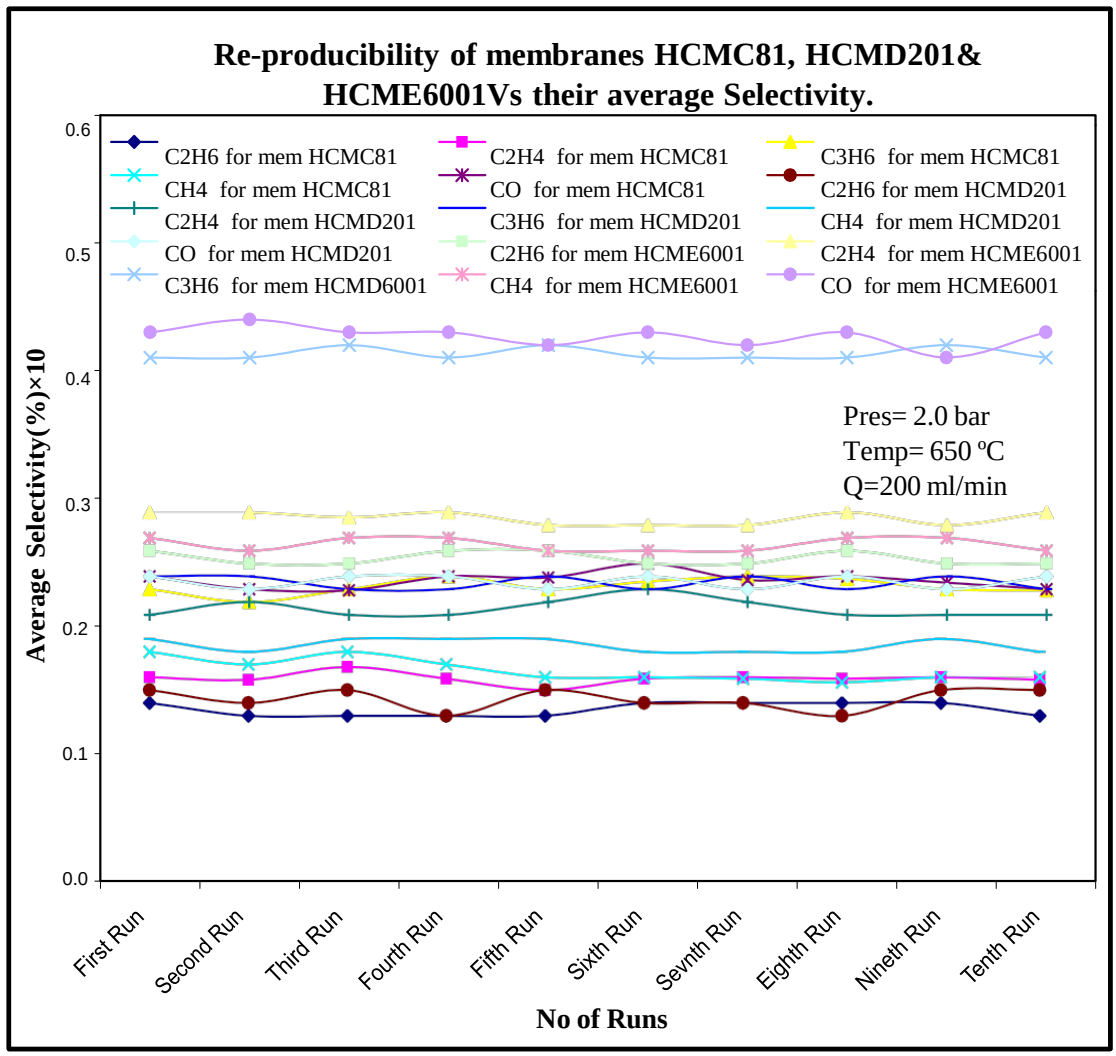

Figure 4.33 Performance comparison curve reproducibility of membranes HCMC81, HCMD201 & HCME6001 vs their average selectivity.

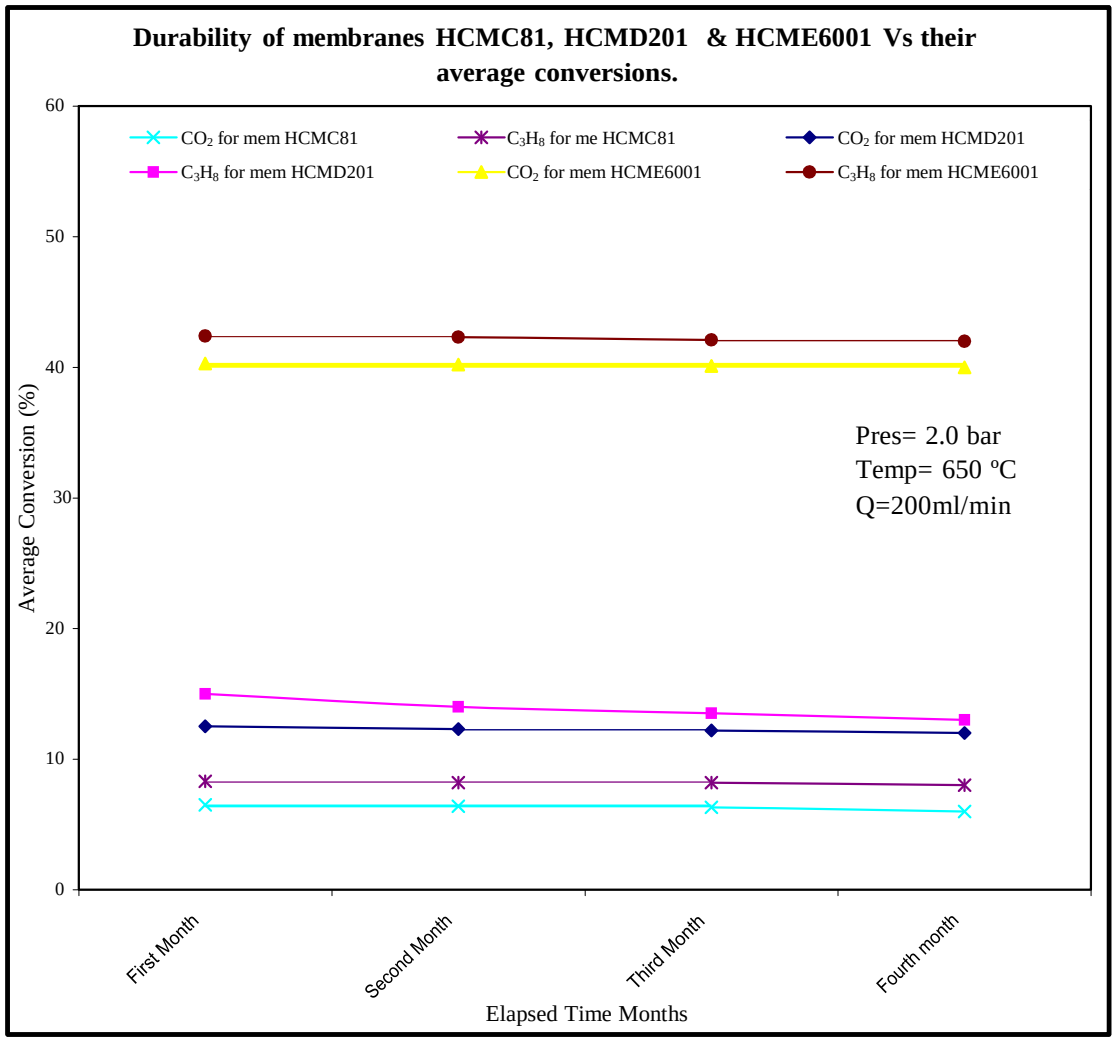

Figure 4.34 Performance comparison curve durability of membranes HCMC81, HCMD201 & HCME6001 vs their average conversion.

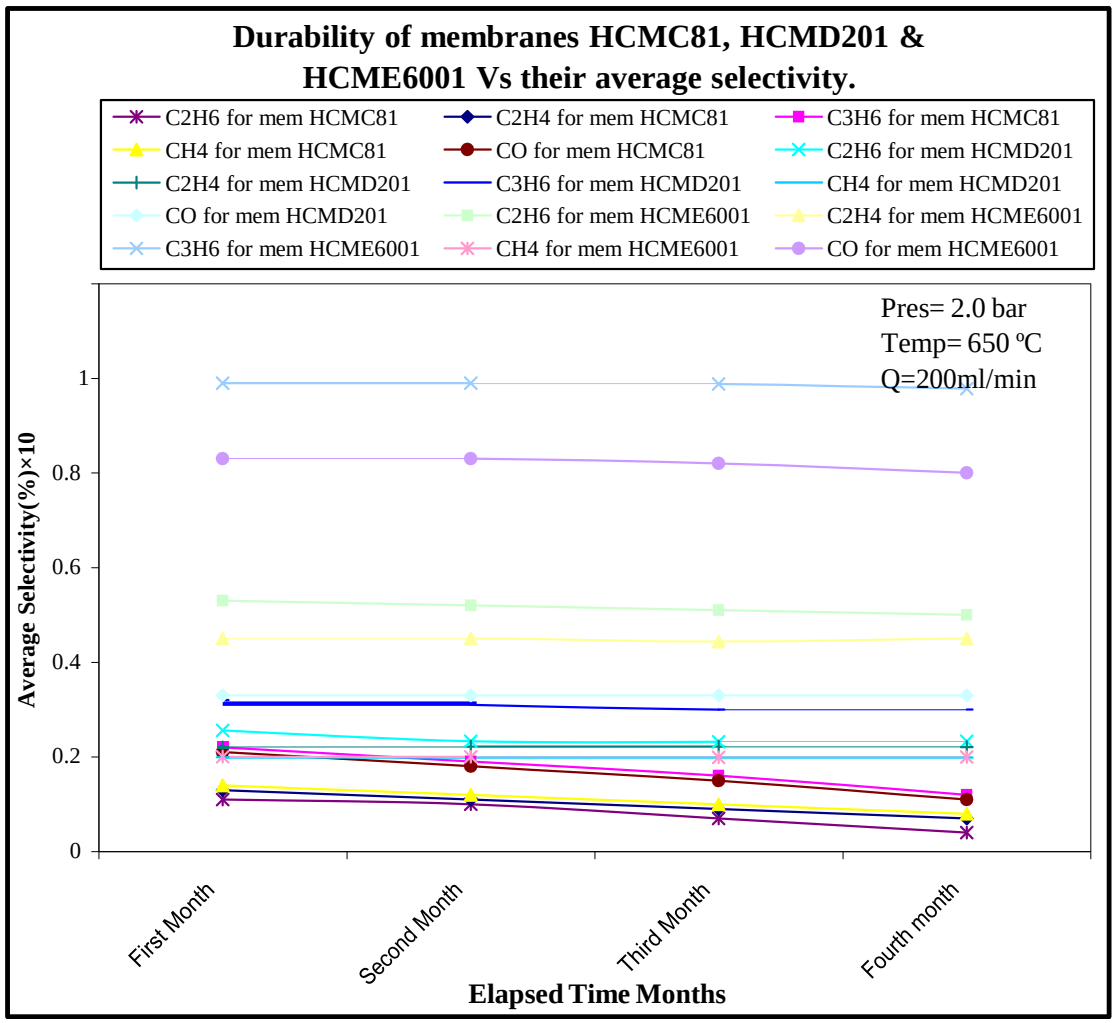

Figure 4.35 Performance comparison curve durability of membranes HCMC81, HCMD201 & HCME6001 vs their average selectivity.

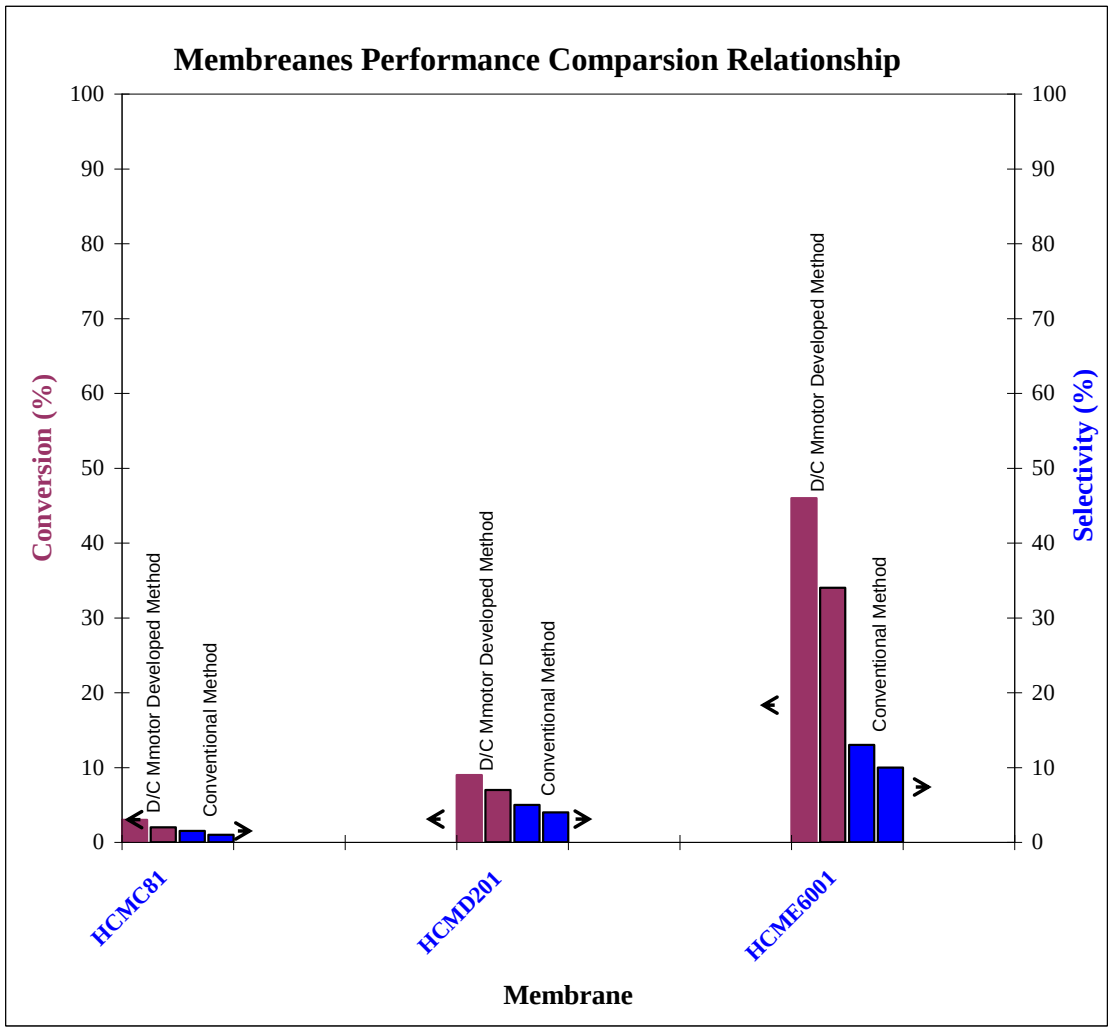

Figure 4.36 Comparison performance plot of HCM type vs average feed reactant gas conversions and their average selectivities using two different membrane preparation techniques.

4.9 HCME6001 membrane typical productive representative sample reactive run result.

Table 4.10 presents the results of the most important findings of this research study. As the experimental phase for the HCME6001 membrane progressed, a few results were gathered to be quantitatively analysed. Thus a typical productive reactive run was nominated and selected to be a representative sample. The experimental reactive run was conducted as shown in Table 4.10 under various operating conditions, including pressure of 1 bar, 2 bars and 3 bars, temperature of 600ºC/873.15ºK, 650ºC/923.15ºK and

700ºC/973.15ºK, and an overall inlet premixed reactant gas flow rate of 100ml/min, 200ml/min and 300ml/min fed at a flow ratio of 2:1. The best experimental fed gas reactant conversion result of 34% and 58% for CO_2 and C_3H_8 respectively, were observed at a pressure of 2 bars, temperature of 650ºC/923.15ºK and flow rate of 200ml/min. These conditions gave production gas selectivities of 41%, 25%, 28%, 26% and 44% for C_3H_6, C_2H_6, C_2H_4, CH_4, and CO, respectively, and some liquid yield (water) and traces of carbon.

4.10 Mass balance.

Mass transfer phenomena play an important role in heterogeneous catalyzed, multiple phase reactions. Dependent on the chosen process parameters, mass transfer can even be the rate determining step. The following mass transfer and reaction steps have to be considered:

1. Mass transfer of the gaseous reactant from the free gas phase into the gas- solid interface;
2. Mass transfer by diffusion of the gaseous reactant in the bulk of the catalyst;
3. Diffusion of the dissolved reactants within the pores of the catalyst to the active sites – pore diffusion;
4. Adsorption of the dissolved reactants at the catalytic active surface – chemisorption ;
5. Chemical reaction at the catalyst surface;
6. Desorption of the product;
7. Diffusion of the product out of the pores to the external surface of the catalyst particle and
8. Diffusion of the product through the external interface into the bulk of the gas.

The slowest step determines the effective rate of the reaction. The aim for process design should be to reduce mass transfer limitations to a minimum because they decrease the effective reaction rate and can promote side reactions. This can be achieved in a catalytic membrane reactor. The membrane reactor investigated in this work for CO_2 reforming reactions operates in pore-flow through mode, using a porous membrane that has no separating functions but acts as a support for the catalyst. The catalyst is immobilized as nanoparticles in the membrane pore structure. By this way, the membrane works as a contact zone for the reactants and the catalyst. Because of fast convective flow internal diffusion limitations are reduced as the products will be immediately removed from the membrane pore which avoids a product accumulation within the membrane. As a consequence, the effective reaction rate is not

influenced by mass transfer limitations and the selectivity for the desired product can be increased. The residence time in the membrane pores is short which suppresses the consecutive reaction. By this way, the forced-through flow concept of membrane reactors has many advantages compared to fixed-bed and slurry reactors:

- pore diffusion can be reduced
- no catalyst separation from the product necessary
- good catalyst accessibility (less catalyst metal necessary)

The concept of a mass balance, also called a material balance, is based on the fundamental laws of physics, which state that mass can neither be produced nor destroyed, but in fact mass is conserved. There is an equally fundamental law for the conservation of energy. Although energy can change in form, it cannot be created or destroyed. These two laws of physics provide the basis for two tools which are used routinely in environmental engineering and science.

In general, the mass balance for any system can be mathematically represented as follows:

Input = output + accumulation.

4.10.1 The material balance for the chemical reactor.

The general form of a mass balance is that the mass that enters a system must, by conservation of mass, either leave the system or accumulate within the system. Mass balances are, therefore, used widely in engineering and environmental analyses. For example, mass balance theory is used to design chemical reactors and analyse alternative processes to produce chemicals.

Input = output + accumulation, or Input - output - accumulation = 0.

4.10.2 General mole balance.

The rate of accumulation of component j = rate of inflow of component j - rate of outflow of component j + rate of generation of component j by chemical reactions:

$$\frac{d}{dt}\int_V cj\,dV = Q_o c_{jo} - Q_1 c_{j1} + \int_V R_j\,dV \qquad 4.17$$

Equation 4.17 applies to every component in the system including inerts, which do not take place in any reactions. j = 1, 2,……, n_s, assuming component j enters and leaves the volume element only by convection with the inflow and outflow streams, i.e. neglecting diffusional flux through the boundary of the volume element due to a concentration

gradient. To solve the reactor material balance, we require an expression for production rates, R_j :

$$R_j \sum_i \nu_{ij} \gamma_i \qquad 4.18$$

In this case, we require γ_i as a function of C_j and we use common reaction-rate expressions without derivation, assuming both the reactant fed gases were well mixed in the reactor and the entire reactor contents are the reactor volume element. Thus the integrals in equation 4.19 are simple to evaluate to produce:

$$\int_{VR} c_j dV = c_j V_R \int_{VR} R_j dV = R_j V_R \qquad 4.19$$

The inflow and outflow stream flow rates are zero, $Q_0 = Q_1 = 0$.

$$\frac{d\left(c_j V_R\right)}{dt} = R_j V_R \qquad 4.20$$

Equation 4.21 applies whether the reactor volume is constant or changes during the reaction, but if the reactor volume is constant (liquids-phase reactions), then,

$$\frac{dc_j}{dt} = R_j \qquad 4.21$$

In this case, we use Equation 4.21 rather than Equation 4.18 if the reactor volume changes significantly during the course of the reaction.

4.11 Mass balance calculation sample of chemical reaction products produced and reactants fed gases consumed.

Although in many cases chemical reactions do not go to completion and only a fraction of the reactants will be converted, the left side of an empirical equation must always equal the right side of the equation. This is due to the most elementary concept of matter balance, which can be expressed in following form:

Input (enters through system boundaries) + generation (produced within system boundaries) − output (leaves through system boundaries) − consumption (consumed within system) = accumulation (build up within system).

In this research study, the chemical reactor was used as shown in figure 4.37, which presents the flow chart of the membrane reactor inputs/outputs of the system involved and the stoichiometric chemical reaction Equation 4.18.

4.11.1 Molecular weight.

$3C_3H_8 + 2CO_2 \longrightarrow C_3H_6 + C_2H_6 + C_2H_4 + CH_4 + 2CO + 2H_2O + C$ 4.22

g mole = mass in g/molecular weight

Reactions of the previously mentioned equation can be expressed stoichiometrically, for example, using equation 4.22, as:

$3[(12 \times 3) + (1 \times 8)]$ g/mole + $2[(12 \times 1) + (16 \times 2)]$ g/mole $\longrightarrow$ $[(12 \times 3) + (1 \times 6)]$ g/mole+$[(12 \times 2)+(1 \times 16)]$g/mole+$[(12 \times 2)+(1 \times 4)]$ g/mole+$[(12\times1)+(1\times4)]$ g/mole+$2[(12\times1)+(1\times16)]$g/mole+$2[(1\times2)+(1\times16)]$g/mole +12

132 g/mol + 88 g/mol = 42 g/mol + 30 g/mol + 28 g/mol+16 g/mol+56 g/mol+ 36 g/mol + 12g/mol.

Mass balance: 220 g/mol = 220 g/mol.

This stoichiometric mole balance calculation is, however, based on the assumption of 100% consumption of the reactant fed gases accompanied by a very small trace of carbon besides other experimental MCR reaction products.

4.11.2 Flow rate.

For mass balance calculations that are based on gas flow rates, a sample of two results obtained for membrane HCME6001 that have been presented in this chapter, were selected to calculate material balance based on flow rate. The results were attained as the intended catalytic membrane was tested under the following operating conditions. The reactant fed gases were premixed via the mixing chamber and introduced into the catalytic reactor at a flow rate of 100ml/min and 300ml/min at ratio of 1:1, CO_2,:C_3H_8 respectively, pressure across the reactor of 2 bars and an average temperature of 650ºC/923.15ºK.

Average selectivities of the CMR chemical reaction product gas after a 6-hr period were used to calculate the material balance, with the following experimental operating conditions:

- Type of flow regime: (1:1) premixed
- Average temperature across the CMR = 650^{o}C/923.15 ^{o}K.
- Pressure = 2 bar abs.
- Inlet flow rate = 100ml/min
- Outlet flow rate = 65ml/min

The calculation results obtained are presented in tables 4.10 and 4.11.

Table 4.10 Mass balance calculation results of the MCR based on gas flow rate of 100 mil/min.

Component	In (mol/min)	Consumed (mol/min)	unconsumed (mol/min)	Out (mol/min)
C_3H_8	0.130	0.053	0.071	0.071
CO_2	0.130	0.051	0.060	0.060
C_3H_6	-	-	-	0.079
C_2H_6	-	-	-	0.001
C_2H_4	-	-	-	0.001
CH_4	-	-	-	0.004
CO	-	-	-	0.026
H_2O + C	-	-	-	0.012
Total	0.260	0.104	0.131	
Total input = 0.260			Total output = 0.260	

Table 4.11 Mass balance calculation results of the MCR based on gas flow rate of 300 mil/min.

Component	In (mol/min)	Consumed (mol/min)	unconsumed (mol/min)	Out (mol/min)
C_3H_8	1.173	0.287	0.987	0.987
CO_2	1.173	0.268	0.889	0.889
C_3H_6	-	-	-	0.321
C_2H_6	-	-	-	0.001
C_2H_4	-	-	-	0.001
CH_4	-	-	-	0.001
CO	-	-	-	0.123
H_2O + C	-	-	-	0.023
Total	2.346	0.555	1.876	0.555
Total input = 2.346			Total output = 2.346	

In order to convert the equivalent of the reactant fed gases into moles of those gases, we apply PV = nRT, substituting for the given operating conditions (i.e. pressure, temperature and flow rate) data, and the results shown in figure 4.37 were obtained:

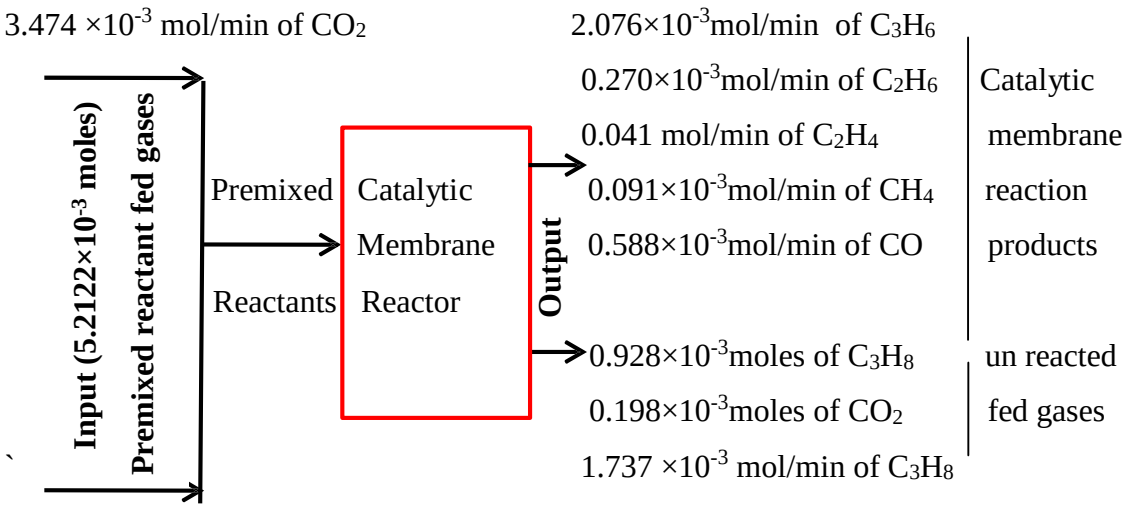

Figure 4.37 flowchart of the membrane reaction system of reactant fed gas art ratio of 2:1.

Figure 4.37 presents the flow chart that is used to summarise the layout of the process as well as to indicate known information about percentages and the state of the process streams.

Total moles of reactant fed gases = 5.2122×10^{-3}, 3.474×10^{-3} moles of which was CO_2 and 1.737×10^{-3} moles C_3H_8. As they were fed into the CMR, they produced 2.076×10^{-3} moles of C_3H_6 + 0.270×10^{-3} moles of C_2H_6 + 0.041×10^{-3} moles of C_2H_4 + 0.091×10^{-3} moles of CH_4 + 0.588×10^{-3} moles of CO + [0.928×10^{-3} moles of C_3H_8 + 0.198×10^{-3} CO_2 moles of un-reacted reactant fed gases] + H_2O + carbon.

This gives us 5.2122×10^{-3} moles = 5.192×10^{-3}. In these circumstances, we may assume that the remaining 0.0202×10^{-3} not accounted for in this reaction represented the liquid yield (i.e. H_2O) and carbon that accompanied the reaction. This proves, therefore, that this mass material balance chemical reaction was balanced because both sides of the equation equaled 100% (in other words 5.2122 moles of reactant fed gases = 5.2122 moles of products).

Table 4.12 shows a summary of the results obtained for the nominated representative reactive run for membrane HCME6001.

Table 4.12 Summary of obtained results for nominated representative reactive run for membrane HCME6001.

Type of gas	Conversion (%)	Selectivity (%)	Pressure (bars)	Temperature (°C)	Flow rate (ml/min)streamed at flow ratio of (2:1)
Propane (C_3H_8)	41 58 43	-	1.0 2.0 3.0	600 650 700	100 200 300
Carbon dioxide (CO_2)	22 34 24	-	1.0 2.0 3.0	600 650 700	100 200 300
Propylene (C_3H_6)	-	32 41 33	1.0 2.0 3.0	600 650 700	100 200 300
Ethane (C_2H_6)	-	18 25 19	1.0 2.0 3.0	600 650 700	100 200 300
Ethylene (C_2H_4)	-	24 28 25	1.0 2.0 3.0	600 650 700	100 200 300
Methane (CH_4)	-	21 26	1.0 2.0	600 650	100 200

		22	3.0	700	300
Carbon monoxide (CO)	-	37 44 38	1.0 2.0 3.0	600 650 700	100 200 300
Water (H_2O)	-	11 18 12	1.0 2.0 3.0	600 650 700	100 200 300
Un reacted propane (C_3H_8)		37			
Un reacted carbon dioxide (CO_2)		23			

4.12 Kinetic activation energy.

In chemistry, activation energy is a term that was introduced in 1889 by the Swedish scientist Svante Arrhenius and is defined as the energy that must be overcome in order for a chemical reaction to occur. Activation energy may also be defined as the minimum energy required starting a chemical reaction. The activation energy of a reaction is usually denoted by **Ea** and given in units of (kjs) per mole [17].

4.13 Determination of activation energy of CMR chemical reactions.

The rate of a reaction depends on the temperature at which it is run. As the temperature increases, the molecules move faster and therefore collide more frequently. The molecules also carry more kinetic energy. Thus, the proportion of collisions that can overcome the activation energy for the reaction increases with temperature. The Arrhenius equation 4.23, shown elsewhere in this study, can be used to calculate the activation energy for chemical reactions. Arrhenius showed that the relationship between temperature and the rate constant for a reaction obeyed the following equation:

$$k = A^* \exp^{(-E/R^*T)} \quad 4.23$$

By rearranging this equation, we obtain:

$$\ln k = \ln A - Ea/RT \quad 4.24$$

This equation is in the form of **y= mx + b**. As the equation of the slope is rearranged, we have E_a= - mR. When the relationship of the LnK (rate constant) is plotted against the inverse of the temperature in °Kelvin, the obtained slope is a straight line. Thus, the slope (m) is equal to $-E_a/R$, when R is a constant that equals 8.314 Jol/mol.K.

Table 4.13 summarises the activation energy values of the chemical reaction between CO_2 and C_3H_8 using the HCME6001 membrane. These values, however, only represent the selected sample that was conducted under certain operating conditions, as indicated in the plots shown in figures 4.44 to 4.49.

Table 4.13 Summary of the activation energy values of the chemical reaction between CO_2 and C_3H_8.

Gas / E	C_3H_8 1	CO_2 1	C_3H_8 1	CO_2 2	C_3H_8 2	CO_2 1
(kJ/mol)	25.1	41.0	57.7	40.0	23.6	113.2

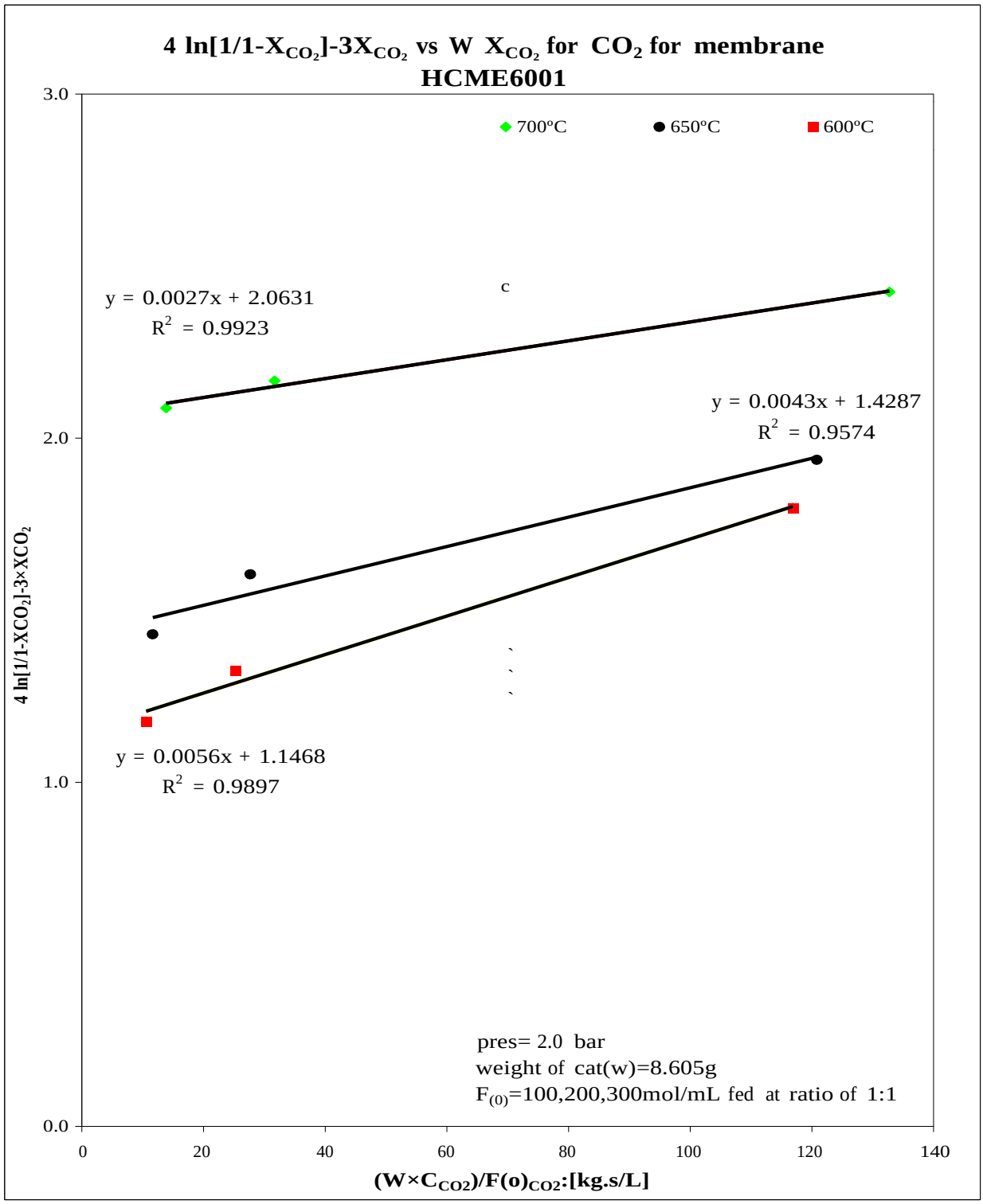

Figure 4.38 Relationship plot of 4 ln[1/1-XCO_2]-3XCO_2 vs W XCO_2 for CO_2 for membrane HCME6001 at various temp, CO_2 reactant fed gas flow rates fed at ratios of 1:1 and Δ P=2.0 bars.

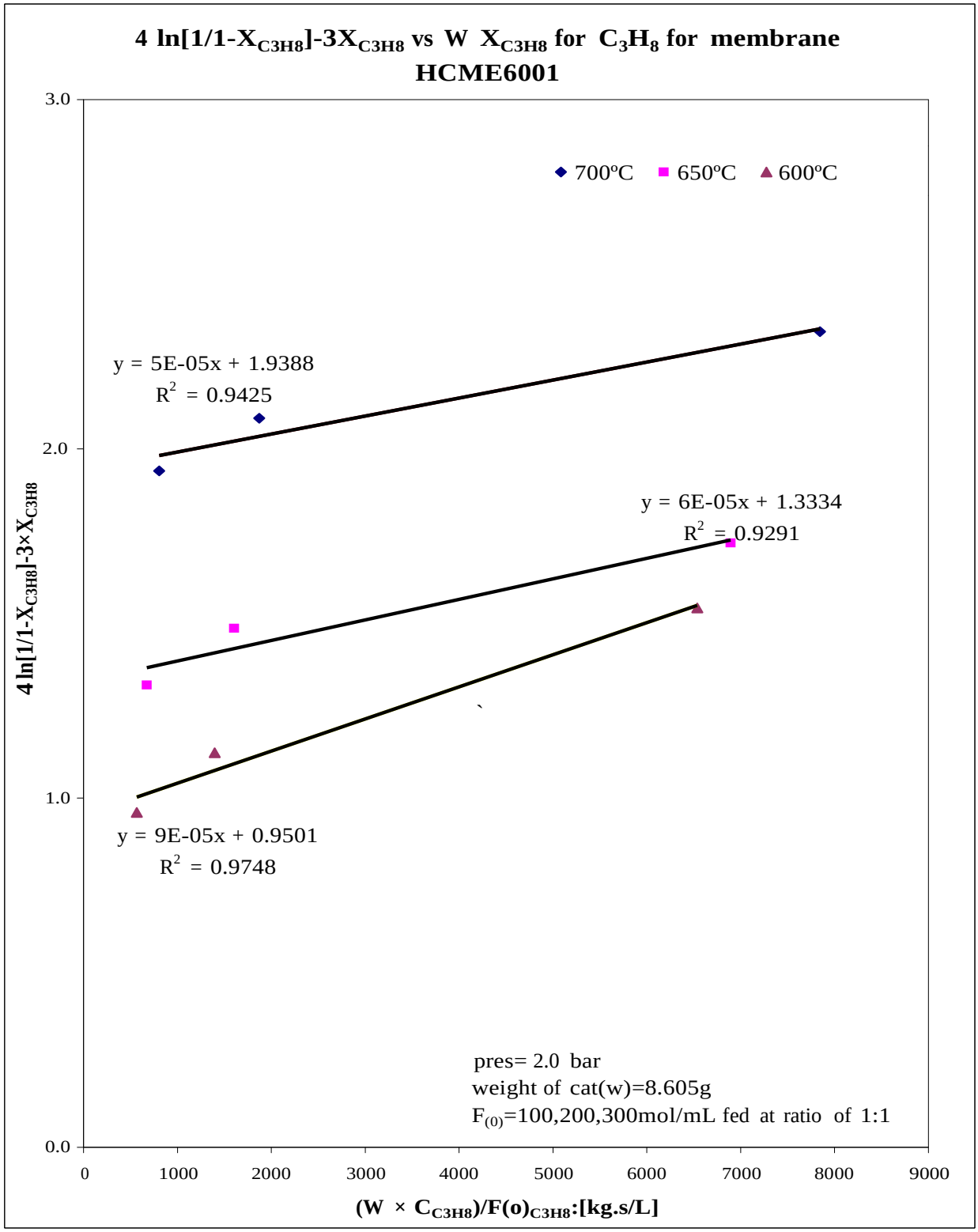

Figure 4.39 Relationship plot of 4 ln[1/1-XC_3H_8]-3XC_3H_8 vs W XC_3H_8 for C_3H_8 for membrane HCME6001 at various temp, C_3H_8 reactant fed gas flow rates fed at ratios of 1:1 and Δ P=2.0 bars.

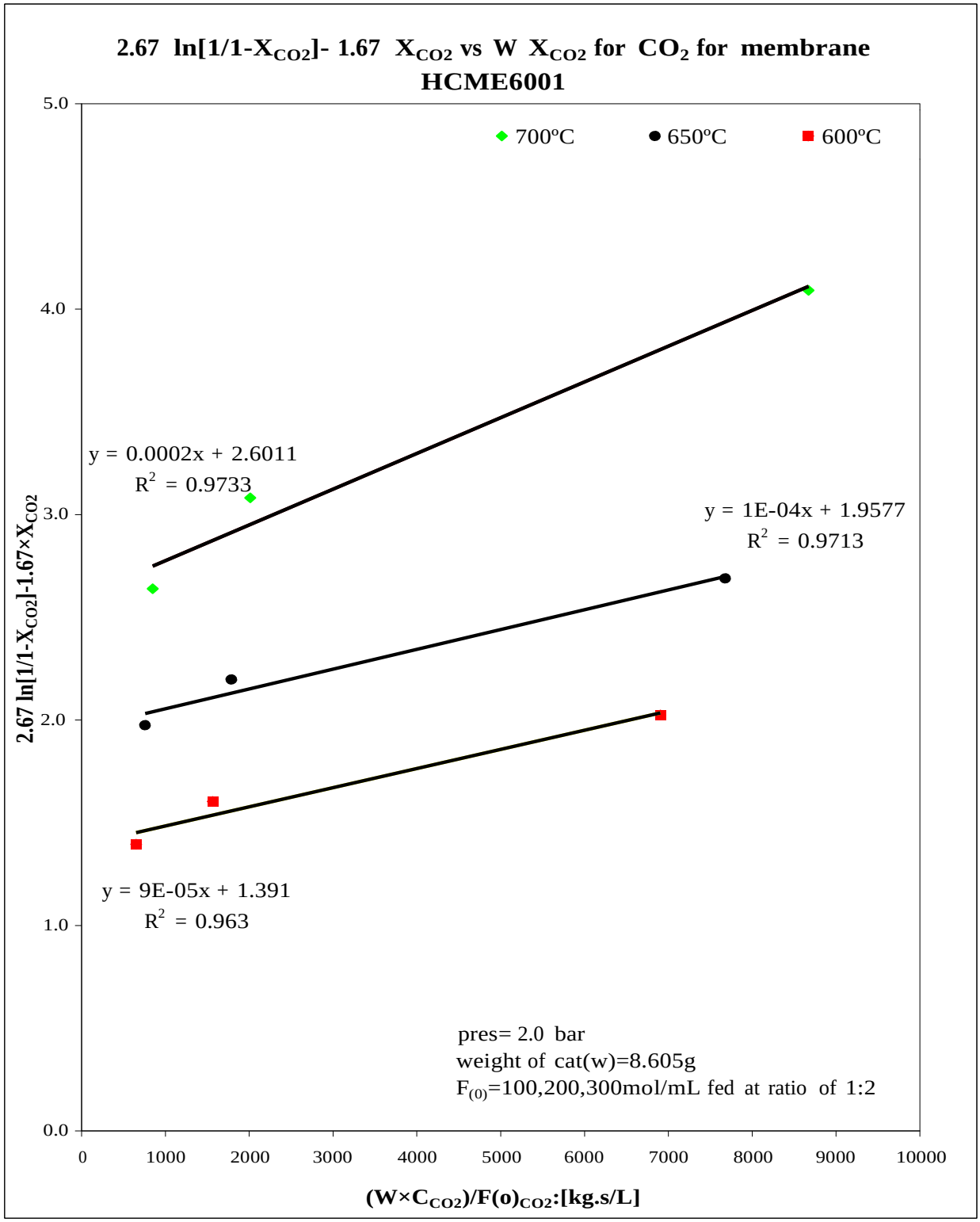

Figure 4.40 Relationship plot of 2.67ln[1/1-XCO_2]-1.67XCO_2 vs W XCO_2 for CO_2 for membrane HCME6001 at various temp, CO_2 reactant fed gas flow rates fed at ratios of 1:2 and Δ P=2.0 bars.

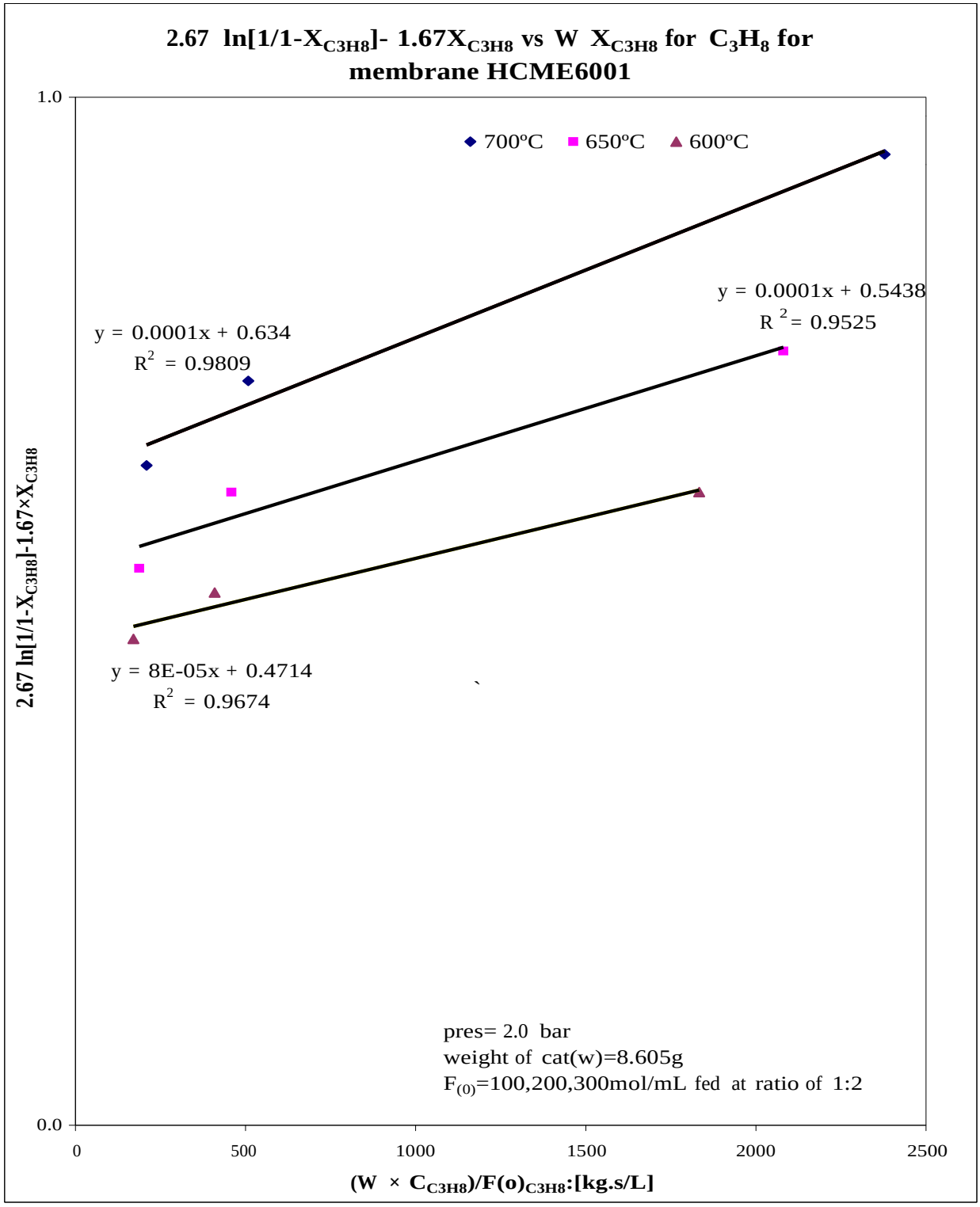

Figure 4.41 Relationship plot of 2.67ln[1/1-XC_3H_8]-1.67X C_3H_8 vs W XC_3H_8 for C_3H_8 for membrane HCME6001 at various temp, C_3H_8 reactant fed gas flow rates fed at ratios of 1:2 and Δ P=2.0 bars.

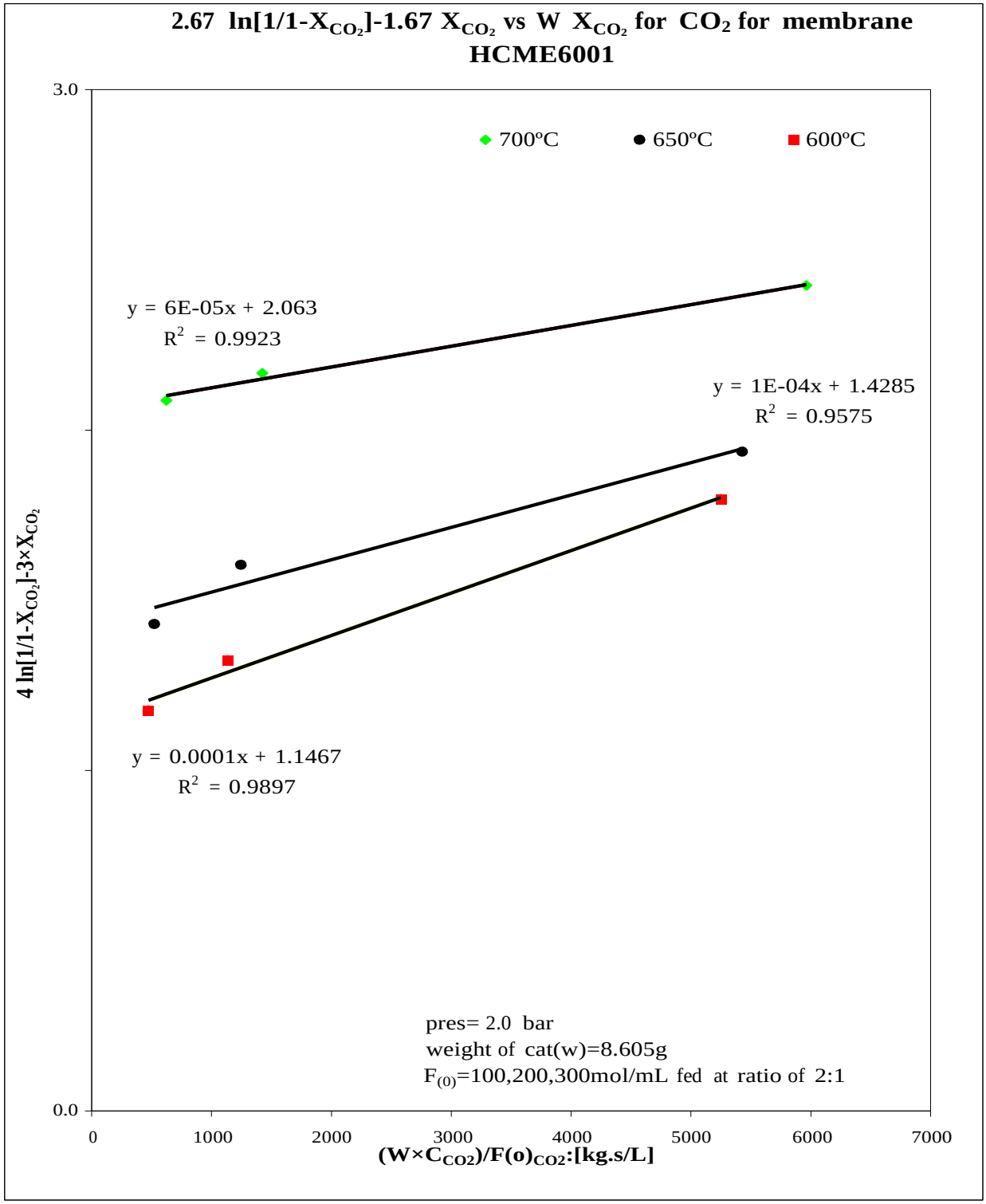

Figure 4.42 Relationship plot of 2.67ln[1/1-XCO2]-1.67XCO$_2$ vs W XCO$_2$ for CO$_2$ for membrane HCME6001 at various temp, CO$_2$ reactant fed gas flow rates fed at ratios of 2: 1 and Δ P=2.0 bars.

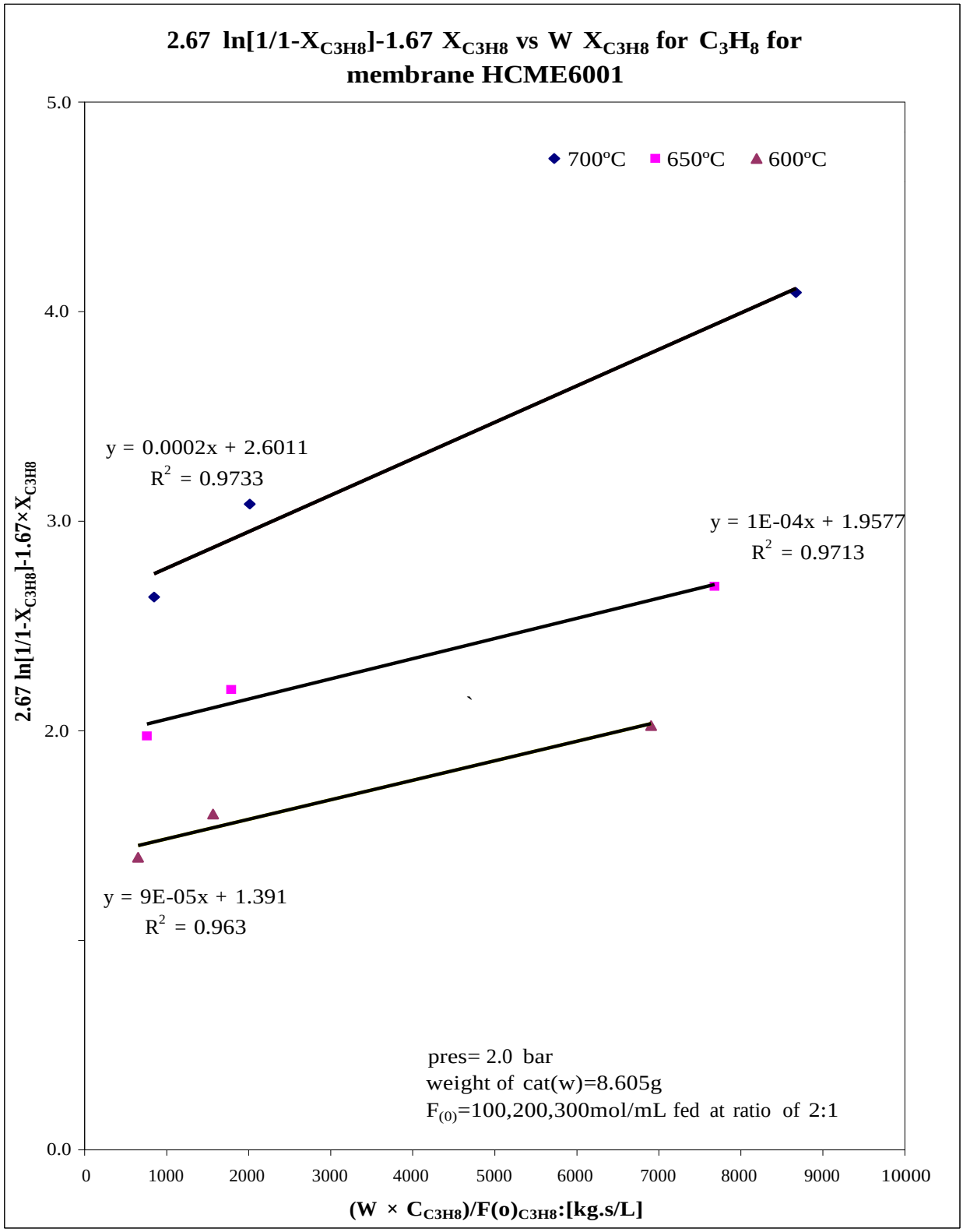

Figure 4.43 Relationship plot of 2.67 ln[1/1-XC_3H_8]-1.67X C_3H_8 vs W XC_3H_8 for C_3H_8 for membrane HCME6001 at various temp, C_3H_8 reactant fed gas flow rates fed at ratios of 2:1 and Δ P=2.0 bars.

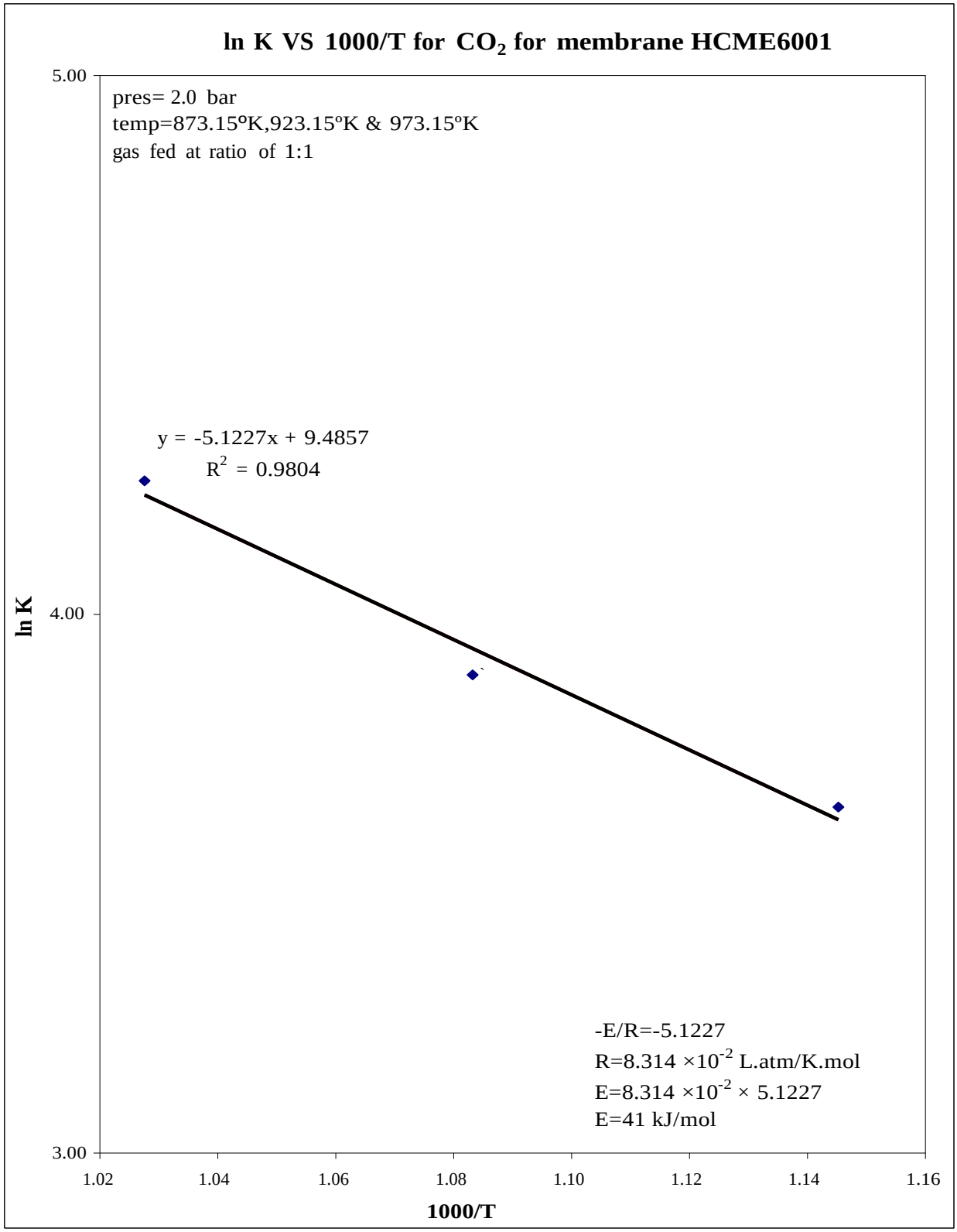

Figure 4.44 Relationship plot of ln K vs 1000/T for CO_2 for membrane HCME6001 at various temp, CO_2 reactant fed gas flow rates fed at ratios of 1:1 and Δ P=2.0 bars.

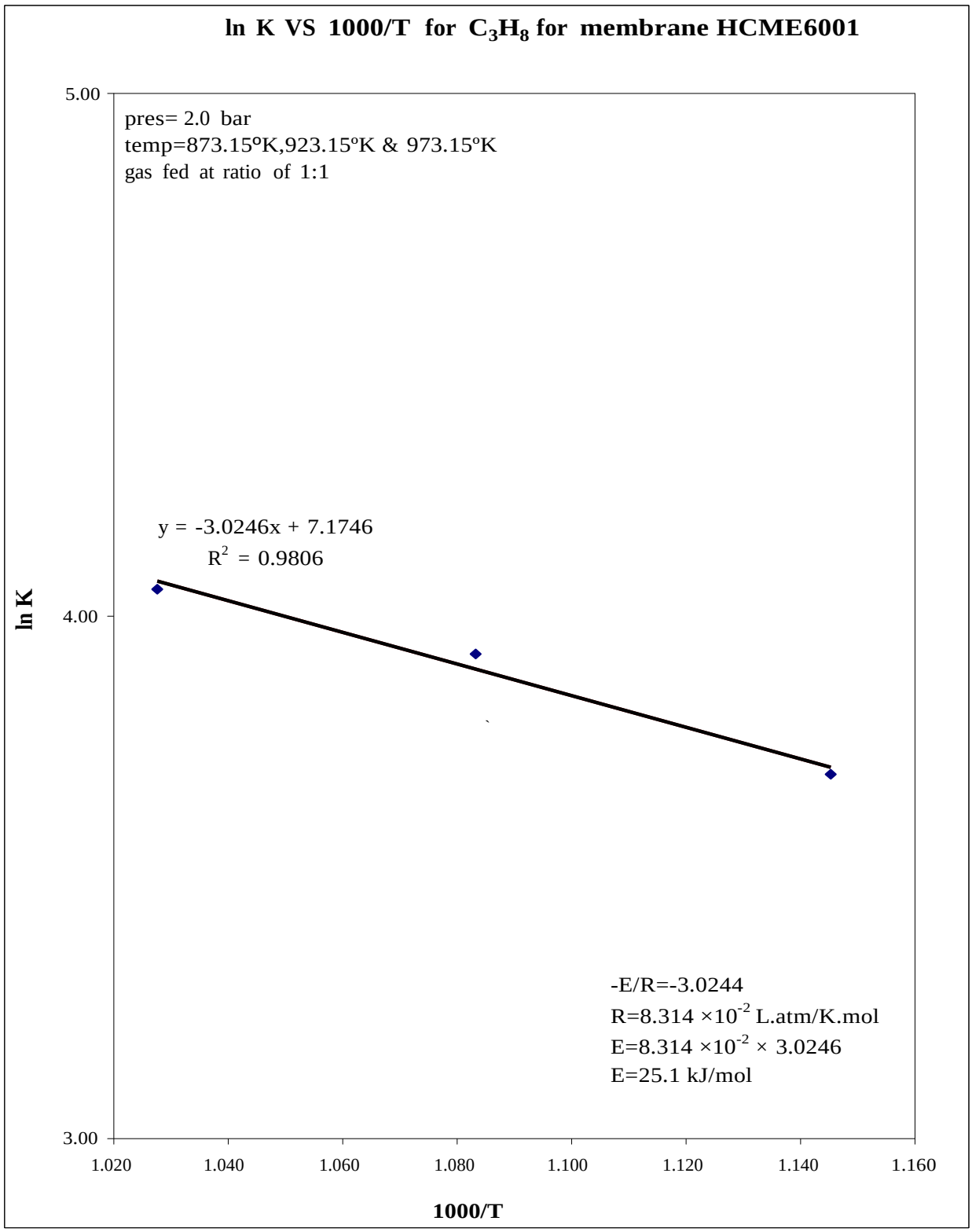

Figure 4.45 Relationship plot of ln K vs 1000/T for C_3H_8 for membrane HCME6001 at various temp, C_3H_8 reactant fed gas flow rates fed at ratios of 1:1 and Δ P=2.0 bars.

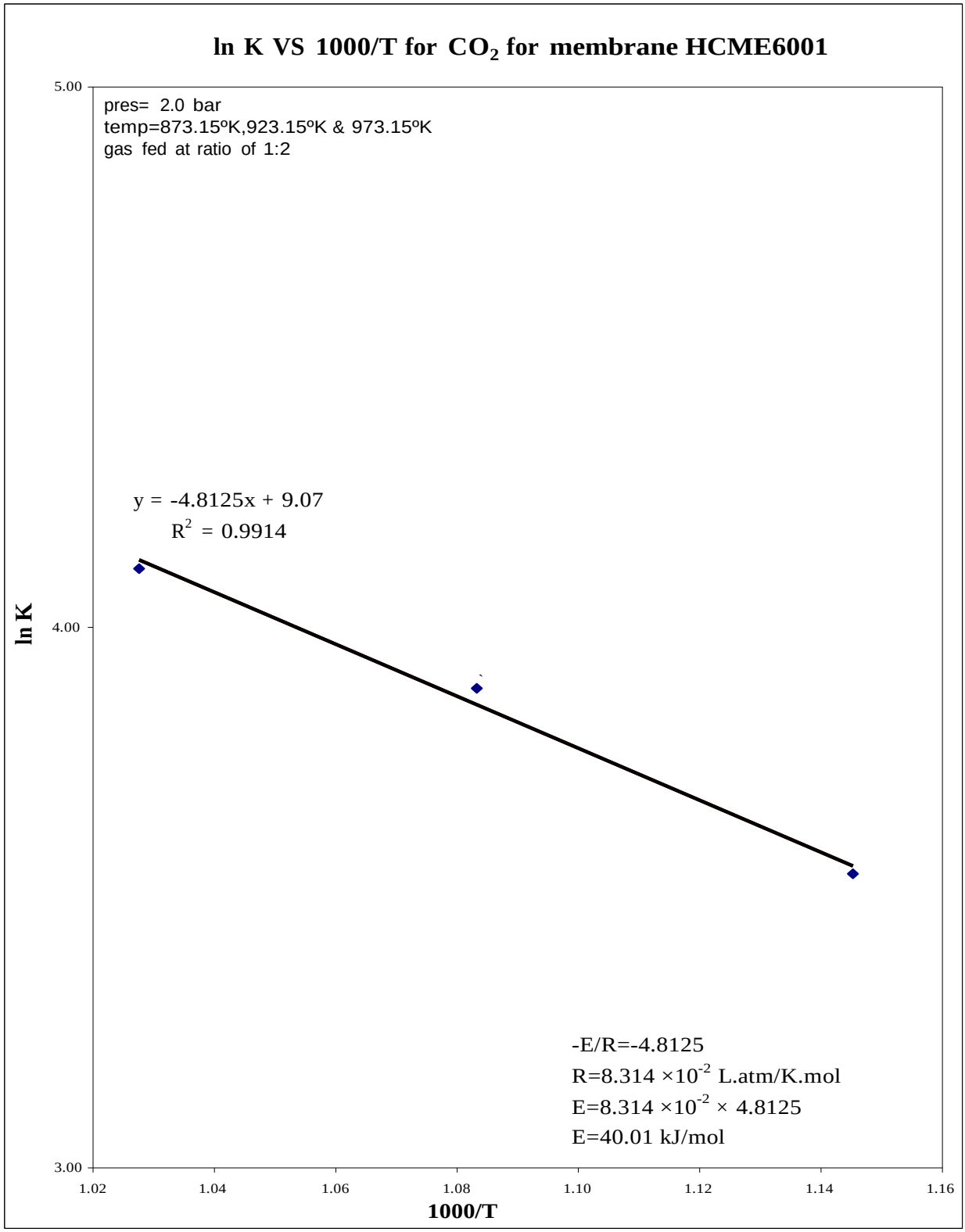

Figure 4.46 Relationship plot of ln K vs 1000/T for CO_2 for membrane HCME6001 at various temp, CO_2 reactant fed gas flow rates fed at ratios of 1:2 and Δ P=2.0 bars.

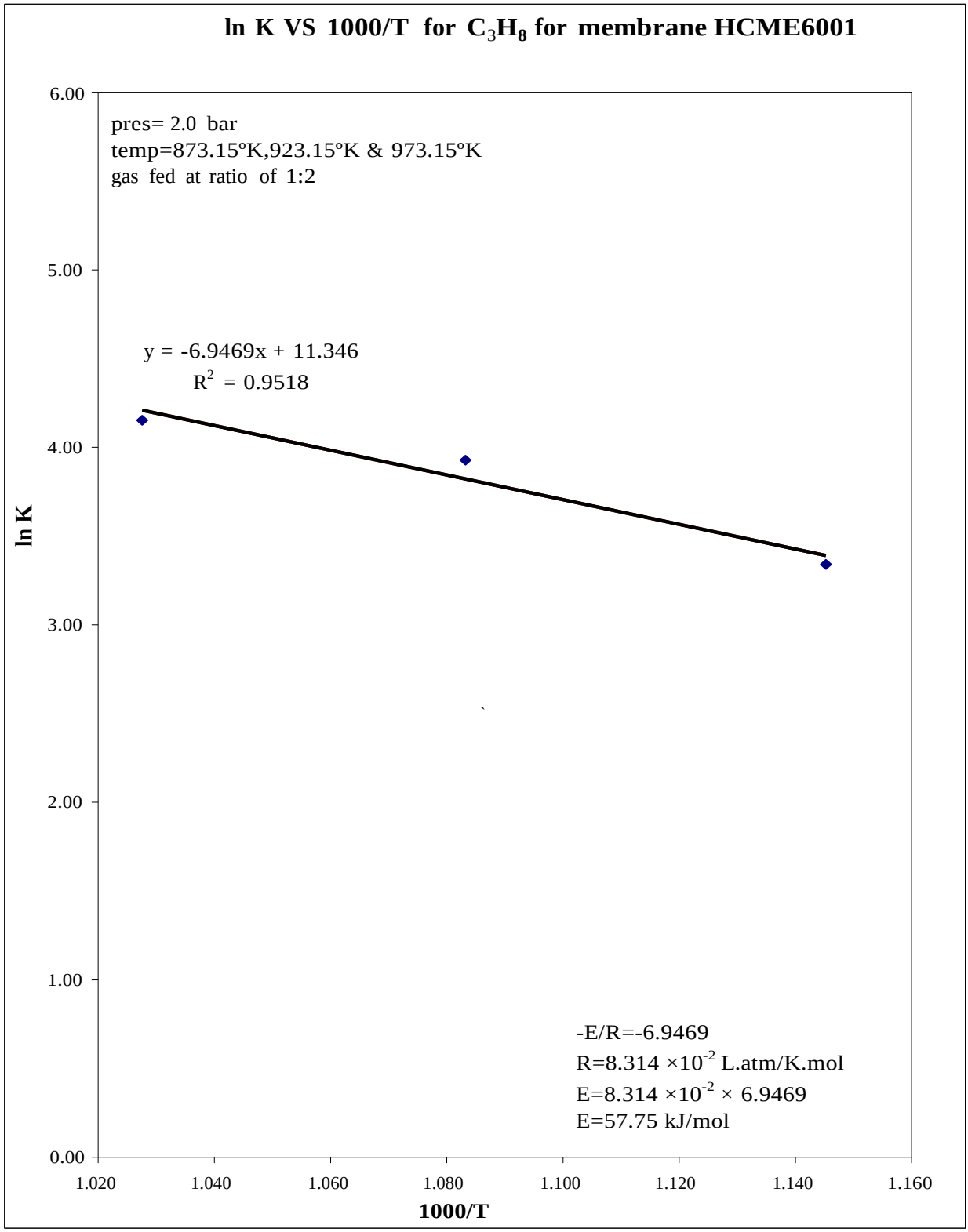

Figure 4.47 Relationship plot of ln K vs 1000/T for C_3H_8 for membrane HCME6001 at various temp, C_3H_8 reactant fed gas flow rates fed at ratios of 1:2 and Δ P=2.0 bars.

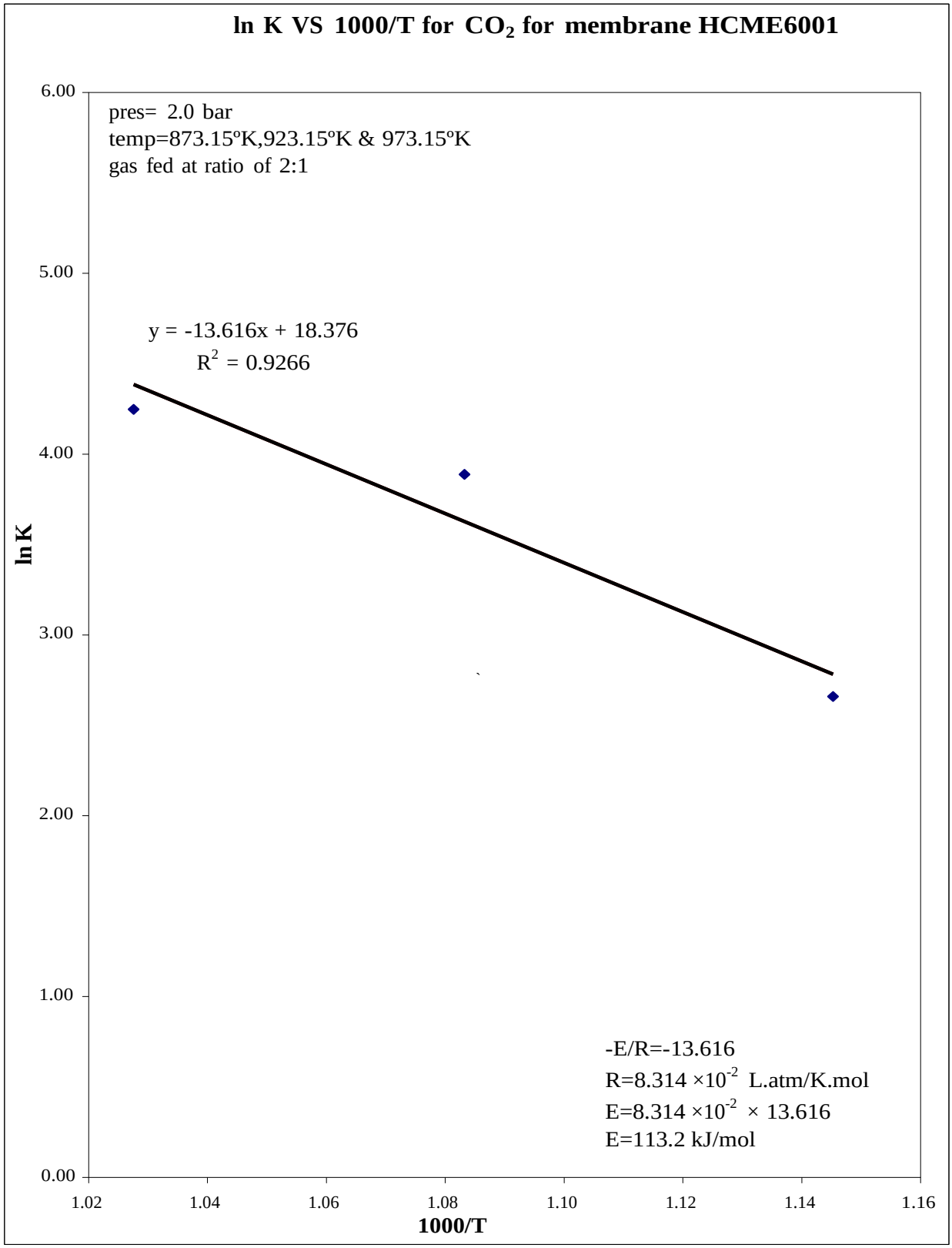

Figure 4.48 Relationship plot of ln K vs 1000/T for CO_2 for membrane HCME6001 at various temp, CO_2 reactant fed gas flow rates fed at ratios of 2:1 and Δ P=2.0 bars.

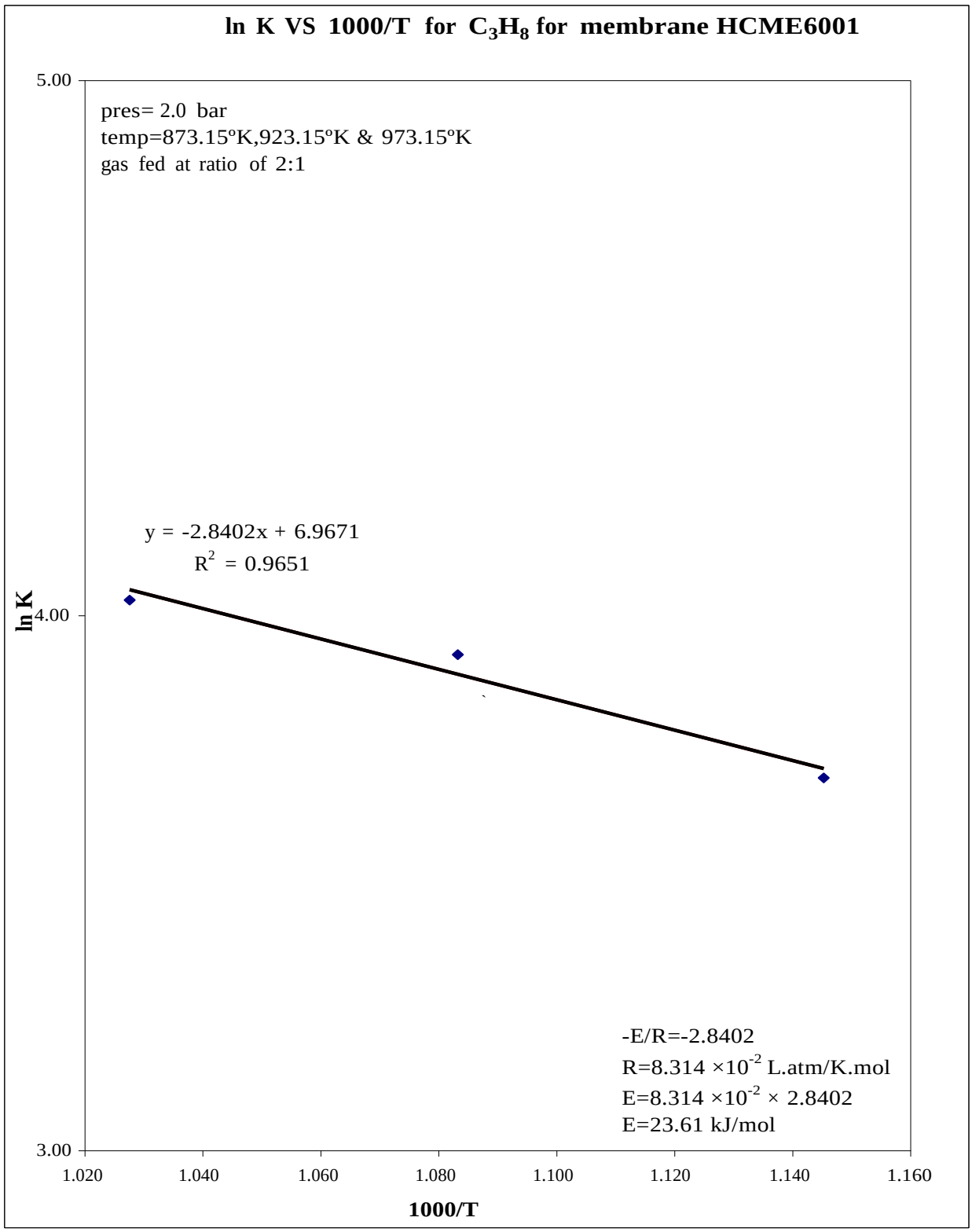

Figure 4.49 Relationship plot of ln K vs 1000/T for C_3H_8 for membrane HCME6001 at various temp, C_3H_8 reactant fed gas flow rates fed at ratios of 2:1 and Δ P=2.0 bars.

Chapter Five

Conclusions and Recommendations for Future Work

CHAPTER 5: Conclusions and recommendations for Future work

5.1 Conclusions.

This research investigated the dry reforming of propane using **H**ybrid **C**eramic **M**embranes (HCMs) incorporating Zr: Ni: Pd: Cu / α- Al_2O_3 $_{catalysts}$. The catalysts were successfully prepared, and used in the HCMs to improve the dry oxidation of C_3H_8 with CO_2 to produce useful gases, mainly C_3H_6 and CO. These are widely considered to be essential raw materials in several industrial areas such as production of PVC and synthesis gas used in GTL. The main objective of this research was to develop a low cost, novel membrane reactor, which was suitable for the production of useful products from associated natural gas. The main focus of activities was the production, characterization and laboratory scale evaluation of catalyst-impregnated membranes based on tubular ceramic supports, and to investigate the feasibility of such catalytic membrane reactors to affect dry reforming.

During the first step of this study, consideration was given to selecting proper ceramic supports with suitable pore diameters that would be practical to use. Consequently, three sets of supports with pore diameters of 80nm, 200nm and 6000nm were chosen. The next stage was to prepare the hybrid solutions using the catalysts and to use them to prepare the HCMs. The detailed procedure of clearing, impregnating, drying and calcining the membrane supports was explained in the experimental chapter. The resulting HCMs were then fully characterised using various techniques including gas permeability measurement, Scanning Electronic Microscopy (SEM), Accelerated Surface Area and Porosimetry analysis (ASAP), nitrogen adsorption, Energy Dispersive X-ray Analysis (EDXA) and X-ray photoelectron spectroscopy (XPS), to have a full understanding of their characteristics and ensure that they were fit for purpose. The experimental rig and its accessories were set up and the prepared HCMs were placed in the reactor for carrying out preliminary tests and investigations on their reactions. These preliminary investigations demonstrated a very promising performance of the catalytic reaction. Success was measured as very good feed reactant gas conversions and good

product gas selectivities. This success may be attributed to the technical modification to the membrane preparation method that was pioneered in this study. This was the use of a low speed d/c motor, which led to almost doubling the amount of catalyst loaded onto the supports. For membranes HCME6001, HCMD201 and HCMC81, catalyst loading gains of 52%, 17%, and 8%, respectively, were obtained compared to the conventional dip coating technique figure4.41 presents a comparison performance plot for the three HCMs and the preparation techniques. This development in the preparation technique boosted the amount of catalyst gain on the membranes and thus contributed to the improvement in their performance in terms of their reactant activation energy. This was especially true for the HCME6001 membrane.

In general, reaction temperatures between 600ºC/873.15ºK and 700ºC/973.15ºK were mainly used in this study. The first challenge, that of selecting proper ceramic supports, therefore had to also consider whether the supports had the strength and ability to withstand operating conditions that included high temperature and pressure. This challenge directed efforts to focus mostly on the development of new HCM catalysts that could achieve this target. The research was, thus, committed to investigating the catalytic performance of dry reforming of propane over Zr: Ni: Pd: Cu / α- Al_2O_3 catalysts under the temperature range of 873.15to 973.15ºK These catalysts, supported on α- Al_2O_3, were used in this study since preliminary studies had shown that they had better selectivity and activity and less deactivation resistance than some other catalysts.

Experimental operating conditions were set up and the permeated gas stream was kept flowing continuously until system stability was approached. The tube-side resulting products were analysed by means of online gas chromatography (GC), and good performance was indicated. With an increase in the reaction temperature, conversion of propane increased rapidly and selectivity of C_3H_6 increased, in addition to some liquid yield product (water). Good thermal stability, excellent gas permeability and hydropholic properties (indicated by the fact that the water vapour accompanying the catalytic membrane reaction could permeate easily) were also observed. Although a further increase in reaction temperature enhanced propane conversion, the selectivity of C_3H_6 was reduced noticeably, along with liquid yield products.

As mentioned, the experimental results show that HCMs exhibit good thermal stability, excellent gas permeability, hydropholic properties and higher separation factors. The water vapour produced by the catalytic membrane reaction could permeate through the HCMs, like the product gases. The membrane reactor could therefore be recommended for H_2O separation processes. In addition, the catalytic tests demonstrated that the intrinsic properties of the membrane reactor are suitable for dry reforming processes. This study also demonstrated the specificity and directivity of the catalytic membranes.

It may be concluded that the performance of the HCMs, especially HCME6001, which has undergone extensive investigation, was very promising. They exhibited high reactant feed gas conversions of about 34% and 58% for CO_2, and C_3H_8, respectively, under operating conditions of 650ºC, 2 bars of pressure and a feed reactant gas flow rate of 200 ml/min at a 2:1 ratio CO_2:C_3H_8. These conditions gave selectivities of 41%, 44%, 25%, 28% and 26% for C_3H_6, CO, C_2H_6, C_2H_4, and CH_4, respectively. These observations support the necessity to further develop these processes as well as other processes available for the conversion of associated natural gas to many useful chemicals.

This conversion process also utilizes CO_2 instead of emitting it to the atmosphere where it causes a range of environmental problems including global warming and climate change. This study identified a way to utilise CO_2 by means of developing a membrane reactor that was capable of being used for the dry reforming process that reacts CO_2 with propane (C_3H_8) to produce very useful gases such as C_2H_4, C_2H_6, CH_4 and C_3H_6, successfully obtaining high feed reactant gas conversions and selectivities. C_3H_6 is, of course, considered to be one of the most useful prime raw materials required by many industries such as PVC manufacturing. It is worth pointing out, however, that the dry reforming process was accompanied by the production of H_2O and CO instead of hydrogen (H_2), probably due to the RWGS reaction that takes place during the process.

The achievements of this research are very promising and encourage further work to be carried out. A similar study conducted by Solymosi *et.al.* (2002), using Rh-Al_2O_3 in a fixed bed continuous-flow reactor for the conversion of C_3H_8 and CO_2 reported that the fixed bed reactor underwent dehydrogenation and cracking on supported Rh at 824ºK-923ºK. C_3H_6 was formed with selectivity of 50-60%, and other major products were C_2H_4 and CH_4. Solymosi, *et.al.* [56] Also reported that the presence of CO_2 basically altered the reaction pathway of propane, and that the formation of H_2 and CO at a ratio

of 0.42-0.52 came into prominence. C_3H_6 was detected only in trace amounts and this led to the assumption that C_3H_6 reacted quickly with CO_2 over Rh after its formation. This obtained very reasonable average conversions of 50% for CO_2 and C_3H_8 feed reactant gases, and therefore good gas average selectivities of about 30% for several productive gases.

Gas permeation tests revealed that there was no separation of the feed gas mixtures, as there was a near absence of Knudsen diffusion. Other potential applications of this membrane reactor technology are anticipated, and economic benefits are massive and global. Another good finding of this study was that catalyst dispersion on the surface and within the pores of the ceramic supports was found to be high, and accounted for the high activity and productivity of the membranes. Moreover, the low pressure used (a maximum of 3 bars as compared to the conventional 10-25 bars for FBCR) could lead to enormous savings in operating costs. The reactor is simple in construction and a scaling up of the system could have membrane reactors operated as an assembly of parallel or a cascade of reactors with intermittent operation.

It was verified, through the analysis of the obtained results with the help of experimental design, that it was possible to optimize the combined process of CO2 dry reforming and associated of natural gas CO_2/C_3H_8 feed at a of ratio of 2:1 and temperature of 650◦C, and a pressure of two bar at these conditions, the response factors were partial C_3H_8 conversion, These conditions gave selectivities of 41%, 44%, 25%, 28% and 26% for C_3H_6, CO, C_2H_6, C_2H_4, and CH_4,and CO respectively. The synthesis gas produced was formed by 34% of hydrogen, without water with a minimum carbon deposition on catalyst surface. However, the temperature and CO_2/C_3H_8 ratio presented the most important effects on the response factors. The spatial velocity had a limited effect because the system approaches thermodynamic equilibrium. In spite of the reduced number of experiments, optimum operation conditions obtained with the three level experimental designs may be regarded as very good. It seems that the phenomenological analysis of a catalytic system cannot be a routine procedure for process optimization problems, because the good performance depends on an accurate kinetic study.

Besides, in this case, parameter estimation may be very difficult and demands significant computation effort, because of the high parameter correlation. Then, it may be said that could be more appropriable once the whole process optimization is aimed at and the kinetic mechanism is not well known and should constitute a basis for catalytic

process optimization in the future.

Overall I consider my research to a certain extent was successful because of the experience that I have gained from the few challenges and problems that I have faced throughout the whole period of my study which of course I had to overcome. In my mind, the better conclusion that could be drawn from all this is that it is really true if there is no pain there is no gain.

5.2 Recommendations for Future work.

The reaction has the potential to be developed in future work and its performance can be improved through the following recommendations:

1. A mathematical model should be developed that will be capable of predicting the optimum membrane area and feed conversion at any given flow rate of the feed gas ratios, to enable the determination of key parameter values for optimum reactor performance.
2. Long-term stability tests could be conducted possibly over 72 hours on a pilot plant unit to confirm the suitability and stability of the catalysts and membranes.
3. The possibility of scaling up this experimental work should be explored to discover if it could be used economically on an industrial commercial scale.
4. Extensive characterisation of the membranes (e.g. pore size, pore volume, SEM, BET surface area, EDXA and XPS analysis) should be carried out.
5. These HCMs seemed to have shown good selectivity for CO gas, which is a very essential raw material for the GTL processes. With a few membrane modifications, similar HCMs could be produced where the support could be coated externally by those substances that were used to produce the HCMs and coated internally by some other substances that would be suitable for GTL processes.
6. An extensive secondary market study should be conducted to ascertain the size of the market likely for such processes.
7. Calculations for both reaction rate analysis and reaction activation energy were not included in this study, so it is highly recommended that such calculations are carried out in any future work.

References

1. Dittmeyer. R., (2001) Membrane reactors for hydrogenation and dehydrogenation processes on supported palladium. Journal of molecular catalysis. A Chemical (2001) p 9-10.
2. K.Scott & R.Hughes.,(1996) Industrial membrane separation technology. Levenspiel, O. (1999). Chemical Reaction Engineering. New York, John Wiley & Sons, Incl.
3. Marcel Mulder., "Basic Principles of Membrane Technology". (1992) P5.
4. Li, K, (2007). Ceramic membranes for separation and reaction. Chichester: John Wiley.
5. Dixon, A.G., 2003. Recent research in catalytic inorganic membrane reactors international Journal of Chemical Reactor Engineering 1 (R6), 1–35.
6. Ghai. R. K "Liquid diffusion of nonelectrolytes: Part I", AIChE Journal, (1973).
7. Tock, R. W. Kammermayer. K., "Temperature separation factor in gaseous diffusion " ALChm. J.1975. 15.p. 715-718.
8. Ulhorn, R. J and Burgraff, A. J. Gas separation with inorganic membranes: Synthesis, characteristics and applications (Ed R.R Bhave) Van Noostrand Reinhold, New York 19981. P.155-176.
9. Brinker, J., Ward, T.L and Headely, T.J, (1993) Ultramicrooporous silica-based supported inorganic membranes. J. Member Sci, 77, p.165-179.
10. Pena, M.A., J.Firro, and J.L.G. Fierro, (1996) " Review: New catalytic routes for syngas and hydrogen production. Applied Catalysis A: General, 144(1-2): p.7-57.
11. Sutton, D.and J.Ross."The CO2 reforming of hydrocarbons present in model gas stream over selected catalysts. " Fuel processing Technology (2002) 75 (45-53).
12. Rostrup-Nielsen, J. " CO2 reforming of Methane over transition metals." Journal of Catalysis. (1993).144: p 38-49.
13. Li, C.F. "Study on application of membrane reactor in direct synthesis DMC from CO_2 and CH3OH over Cu-KF/MgSiO catalyst", Catalysis Today, (2003).
14. Olsbye. U., A. Slagtern, ‘‘an investigation of coking properties of fixed fluid bed reators during methane-to-synthesis gas reactions. " Applied Catalysis A: General (2002) 228. P.289-303.
15. Asami. K., K. Fujimoto, (2003) " CO2 reforming of CH_4 over ceria- supported metal catalysis." Catalysis Today 84. p 231.
16. Nagaoka, K., K. Aolka, ‘‘Carbon Deposition during CO2 reforming of methane-Comparison between Pt/Al2O3 and Pt/ZrO2". Journal of Catalysis. (2001) 197: p34-42.

17. http://www.en.wikipedia.org.
18. http://www.uop.com.
19. Perry's chemical engineers standards " Handbook of Engineers calculations" (1984).
20. Hardiman, K., T, Ying, ''Performance of a CO-Ni catalyst for propane reforming under low steam-to- carbon ratios. " Chemical Engineering Journal (102). (2004). P 119-130.
21. Mohammed, M. Characterisation and Deactivation Studies of a Coke Induced Deactivated Catalyst. Chemical engineering and Industrial Chemistry. Sydney, University of New south Wales (2002) p 79.
22. Wilhelm,D., A. Karp, " Syngas production for gas-to-Liquids applications technologies, issues and outlook." Fuel Processing Technology (2001).71: p139-148.
23. Rose, J., A. V. Keulen, ''the catalytic conversion of natural gas to useful products." Catalysis Today (1996). 30:p 193-199.
24. Wang, S. and Lu.M " Co2 reforming of Methane on Ni catalysts: Effects of support phase and preparation technique." (1998) Applied Catalysis B: Environmental 16:269-277.
25. Cheng, Z., J. Li, ''Role of support in CO2 reforming of CH_4 over a Ni/-Al2O3 catalyst" Applied Catalysis A: General (2002) 205: p 31-36.
26. Ziaka., Z.D. "A high temperature catalytic membrane reactor for propane dehydrogenation" Journal of Membrane Sci (1993).Vol 77, P 221-232.
27. Yildirim. Y, E. Gobina., R. Hughes " Membrane technology in the chemical industry." Journal of Mem Sci, (1997). 43. p11-12.
28. Coronas, J., Santamaria, J. (1999). Catalytic reactors based on porous ceramic membranes. Catalysis Toda, 51.P, 382.
29. Quicker. P., ''Catalytic dehydrogenation of hydrocarbons in palladium composite membrane reactors" Catalysis Today,(2000), Vol.56 P 21-34.
30. Reo. C. and C .Lund." Defining conditions where the use of porous membrane reactors can be justified solely on basis of improved yield",(1997),Chemical Eng Sci 52 (18) 3075-2083.
31. Dittmeyer, R., Svajda, K., Reif, M, 2004 A review of catalytic membrane layers for gas/liquid reactions. Topics in Catalysis 29 (1), 3–27.
32. Schom¨acker, R.,Schmidt,A., Frank, B., Haidar, R., Seidel-Morgenstern, A., 2005.
33. Westermann, T., Melin, T., 2009. Flow-through catalytic membrane reactors principles and applications. Chemical Engineering and Processing Process Intensification 48 (1), 17–28.

34. Butt, J. (2002). " Reaction Kinetics Reactor Design, Marcel Decker, Inc.
35. Sheitntuch M., and Sznejer G, "Application of a membrane reactor for dehydration reaction" Chemical Eng Sci (1996).vol 59 p 2013 2021.
36. Weyten H., and Keizer K., " dehydrogenation of propane using a packed -bed membrane reactor''. (1997). AIChe Journal vol 43 p 1819-1827.
37. Bitter J.G Tosotsis T (1988) a high temperature catalytic membrane reactor for propane dehydration'. Chemical Eng Sci Vol 45 -8 P 2423-2429.
38. Solymosi, F., Tomlmacsov.P (2005)."Dry reforming of propane over supported Re catalyst." Journal of catalysis 233:51-59.
39. Zhang, Z. and Verykios.X (1994)." CO_2 reforming of Methane to synthesis gas over supported Ni catalysts." 21:589.
40. Solymosi, F., Tomlmacsov.P "CO"2 reforming of propane over supported Rh", Journal of Catalysis, (2003)216:377-385.
41. Opoku-Gymmfi, K and Adsesina A. (1999). " Forced composition cycling of a novel thermally self-sustaining fluidised-bed reactor for Methane reforming." Chem Eng Sci 54 p 25-75.
42. Zhong, H S.H.W.Sun, X.T.Wang, H.Q.Shao and J.B.Guo. (2005).
43. Slamgtern, A, Schwarman Y, (1997)." Specific Features Concerning the Mechanism of Methane reforming by carbon Diooxide over Ni/La2O3 catalyst,." Journal of catalsis 172:118.
44. Birtill, J (2003). "But will it last until the shutdown? Deciphering catalyst decay" Catalysis Today: p531-545.
45. Bartholomew, C., (1982) " Carbon deposition in steam reforming and methanation." Catal Rev Sci Eng 24:67-112.
46. Fogler, H. (1999) Elements of Chemical Reaction Engineering. Prentice Hall PTR.
47. Furimsky, E (1999) " Deactivation of hydro processing catalysts " Catalytic Today 381-495.
48. Lippens, B.C. and J.H.d. Boer, Studies on pore systems in catalyst v. the t method Journal of Catalysis, 1965. 4: p. 319-323.
49. Qui, X., Tsubaki, N., Fujimoto, K. (2001). Journal of Chemical Engineering of Japan, 34(11), pp.1366-1372.
50. Briggs, D., M.P. Seah, and Wiley, Practical surface analysis. Auger and x-ray photoelectron spectroscopy. Vol. 1.

51. Barret, E.P., L.G. Joyner, and P.P. Halenda, (1951) the determination of pore volume and area distribution in porous substances, I Computations from nitrogen isotherms Journal of American Chemical Society, 73: p 373-380.
52. Lindlar, B., Chemical modification of high-quality large-pore M41S materials Journal of Materials Chemistry, 2002. 12: p. 528-533.
53. Tough, I Quantitative X-ray Analysis Using the Scanning Electronic Microscopic 2001 Class notes. Department of Applied Science- The Robert Gordon University.
54. Brunauer, S., P.H. Emmet, and E. Teller, (1938) Adsorption of gases in multimolecular layers. Journal of American Chemical Society, p. 309-319.
55. Solymosi, F., Tomlmacsov.P (2002).,"Decomposition of propane and its reaction with CO2 over alumina-supported Pt metals", Catalysis letters 83(Nov) :p 183-168.
56. Tough, I, An introduction to the Scanning Electron Microscope.2001. Class notes. Department of Applied Science. The Robert Gordon University.

Appendix One

Membrane surface area and volume calculations

Hence the membrane support is of the form of cylinder therefore its outside surface are would be calculated using the formula for surface area of cylinder.

Surface area the membrane support with the following dimensions

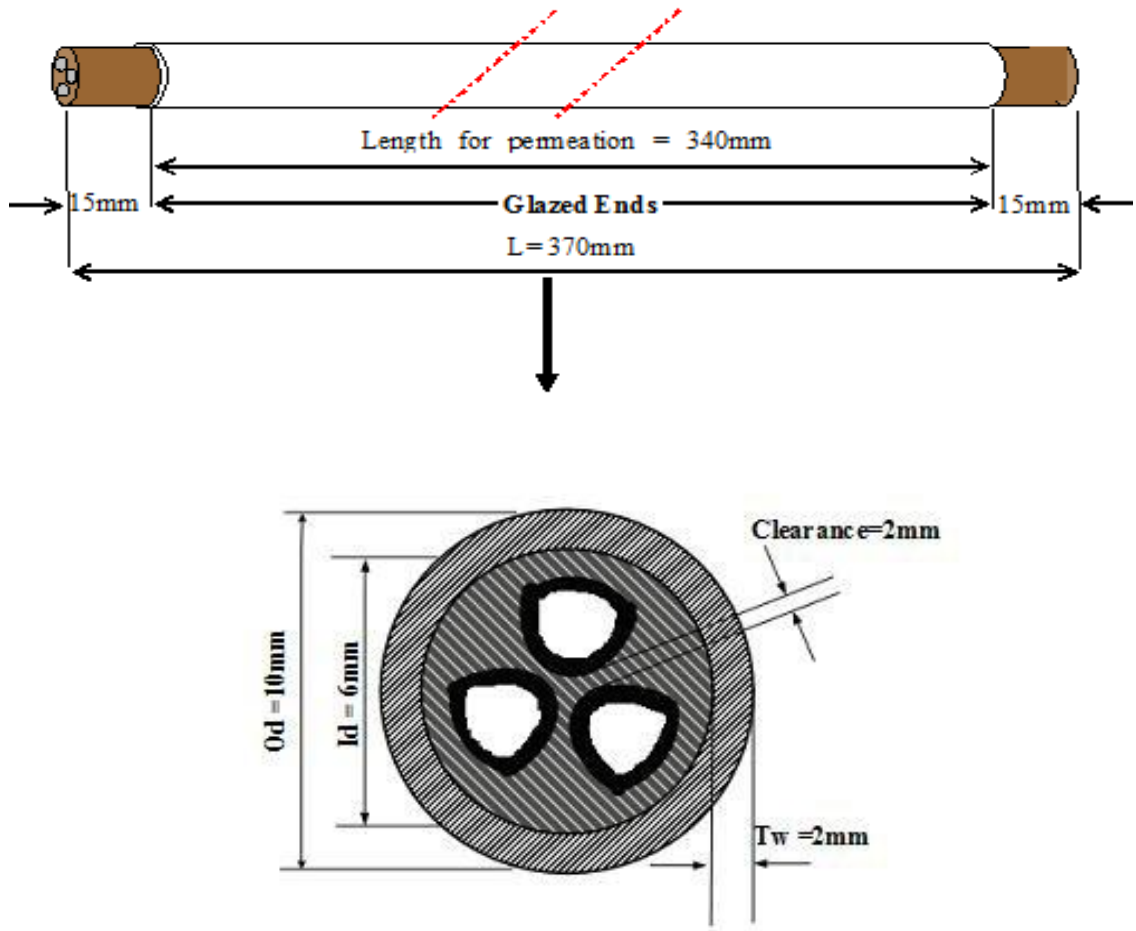

Figure A1.1 Geometric details of fresh support.

Active surface area = 2 × 22/7 × r × h = 2 × 22/7 × 0.5 × 3.4= 10.685 cm^2

Catalyst loading per unit surface area using low speed d/c motor =8.605/10.685=0.805 g/cm^2

Catalyst loading per unit surface area using conventional method =4.113/10.685=0.384g/cm^2

Also volume of the membrane support = 22/7 × r^2 × h = 22/7× $(0.5)^2$ × 3.4 = 2.671 cm^3

Print Date: Thu Jun 12 11:22:59 2008 Page 1 of 1

Title :
Run File : c:\star\data\3800.45018.run
Method File : C:\Star\GC2\ali 40.mth
Sample ID : Manual Sample

Injection Date: 12/06/2008 10:53 Calculation Date: 12/06/2008 11:19

Operator :
Workstation: RGU13846
Instrument : Varian Star #1
Channel : Front = TCD

Detector Type: 3800 (10 Volts)
Bus Address : 45
Sample Rate : 10.00 Hz
Run Time : 25.973 min

** GC Workstation Version 6.41 ** 00756-24C0-C65-00B4 **

Run Mode : Analysis
Peak Measurement: Peak Area
Calculation Type: External Standard

Peak No.	Peak Name	Result ()	Ret. Time (min)	Time Offset (min)	Area (counts)	Sep. Code	Width 1/2 (sec)	Status Codes
1	CO2	14.9310	3.616	-0.002	1653766	BB	10.8	
2	ETHYLENE	4.9738	5.539	-0.002	573723	BV	0.0	
3		0.0000	6.180	0.000	12038	VB	16.0	
4	PROPYLENE	34.8669	15.744	-0.002	2580389	BV	51.8	
5		0.0000	17.111	0.000	10192	VV	0.0	
6	PROPANE	14.9181	17.709	-0.004	1172908	VB	78.1	
7	NITROGEN	5.0026	21.717	-0.002	206715	BV	4.9	
8	METHANE	4.9679	22.628	-0.003	182020	VV	7.4	
9	CO	19.9849	24.275	-0.007	828518	VB	12.5	
	Totals:	99.6452		-0.022	7220269			

Total Unidentified Counts : 22230 counts

Detected Peaks: 9 Rejected Peaks: 0 Identified Peaks: 7

Multiplier: 1 Divisor: 1 Unidentified Peak Factor: 0

Baseline Offset: -19 microVolts LSB: 1 microVolts

Noise (used): 2 microVolts - monitored before this run

Figure A1.2 GC calibration run results print out.

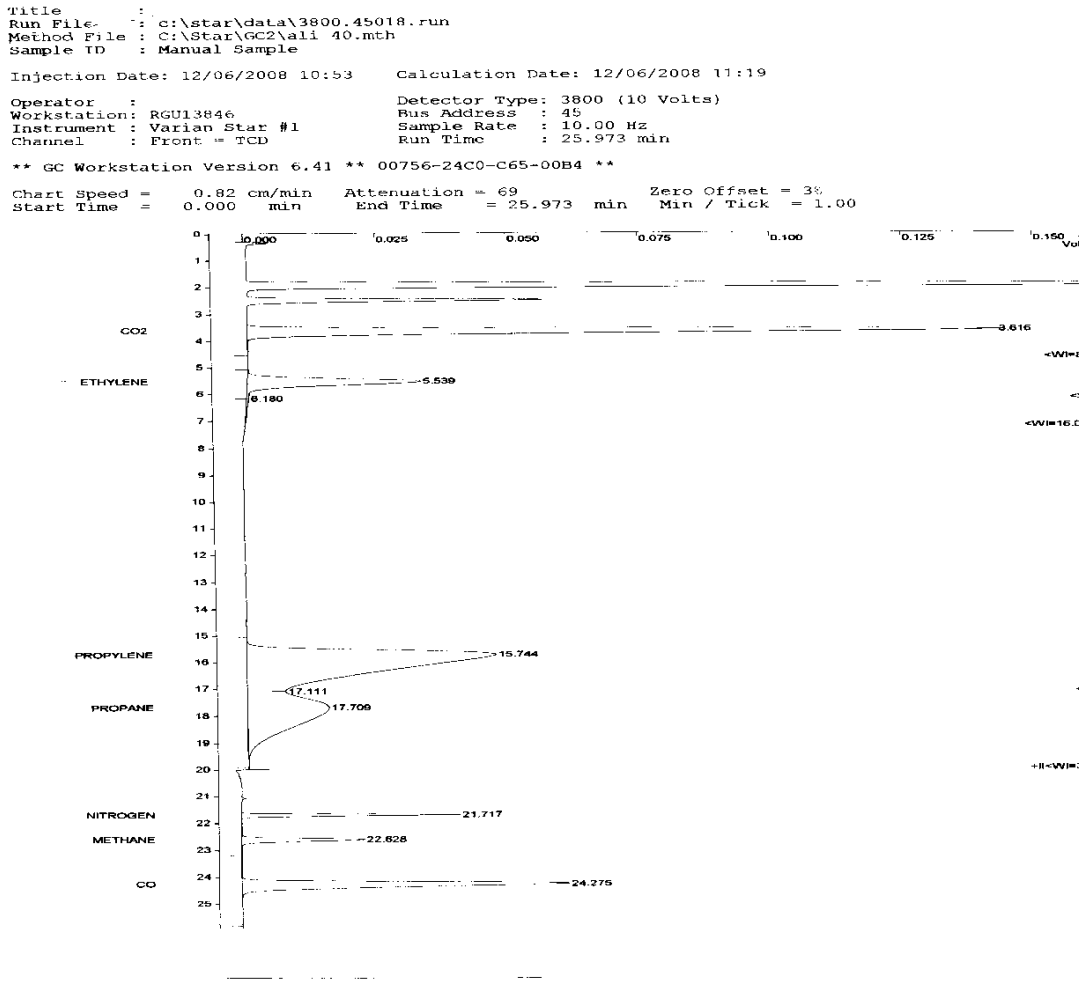

Figure A1.3 An example of the peaks of GC calibration runs using the standard calibration cylinder.

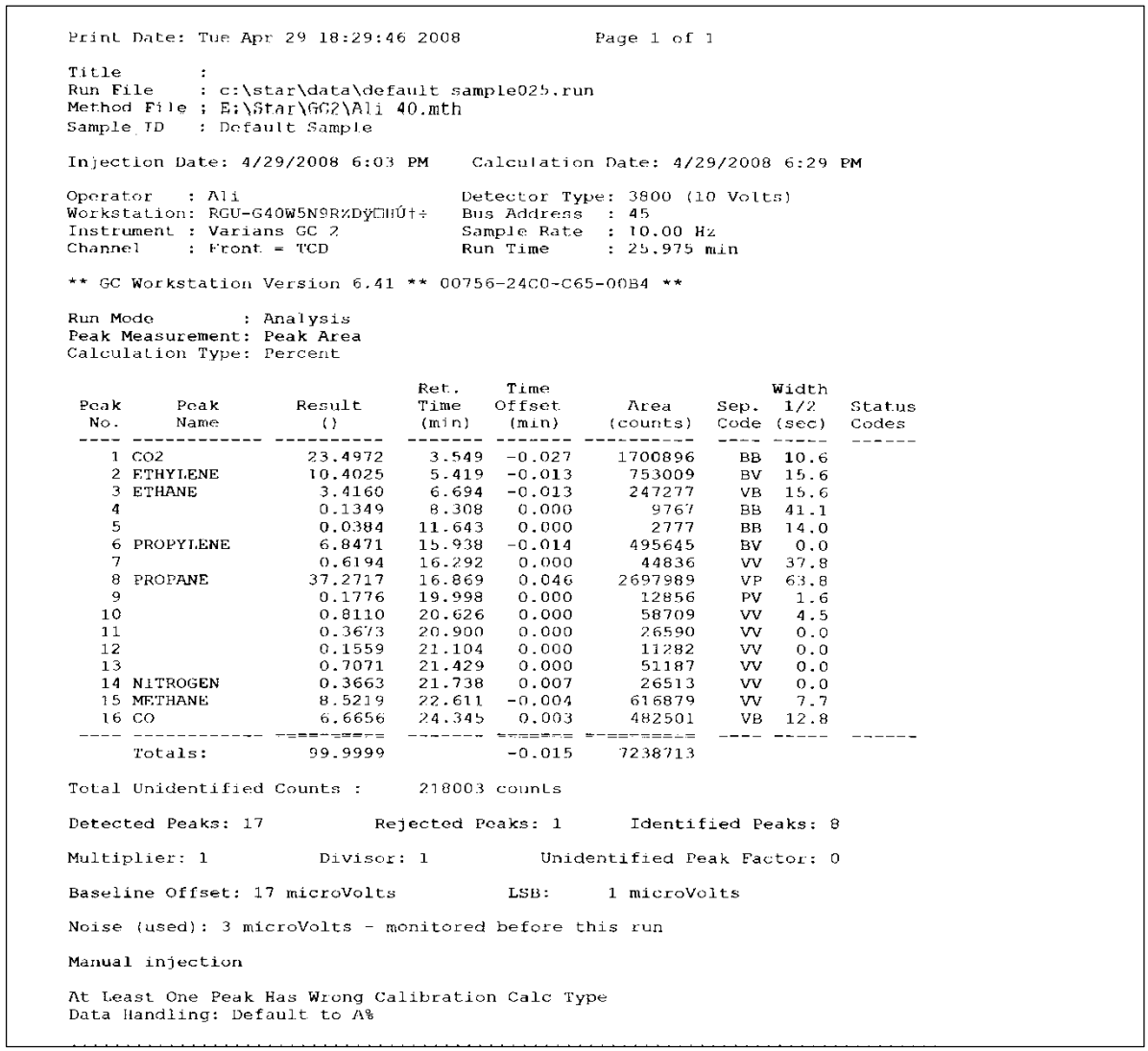

```
Print Date: Tue Apr 29 18:29:46 2008            Page 1 of 1

Title       :
Run File    : c:\star\data\default sample025.run
Method File : E:\Star\GC2\Ali 40.mth
Sample ID   : Default Sample

Injection Date: 4/29/2008 6:03 PM    Calculation Date: 4/29/2008 6:29 PM

Operator    : Ali                    Detector Type: 3800 (10 Volts)
Workstation: RGU-G40W5N9RZDÿ□HÚ†÷    Bus Address  : 45
Instrument : Varians GC 2            Sample Rate  : 10.00 Hz
Channel     : Front = TCD            Run Time     : 25.975 min

** GC Workstation Version 6.41 ** 00756-24C0-C65-00B4 **

Run Mode         : Analysis
Peak Measurement: Peak Area
Calculation Type: Percent

                                Ret.    Time                      Width
Peak      Peak        Result    Time   Offset      Area    Sep.   1/2    Status
 No.      Name          ()     (min)   (min)     (counts) Code  (sec)  Codes
---- ------------ ---------- ------- ------- ---------- ---- ------ ------
   1 CO2             23.4972   3.549  -0.027    1700896   BB   10.6
   2 ETHYLENE        10.4025   5.419  -0.013     753009   BV   15.6
   3 ETHANE           3.4160   6.694  -0.013     247277   VB   15.6
   4                  0.1349   8.308   0.000       9767   BB   41.1
   5                  0.0384  11.643   0.000       2777   BB   14.0
   6 PROPYLENE        6.8471  15.938  -0.014     495645   BV    0.0
   7                  0.6194  16.292   0.000      44836   VV   37.8
   8 PROPANE         37.2717  16.869   0.046    2697989   VP   63.8
   9                  0.1776  19.998   0.000      12856   PV    1.6
  10                  0.8110  20.626   0.000      58709   VV    4.5
  11                  0.3673  20.900   0.000      26590   VV    0.0
  12                  0.1559  21.104   0.000      11282   VV    0.0
  13                  0.7071  21.429   0.000      51187   VV    0.0
  14 NITROGEN         0.3663  21.738   0.007      26513   VV    0.0
  15 METHANE          8.5219  22.611  -0.004     616879   VV    7.7
  16 CO               6.6656  24.345   0.003     482501   VB   12.8
---- ------------ ---------- ------- ------- ---------- ---- ------ ------
     Totals:         99.9999           -0.015    7238713

Total Unidentified Counts :      218003 counts

Detected Peaks: 17          Rejected Peaks: 1       Identified Peaks: 8

Multiplier: 1           Divisor: 1           Unidentified Peak Factor: 0

Baseline Offset: 17 microVolts           LSB:      1 microVolts

Noise (used): 3 microVolts - monitored before this run

Manual injection

At Least One Peak Has Wrong Calibration Calc Type
Data Handling: Default to A%
```

Figure A1.4 A GC proper run result print out for membrane HCME6001.

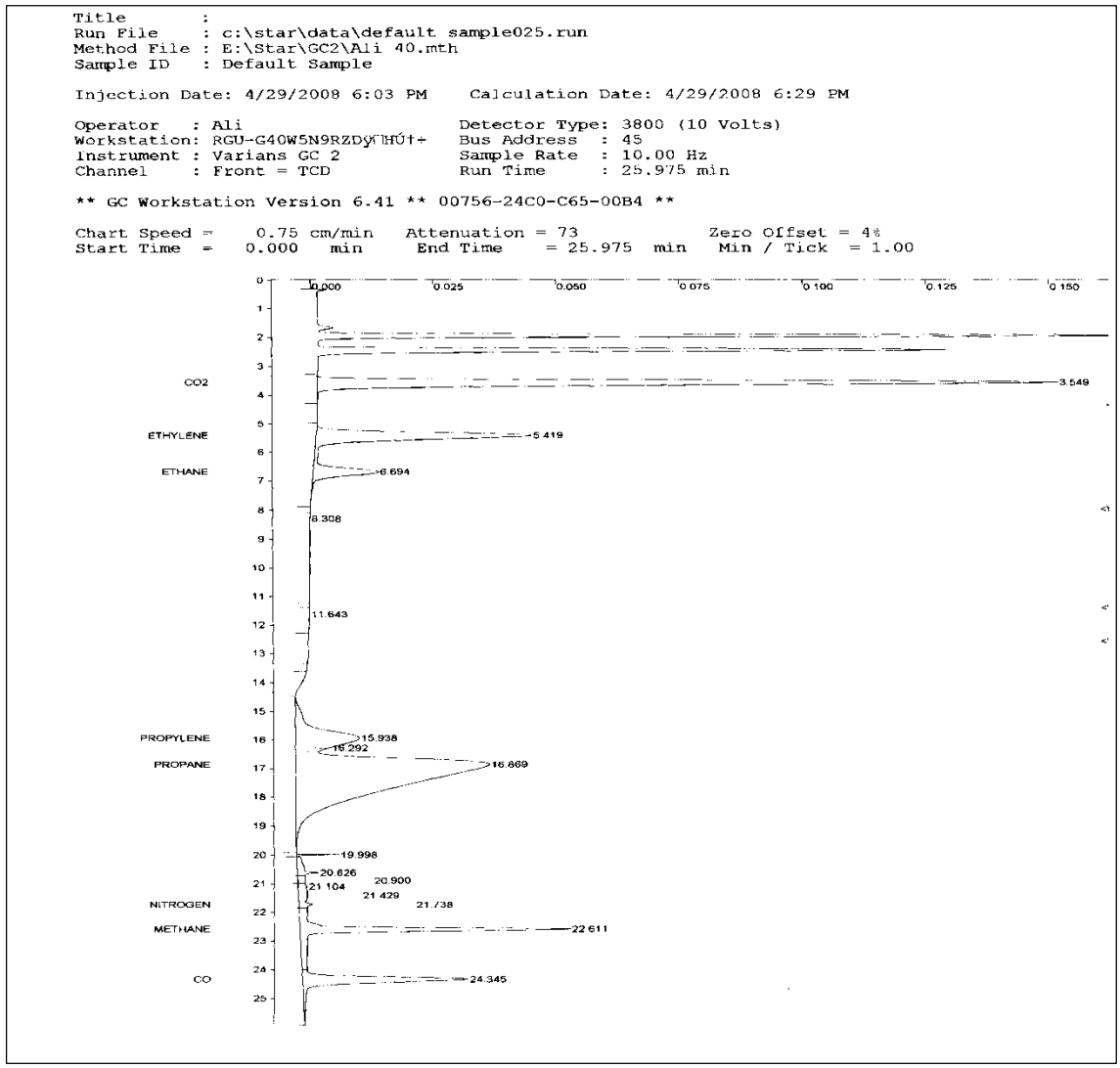

Figure A1.5 An example of the peaks of a GC runs for membrane HCME6001.

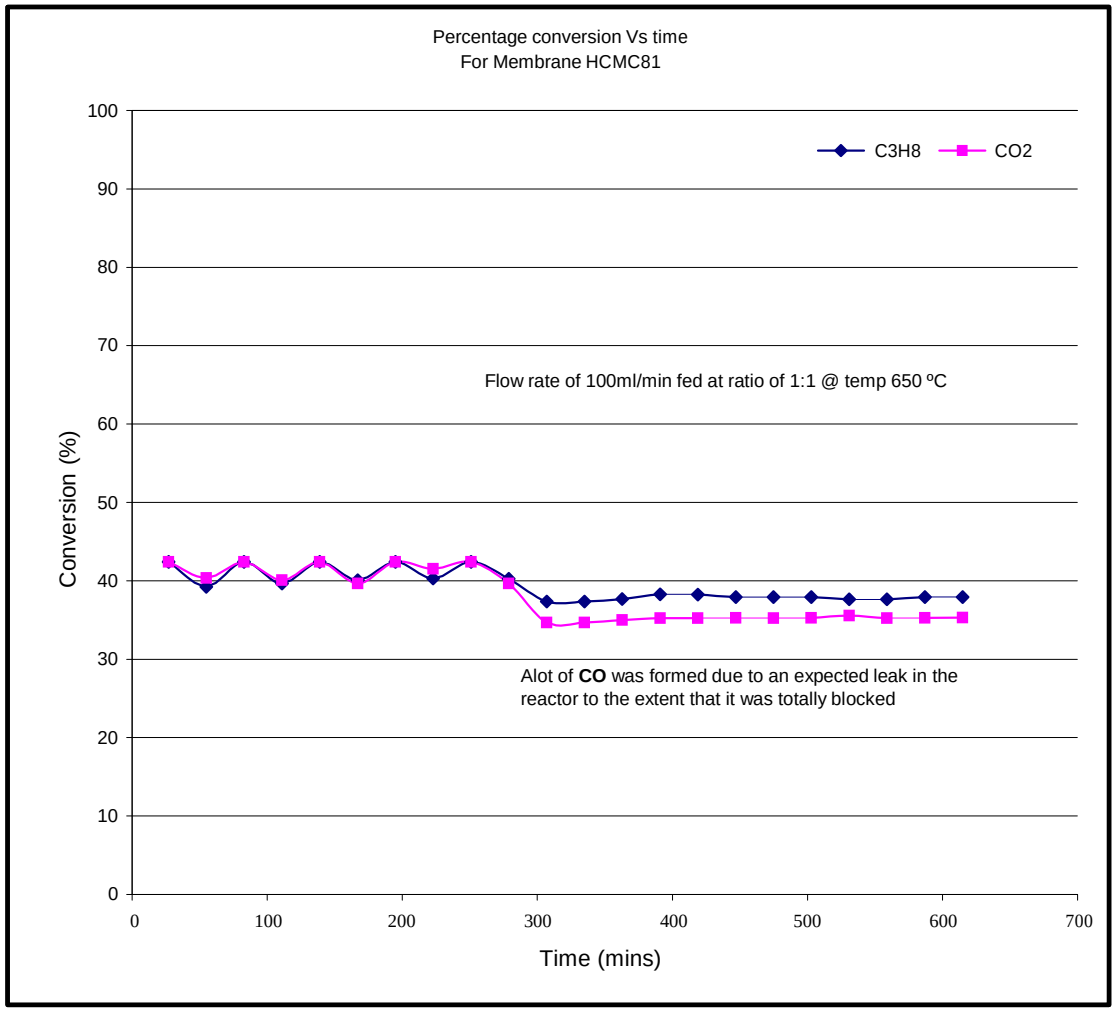

Figure A1.6 Shows the percentage conversion vs time for membrane HCMC81.

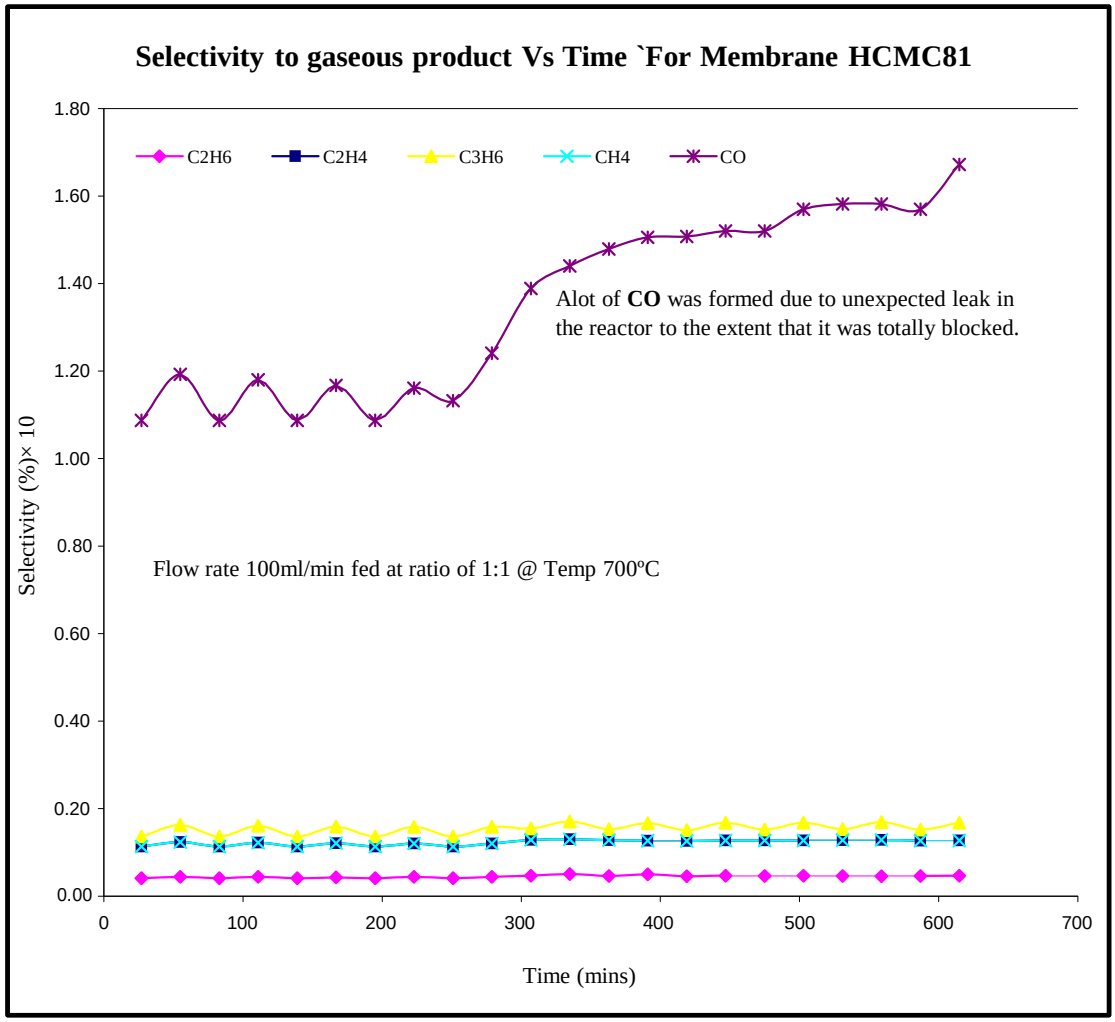

Figure A1.7 Shows the selectivity to gaseous product vs time for membrane HCMC81.

Figure A1. 8 Shows pictorial view for membrane HCME6001 that proves the presences of traces of carbon (coking).

Appendix Two

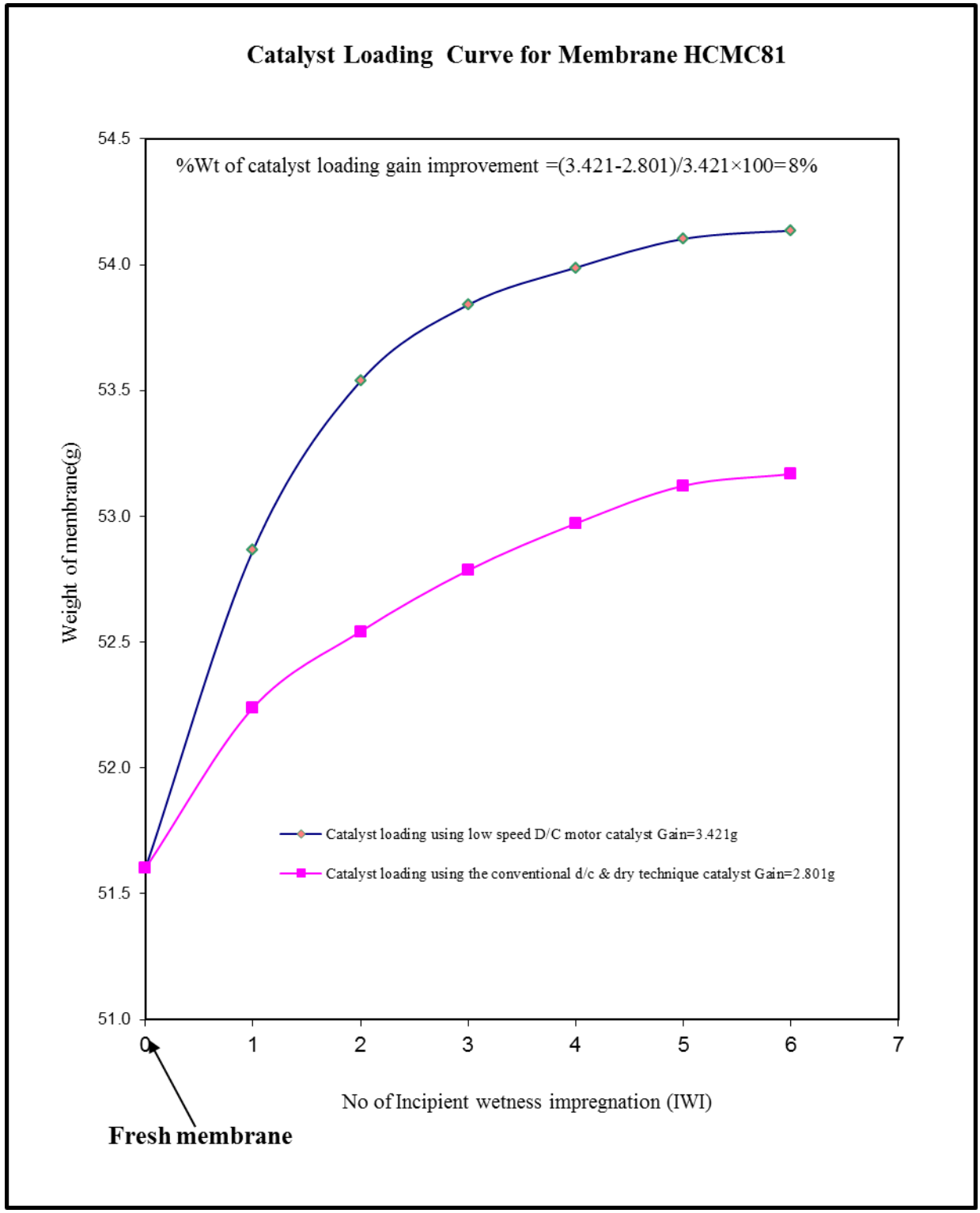

Figure A2. Catalyst [PdCl2-Cu (NO3)2 +ZrCl2-Ni (NO3)2] loading curve for membrane HCMC81.

EM Images

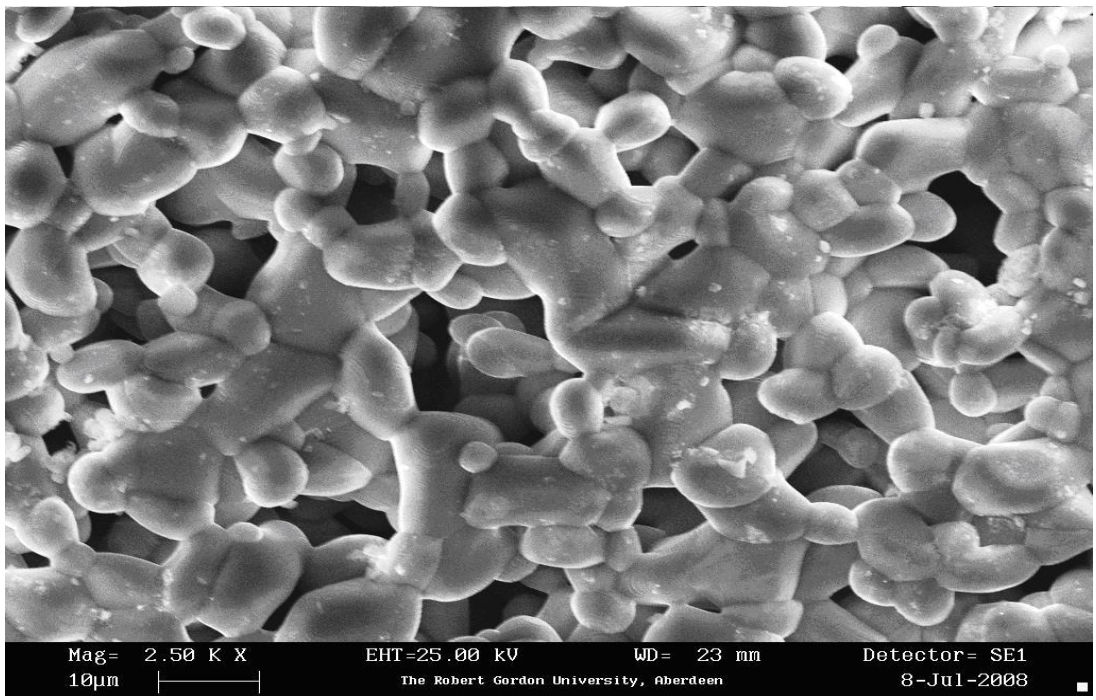

For C80nm fresh support

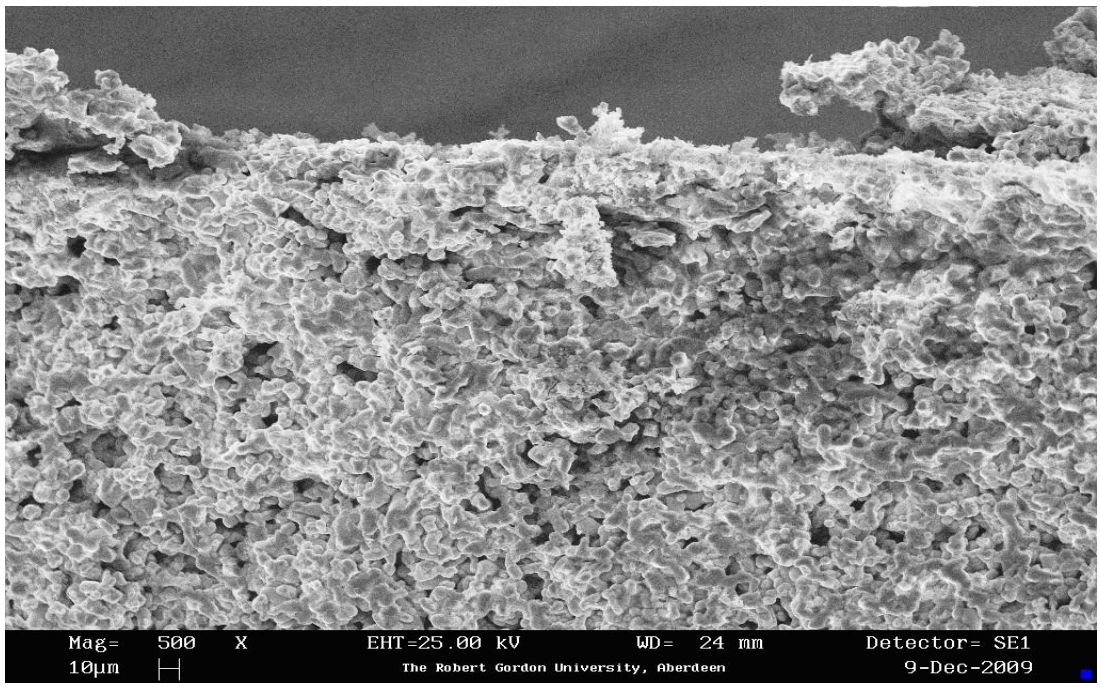

For Membrane HCMC81 3rd Dip-coating

Figure A2.2 SEM images for fresh support C81 and membrane HCMC81.

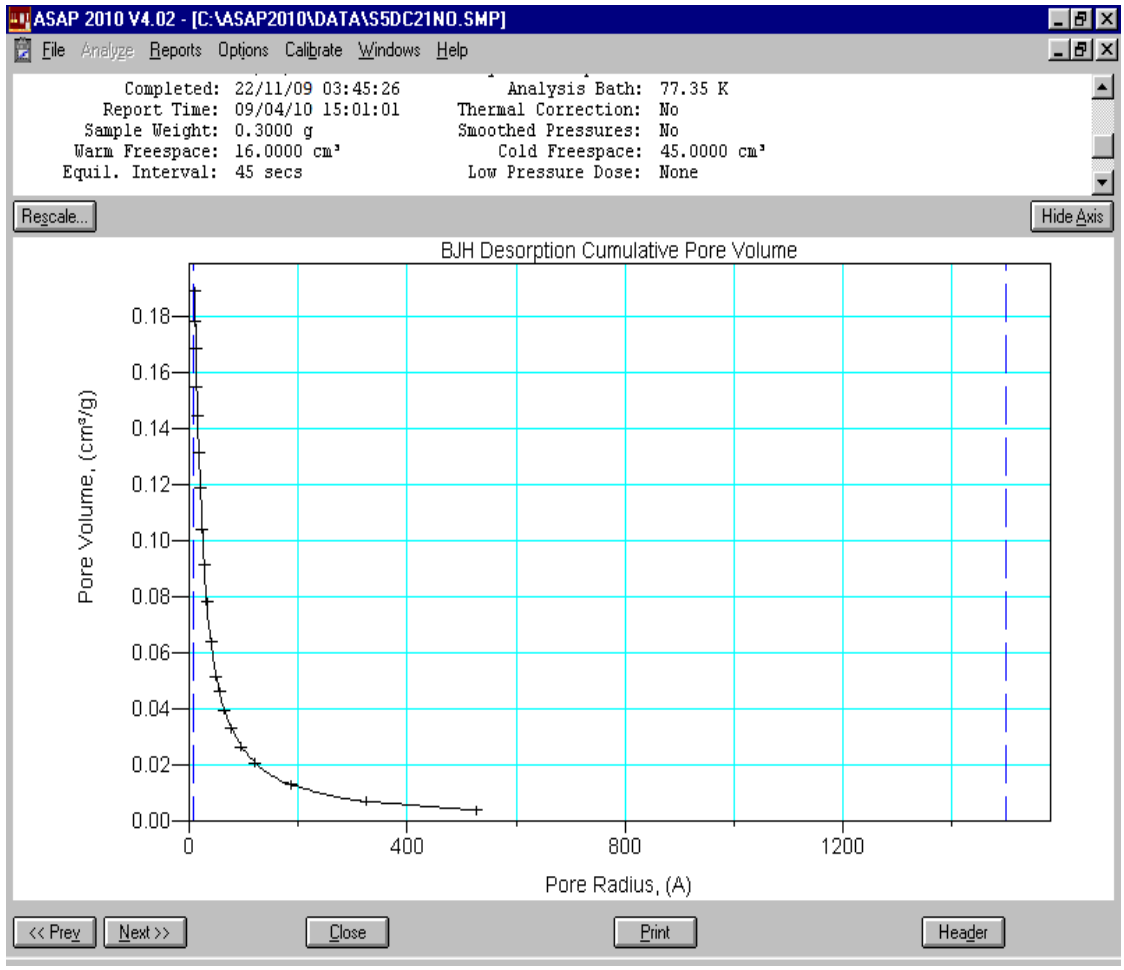

Figure A2.3 ASAP curve for C80nm fresh support.

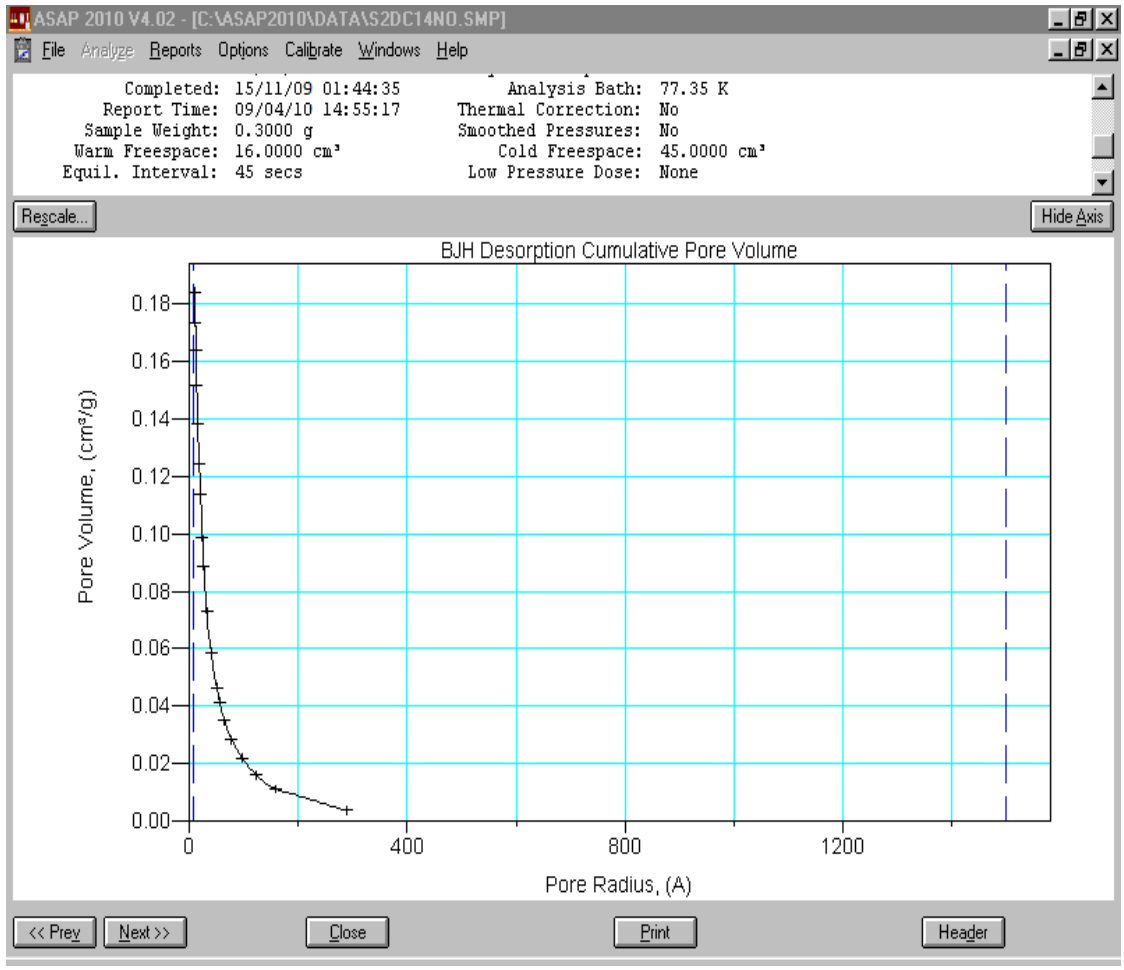

Figure A2.4 ASAP curve for membrane HCMC81 3rd dip-coating.

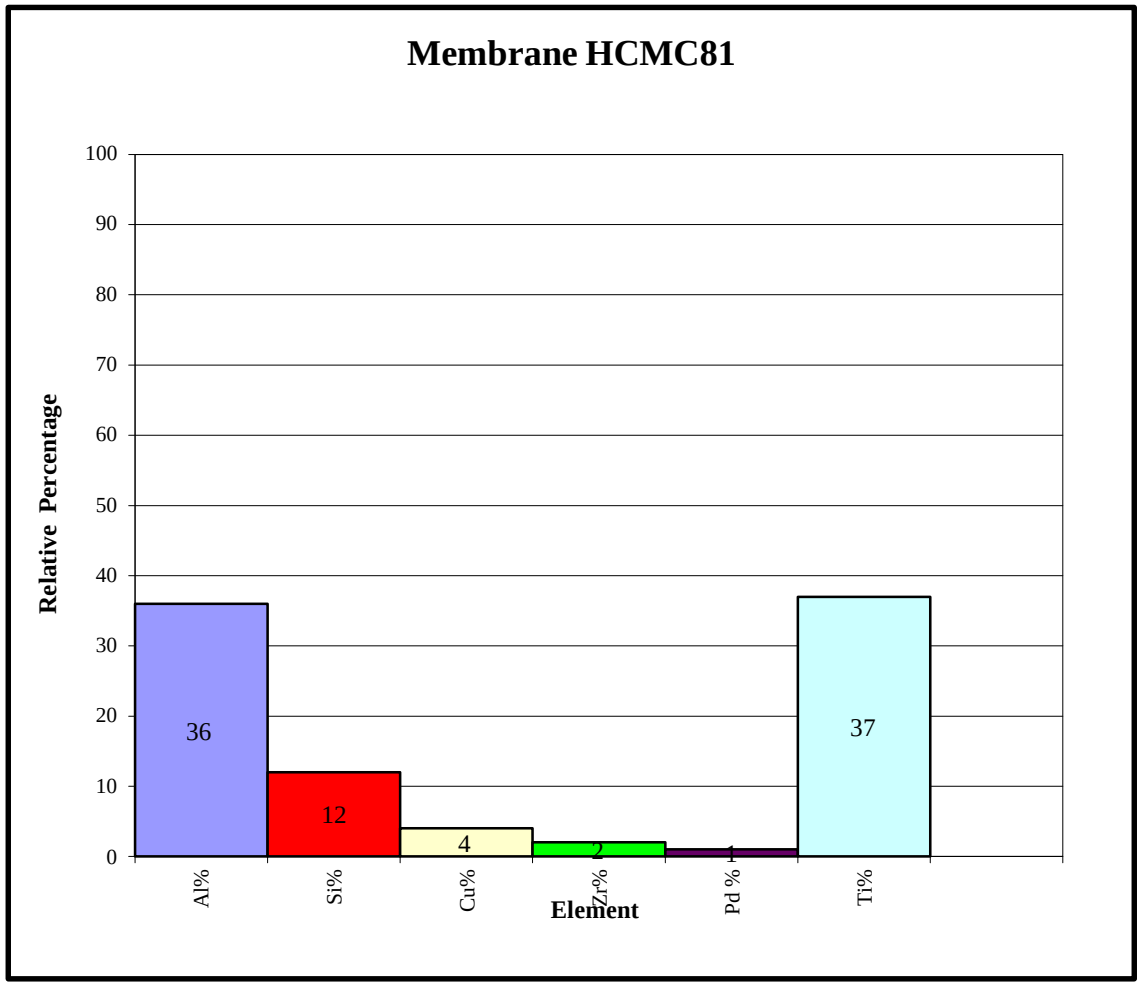

Figure A2.5 The EDXA plots for membrane HCMC81.

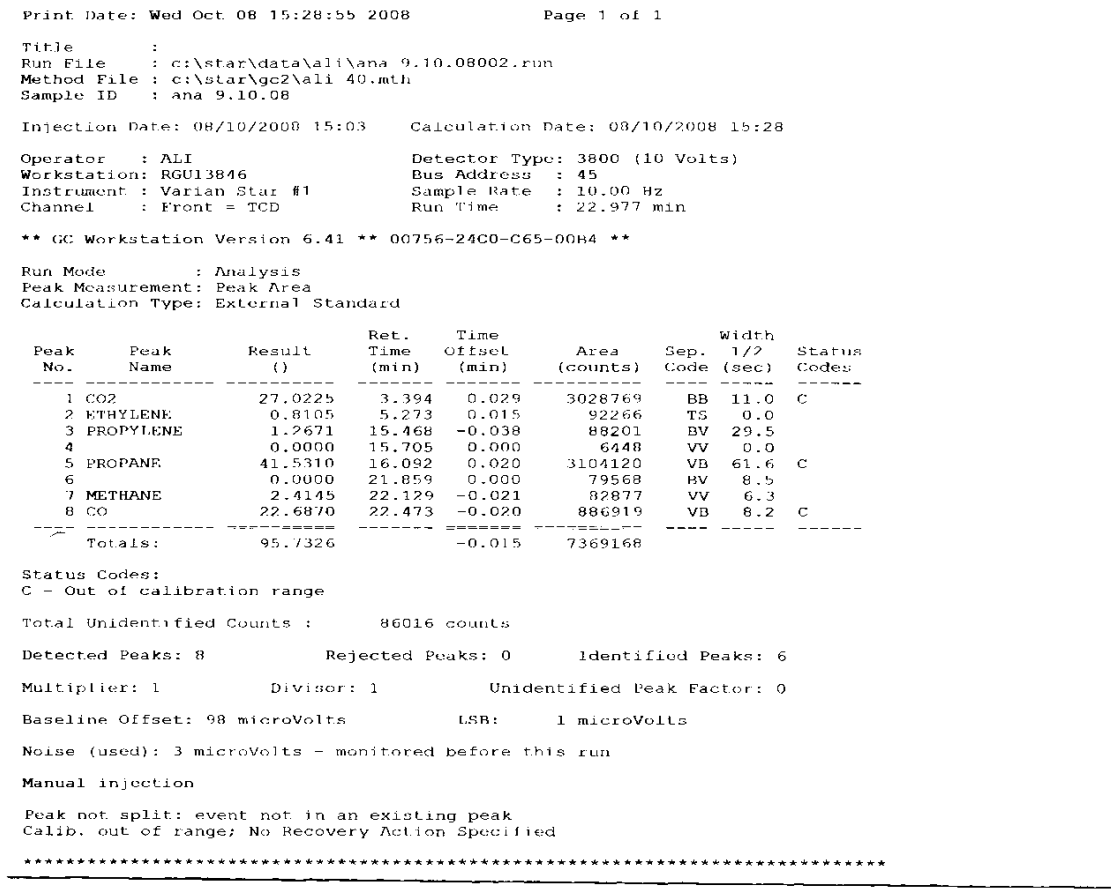

Print Date: Wed Oct 08 15:28:55 2008 Page 1 of 1

Title :
Run File : c:\star\data\ali\ana 9.10.08002.run
Method File : c:\star\gc2\ali 40.mth
Sample ID : ana 9.10.08

Injection Date: 08/10/2008 15:03 Calculation Date: 08/10/2008 15:28

Operator : ALI Detector Type: 3800 (10 Volts)
Workstation: RGU13846 Bus Address : 45
Instrument : Varian Star #1 Sample Rate : 10.00 Hz
Channel : Front = TCD Run Time : 22.977 min

** GC Workstation Version 6.41 ** 00756-24C0-C65-00B4 **

Run Mode : Analysis
Peak Measurement: Peak Area
Calculation Type: External Standard

Peak No.	Peak Name	Result ()	Ret. Time (min)	Time Offset (min)	Area (counts)	Sep. Code	Width 1/2 (sec)	Status Codes
1	CO2	27.0225	3.394	0.029	3028769	BB	11.0	C
2	ETHYLENE	0.8105	5.273	0.015	92266	TS	0.0	
3	PROPYLENE	1.2671	15.468	-0.038	88201	BV	29.5	
4		0.0000	15.705	0.000	6448	VV	0.0	
5	PROPANE	41.5310	16.092	0.020	3104120	VB	61.6	C
6		0.0000	21.859	0.000	79568	BV	8.5	
7	METHANE	2.4145	22.129	-0.021	82877	VV	6.3	
8	CO	22.6870	22.473	-0.020	886919	VB	8.2	C
	Totals:	95.7326		-0.015	7369168			

Status Codes:
C - Out of calibration range

Total Unidentified Counts : 86016 counts

Detected Peaks: 8 Rejected Peaks: 0 Identified Peaks: 6

Multiplier: 1 Divisor: 1 Unidentified Peak Factor: 0

Baseline Offset: 98 microVolts LSB: 1 microVolts

Noise (used): 3 microVolts - monitored before this run

Manual injection

Peak not split: event not in an existing peak
Calib. out of range; No Recovery Action Specified

Figure A2.6 An example of the GC peaks for the products for membrane HCMC81.

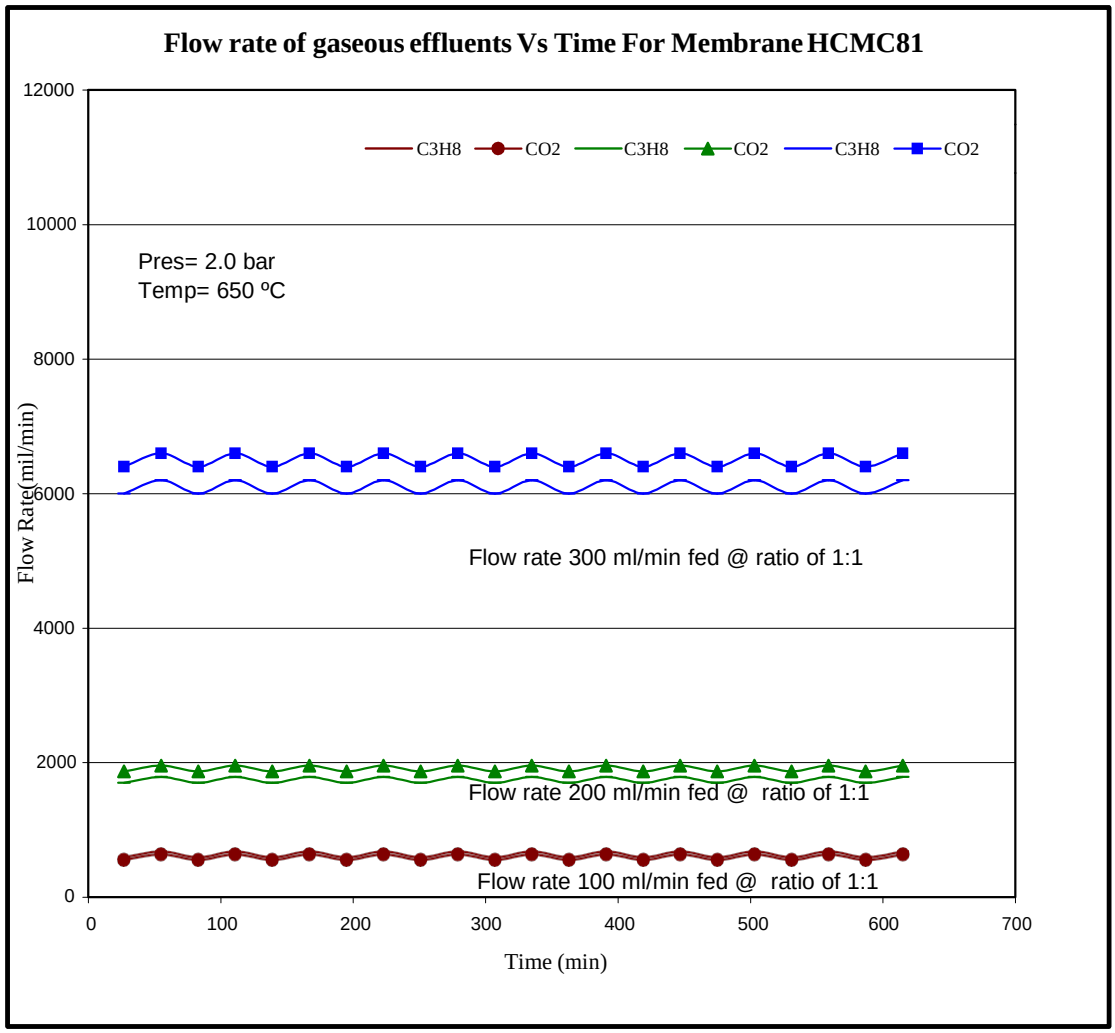

Figure A2.7 Flow rates of gaseous effluents vs time for membrane HCMC81 fed at ratio of 121.

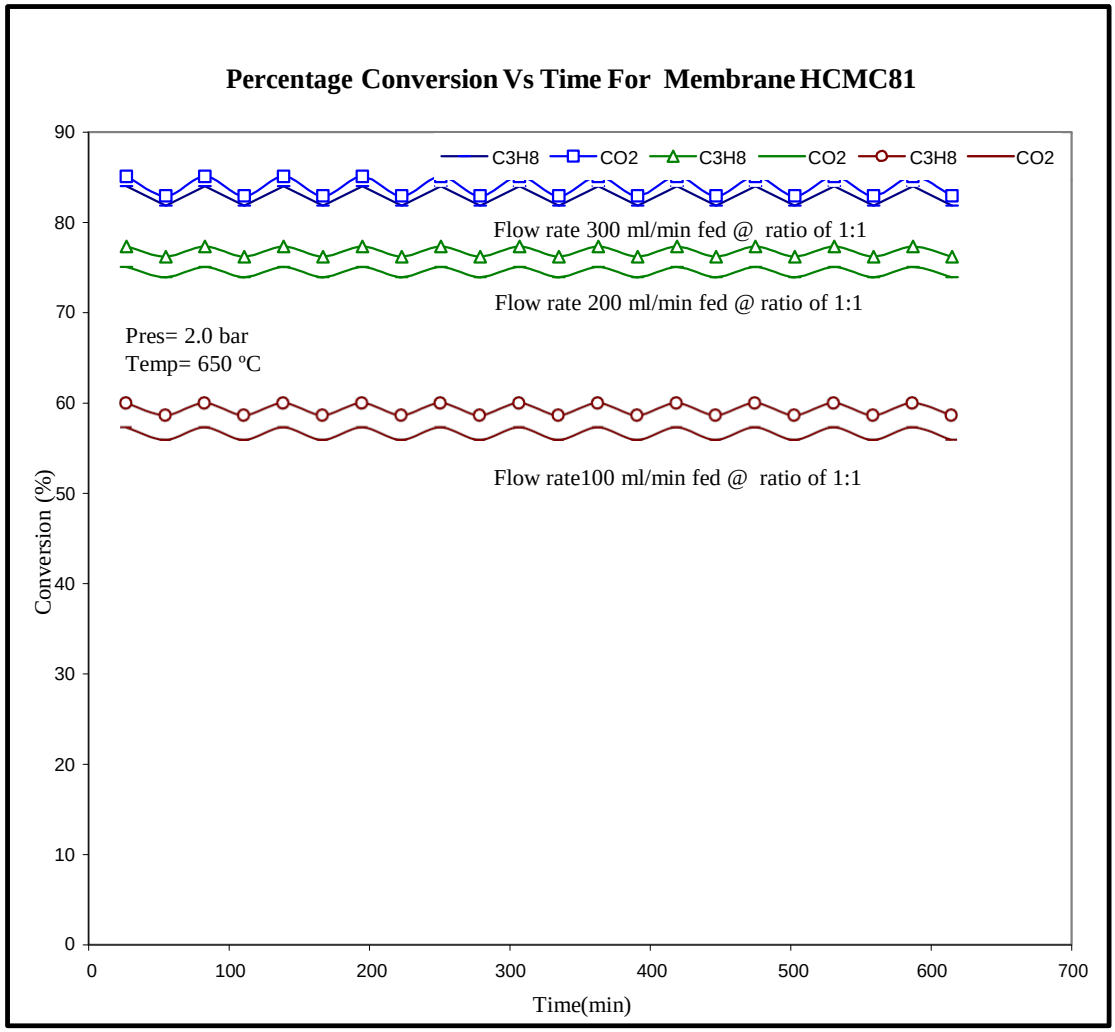

Figure A2.8 Percentage conversion vs time for membrane HCMC81 fed at ratio of 121.

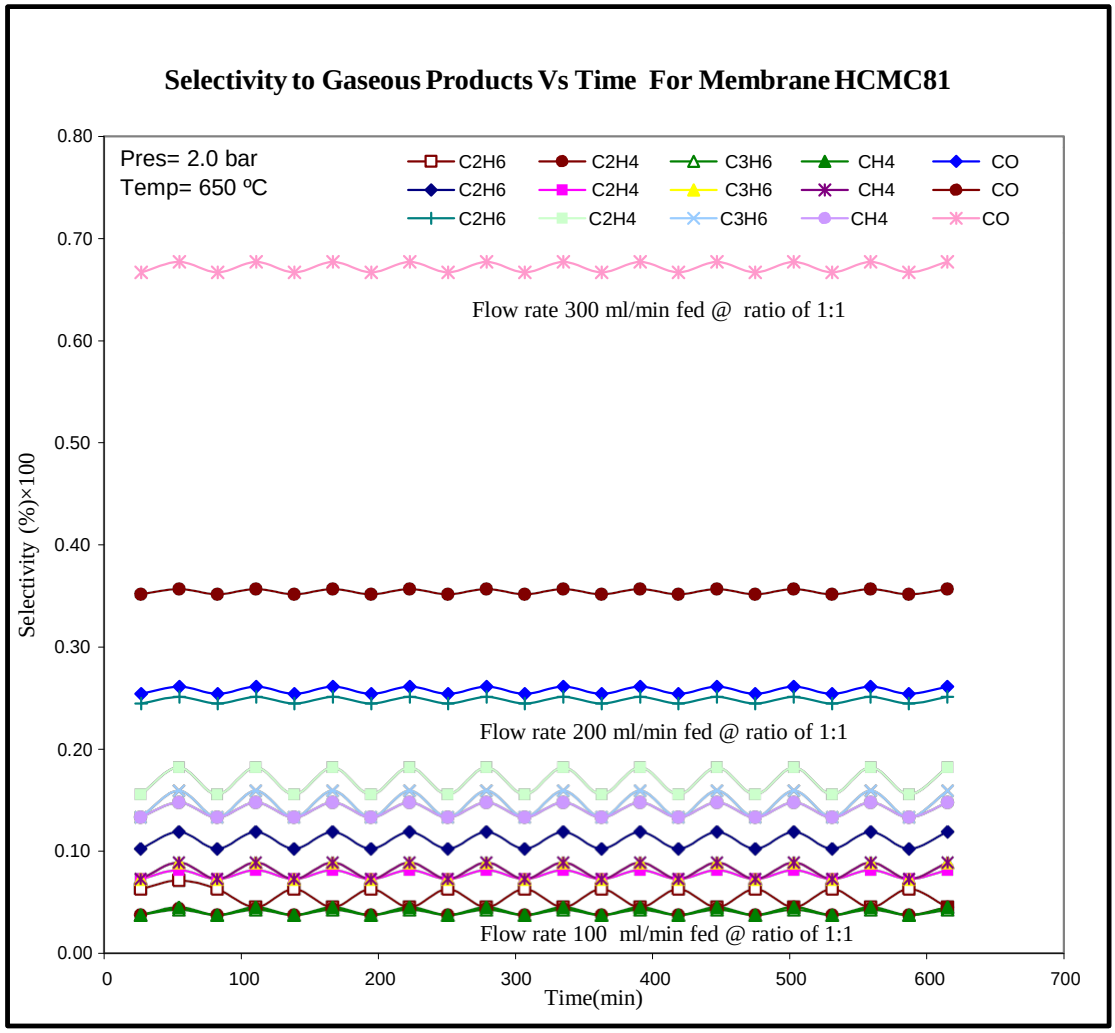

Figure A2.9 Selectivity to gaseous products vs time for membrane HCMC81 fed at ratio of 121.

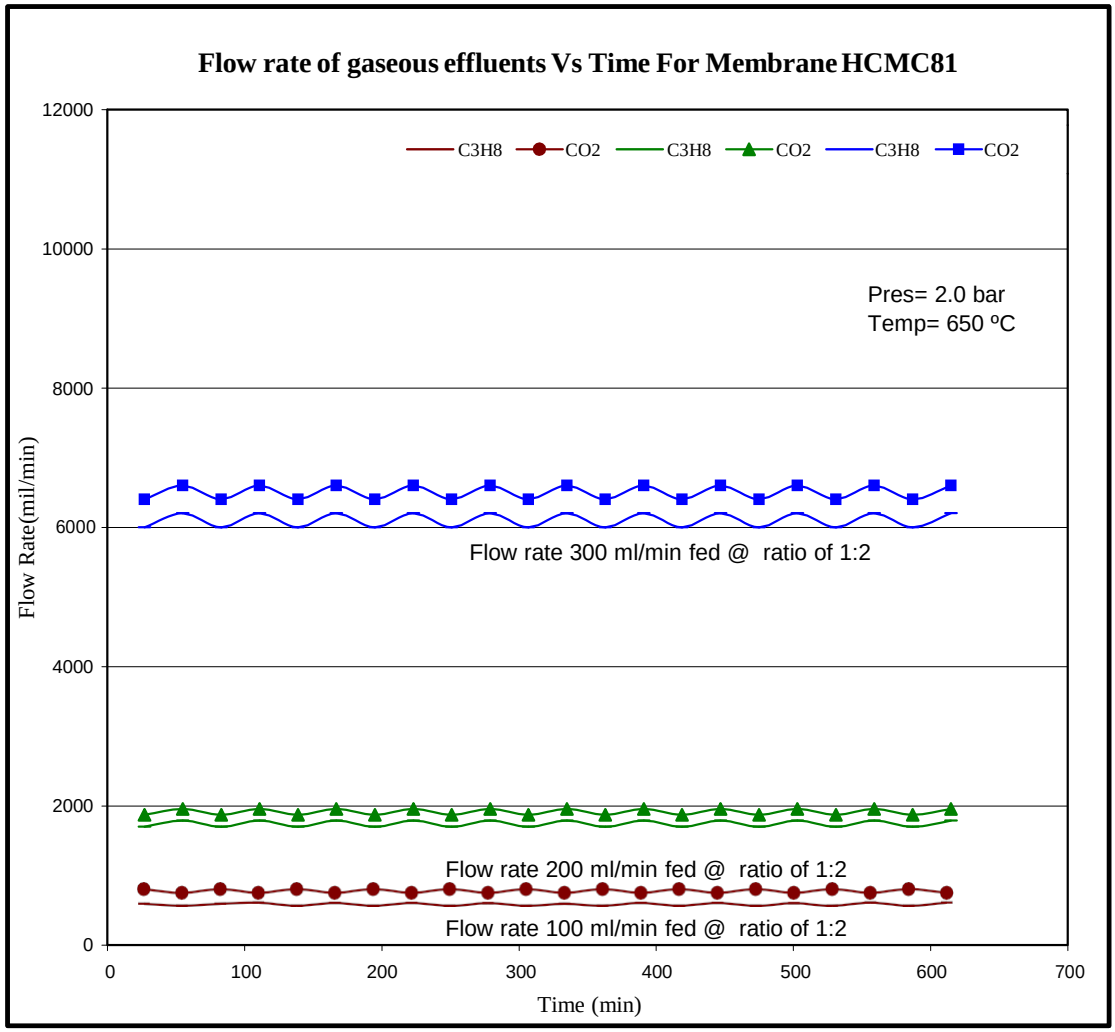

Figure A2.10 Flow rates of gaseous effluents vs time for membrane HCMC81 fed at ratio of 122.

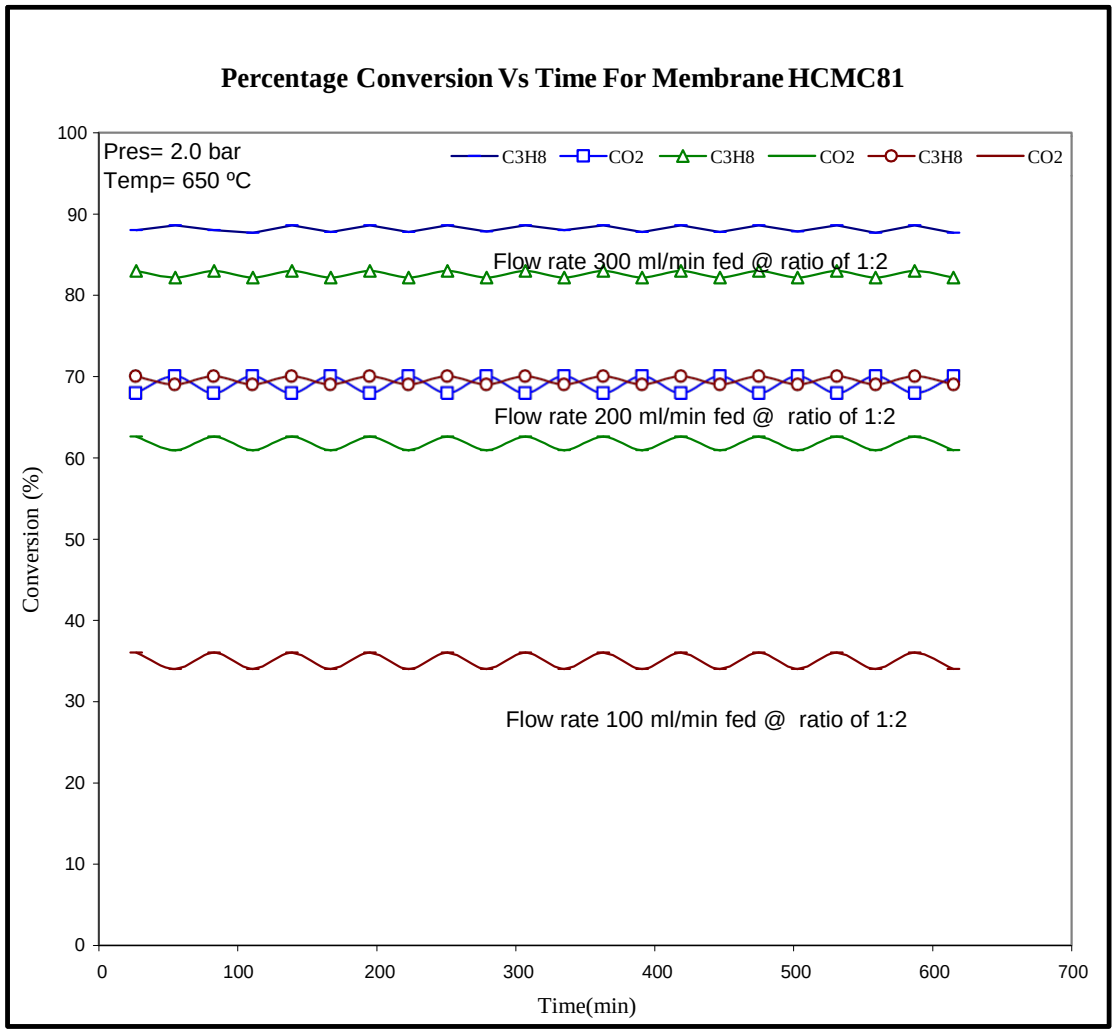

Figure A2.11 Percentage conversion vs time for membrane HCMC81 fed at ratio of 122.

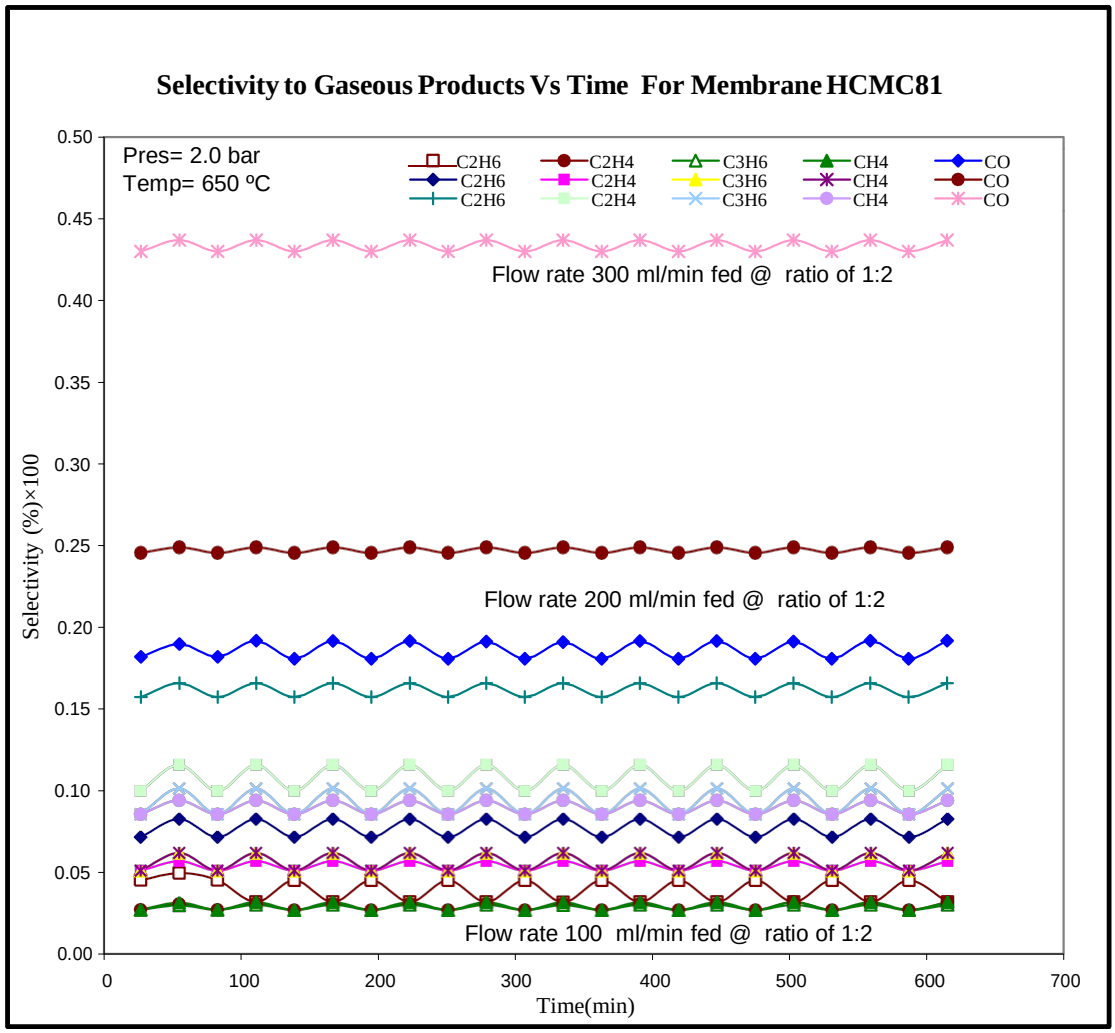

Figure A2.12 Selectivity to gaseous products vs time for membrane HCMC81 fed at ratio of 122.

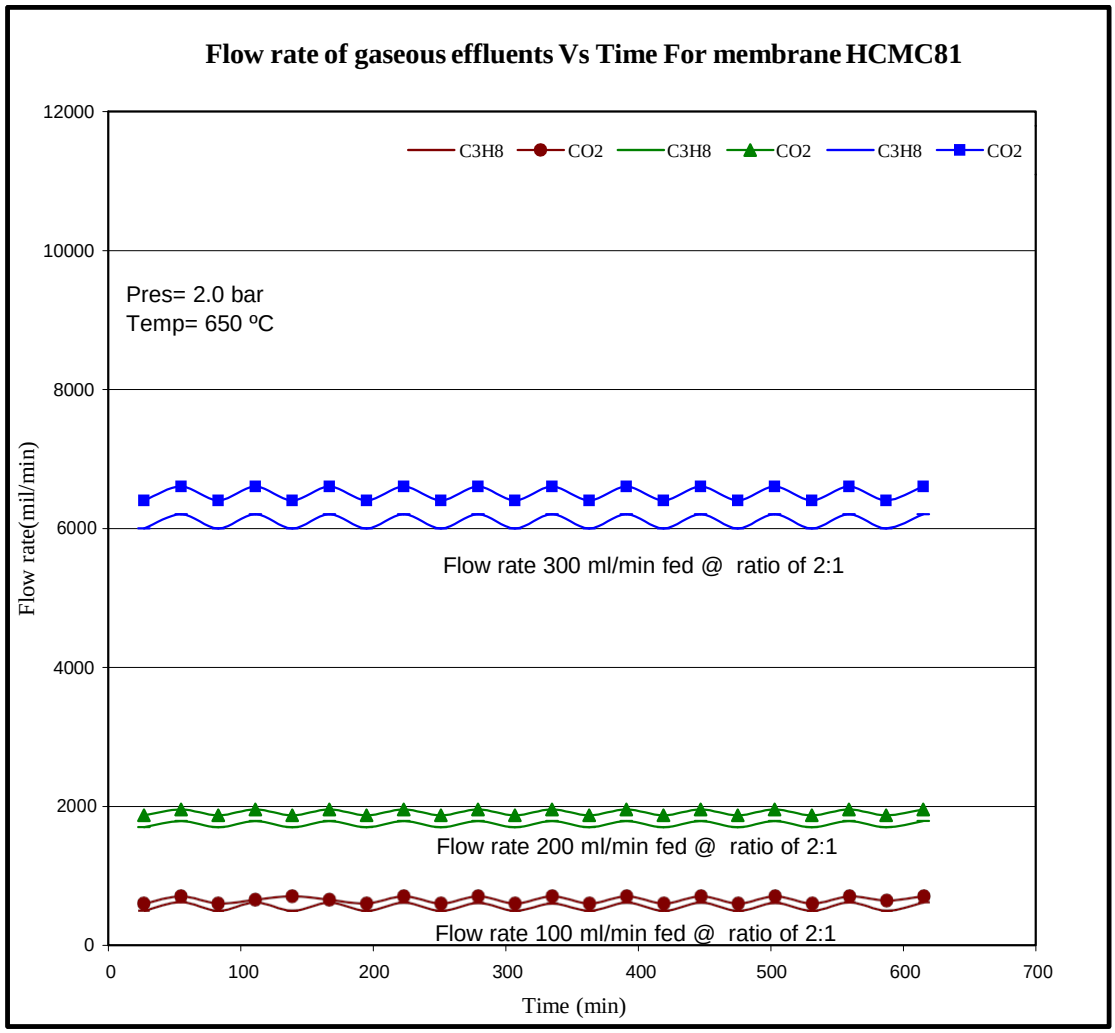

Figure A2.13 Flow rate of gaseous effluent vs time for membrane HCMC81 fed at ratio of 221.

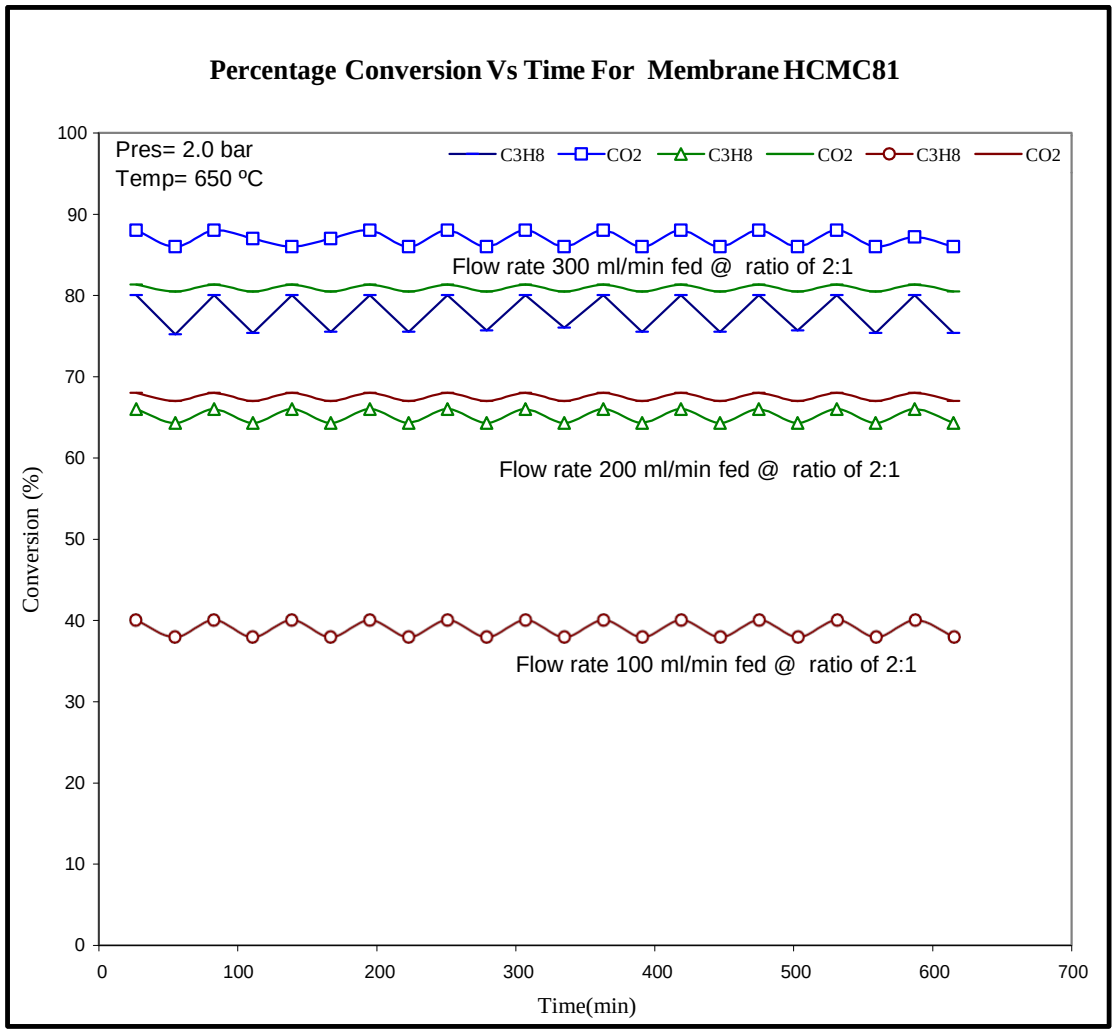

Figure A2.14 Percentage conversion vs time for membrane HCMC81 fed at ratio of 221.

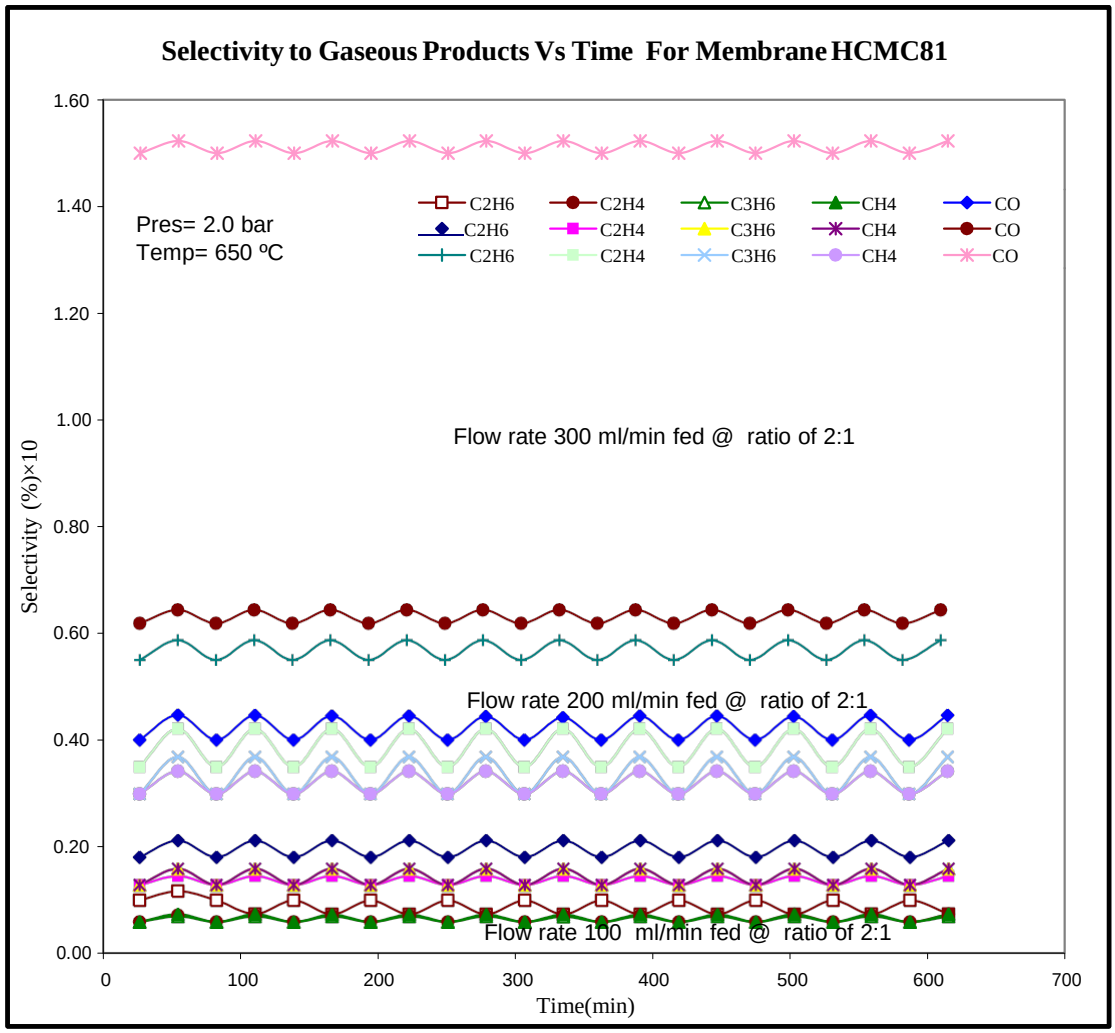

Figure A2.15 Selectivity to gaseous products vs time for membrane HCMC81 fed at ratio of 221.

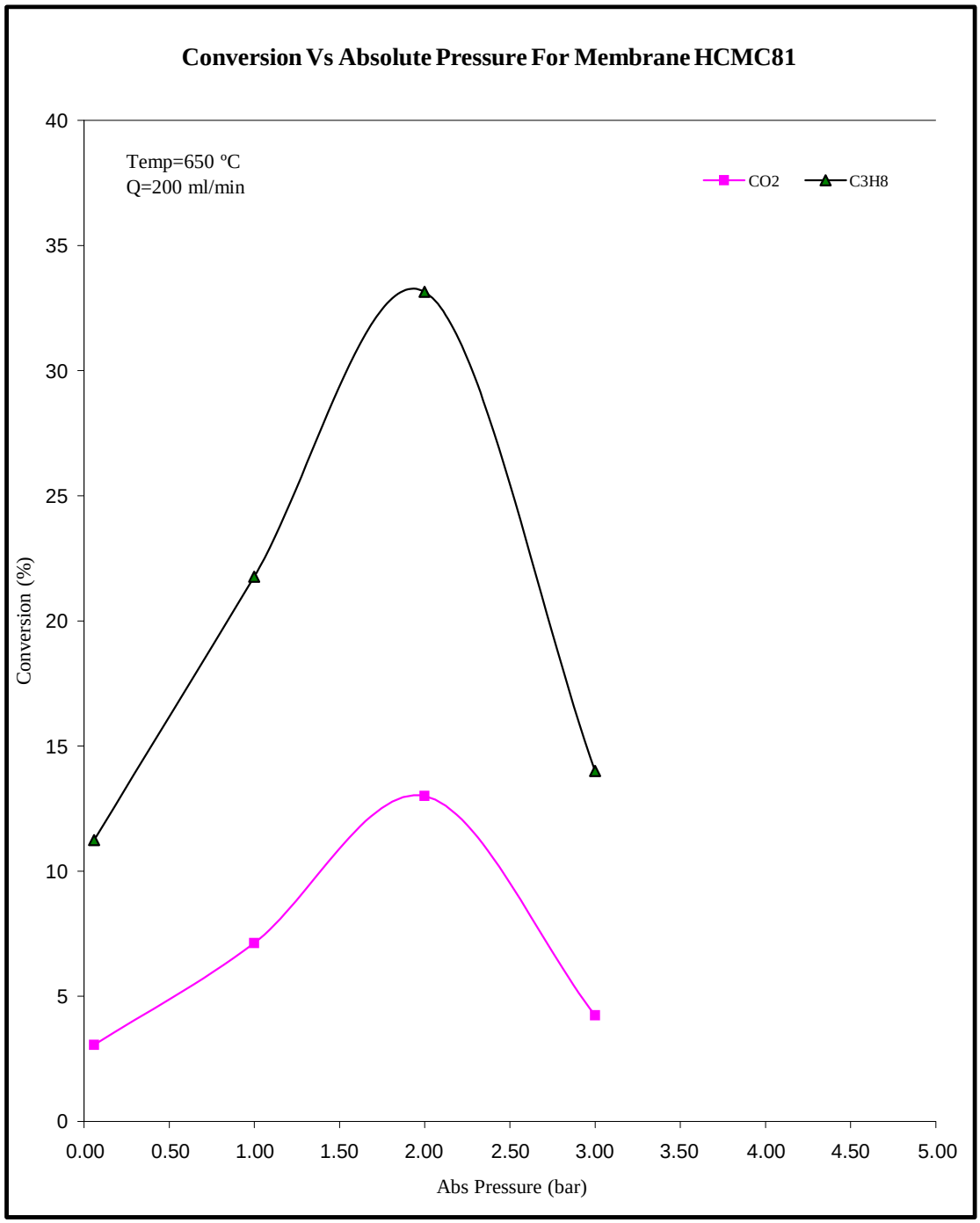

Figure A2.16 Conversion vs Absolute pressure for membrane HCMC81.

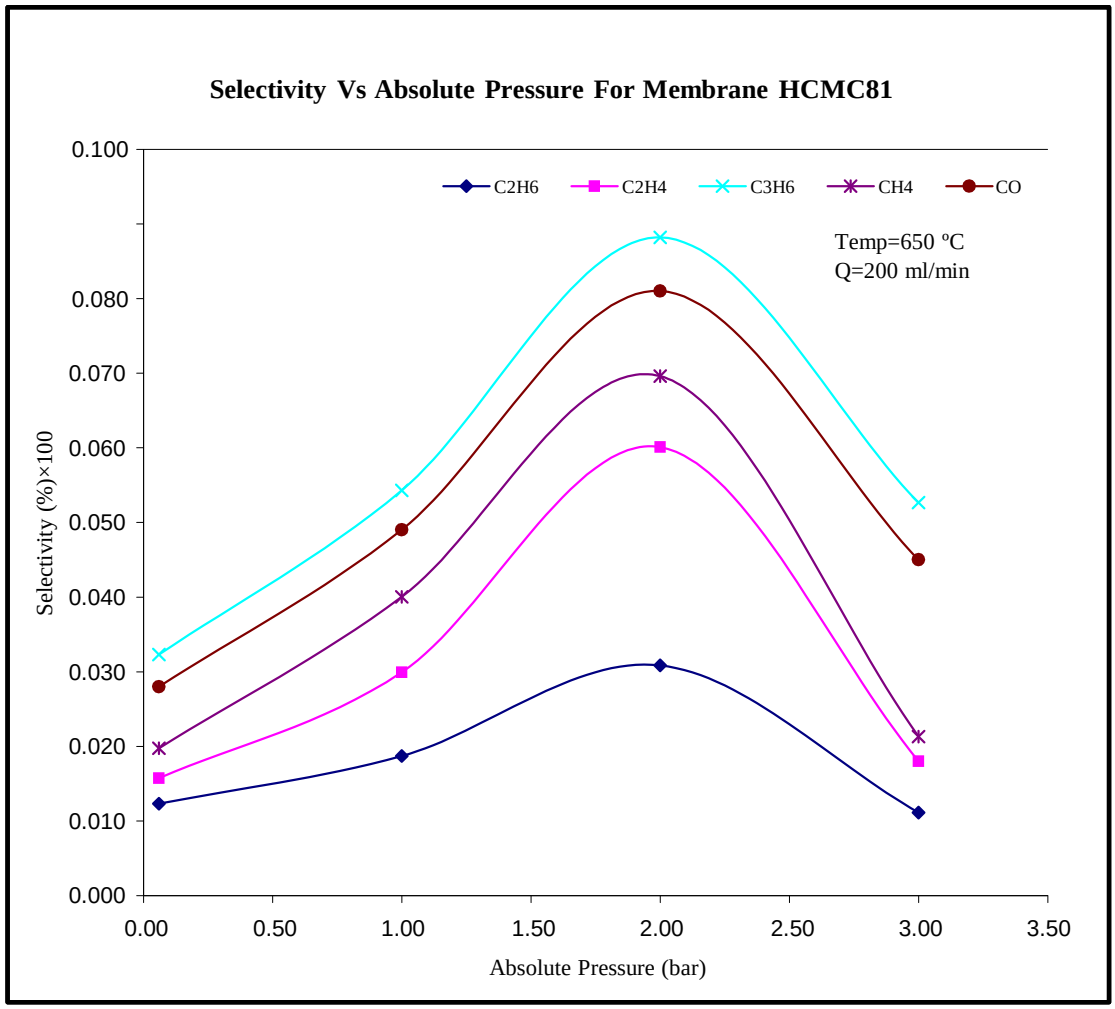

Figure A2.17 Selectivity vs absolute pressure for membrane HCMC81.

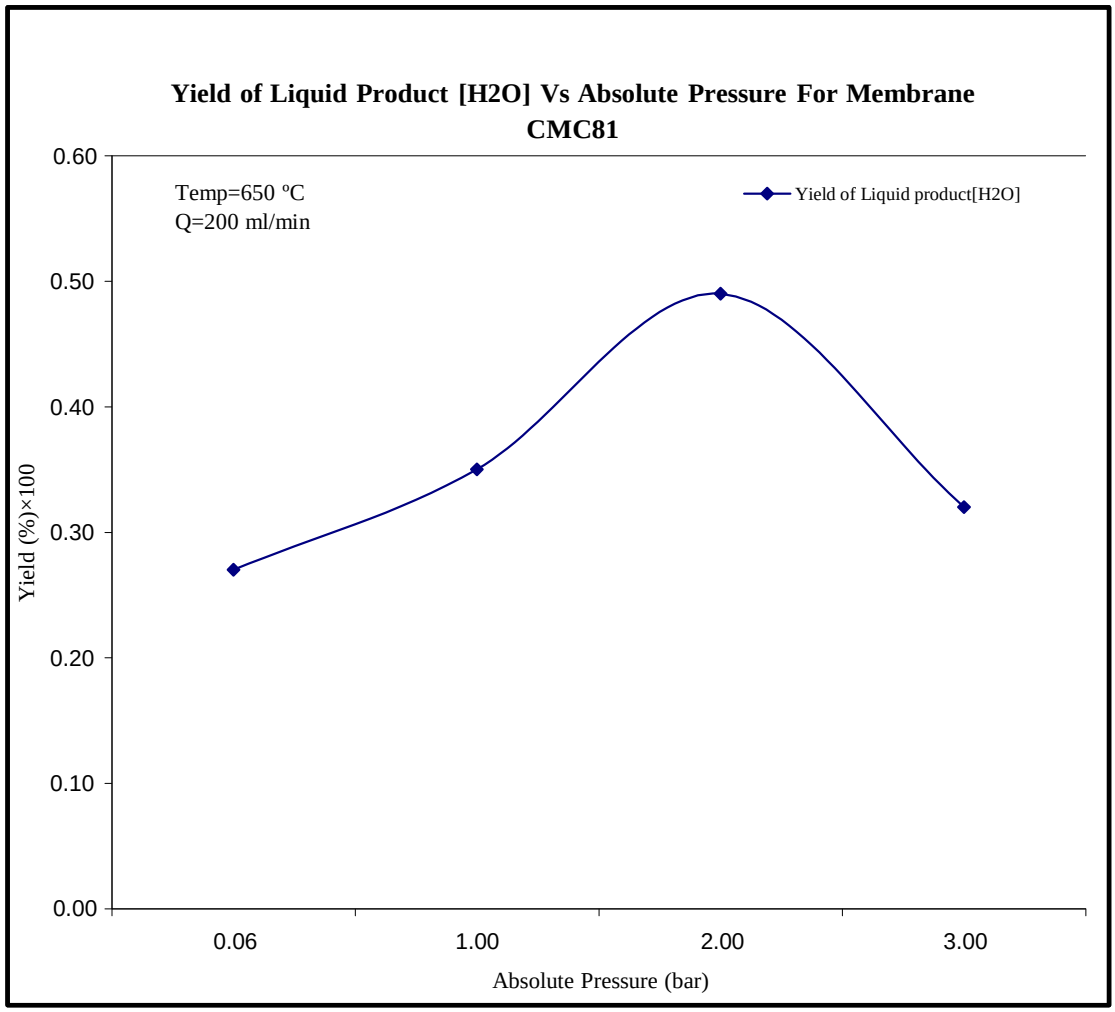

Figure A2.18 Yield of liquid products (H_2O) vs absolute pressure for membrane HCMC81.

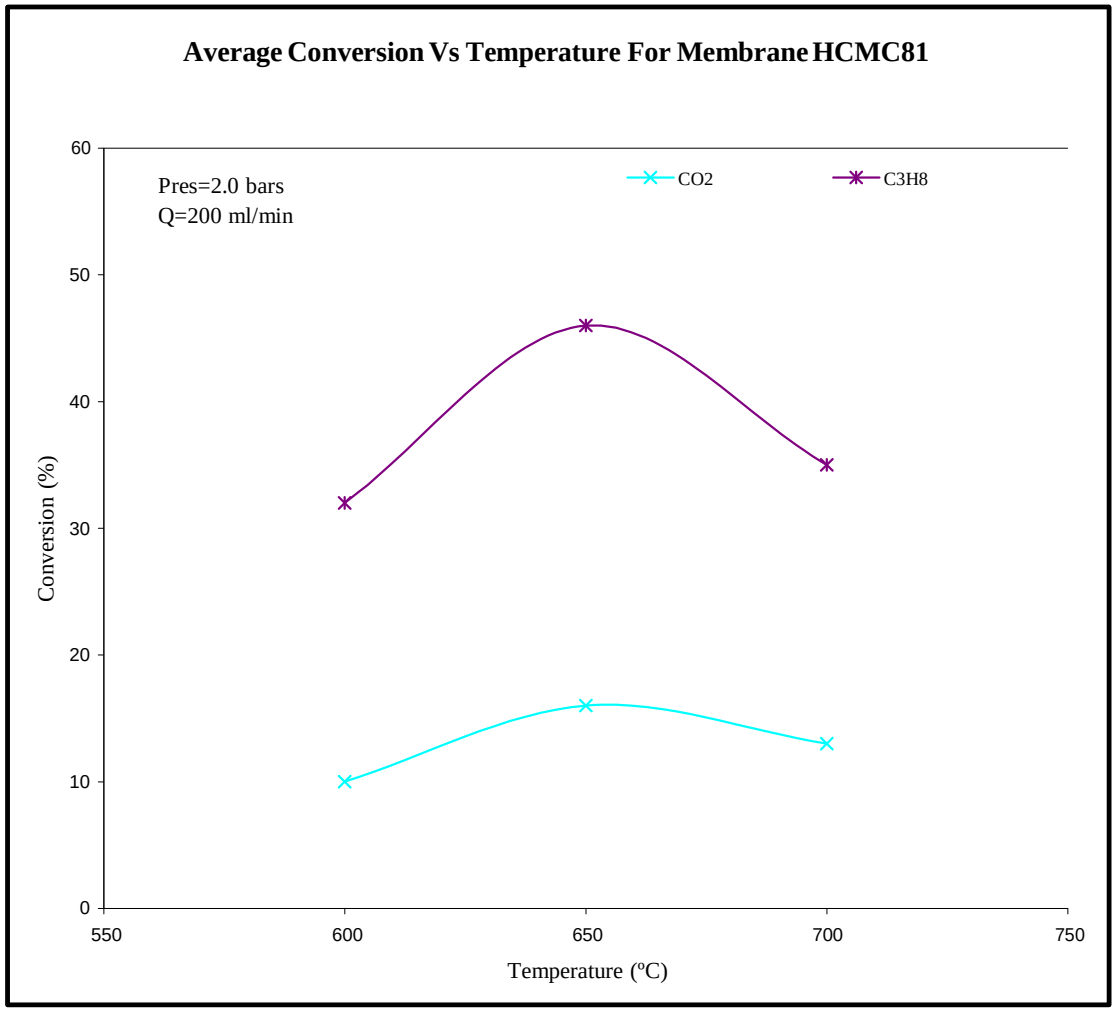

Figure A2.19 Average conversion vs temperature for membrane MCHC81.

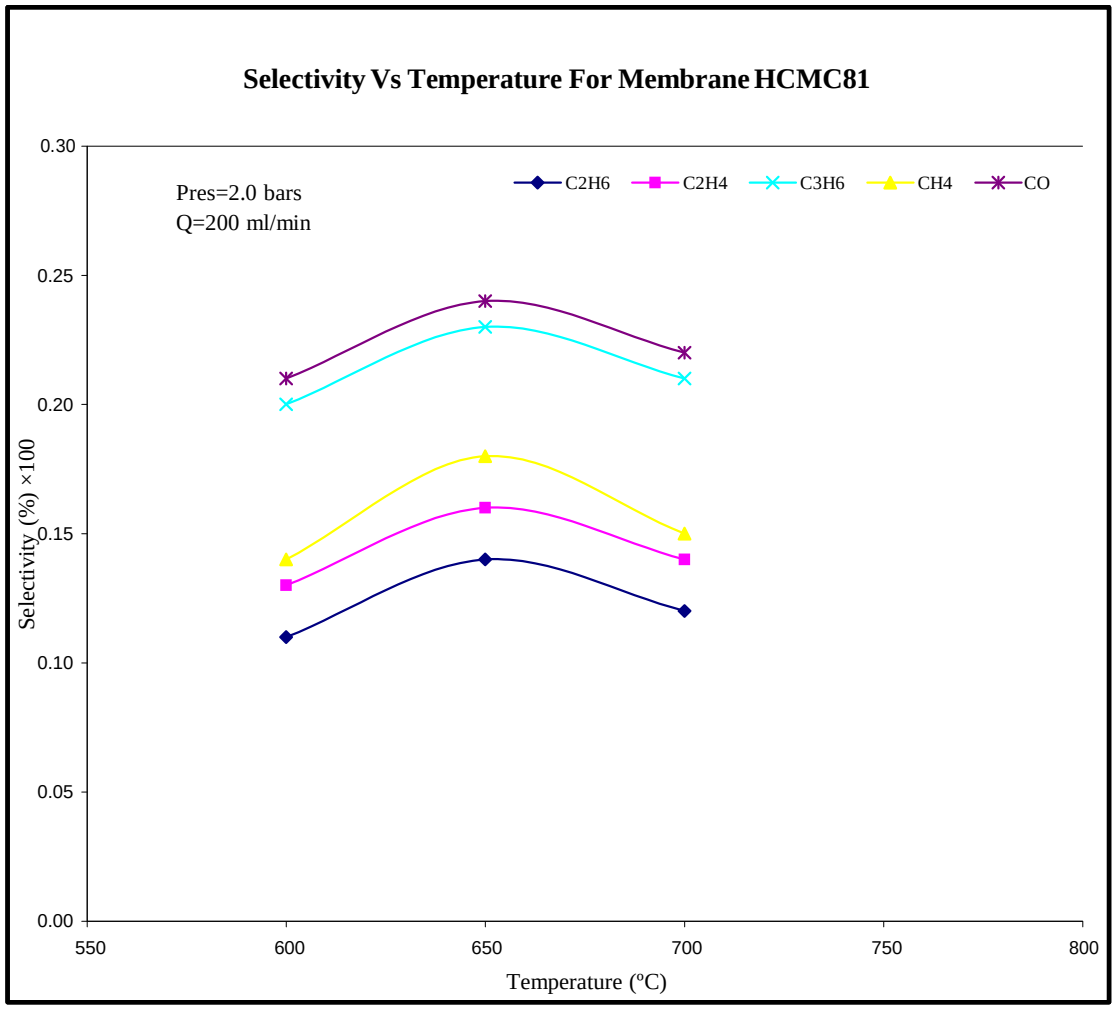

Figure A2.20 Selectivity vs temperature for membrane HCMC81.

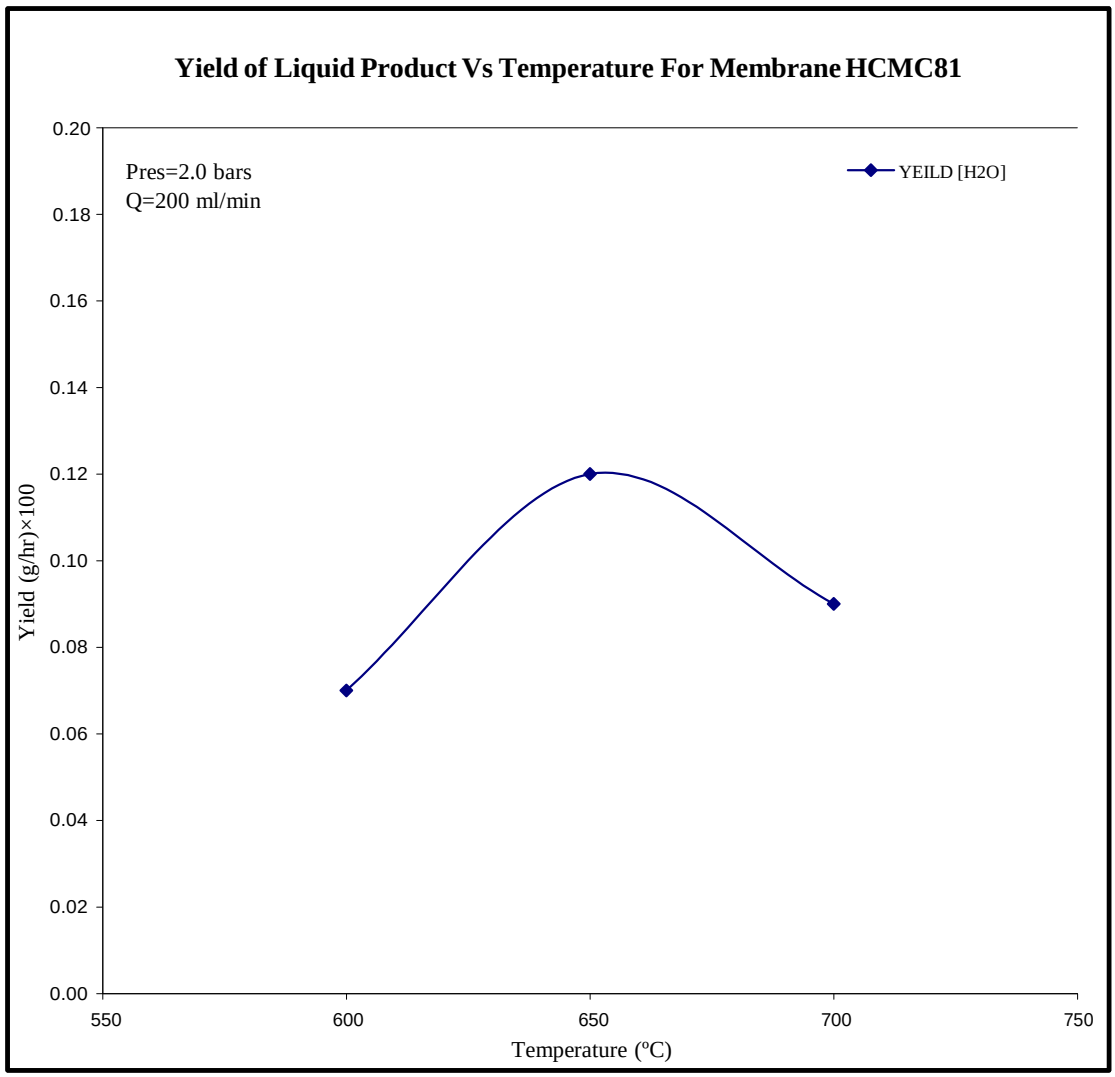

Figure A2.21 Yield of liquid products (H2O) vs temperature for membrane HCMC81.

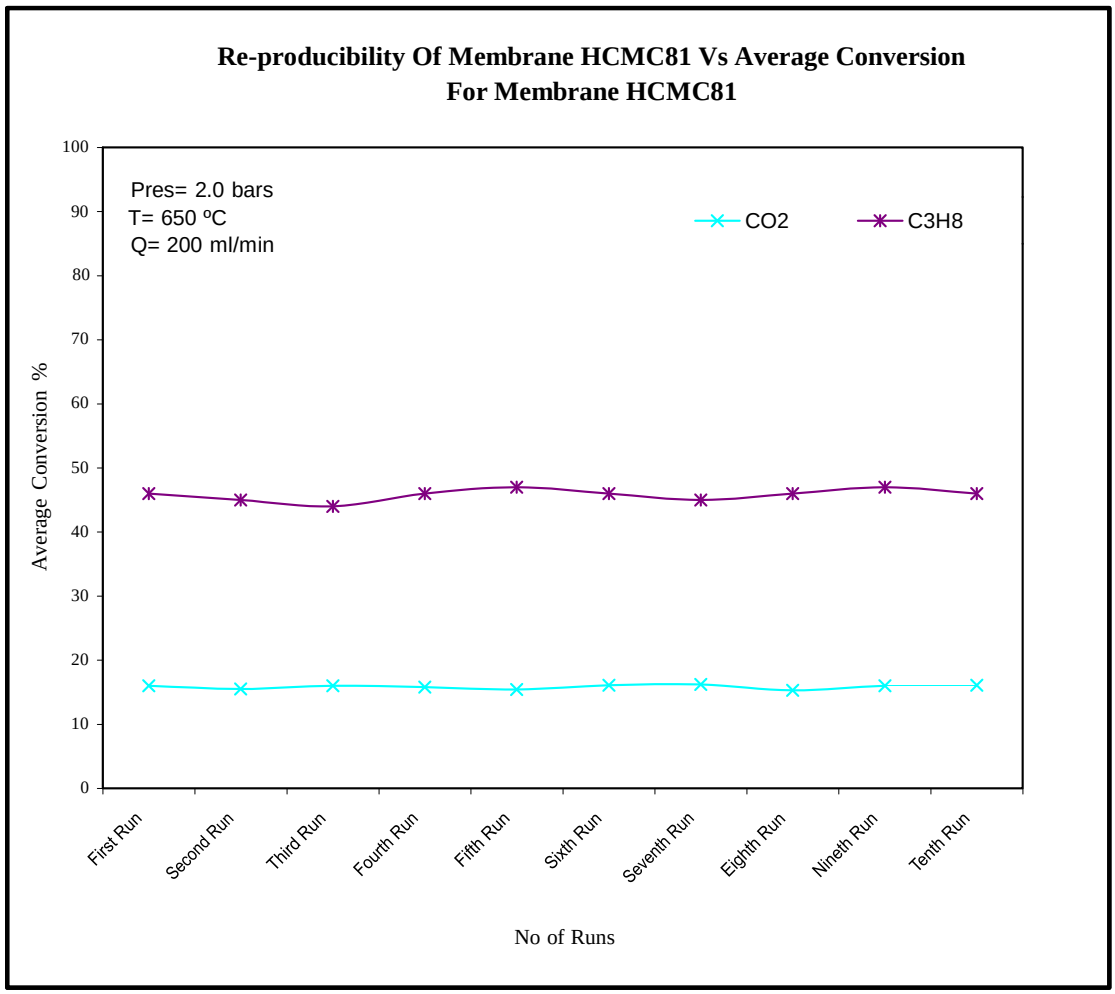

Figure A2.22 Re-reducibility of membrane HCMC81 vs average conversion for membrane HCMC81.

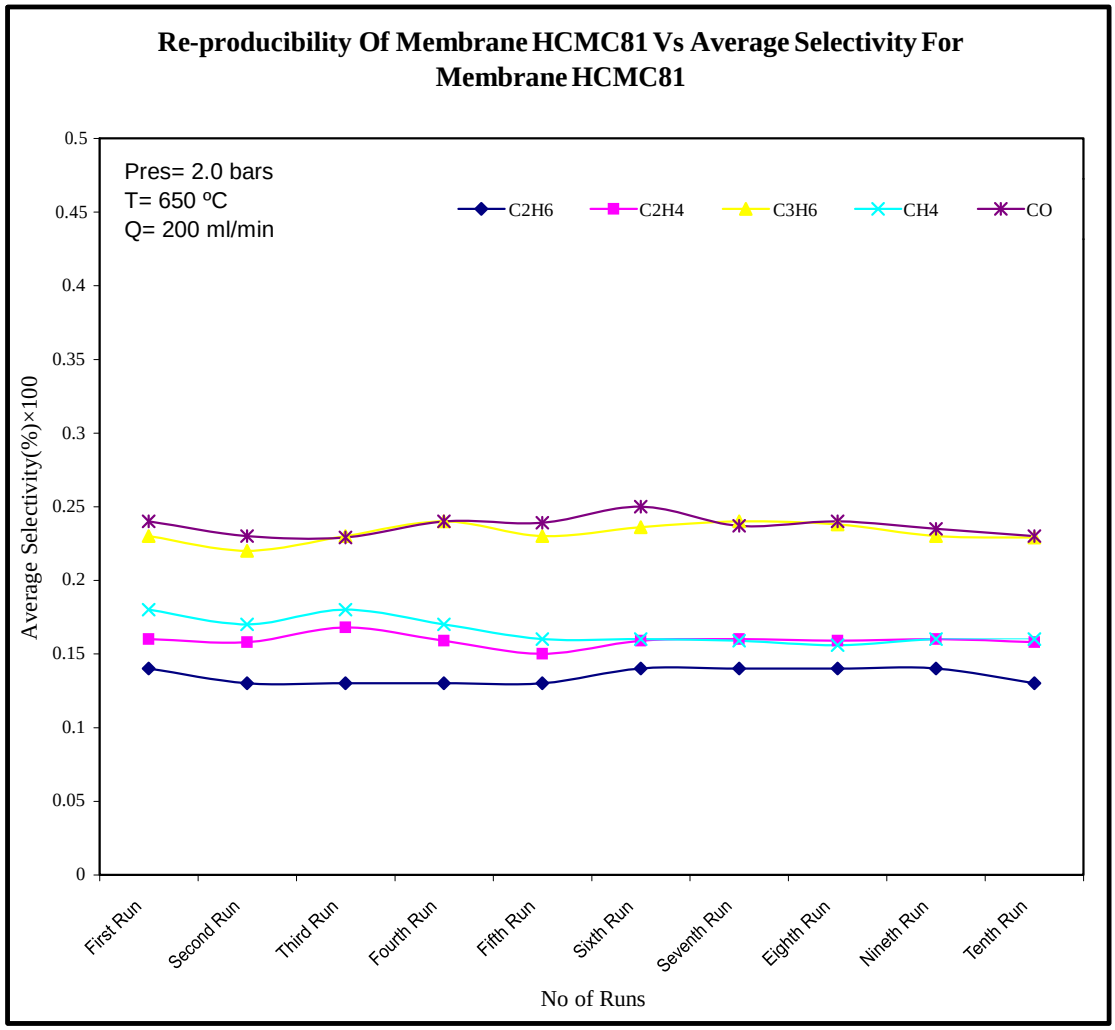

Figure A2.23 Re-reducibility of membrane HCMC81 vs average selectivity for membrane HCMC81.

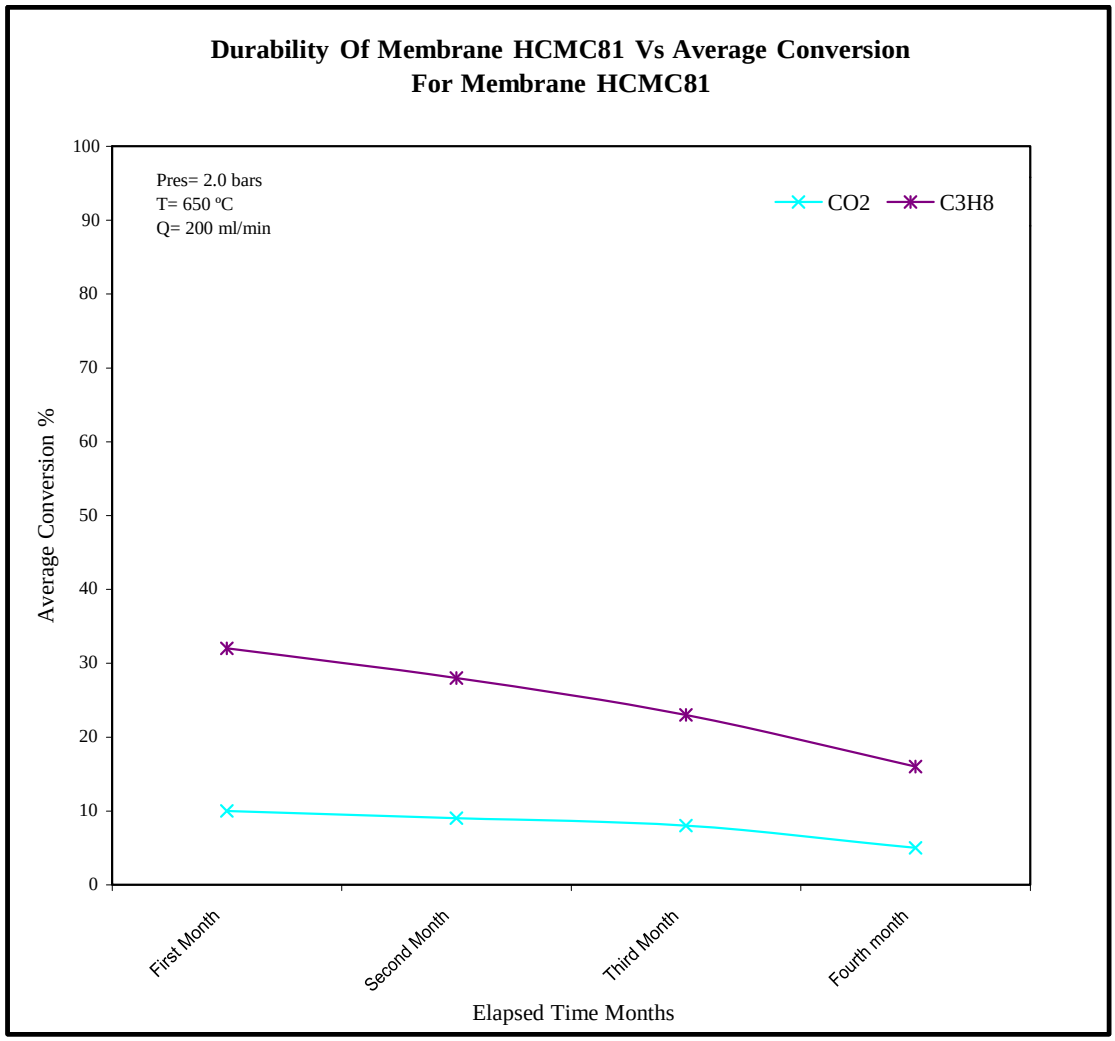

Figure A2.24 Durability of membrane HCMC81 vs average conversion for membrane HCMC81.

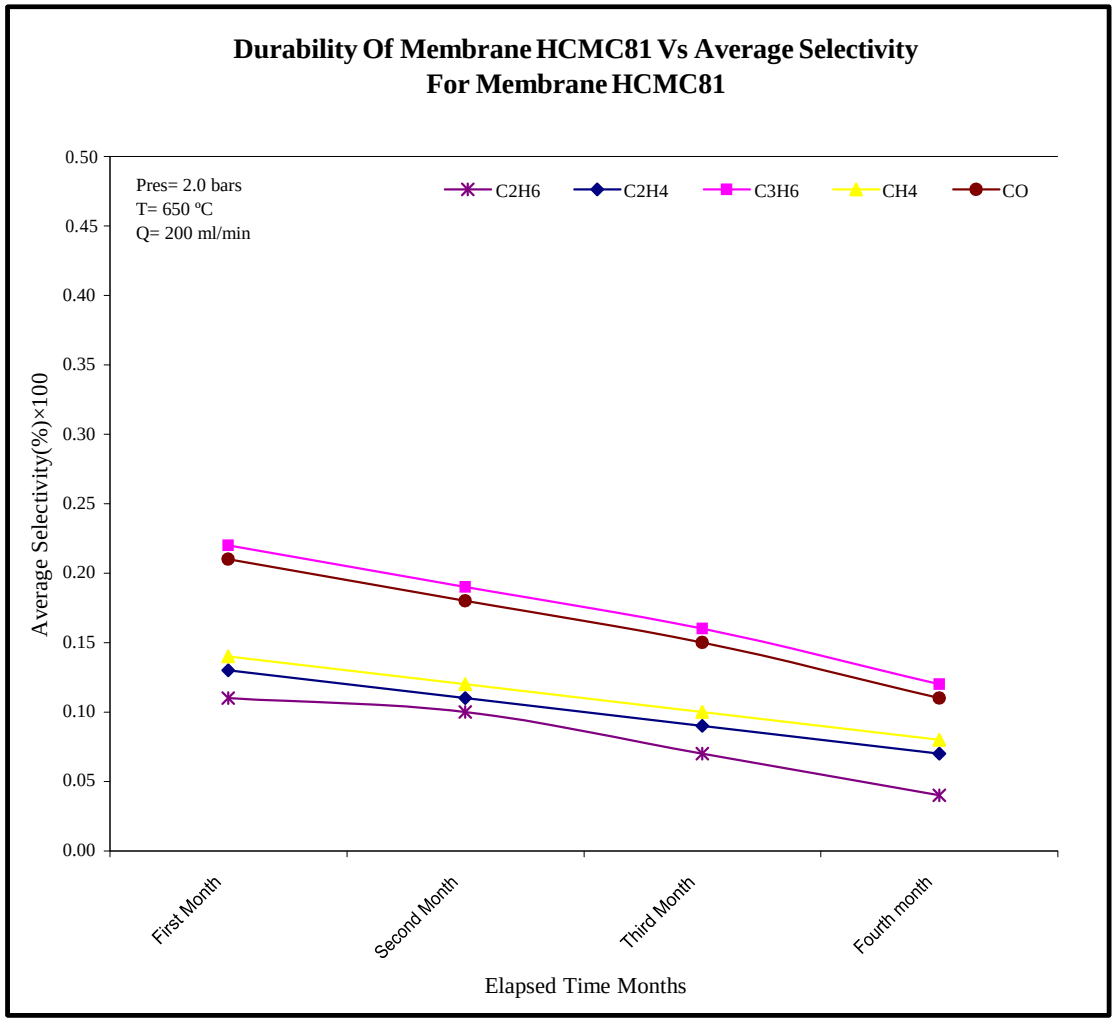

Figure A2.25 Durability of membrane HCMC81 vs average selectivity for membrane HCMC81.

Appendix Three

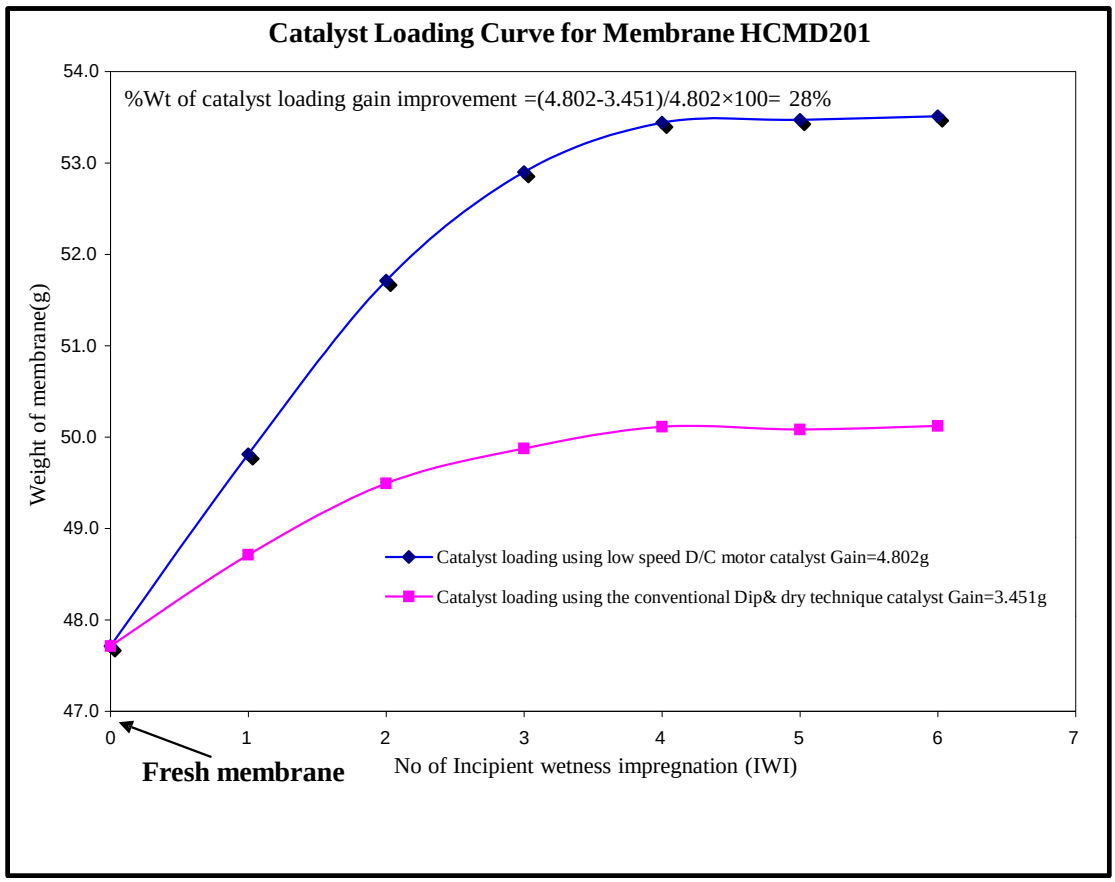

Figure A3.1 The catalyst [$PdCl_2$-Cu (NO_3)2 +$ZrCl_2$-Ni (NO_3)2] loading curve for membrane HCMD201.

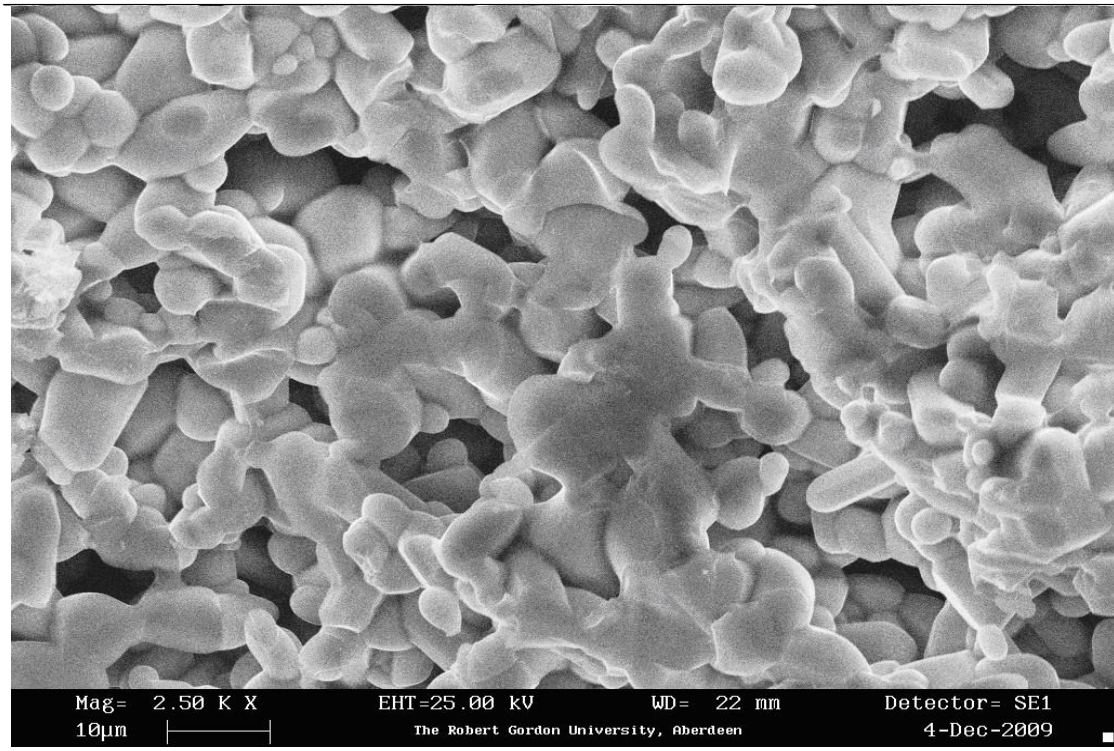

For D200nm Fresh Support

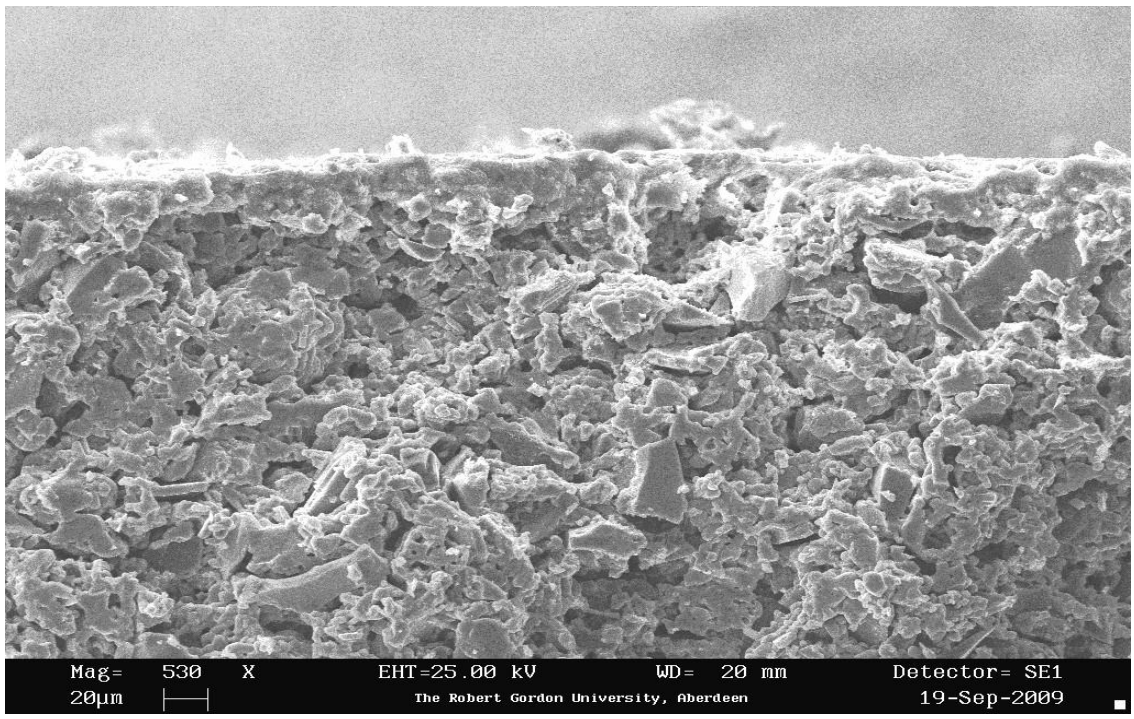

For Membrane HCMD201 3rd Dip-coating

Figure A3.2 SEM images for fresh support D200 and membrane HCMD201.

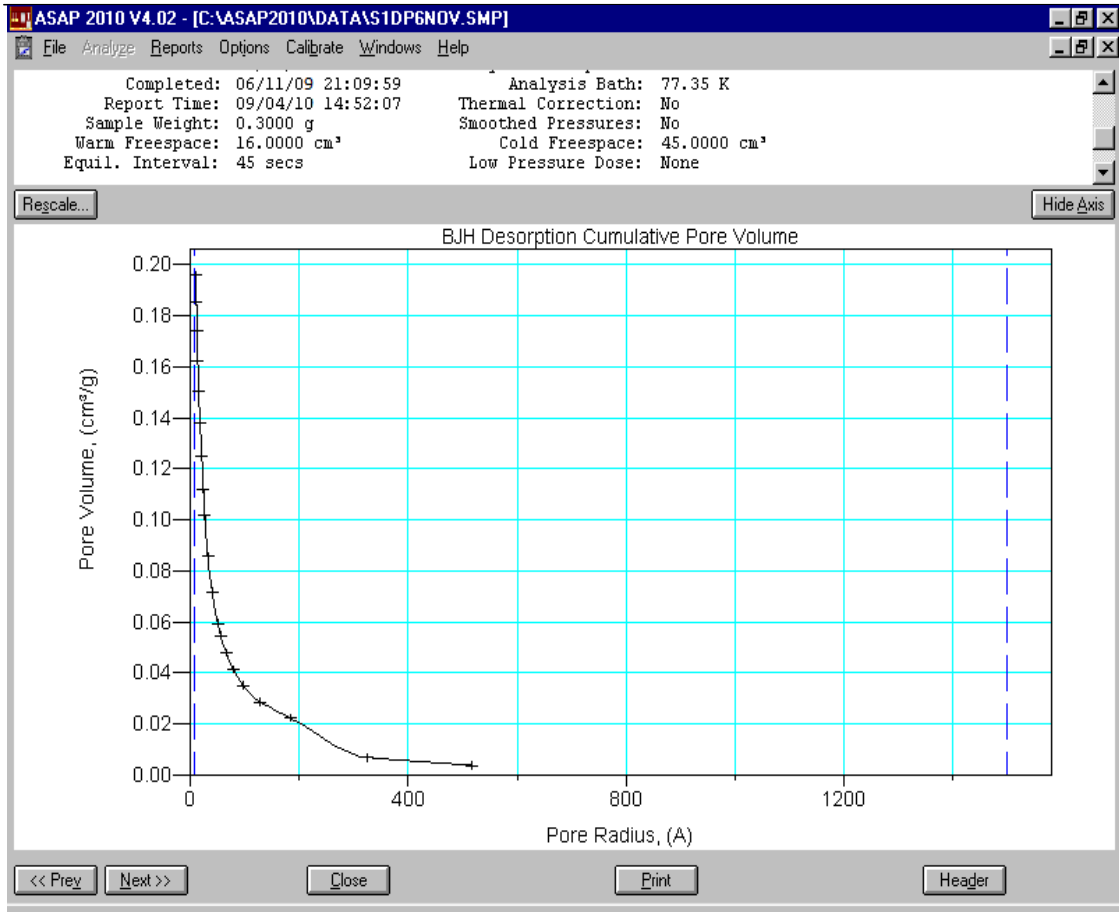

Figure A3.3 ASAP curve for D200nm fresh support.

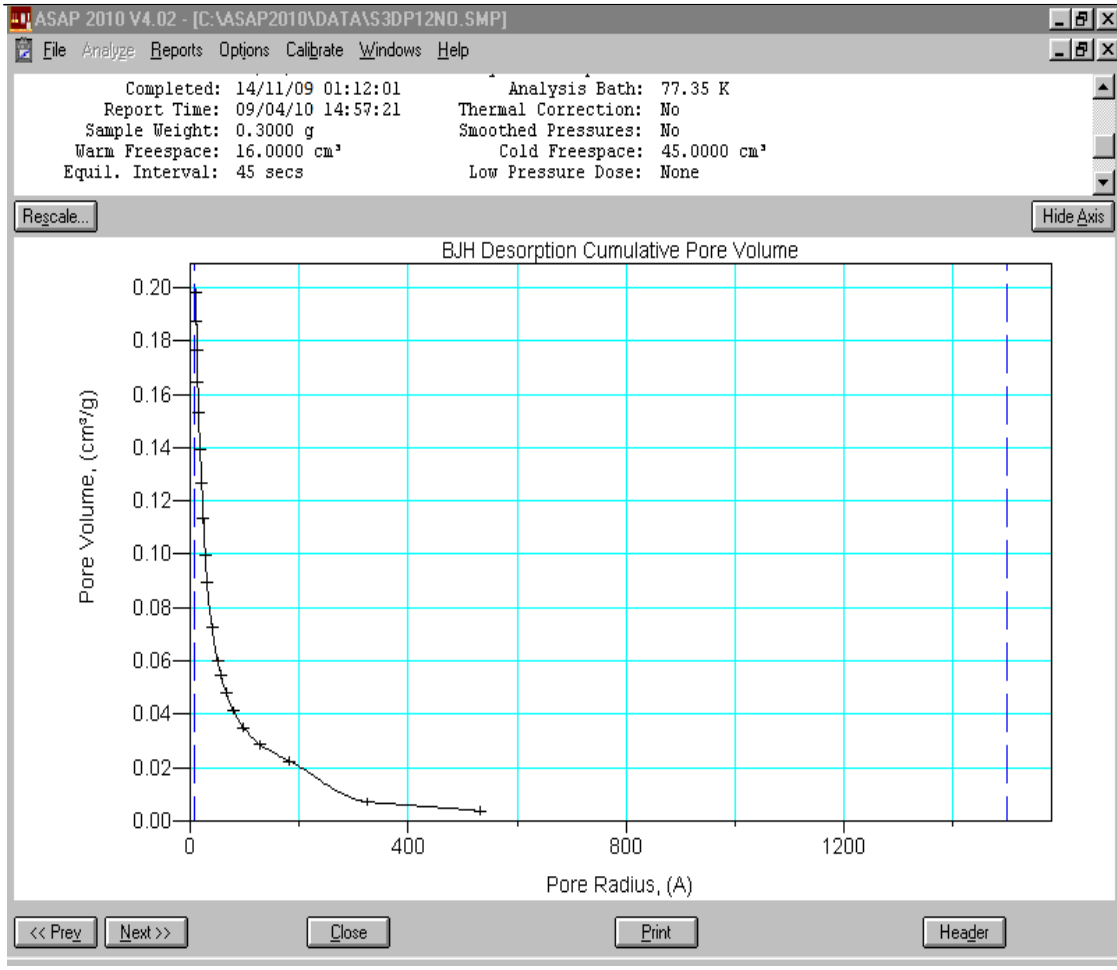

Figure A3.4 ASAP curve for membrane HCMD201 3rd dip-coating.

Print Date: Tue Feb 10 17:15:43 2009 Page 1 of 1

Title :
Run File : c:\star\data\3800.45116.run
Method File : c:\star\3800.45116-front.mth
Sample ID : Manual Sample

Injection Date: 10/02/2009 16:51 Calculation Date: 10/02/2009 17:15

Operator : ALI Detector Type: 3800 (10 Volts)
Workstation: RGU13846 Bus Address : 45
Instrument : Varian Star #1 Sample Rate : 10.00 Hz
Channel : Front = TCD Run Time : 23.477 min

** GC Workstation Version 6.41 ** 00756-24C0-C65-00B4 **

Run Mode : Analysis
Peak Measurement: Peak Area
Calculation Type: External Standard

Peak No.	Peak Name	Result ()	Ret. Time (min)	Time Offset (min)	Area (counts)	Sep. Code	Width 1/2 (sec)	Status Codes
1	CO2	21.5558	3.463	0.086	2416041	BB	10.8	C
2	ETHYLENE	2.4430	5.320	0.013	280185	BB	15.2	
3	PROPYLENE	2.9110	15.680	-0.027	202622	BV	0.0	
4		0.0000	15.982	0.000	1595	VV	29.4	
5	PROPANE	35.9983	16.413	-0.079	2690599	VB	61.0	C
6		0.0000	21.740	0.000	129757	BV	7.4	
7	METHANE	4.9444	22.155	0.002	169714	VV	6.9	
8	CO	15.2371	22.455	0.010	595672	VB	7.9	
	Totals:	83.0896		0.005	6486185			

Status Codes:
C - Out of calibration range

Total Unidentified Counts : 131353 counts

Detected Peaks: 8 Rejected Peaks: 0 Identified Peaks: 6

Multiplier: 1 Divisor: 1 Unidentified Peak Factor: 0

Baseline Offset: 6 microVolts LSB: 1 microVolts

Noise (used): 3 microVolts - monitored before this run

Manual injection

Peak not split: event not in an existing peak
Calib. out of range; No Recovery Action Specified

Figure A3.5 An example of the GC peaks for the products for membrane HCMD201.

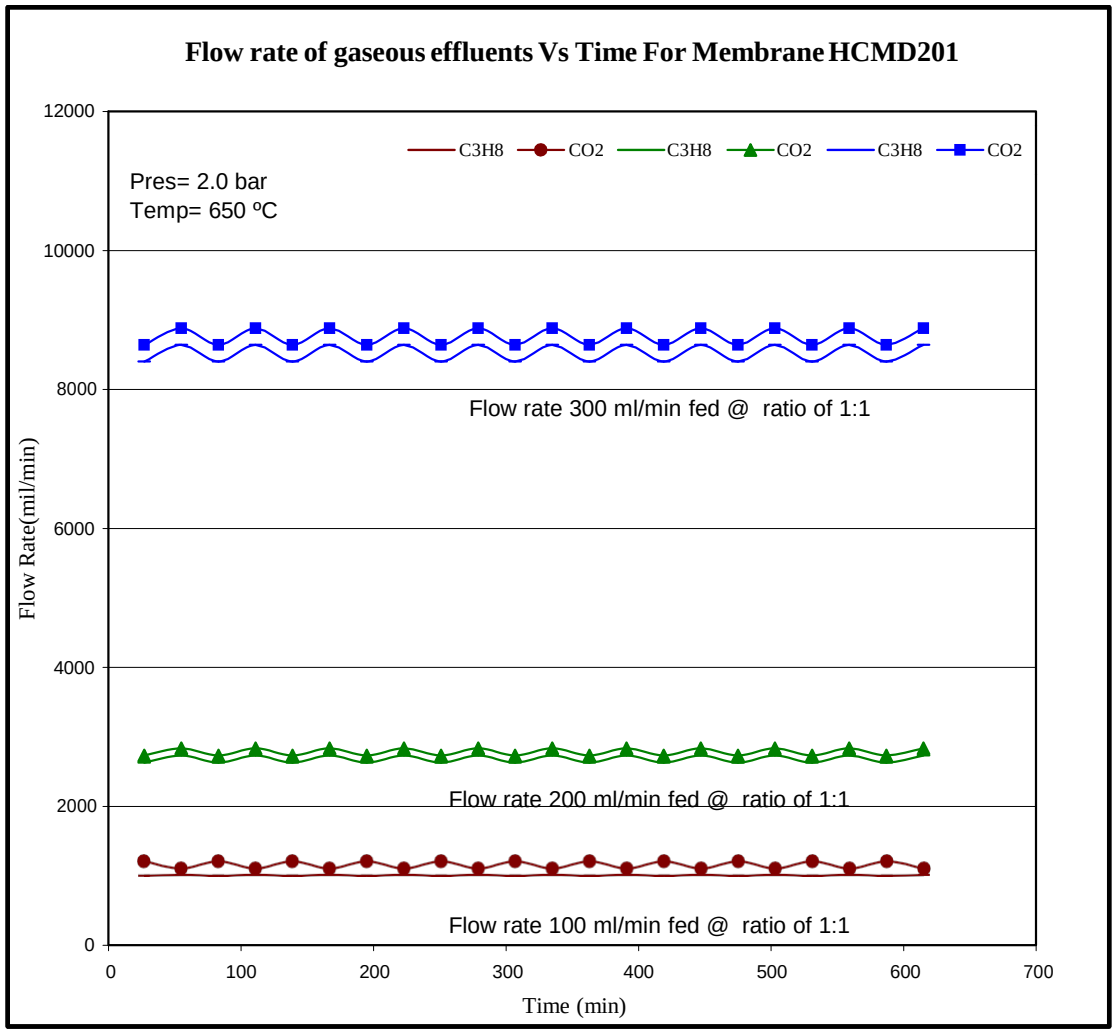

Figure A3.6 Flow rates of gaseous effluents vs time for membrane HCMD201 fed at ratio of 121.

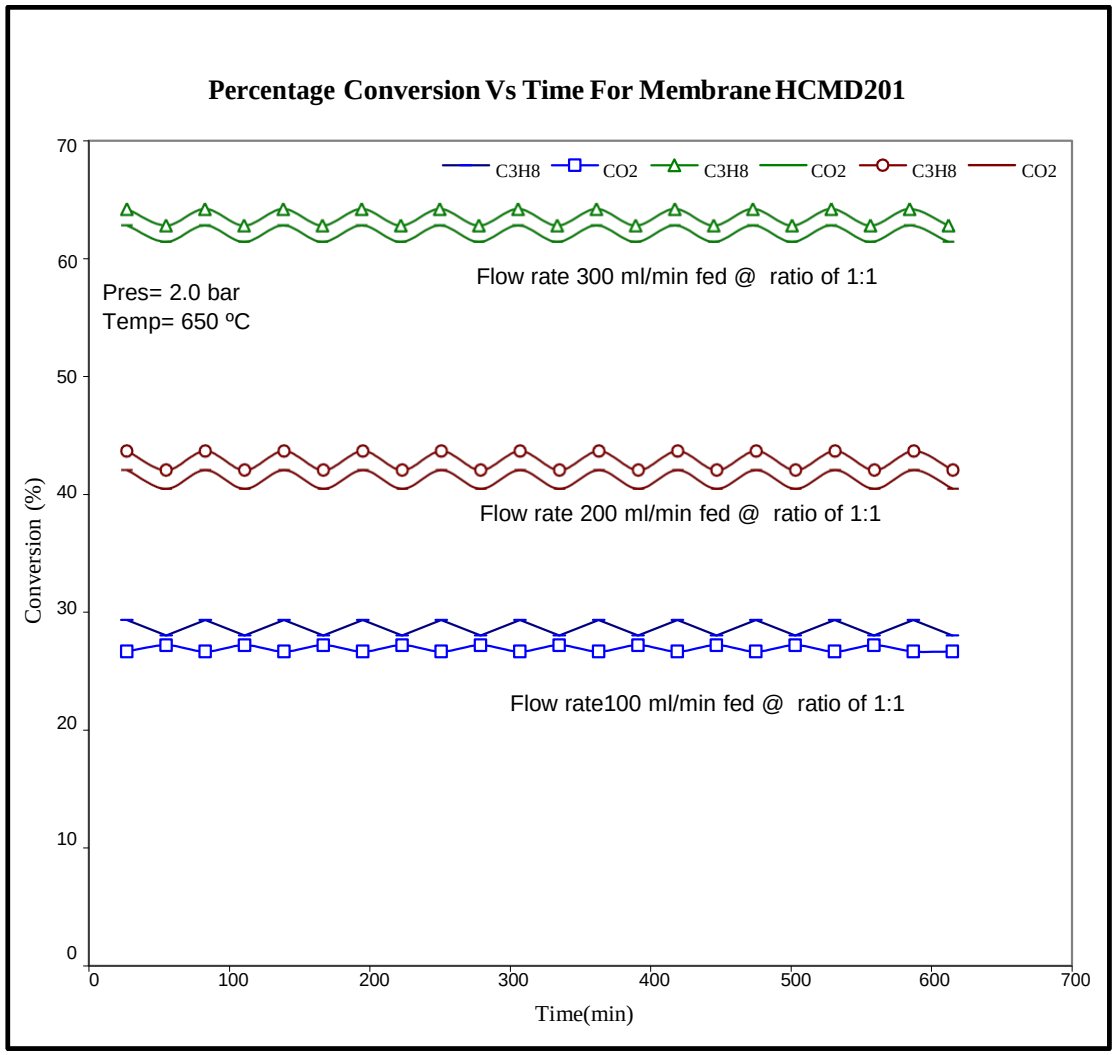

Figure A3. 7 Percentage conversion vs time for membrane HCMD201 fed at ratio of 121.

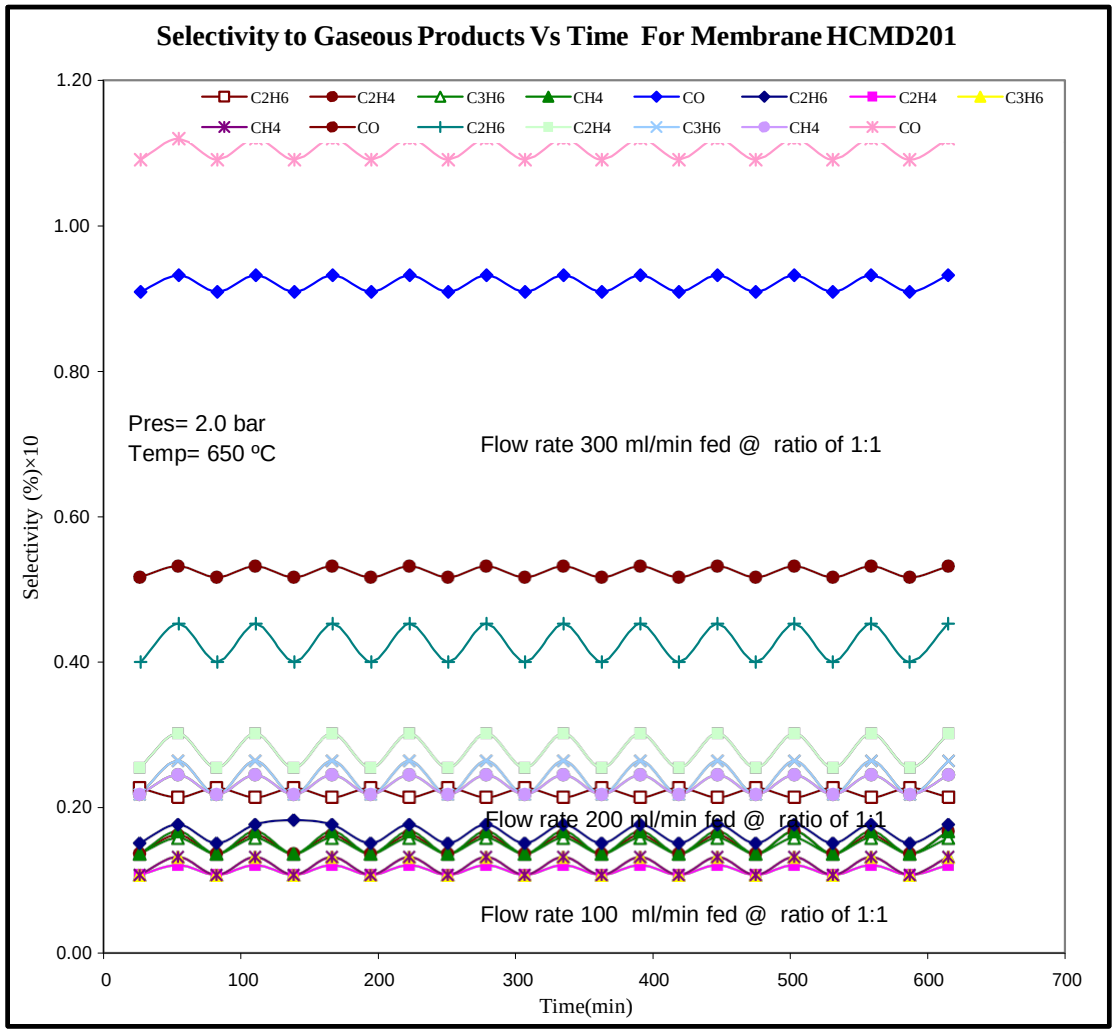

Figure A3.8 Selectivity to gaseous products vs time for membrane HCMD201 fed at ratio of 121.

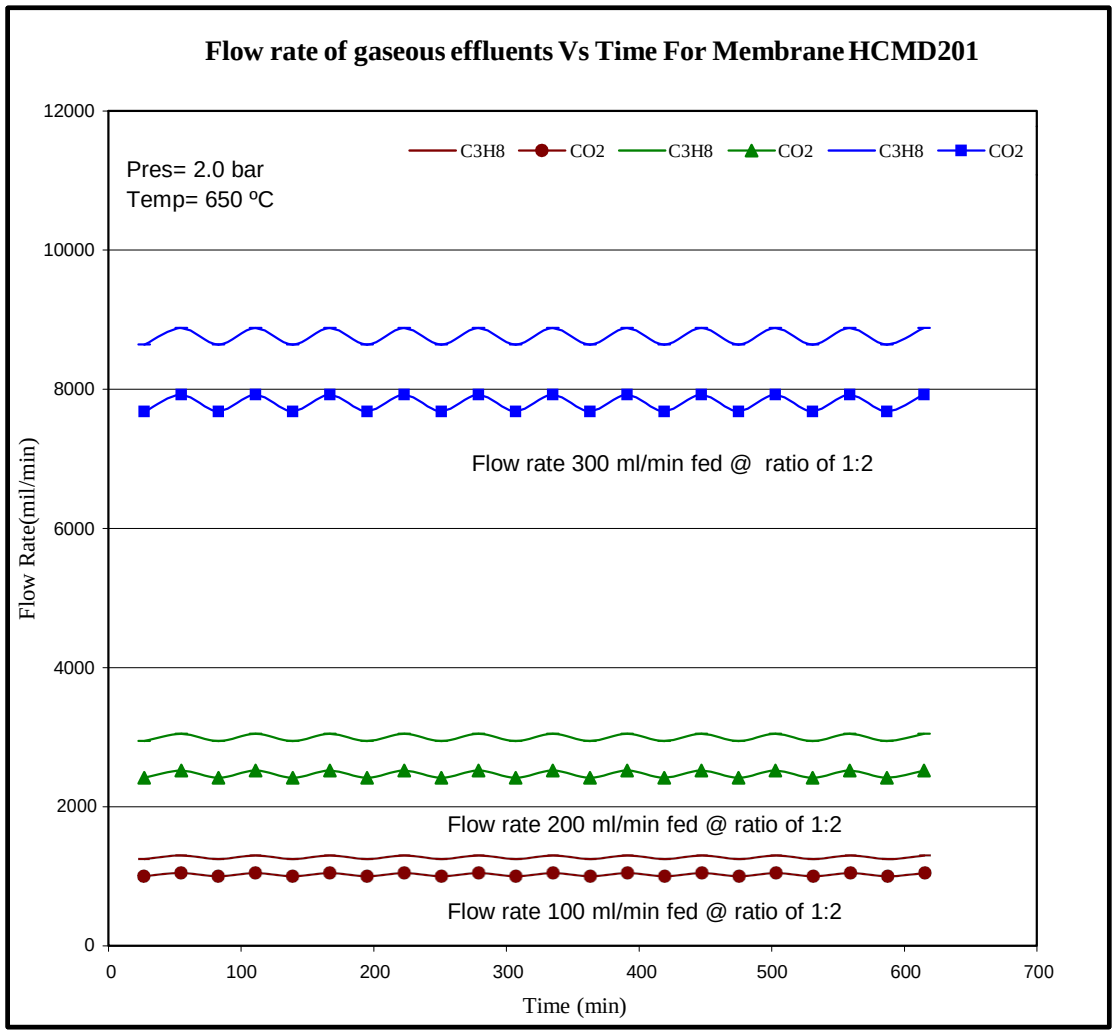

Figure A3.9 Flow rates of gaseous effluents vs time for membrane HCMD201 fed at ratio of 122.

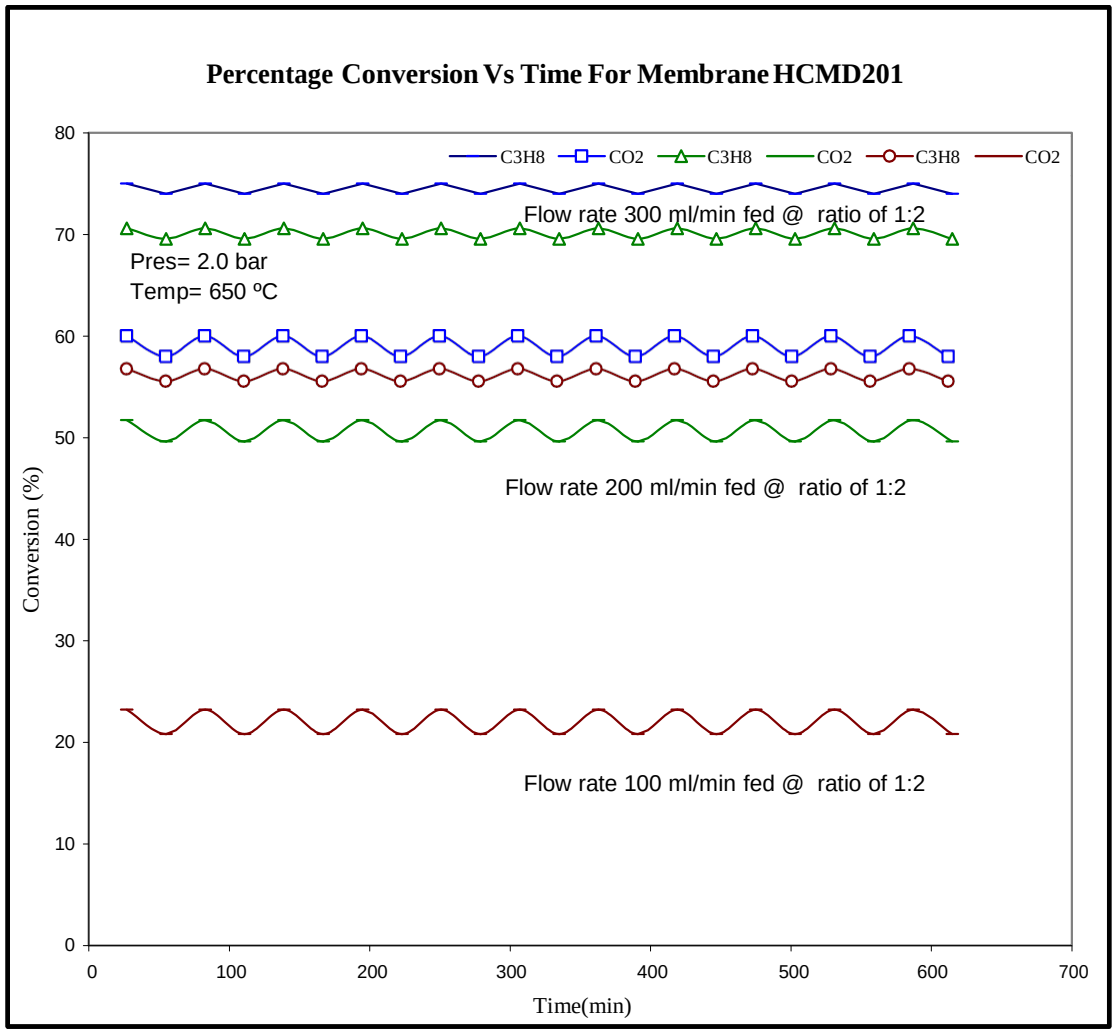

Figure A3.10 Percentage conversion vs time for membrane HCMD201 fed at ratio of 122.

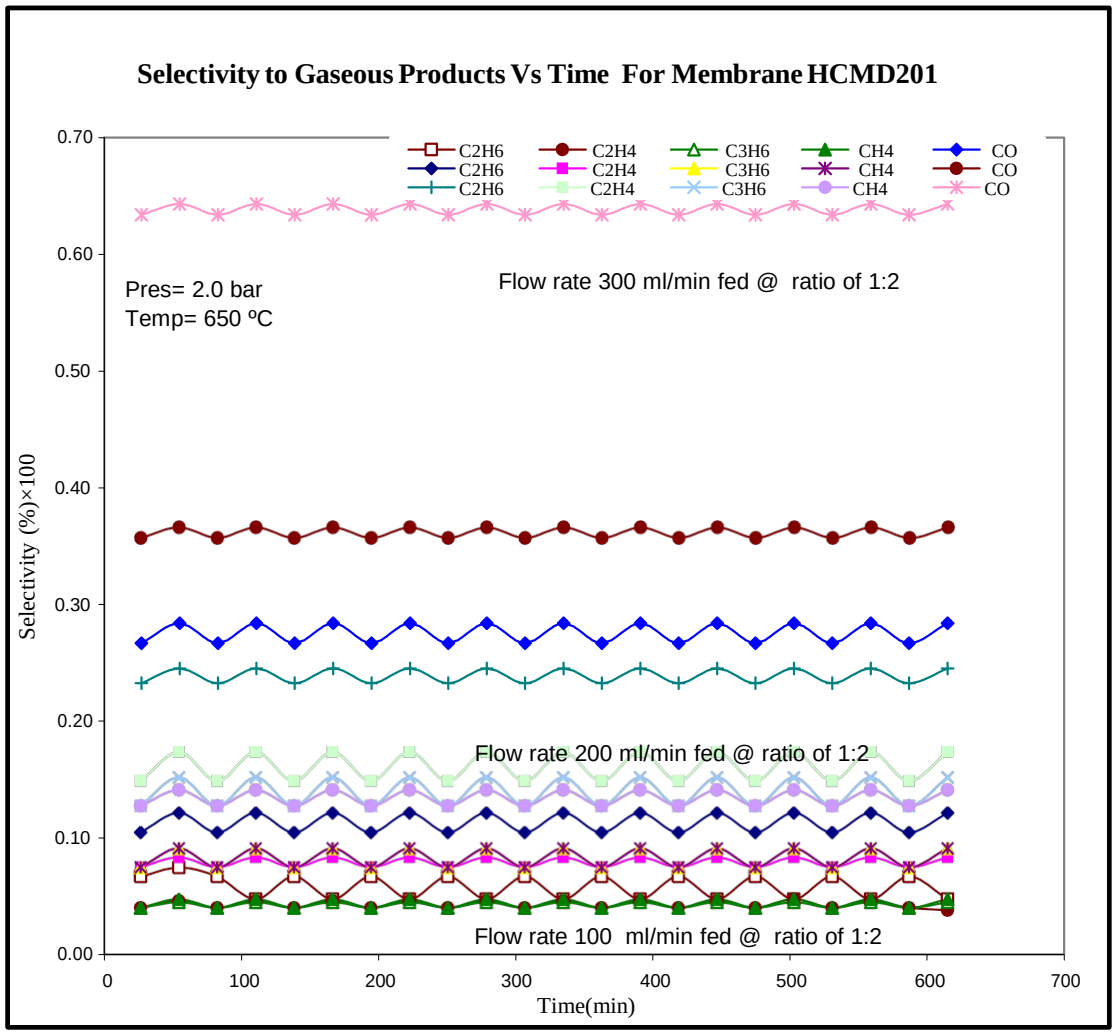

Figure A3.11 Selectivity to gaseous products vs time for membrane HCMD201 fed at ratio of 122.

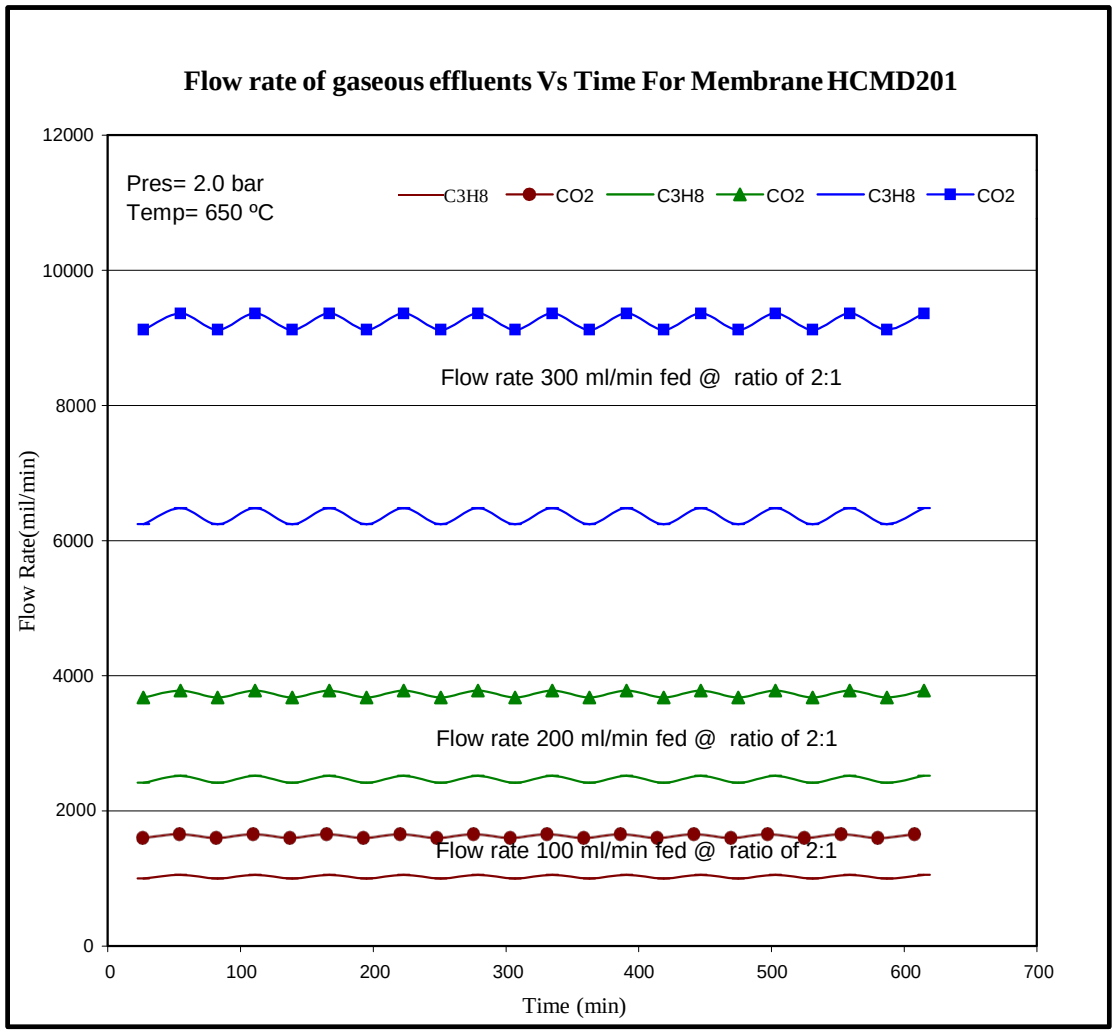

Figure A3.12 Flow rates of gaseous effluents vs time for membrane HCMD201 fed at ratio of 221.

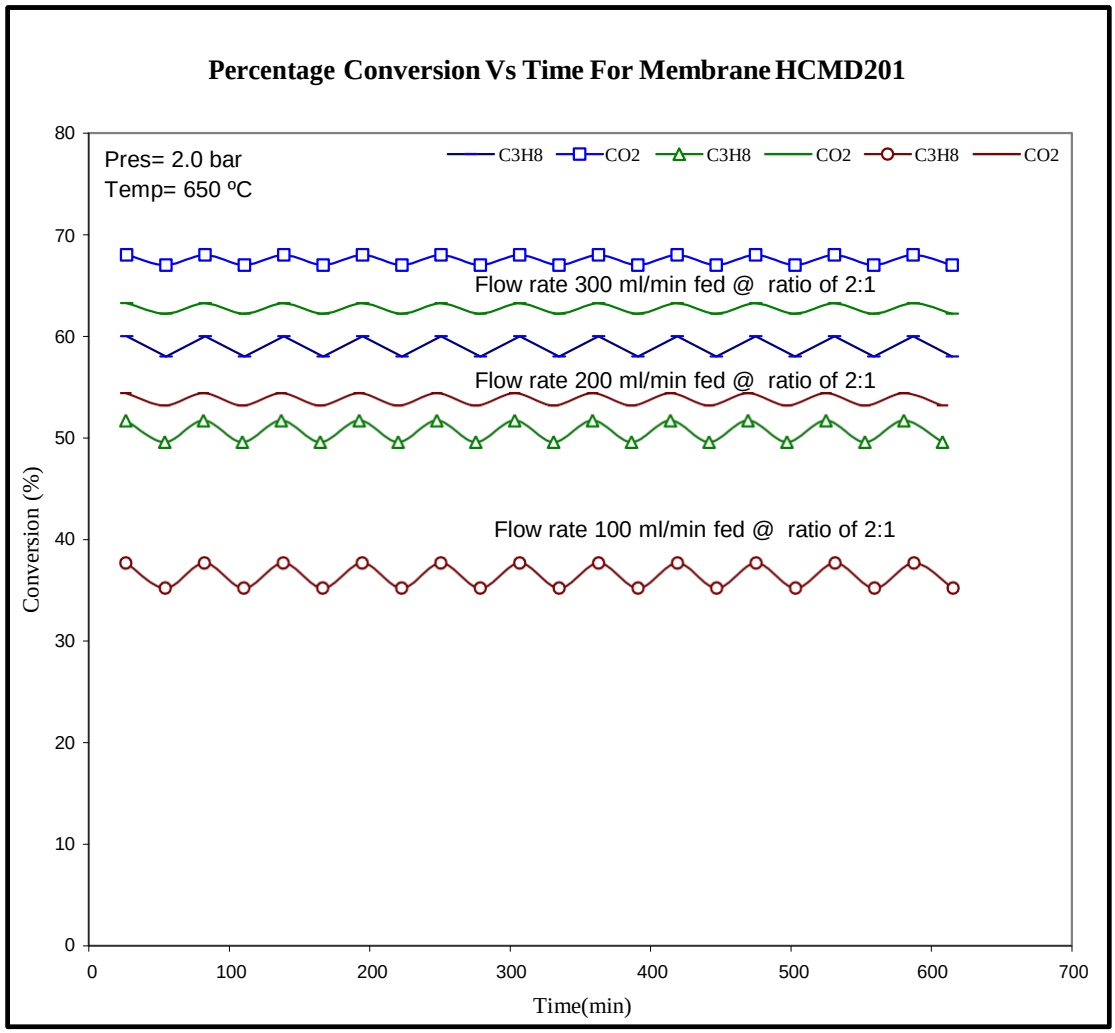

Figure A3.13 Percentage conversion vs time for membrane HCMD201 fed at ratio of 221.

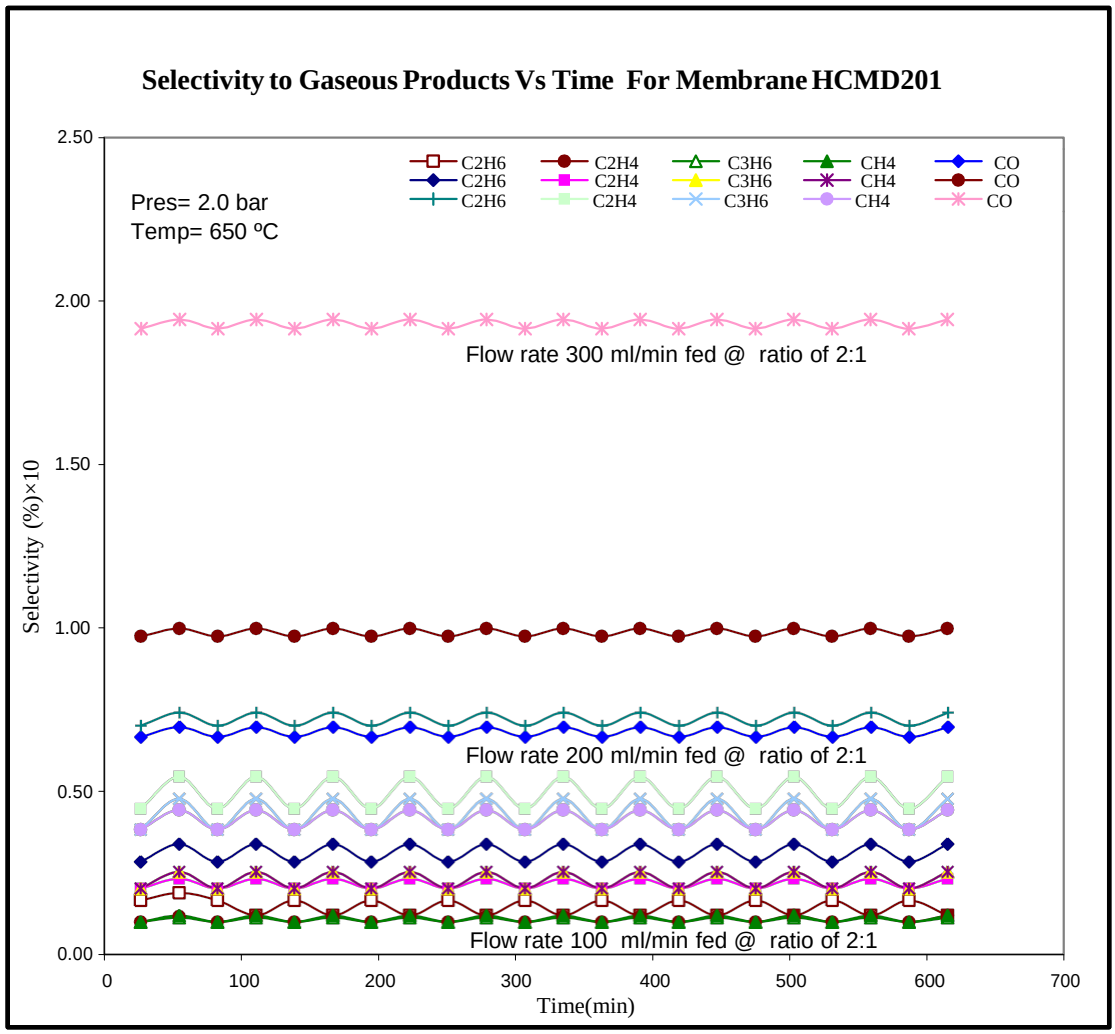

Figure A3.14 Selectivity to gaseous products vs time for membrane HCMD201 fed at ratio of 221.

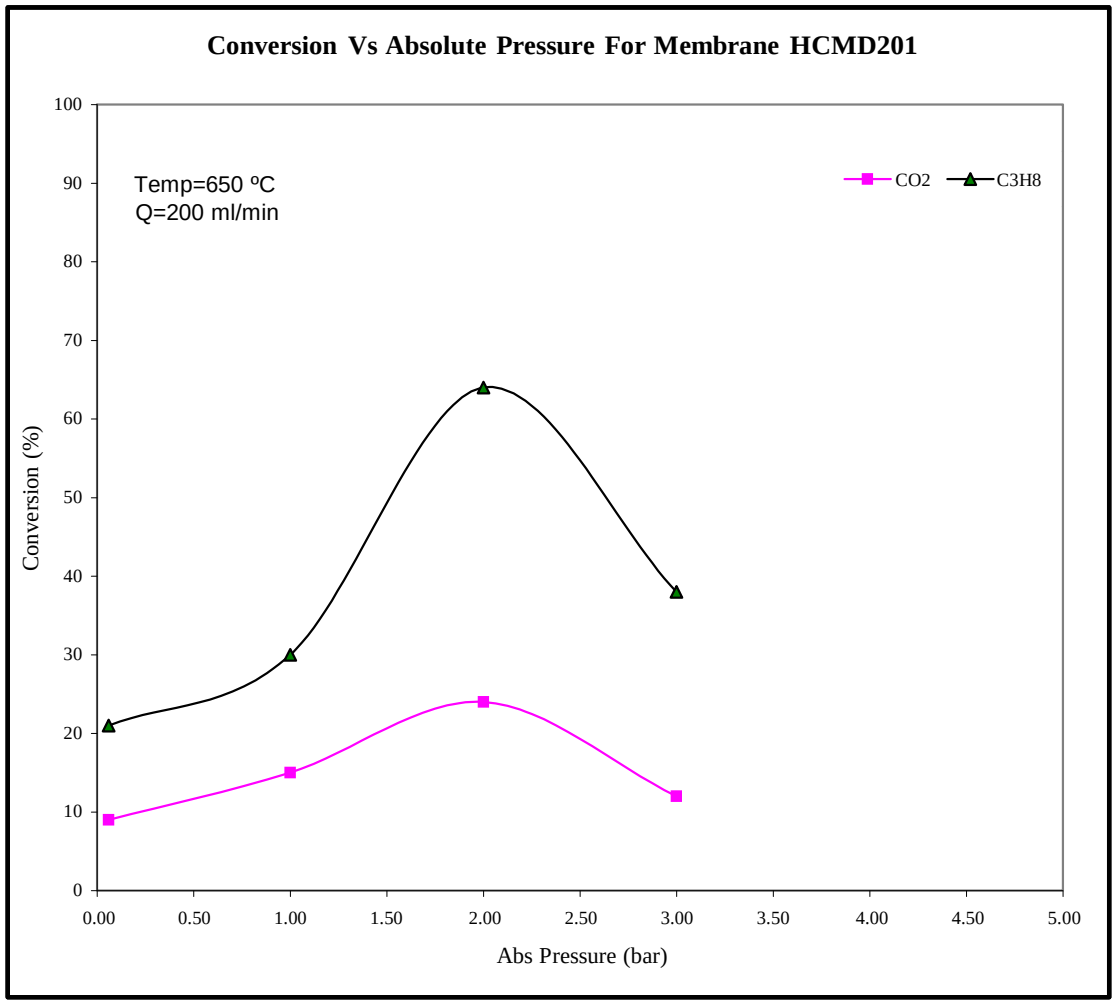

Figure A3.15 Conversion vs absolute pressure for membrane HCMD201.

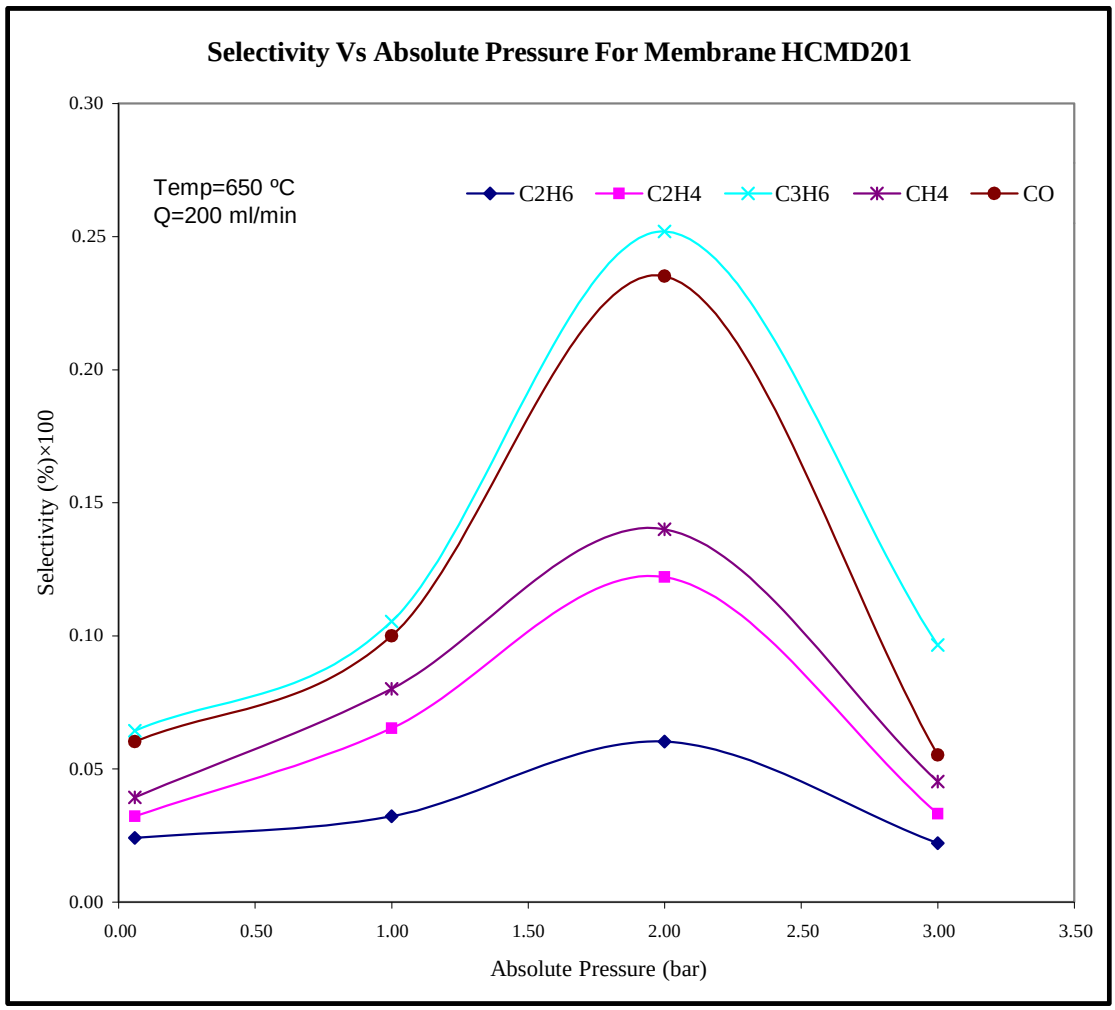

Figure A3.16 Selectivity vs absolute pressure for membrane HCMD201.

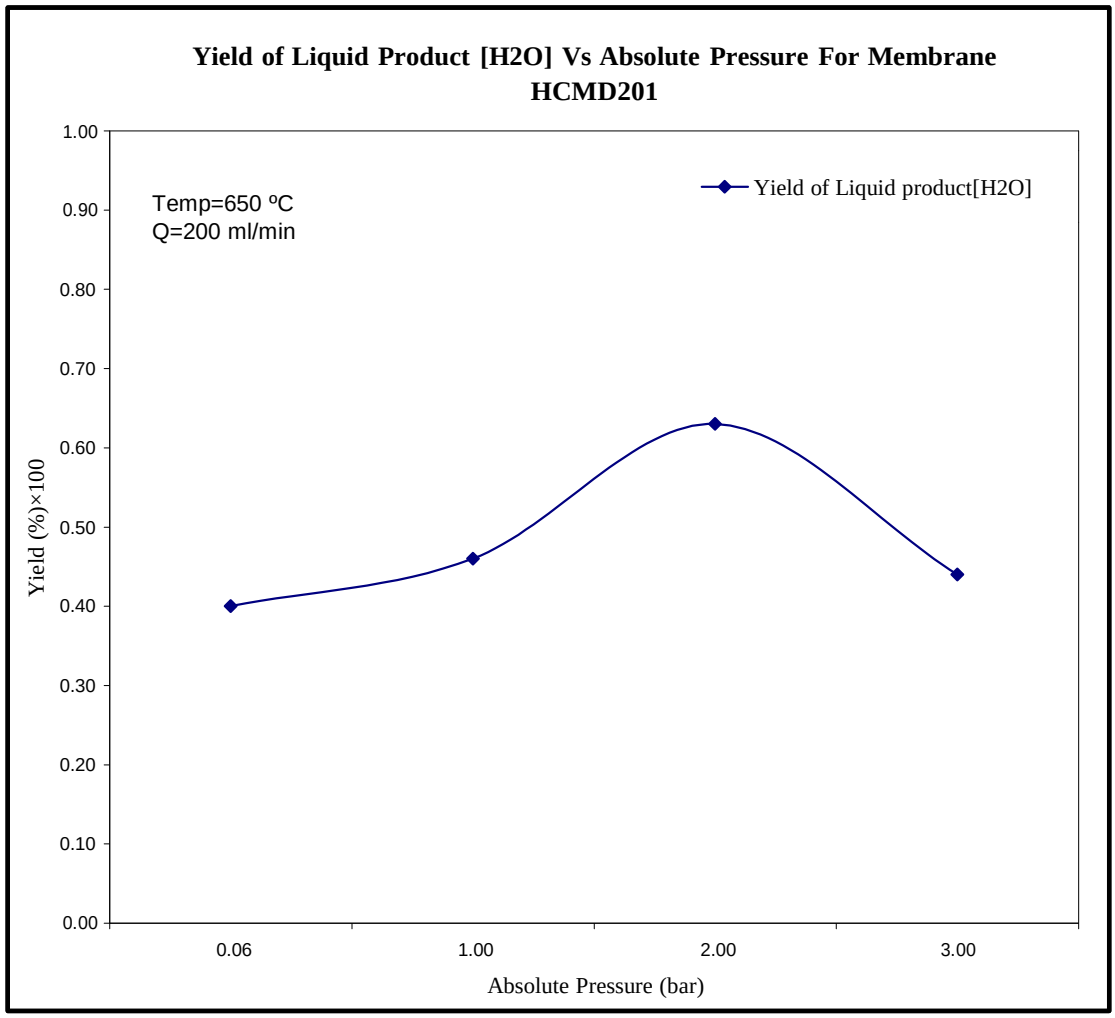

Figure A3.17 Yield of liquid products (H_2O) vs absolute pressure for membrane HCMD201.

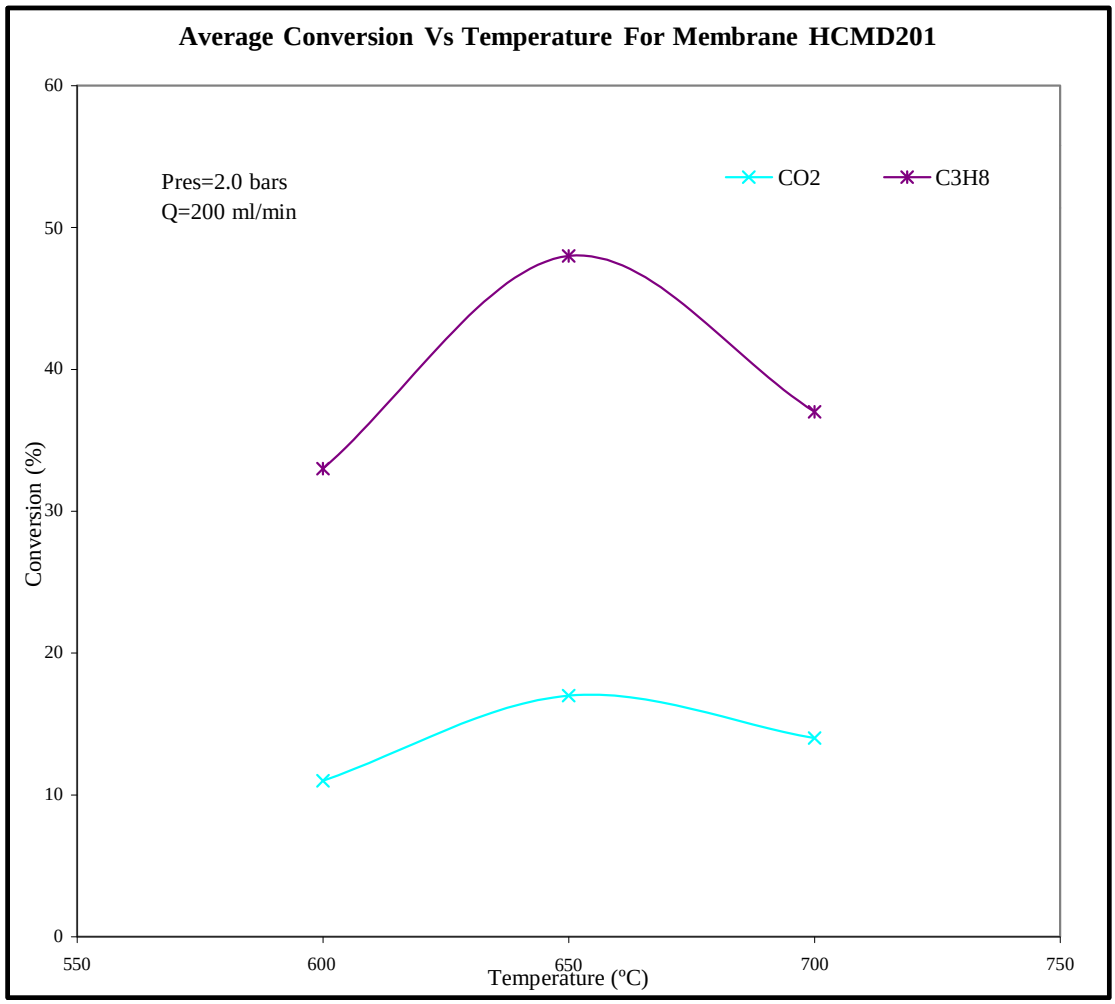

Figure A3.18 Average conversion vs temperature for membrane HCMD201.

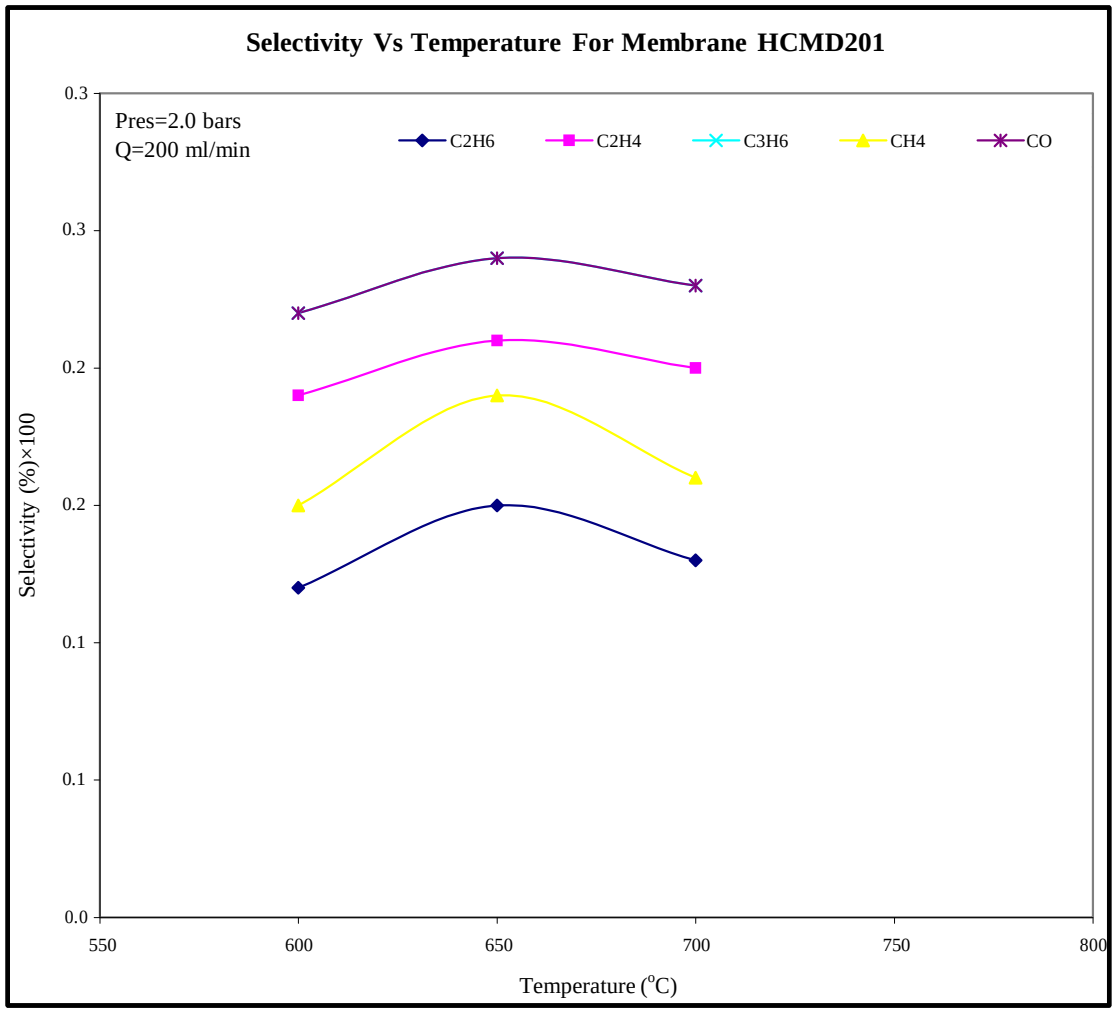

Figure A3.19 Selectivity vs temperature for membrane HCMD201.

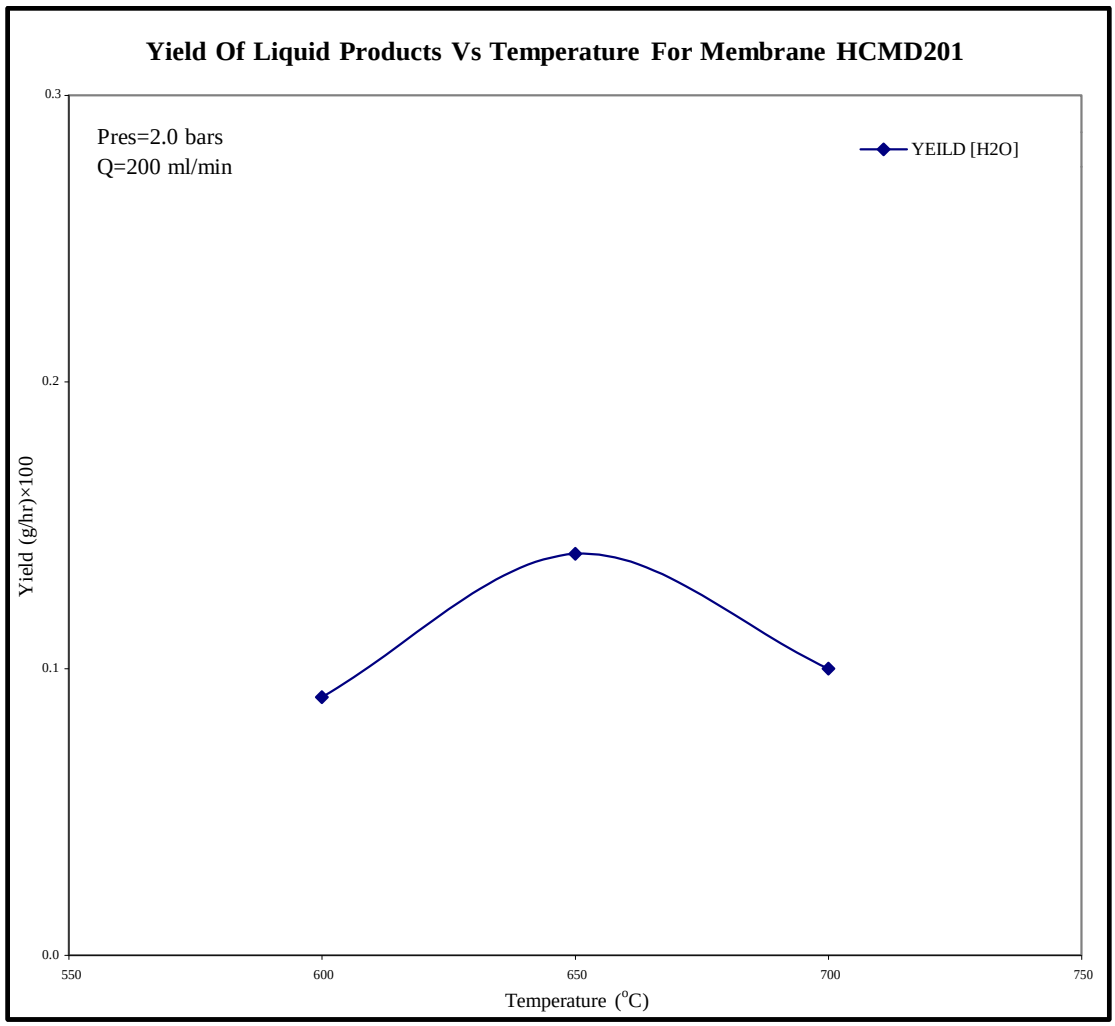

Figure A3.20 Yield of liquid products vs temperature for membrane HCMD201.

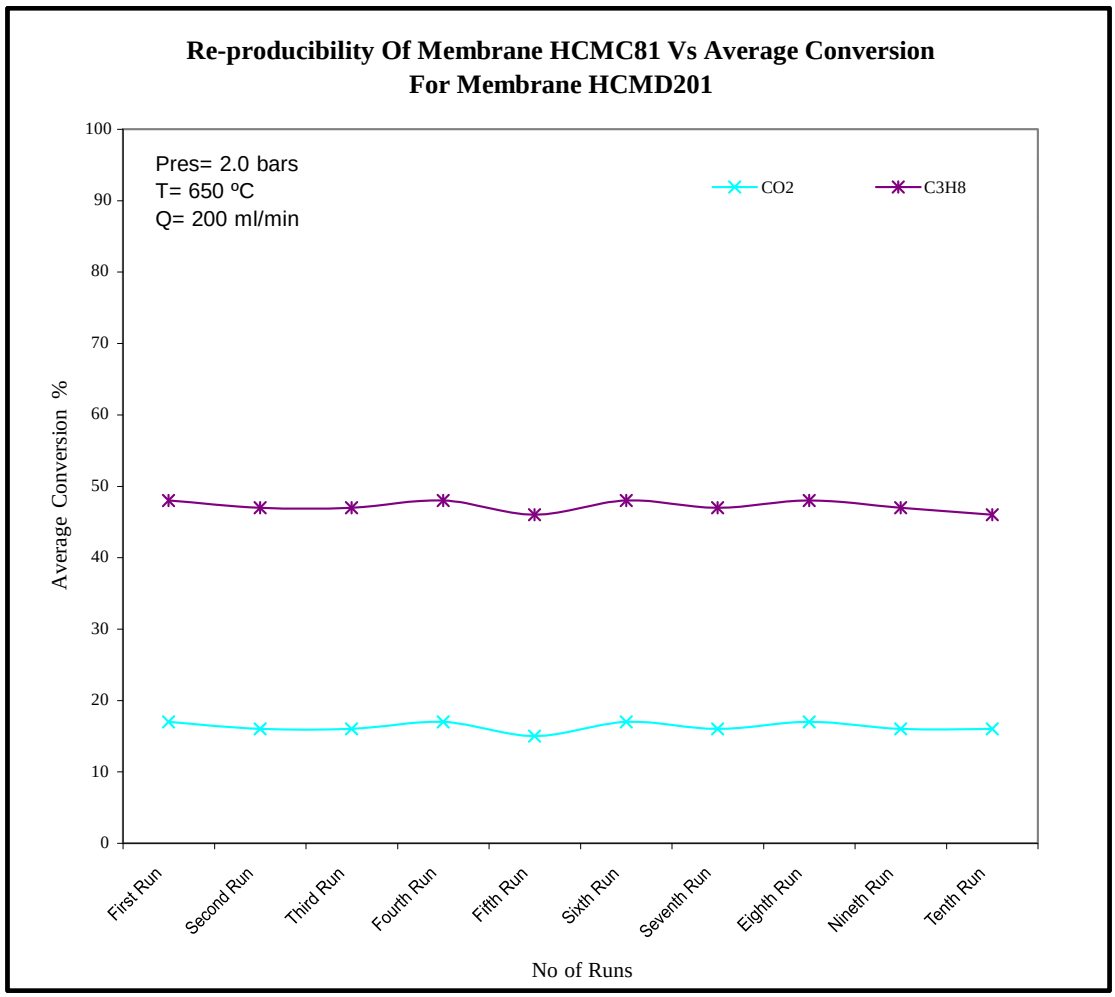

Figure A3.21 Re-reducibility of membrane HMCD201 vs average conversion for membrane HCMD201.

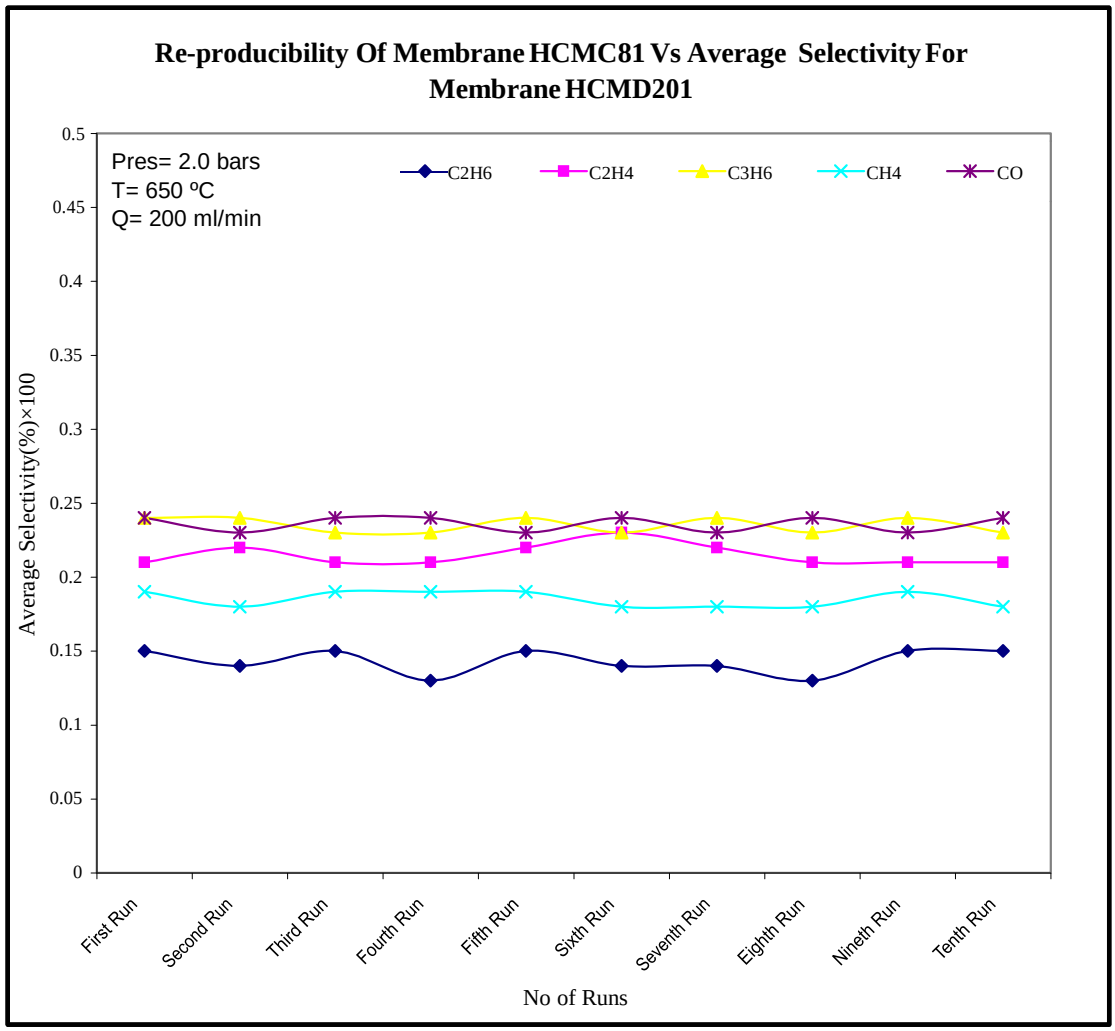

Figure A3.22 Re-reducibility of membrane HMCD201 vs average selectivity for membrane HCMD201.

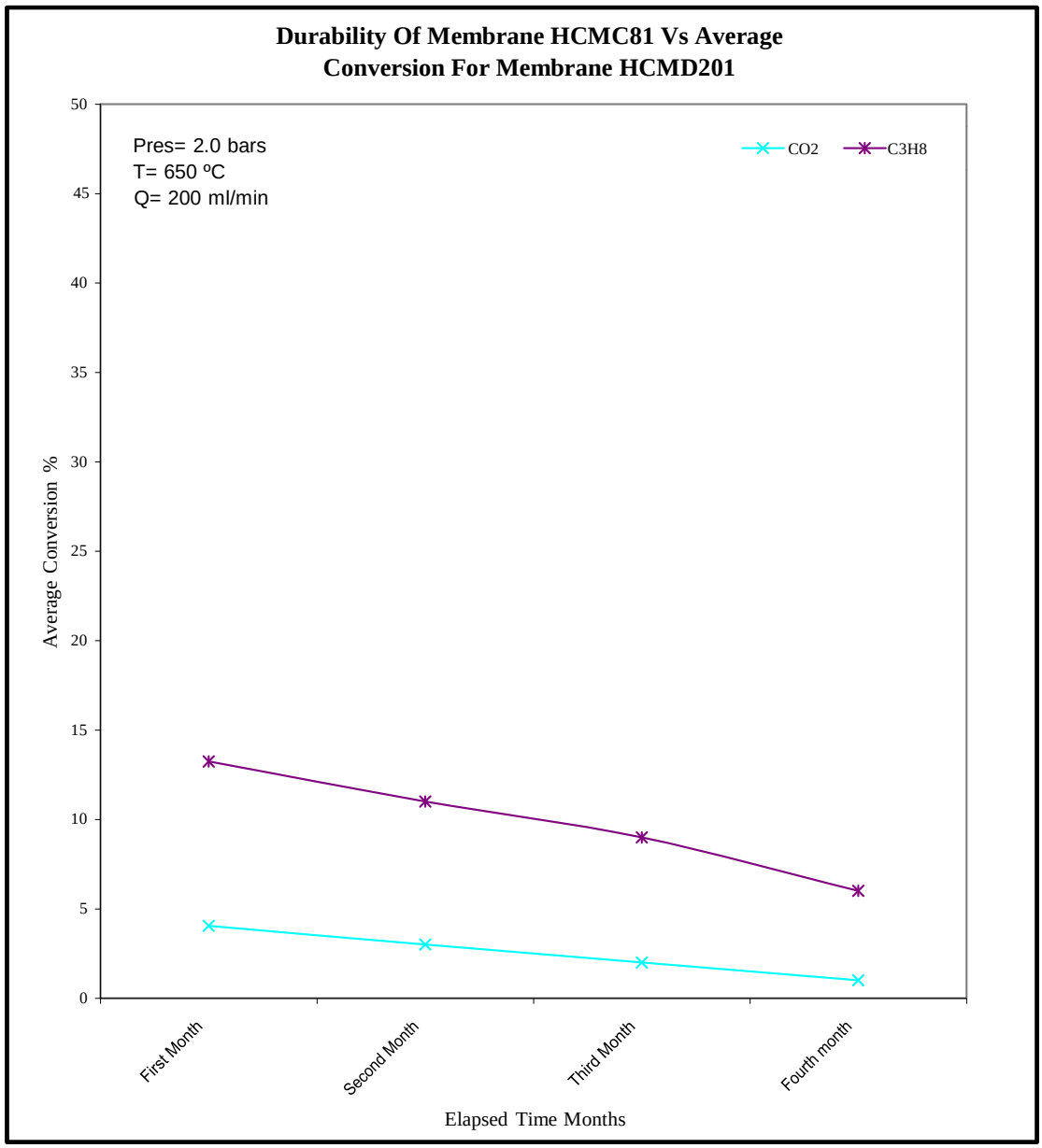

Figure A3.23 Durability of membrane HMCD201 vs average conversion for membrane HCMD201.

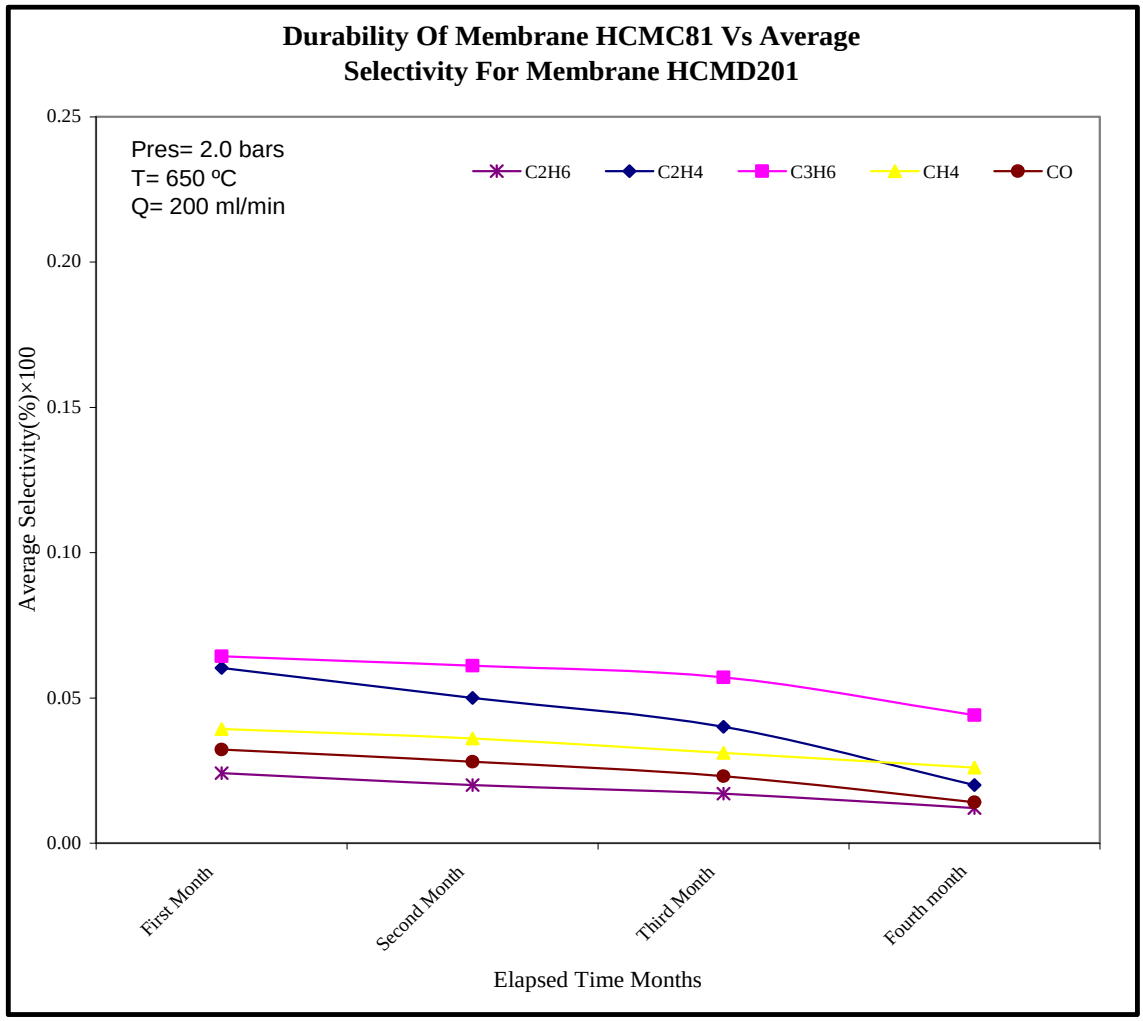

Figure A3.24 The durability of membrane HMCD201 vs average selectivity for membrane HCMD201.